THEORETICAL AND EXPERIMENTAL STUDY ON THE ULTRASONIC FUEL INJECTOR VALVE

A thesis submitted to the
University of Sheffield for
the degree of Doctor of Philosophy
in the Department of Mechanical Engineering

by

Hazim Muhammade Ali Al-Hussaini
B.Sc., M.Sc.

May, 1980.

To my parents -

to whom I owe everything.

ACKNOWLEDGEMENTS

This investigation was carried out in the Department of Mechanical Engineering of the University of Sheffield where the equipment, materials and facilities used were gratefully provided by Professor Royle.

Above all, the author particularly wishes to express his profound gratitude and appreciation in acknowledging with thanks the supervision, assistance and encouragement given him throughout the research programme by Dr. R. F. Boucher.

Much assistance was given to the author during the research programme by many technicians in the department. For this, he would like to thank the technicians in the Fluidics Laboratory.

The author wishes to thank his colleague, Mr. K. Bulmer, for his assistance in the presentation of the thesis. Thanks are also due to Mrs. Ann Brewster for her skill and speed in typing the thesis.

Finally the author wishes to thank his family for their financial support.

SUMMARY

This thesis describes a theoretical and experimental investigation of a novel ultrasonic fuel injector valve constructed from a tapered metal horn whose wide end is bonded to a quartz crystal. Fuel enters sideways at the longitudinal antinode and passes along a central hole to a ball valve at the tip. When the crystal is driven by an oscillatory pulse, it excites longitudinal vibrations, bouncing the ball from its seat and releasing fuel.

The ball motion without any liquid resistance has been studied theoretically through a computer program. Parameters such as the maximum gap between the ball and the seat, the frequency, amplitude and initial condition of the tip motion, and the time of impact have been studied, and compared with measurements of ball motion in a large vibrating model.

The injector tip motion has been measured using a laser technique. The measurements have been made with and without fuel flow. The effects of the fuel supply pressure and pulse width on the tip motion have been studied. Using this data, the effect of the actual (non-ideal) motion of the tip on the behaviour of the ball was studied theoretically.

A model of the valve was designed so that flow forces on the ball and the flow rates through the various passages could be measured. Using this data, the ball motion with fluid resistance was computed under various conditions. This in turn permitted the fluid flow from the injector valve to be predicted.

Five scale models of new valve geometries were designed and installed on an improved test rig. By this means, the effect of valve geometry on flow force and the flow rates within the valve were studied. The behaviour of actual injector flow during flow pulses was studied using laser anemometry.

The main findings of this investigation were as follows. The ball moves with a random frequency. An increase in the maximum gap between the ball and the seat caused, in general, a decrease in the frequency spectrum of the ball. Tip motion was found to build up in 5 ms to the steady state. Increasing the supply pressure caused a reduction in the amplitude of the tip motion. A decay of 1.5 ms in the tip motion was observed after switching off the injector. The effect of various geometrical changes in the design of the tip and its passageways on ball force and flow rates has been demonstrated. Ball motion built up in 1.5 - 2 ms, and decayed in 3 ms. The liquid resistance was found to have a significant influence on the ball motion. The flow rate built up to the steady state in 2- 3 ms and decayed in 2 ms. The total flow was found to have linear characteristics after 1.5 - 2 ms from switching on the injector.

Of particular significance, it was predicted theoretically and measured experimentally that the flow rate was independent of supply pressures over 40 psi.

CONTENTS

Page No.

NOTATIONS

a Acceleration of the tip at any instance.

A Ratio of the tip velocity at any instance to the maximum velocity of the tip.

A_{cs} Area of the measuring cross section.

A_{mt} Area of the tip inlet of the model.

A_r Projected area of the uppar half of the ball.

A_{vt} Area of the top inlet of the valve.

A_o Ratio of the initial velocity of the ball to the maximum velocity of the tip.

A_{o1} Ratio of the velocity of the ball after the collision to the maximum velocity of the tip.

A_1, A_2, A_3 and A_4 Cross sectional areas between the ball and the lower wall of the valve at sections 1, 2, 3 and 4 respectively.

A_{1-2}, A_{2-3}, A_{3-4} and A_{4-5} Projected areas of the lower half of the ball between sections 1 and 2, 2 and 3, 3 and 4 and 4 and 5 respectively.

B Constant.

B_o Ratio of the initial position of the ball from a fixed datum to the maximum gap between the ball and the seat.

B_{og} Ratio of the position of the ball from a fixed datum at the instance of the reversal in the direction due to the gravity to the maximum gap between the ball and the seat.

c_o Velocity of the sound.

C_{Dm} Coefficient of drag of the model.

C_{Dv} Coefficient of drag of the valve.

d_{mt} Diameter of the top inlet of the model.

d_{vt} Diameter of the top inlet of the valve.

D Ratio of the maximum amplitude of the tip to the maximum gap between the ball and the seat.

D_m Diameter of the ball of the model.

D_v Diameter of the ball of the valve.

E Young's modulus.

E_v Euler's number of the valve.

f Frequency of the tip (c/s).

f_D Doppler shift frequency.

f_{Dm} Maximum instantaneous Doppler frequency.

F_e Measured net force on the ball.

F_g Gravity force on the ball.

F_l Flow force on the lower half of the ball.

F_{mb} Buoyancy force on the ball of the model.

F_{mf} Flow force on the ball of the model.

F_u Flow force on the upper half of the ball.

F_{vb} Buoyancy force on the ball of the valve.

F_{vf} Flow force on the ball of the valve.

F_{vo} Flow force on the ball of the valve when it is on the seat.

g Gravitational acceleration.

g_1 Acceleration of the ball due to the fluid and gravity forces.

G_m Ratio of the parameter of damped vibration to the tip frequency.

K Spring constant.

L Fundamental variable of length.

L_o Fundamental dimension of length.

m Mass of the ball.

M Mass of the ball plus the added mass.

n Natural frequency of the spring-mass system.

N Number of the tip cycles at any instance.

N_m Maximum number of the tip cycles.

p_a Atmospheric pressure.

p_{mo} Static pressure at the outlet of the model.

p^*_{mo} Piezometric pressure at the outlet of the model.

p_{mt} Static pressure at the top inlet of the model.

p_w Pulse width.

p_{vo} Static pressure at the outlet of the valve.

p^*_{vo} Piezometric pressure at the outlet of the valve.

p_{vt} Static pressure at the top inlet of the valve.

p^*_1, p^*_2, p^*_3, p^*_4 and p^*_6 Piezometric pressures at sections 1, 2, 3, 4 and 6 respectively.

P_{mt} Supply pressure at the top inlet of the model.

P_v Supply pressure to the valve.

P_{vt} Supply pressure at the top inlet of the valve.

Q_{mt} Flow rate at the top inlet of the model.

Q_{vL} Instantaneous flow rate of the valve.

Q_{vN} Total flow for each increment of time.

Q_{vs} Side inlets flow rate of the valve.

Q_{vt} Top inlet flow rate of the valve.

Q_{vT} Total flow rate of the valve.

r Radius of the ball.

R_e Reynolds number.

R_{em} Reynolds number of the model.

R_{ev} Reynolds number of the valve.

$\bar{R}_{ev}$ Reynolds number of the valve based on the relative velocity between the ball and the flow at the top inlet.

R_1 Resistance due to the area of the top inlet.

R_2 Resistance due to the area above the ball.

R_3 Resistance due to the area of the side inlets.

R_4 Resistance due to the area under the ball.

R_5 Resistance due to the area of the outlet.

s Initial phase angle of the tip.

t Time at any instance after switching on the injector.

t_c Time in which the ball makes one cycle.

t_{co} Time between two successive collisions.

t_g Time in which the velocity of the ball becomes zero due to the gravity.

t_i Time at which the impulse was applied.

t_1 Time at any instance between two successive collisions.

T Number of the tip cycles in which the ball makes one cycle.

T_o Fundamental dimension of time.

v Velocity of the tip at any instance.

v_b Velocity of the ball at any instance between two successive collisions.

v_f Velocity of the tip after the collision.

v_o Initial velocity of the ball.

v_{o1} Velocity of the ball after the collision.

v_r Relative velocity between the ball and the flow at the top inlet.

v_i Tip velocity before the collision.

v_{ib} Ball velocity before the collision.

V_{mo} Flow velocity at the outlet of the model.

V_{mt} Flow velocity at the top inlet of the model.

V_T Maximum velocity of the tip

V_{vL} Flow velocity at the test section.

V_{vo} Flow velocity at the outlet of the valve.

V_{vt} Flow velocity at the top inlet of the valve.

w_d Damped natural frequency.

w_o Frequency of the tip (rad/s).

W Tip cycles (in radian) at any instance.

W_G Tip cycles (in radian) in which the velocity of the ball becomes zero due to the gravity force.

W_m Ratio of the tip frequency to the damped natural frequency.

W_n Injector tip natural frequency.

W_s Number of the tip cycles (in radian) in which the separation of the ball from the seat occurs.

W_1 Tip cycles (in radian) at any instance between two successive collisions.

y Gap between the ball and the seat.

y_{max} Maximum value of y.

y_{min} Minimum value of y.

y_o Initial position of the ball from a fixed datum.

y_{og} Position of the ball from a fixed datum at the instance of the reversal in its direction due to the gravity force.

y_w Maximum gap between the ball and the seat.

y_x Maximum amplitude of the tip.

y_1 Position of the tip from a fixed datum.

y_2 Position of the ball from a fixed datum.

$\bar{y}$ Argument of the polynomial.

Y_1 Ratio of the position of the tip from a fixed datum to the maximum gap between the ball and the seat.

Y Ratio of the gap between the ball and the seat to the maximum gap between the ball and the seat.

z_{mo} Height of the outlet of the model from the datum.

z_{mt} Height of the top inlet of the model from the datum.

z_{vo} Height of the outlet of the valve from the datum.

z_{vt} Height of the top inlet of the valve from the datum.

Z Ratio of the gravitational acceleration to the maximum acceleration of the tip.

τ Time of impact.

σ Poisson's ratio.

λ Beam wave length.

θ Beam intersection angle.

δ Initial phase angle of the steady state motion of the tip.

γ Parameter of damped vibration.

β Initial phase angle of the free vibration of the tip.

α Parameter of damped vibration.

ΔW Increment of W.

ν_m Kinematic viscosity of the liquid in the model.

ν_v Kinematic viscosity of the liquid in the valve.

ρ_m Density of the liquid in the model.

ρ_v Density of the liquid in the valve.

Chapter One

INTRODUCTION

1.1 GENERAL

The ultrasonic fuel metering valve has been designed by Plessey Company - U.K. The metering valve consists of a ball valve in the tip of an ultrasonic oscillator (horn). When the horn is oscillating, the ball is caused to bounce off its seat releasing fluid. The valve has been designed to provide precisely metered quantities of fuel, suitable for distribution and combustion when signalled by a controlling source. The metering valve provides an uncomplicated, cost effective response to increasing demands for fuel economy and low pollution combustion. For this reason, the ultrasonic fuel metering valve has become an object of extensive studies.

1.2 THE NEED FOR THE INVESTIGATION

It was found by The Plessey Company that the flow per pulse for small pulse widths (such as 1 ms) fluctuated (1). This indicated that the flow on each stroke of the engine would be different. This phenomenon is most undesirable. In order to determine the reason for this phenomenon, parameters which affect the behaviour of the valve should be studied. This would hopefully give an improved understanding of the injector and lead to better performance. A search through the literature revealed that very little is known about the parameters which affect the behaviour of the valve.

It is therefore considered that a theoretical and experimental study is needed.

1.3 SCOPE AND PURPOSE OF THE PRESENT INVESTIGATION

The general purpose of this investigation is to study:

1. The motion of the ball in various injector valves.
2. The consequent fuel flow, with a view to improving performance.

The ball motion without any liquid resistance has been studied theoretically through a computer program. Parameters such as the maximum amplitude of the injector tip, the maximum gap between the ball and the seat, the frequency of the tip, the initial conditions of the tip motion, and the time of impact have been studied.

The ball motion without any liquid resistance was measured in a large model of the injector valve. The purpose of these measurements was to check the results of the theoretical analysis of the ball motion, and to get an understanding of the ball motion between two vibrating walls.

The ultrasonic fuel injector was set up in the laboratory for measuring the amplitude of the vibration of the tip and the total flow rate from the injector.

In an attempt to find the effect of the tip motion on the behaviour of the valve, the tip motion has been measured by using a laser technique. The measurements have been made with and without fuel flow. The effects of the supply pressure and the pulse width on the tip motion have been studied.

The effect of the non-ideal motion of the tip on the behaviour of the ball has been studied theoretically by using the laser data in the previous theoretical analysis of the ball motion.

A large scale model of the injector valve has been designed, and a rig has been set up in an attempt to measure the force of the fluid on the ball and the flow rate in the model. The purpose of doing these measurements was to permit calculation of the forces of the fluid on the ball and the flow rate in the valve of the injector.

In an attempt to find the effect of the liquid resistance on the ball motion, the ball motion with the fluid resistance has been studied theoretically through a computer program. Consequently the fluid flow from the injector valve was predicted theoretically through a computer program.

Five scale models of different geometries of the valve were designed and a new test rig was set up for measuring the force of the fluid on the ball and the flow rate in these models. The fluid force on the ball and the flow rate were calculated in the corresponding injector valves. The aim of this study was an attempt to find the effect of the geometry of the valve on the fluid force on the ball and the flow rate in the valve.

To study the behaviour of the actual injector flow during the pulse, the flow rate to the injector has been measured by using the laser technique.

Chapter Two

ULTRASONIC FUEL INJECTOR

2.1 INTRODUCTION

This chapter is devoted to getting an idea about the ultrasonic fuel injector. The need for the ultrasonic fuel injector, background development, description of the injector and the recent studies on the injector are given below.

2.2 THE NEED FOR THE ULTRASONIC FUEL INJECTOR

The need for an improvement over the conventional carburettor has become apparent in recent years in the automotive industry. The emphasis on reduction of exhaust emissions of a harmful nature first showed up the deficiencies of this device. Recently the rising cost of petroleum products and the need to conserve resources has increased the momentum of the search for improved combustion in spark engines. In order to accomplish improvement in combustion, it is necessary to meter the fuel accurately to the cylinder, to prepare the fuel by fine atomisation and to achieve a high response rate from the injectors. A new technological approach to the metering of fuel is now needed to meet the new requirements. Such an approach is offered by the Plessey system. The basis of the Plessey fuel system is the ultrasonic fuel injector (2).

The ultrasonic fuel injector is a transducer designed to have a minimum of mechanical complexity, be producible at low cost and provide that vital link between the control system and the fuel supply. It has only one moving part, which is non-sliding and low

mass, is simple to manufacture, uses low cost, wide tolerance components and has excellent response characteristics. Durability has been proven on life tests with injectors operating for over 4000 hours and still performing within manufacturing specification. In addition to the obvious advantages over the better known electro-magnetic valves, such as: inherent simplicity, good fuel preparation, long life and low cost, it also offers unique operational characteristics beneficial to the system designer. The non existence of sliding parts and the small surface area of the ball also make the injector suitable for use with the more viscous fuels such as diesel (3). In a single point system, the ultrasonic fuel injector is positioned to inject fuel into the manifold at a point so that all the cylinders are supplied with an air/fuel mixture created at this point (fig. (2.1)) (2).

2.3 BACKGROUND DEVELOPMENT

Plessey commenced research into the use of ultrasonics as a means of fuel management more than 12 years ago. Early work was concerned mainly with ultrasonic atomisation of fuels for improved combustion, particularly liquid fuels heavier than gasolene. Some experience was gained in mixture preparation for operating low compression ratio spark ignition engines on kerosine and diesel fuel. Improved light up of small gas turbines was successfully demonstrated, as was a device for re-igniting aero engines following high altitude flame out. The next stage of development introduced a means of flow control in addition to the capabilities. A solid state metering valve termed an Electro Fluidic Divider was

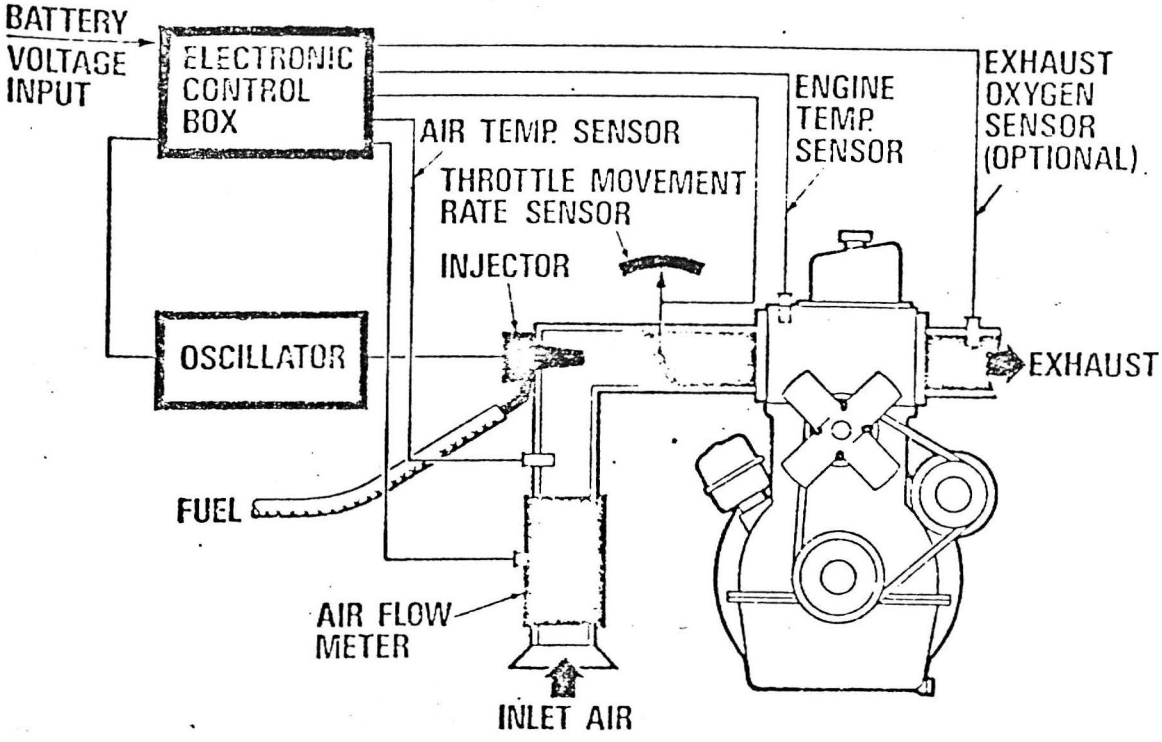

FIG. 2.1 ULTRASONIC FUEL INJECTOR IN A SINGLE POINT SYSTEM

developed and comprised a small sharp edged metered orifice, situated in the tip of an ultrasonic velocity transformer. In its quiescent state fuel passed through the orifice and emerged in a coherent stream where it was wholly collected by a small capillary collector tube facing the orifice a short distance from it. This fuel was then returned to some convenient part of the fuel pumping system. When the fluidic divider was activated, cavitation created on the back of the orifice caused a disintegration of the fuel stream, the majority of which by-passed the collector tube in the form of a fine spray. Thus by controlling the excitation period and repetition frequency the fuel could be both metered and atomised. Further multi-fuel research was carried out using this device and some considerable success was achieved operating two-stroke outboard engines on kerosene, and a small Wankel engine on kerosene and diesel fuel. At about this time several automotive companies expressed their interest in the fluidic divider for volume automotive fuel control systems. There were two main disadvantages with this design when used with gasolene. Firstly, a possibility of fuel vapourisation from the jet during the activated state, especially at high temperature and low ambient pressure. Secondly, the problem of continuously cycling the fuel. Its main attractions, however, were that it was truly solid state and inexpensive to produce. The prospect of a high volume market for the injector in the automotive industry led to an increase in development activity, which has culminated in the present ball valve injector design. This injector is now passing from its development stage to the production engineering phase (3).

2.4 DESCRIPTION OF THE INJECTOR

2.4.1 General

The injector (which is shown in fig. (2.2)) comprises a steel body (see fig. (2.3)), shaped as a velocity transformer with a length equal to one half wave length at approximately 60 KHz. A piezoelectric ceramic disc is bonded to the low amplitude end and a metering ball valve located at the high amplitude end of the body. Fuel is introduced at or near the vibration nodal plane and the injector is also mounted in this plane. The injector is vibrated at its resonant frequency by an electronic drive oscillator. In its non activated state the ball is held against its seat by the fuel pressure. When commanded by the control unit the drive oscillator output excites the injector body into resonance and the valve seat vibrations shake the ball from its closed position, allowing atomised fuel to pass from the valve. When the oscillator is switched off vibrations cease and the ball returns, under the action of fuel pressure, to its seat.

2.4.2 Injector Ball Valve

The metering valve itself (fig. (2.4)) is an important component of the injector and consists of three main parts:

(1) A valve seat.

(2) A steel ball of 2 mm diameter.

(3) A ball location housing.

Current designs enable this valve to be manufactured and subjected to certain performance and quality control criteria which can be related to its metering accuracy in the finally assembled

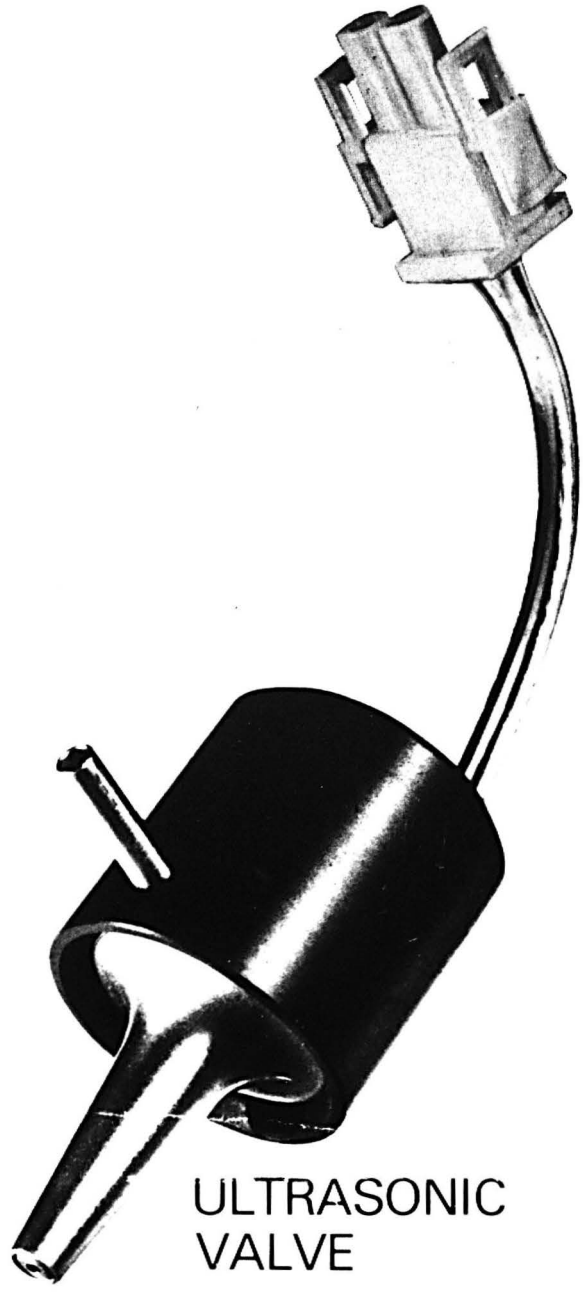

FIG. 2.2 - ULTRASONIC VALVE

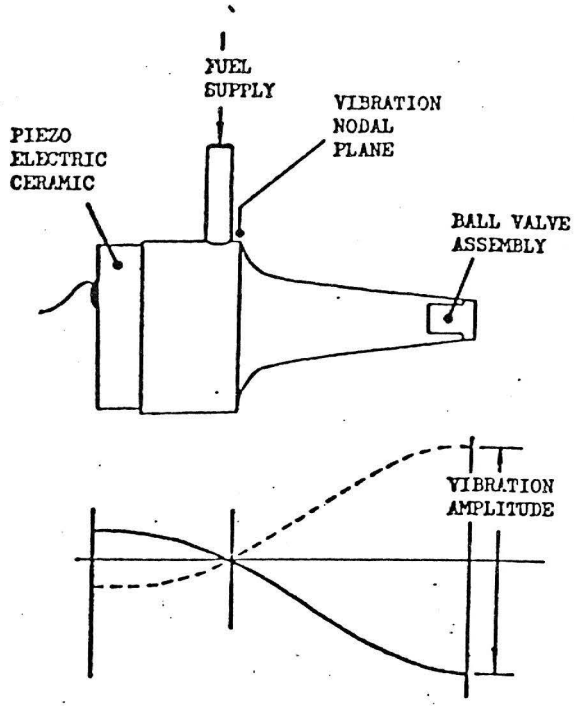

FIG. 2.3 ULTRASONIC INJECTOR

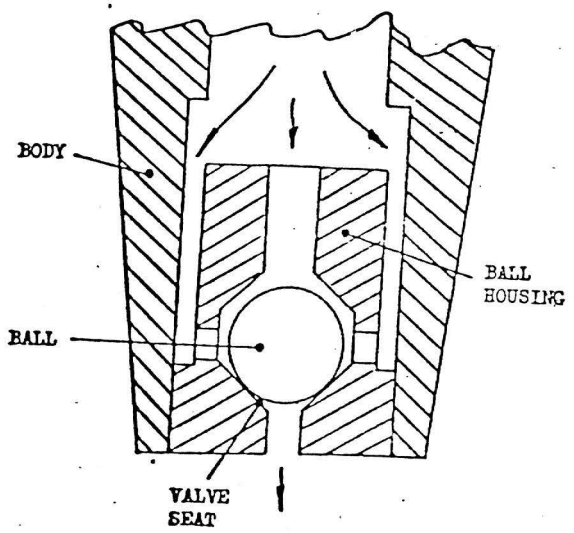

FIG. 2.4 BALL VALVE ASSEMBLY

injector. This enables the valve to be rejected at an early low cost state before any significant value is added (3).

The main metering orifice is not the exit orifice, but the varying orifice between ball and seat. Thus, if the ball movement during a pulse is predictable within certain finite limits, the metering accuracy is not affected by contamination as it is continually cleaned by ball contact over a defined area of the seat (3).

The ball location housing is designed to control the very complex ball movements and fluid dynamics within the valve (3).

2.4.3 Injector Body

The piezo ceramic disc is bonded to the rear face at the low amplitude end of the injector body which is shaped to give sufficient amplification of the piezo disc vibrations for correct valve operation. The injector must be mounted close to its vibration node because of the dynamic nature of its operation and care must be exercised when mounting to avoid undue damping of the vibrations. By careful design, a simple, reliable mounting arrangement was developed which provides a reliable means of introducing fuel (fig. (2.5)), thereby eliminating the need for a conventional rubber hose with all its inherent problems of rubber deterioration, poor sealing, etc. (3).

2.4.4 Drive Circuits

Drive to the injector is supplied from a power oscillator, the injector forming one part of the resonant loop thereby controlling the drive frequency at the resonant frequency of the injector. The

response of the oscillator is excellent and resonant frequency and maximum drive volts are achieved within 3 cycles of oscillation after switch-on. Power requirements for the injector when operating at maximum duty cycle can be from 8 to 15 watts, depending on the maximum flow rate of the injector (3).

2.5 RECENT STUDIES ON THE INJECTOR

The recent studies on the injector have been done only by the Plessey Company Limited.

Grubb, Milsom and Abram (1) have examined the tip motion under a microscope. It was found that although the tip motion was detectable, the amplitude was too small to allow accurate measurement by this method.

Grubb, Milsom and Abram (1) have also measured the tip motion by a capacitive measuring technique. The injector was filled with fuel, but without atomization. It was deduced that the amplitude of vibration of the tip was 0.0026 mm. Also it was found that the motion of the tip was built up to the final amplitude over several milliseconds.

The motion of the ball was studied theoretically through a computer program by (1). It was assumed that the ball was bouncing between the top wall and the seat of the injector valve without any fluid resistance. The coefficient of restitution for the ball-wall collisions was taken to be unity, and the tip motion was assumed to be sinusoidal. The maximum amplitude of the tip motion, the frequency of the tip and the maximum gap between the ball and the seat were 0.0025 mm, 60 KHz and 0.25 mm respectively.

It was found that the ball was moving in a random motion. Martin and Sumal (3) have found that the injector had linear characteristics for fuel flow versus pulse width, with only a slight change in the slope at about 0.8 ms pulse width (fig. (2.6)). It was also found in (3) that the flow versus the supply pressure characteristics of the injector were unique (fig. (2.7)). Their explanation of the results was that when the supply pressure increased, the flow rate increased as a function of the square root of the pressure drop across the exit orifice. But at the same time the force on the ball increased by the increase of the supply pressure, and hence the ball movement decreased. This meant that the area between the ball and the seat was a function of the reciprocal of the square root of the pressure drop across this orifice.

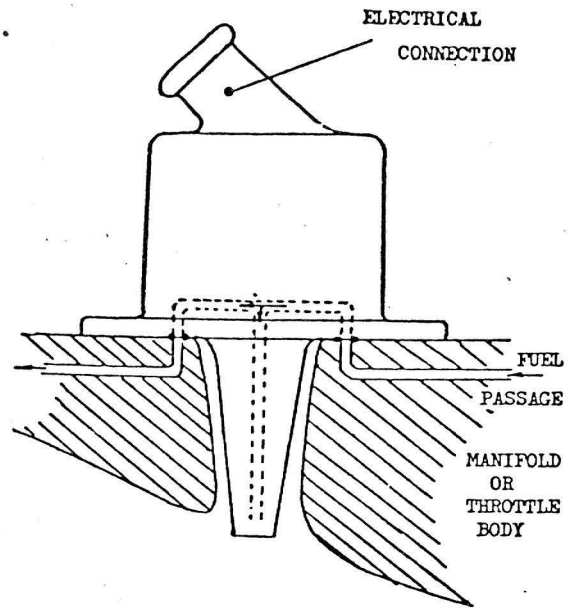

FIG. 2.5 SCHEMATIC VIEW OF FLOW THROUGH FUEL SUPPLY ARRANGEMENT

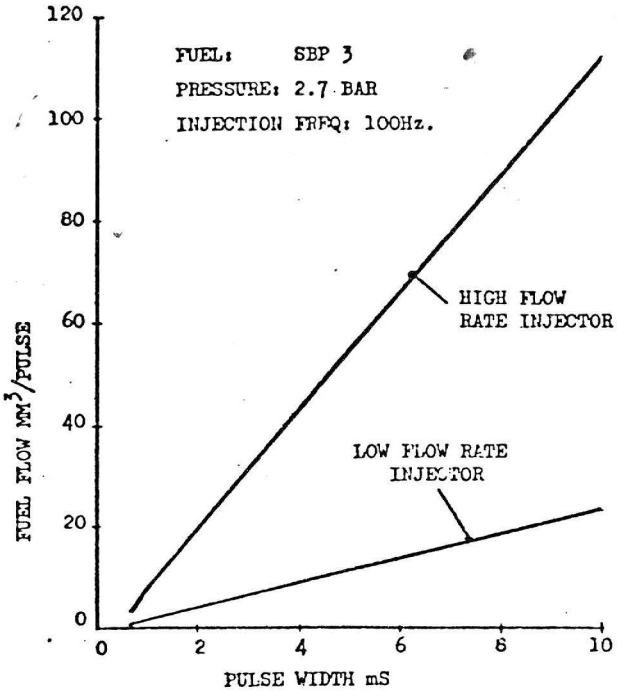

FIG. 2.6 FUEL FLOW vs PULSE WIDTH FOR TWO TYPICAL INJECTORS

1. FUEL VELOCITY
2. EFFECTIVE ORIFICE AREA
3. NET FLOW FROM ULTRASONIC INJECTOR

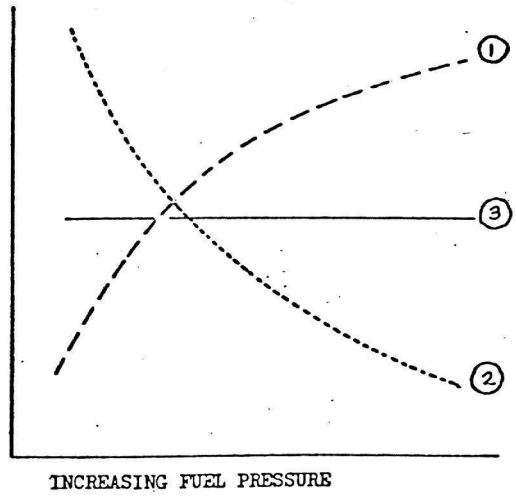

FIG. 2.7 EFFECT OF FUEL PRESSURE ON FLOW

Chapter Three

THEORETICAL ANALYSIS OF THE BALL MOTION WITHOUT FLUID RESISTANCE

3.1 INTRODUCTION

Since when the ball collides at the exit orifice of the valve, it closes the valve, the flow rate from the injector will be affected by the motion of the ball. The motion of the ball can thus be considered of importance in the design of the ultrasonic fuel injector.

The only research which has been done on this problem was by Grubb, Milsom and Abram (1). It was assumed by them that the ball was bouncing between the upper and lower walls of the valve without any fluid resistance. The transient or stochastic nature of the starting process and the time of impact were not considered. It was found that the ball was moving in random frequency.

In this chapter the ball motion has been studied theoretically using a computer program. Parameters such as the maximum amplitude of the injector tip, the frequency of the injector tip, the maximum gap between the ball and the seat, the time of impact and the starting condition of the injector tip were studied.

3.2 THEORY

3.2.1 Injector Tip Motion

3.2.1.1 Equation of Motion of the Injector Tip

The injector tip was assumed moving sinusoidly. The following equation represented the motion of the tip from a fixed datum which was assumed as the line passing through the seat at t = o,

$$y_1 = y_x \sin(w_o t + s) \qquad (3.1)$$

where y_x represents maximum amplitude of the tip, w_o frequency of the tip, t time at any instance after switching on the injector, and s initial phase angle of the tip.

3.2.1.2. Starting Conditions of the Tip Motion

Two starting conditions have been assumed:

1. The tip was moving down at $t = o$, i.e. $s = \pi$
2. The tip was moving up at $t = o$, i.e. $s = o$.

3.2.2 Motion of the Ball

3.2.2.1 Equation of Motion of the Ball

The ball was assumed to move in one dimension, fig. (3.1). The motion of the ball was assumed without any fluid resistance. The forces which were assumed acting on the ball were the collision and the gravity forces.

The following equation represented the motion of the ball from the same datum as the tip:

$$y_2 = -g\, t_{1/2}^2 + v_o\, t_1 + y_o \qquad (3.2)$$

where y_2 represents the position of the ball from a fixed datum, g gravity acceleration, t_1 time at any instance between two successive collisions, v_o initial ball velocity and y_o initial position of the ball from a fixed datum.

3.2.2.2 Starting Conditions of the Ball Motion

Two starting conditions have been assumed:

1. At $t = o$, $t_1 = o$, $y_o = y_1$, and the ball was moving down with v_o equal to the maximum velocity of the tip.

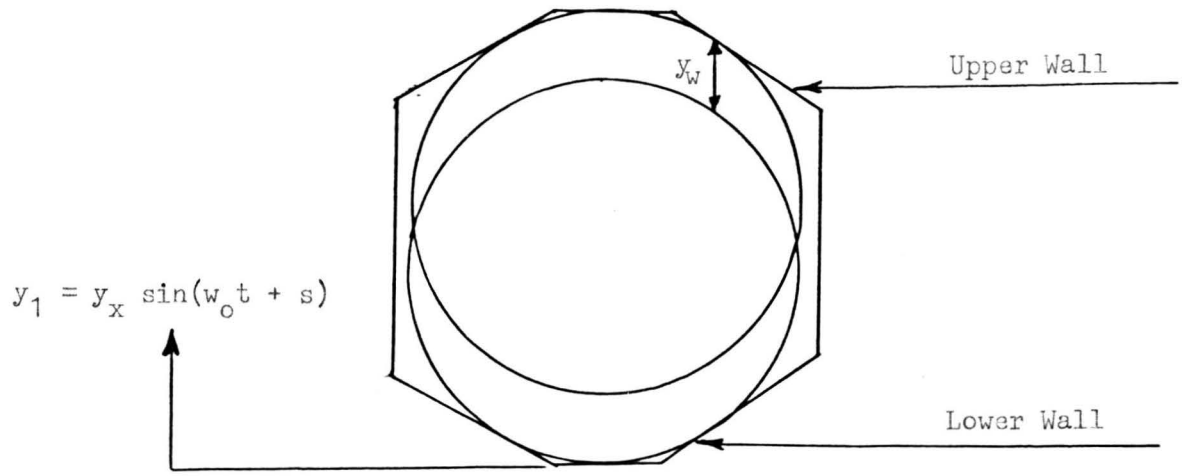

FIG. 3.1 THEORETICAL MODEL OF THE INJECTOR VALVE

2. At $t = o$, $t_1 = o$, $y_o = y_1$, and the ball was moving up with v_o equal to zero.

3.2.2.3 Equation of the Gap between the Ball and the Seat

The gap between the ball and the seat was found by subtracting eqn. (3.1) from eqn. (3.2):

$$y = y_2 - y_1 \tag{3.3}$$

$$y = -g\, t_{1/2}^2 + v_o\, t_1 + y_o - y_x \sin(w_o\, t + s) \tag{3.4}$$

3.2.2.4 Collision between the Ball and the Walls of the Valve

The collision between the ball and the seat occurred when $y = o$, and the collision between the ball and the upper wall occurred when $y = y_w$. When the collision occurred, t_1, y_o and v_o changed and became as follows:

$$t_1 = t_{co} \ ,$$

$$y_o = y_1 \ ,$$

$$v_o = v_{o1} \ ,$$

where t_{co} represents the time between two successive impacts and v_{o1} the velocity of the ball after the collision.

Since the material of the ball and the walls of the valve were the same (steel), the coefficient of restitution was assumed to be unity. Since the mass of the injector horn was large compared to the mass of the ball, the velocity of the tip was assumed unaffected by the collision with the ball.

From (4) the velocity (v_{o1}) of the ball after the collision

was: $$v_{o1} = v_f + v_i - v_{ib} \quad (3.5)$$

When the time of impact was not considered in the analysis:

$v_f = v_i = v$ at the instance of the impact,

and

$v_{ib} = v_b$ at the instance of the impact,

where v_f represents the velocity of the tip after the collision, v_i the velocity of the tip before the collision, v the velocity of the tip at any instance between two successive collisions, v_{ib} the velocity of the ball before the collision and v_b the velocity of the ball at any instance between two successive collisions.

Hence

$$v_{o1} = 2 v_f - v_{ib} \quad (3.6)$$

v_f was found from the derivative of y_1 with respect to t:

$$v_f = y_x \ w_o \ \cos (w_o t + s) \quad (3.7)$$

v_b was found from the derivative of y_2 with respect to t_1:

$$v_b = -g \ t_1 + v_o \quad (3.8)$$

At the instance of the impact $t_1 = t_{co}$ and hence:

$$v_{ib} = -g \ t_{co} + v_o \quad (3.9)$$

By substituting eqn. (3.7) and eqn. (3.9) in eqn. (3.6) we obtained:

$$v_{o1} = 2 y_x \ w_o \ \cos (w_o t + s) + g \ t_{co} - v_o \quad (3.10)$$

3.2.2.5 Equation of the Gap After the Reversal in the Direction of the Ball Due to Gravity

The time in which the velocity of the ball reached zero was

found by equating eqn. (3.8) to zero:

$$t_g = \frac{v_o}{g} \quad . \tag{3.11}$$

Equation of the gap after the reversal in the direction of the ball due to gravity was found in a similar way to that in which eqn. (3.4) has been found:

$$y = -g\, t_{1/2}^2 + y_{og} - y_x \quad \sin(w_{ot} + s) \quad , \tag{3.12}$$

where t_1 represents t_g plus the time at any moment between the instance of the reversal in the direction and the instance of the following impact, and y_{og} the position of the ball from a fixed datum at the instance of the reversal in the direction.

3.2.2.6 Steady State Motion of the Ball

Since the flow rate from the injector should be constant during the pulse width, and since the main metering orifice was not the exit orifice, but the varying gap between the ball and the seat, (3), the time of the ball cycle was considered of importance in controlling the flow rate from the injector. The cycle of the ball was considered as the movement of the ball between two successive impacts with the seat. The flow rate from the injector would be constant during the pulse width when the period of the ball cycle was constant during the pulse and this motion of the ball was considered as the steady state motion.

3.2.3 Dimensional Analysis

Dimensional analysis has been used in this analysis because it does yield information about the form of mathematical relations

connecting the relevant variables and suggests the most effective way of grouping the variables together.

It could be seen from eqn. (3.4) that the gap between the ball and the seat was affected by the following variables:

$$w_o\ ,\ y_x\ ,\ y_w\ ,\ t\ ,\ s\ ,\ g\ ,\ t_1\ ,\ v_o\ ,\ y_o$$

$$\text{i.e.}\quad y = \phi\,(\,w_o, y_x, y_w, t, s, g, t_1, v_o, y_o\,)\,. \qquad (3.13)$$

The group method was used in applying the dimensional analysis as follows:

Using the mass, length and time system, the dimensional matrix was:

	y	w_o	y_x	y_w	t	s	g	t_1	v_o	y_o
M	0	0	0	0	0	0	0	0	0	0
L	1	0	1	1	0	0	1	0	1	1
T	0	-1	0	0	1	0	-1	1	-1	0

The variables included dimensions of length and time. So that two fundamental variables were used to include these dimensions. Selecting y_x and w_o, the fundamental dimensions of length and time were expressed in terms of these:-

$$[\,y_x\,] = [\,L_o\,] \qquad \text{giving} \qquad [\,L_o\,] = [\,y_x\,]\ ,$$

$$[\,w_o\,] = [\,T_o^{-1}\,] \qquad \text{giving} \qquad [\,T_o\,] = [\,w_o^{-1}\,]\,.$$

Group $\pi_1\,.\,[\,y\,] = [\,L_o\,] = [\,y_x\,]\,.$

Whence $y = \pi_1\ y_x$ and $\pi_1 = \dfrac{y}{y_x}$.

Group $\pi_2\,.\,[\,y_w\,] = L_o = [\,y_x\,]$

Whence $y_w = \pi_2\ y_x$ and $\pi_2 = \dfrac{y_w}{y_x}$

Group $\pi_3 \cdot [t] = [T_o] = w_o^{-1}$.

Whence $t = \pi_3 w_o^{-1}$ $\pi_3 = t w_o$

Group $\pi_4 \cdot [s] = [o]$.

Whence $s = \pi_4$ and $\pi_4 = s$.

Group $\pi_5 \cdot [g] = [L_o T_o^{-2}] = y_x w_o^2$.

Whence $g = \pi_5 y_x w_o^2$ and $\pi_5 = \frac{g}{y_x w_o^2}$.

Group $\pi_6 \cdot [t_1] = [T_o] = [w_o^{-1}]$.

Whence $t_1 = \pi_6 w_o^{-1}$ and $\pi_6 = t_1 w_o$.

Group $\pi_7 \cdot [v_o] = [L_o T_o^{-1}] = [y_x \cdot w_o]$.

Whence $v_o = \pi_7 y_x w_o$ and $\pi_7 = \frac{v_o}{y_x w_o}$.

Group $\pi_8 \cdot [y_o] = [L_o] = [y_x]$.

Whence $y_o = \pi_8 y_x$ and $\pi_8 = \frac{y_o}{y_x}$.

$$\frac{y}{y_x} = \Psi\left(\frac{y_w}{y_x}, t w_o, s, \frac{g}{y_x w_o^2}, t_1 w_o, \frac{v_o}{y_x w_o}, \frac{y_o}{y_x}\right), \quad (3.14)$$

or

$$\frac{y}{y_w} = \Psi\left(\frac{y_x}{y_w}, t w_o, s, \frac{g}{y_x w_o^2}, t_1 w_o, \frac{v_o}{y_x w_o}, \frac{y_o}{y_w}\right). \quad (3.15)$$

Putting $\frac{y}{y_w} = Y$, $\frac{y_x}{y_w} = D$, $t\, w_o = W$, $\frac{g}{y_x\, w_o^2} = Z$,

$$t_1\, w_o = W_1\,, \quad \frac{v_o}{y_x\, w_o} = A_o\,, \quad \frac{y_o}{y_w} = B_o\,,$$

therefore

$$Y = \Psi\,(D\,, W\,, s\,, Z\,, W_1\,, A_o\,, B_o) \qquad (3.16)$$

If the same dimensionless groups are used in eqn. (3.4) it becomes:

$$Y = D\,(-Z\,W_1^2/2 + A_o\,W_1 + B_o) - D\,\sin\,(s + W) \qquad (3.17)$$

When $Y = 0$, the collision was with the lower walls and when $Y = 1$, the collision was with the upper wall. Eqn. (3.10), for the velocity of the ball after collision, becomes:

$$A_{o1} = 2\,\cos\,(W + s) + (Z\,W_1 - A_o)\,. \qquad (3.18)$$

From eqn. (3.11), the ball velocity becomes zero in WG radians due to the gravity f where

$$WG = \frac{A_o}{Z} \qquad (3.19)$$

Eqn. (3.12), for the gap after the reversal in the direction of the ball due to gravity, becomes

$$Y = D\,(-Z\,W_1^2/2 + B_{og}) - D\,\sin\,(W + s)\,. \qquad (3.20)$$

3.2.4 Time of Impact

Since the shape of the upper and lower walls of the valve look like a cone, and the ball collided with the walls of the valve all round, the time of impact was a complicated problem. To simplify the problem, impact was assumed between the ball and a plane surface (of a massive body at one point). This time of impact was probably longer than that of the actual case. The time of impact of this assumption was calculated and compared with the time of the cycle of the ball to find if the time of impact was important or not.

Many investigators have studied the problem of the time of impact with a plane surface of a massive body of the same material.

S. C. Hunter (5) has calculated the absorption of vibrational energy in the form of elastic waves generated by a transient localized force acting normally to a free surface of a simi-infinite solid in terms of Fourier components of the force. He has applied this result to the Hartzian collision of a small body with a plane surface of a massive specimen. He has concluded that for impact velocities which were small compared to the propagation velocity of elastic waves in the specimen, a negligible proportion of the original kinetic energy of the small body was transferred to the specimen during the collision. Hunter considered this result as conforming the validity of the Hertz theory (see Love (6)). for the detail of this theory) for collisions between a small and a massive body. It has been stated by Hunter that this analysis became applicable only when the thickness of the massive body was sufficient to prevent the first reflected elastic wave returning to

the contact area before the impact terminated, and also

$$\left(\frac{v_{ib} - v_i}{c_o}\right)^{1/5} \ll 1$$

Goodier, Jashman and Ripperger (7) have measured the time of impact between a steel ball with a steel block. It was their observation that the duration of contact given by Hertz agreed well with their measurements provided that the height through which the ball was dropped was small. Lifshitz and Kolsky (8) have measured the time of impact between a steel ball with steel block. They have observed that the time of impact had the values predicted by the Hertzian treatment for elastic deformations even when the velocities of impact were as much as eight times the velocity first required to initiate plastic yield.

One of the premises on which Hertz's mathematical theory of collision of elastic bodies was based was that the strains produced in the immediate neighbourhood of the region of contact are determined by the pressure subsisting at any instant between the bodies, and were practically the same as under static conditions. Raman (9) has shown that this premise was valid even when the impinging bodies did not move as rigid bodies, and the impact caused to conversion of part of the translational kinetic energy into energy of elastic wave-motion in the solid. Based on a series of experiments on the transverse impact of a solid sphere on an infinitely extended elastic plate of finite thickness, he calculated the coefficient of restitution, assuming that this coefficient was a function of the elastic constants and densities of the materials, the diameter of the sphere, the thickness of the plate, and the velocity of impact.

Raman stated that when the velocity of impact was not very large and the thickness of the plate was not much smaller than the diameter of the impingion sphere, the time of impact predicted by Hertz's theory agreed well with the time of impact necessary in the calculation of the coefficient of restitution.

From the literature cited above the Hertz theory could provide excellent evaluation of the time of impact between the ball and the walls of the valve. In this analysis Hertz theory was used and from Hunter (5) the equation of the time of impact was:

$$\overline{C} = 2.94 \left[\frac{15}{8} m \left(\frac{1-\sigma^2}{E}\right)\right]^{2/5} r^{-1/5} (v_{ib} - v_i)^{-1/5} , \qquad (3\ 21)$$

where m represents the mass of the ball, σ Poisson's ratio, E Young's modulus, r radius of the ball, v_{ib} velocity of the ball before the collision and v_i velocity of the tip before the collision.

The two conditions which have been stated by Hunter, for the application of Hertz theory to this problem were also applied in this analysis:

1) $\left(\frac{v_{ib} - v_i}{c_o}\right)^{1/5} \ll 1$

2) The mass of the horn of the injector was very large compared to the mass of the ball, and the horn was long enough to prevent the first reflected elastic wave returning to the contact area before the impact terminated, i.e. the time of impact was smaller than the time which the first elastic reflected wave took to come back to the contact area again.

When the time of impact was included, eqn. (3.4) becomes:

$$y = -g\, t_1^2/2 + v_o\, t_1 + y_o - y_x \left[\sin\ w_o(t+\tau) + s\right], \quad (3.22)$$

eqn. (3.7) becomes:

$$v_f = y_x\, w_o\ \cos\left[w_o\,(t+\tau) + s\right], \quad (3.23)$$

and eqn. (3.9) becomes:

$$v_{o1} = y_x\, w_o\ \cos\left[w_o(t+\tau) + s\right] + y_x\, w_o\ \cos\,(w_o\, t + s) + g\, t_{co} - v_o \quad (3.24)$$

3.3 COMPUTER PROGRAMS

3.3.1 Computer Program Without the Time of Impact

Fig. (3.2) shows the flow chart of the computer program. Fortran language was used on the ICL 1906 computer at Sheffield University.

The value of Y was calculated for each increment ΔW and this process was continued until Y became ≤ 0, i.e., the collision was with the lower wall, or Y became 1, i.e., the collision was with the upper wall. The value of W for which Y was equal 0, or Y equal 1 was found by using C05ACF subroutine which was stored in the library of the computer. This subroutine was based on bisection method. The computer program is shown in appendix (2).

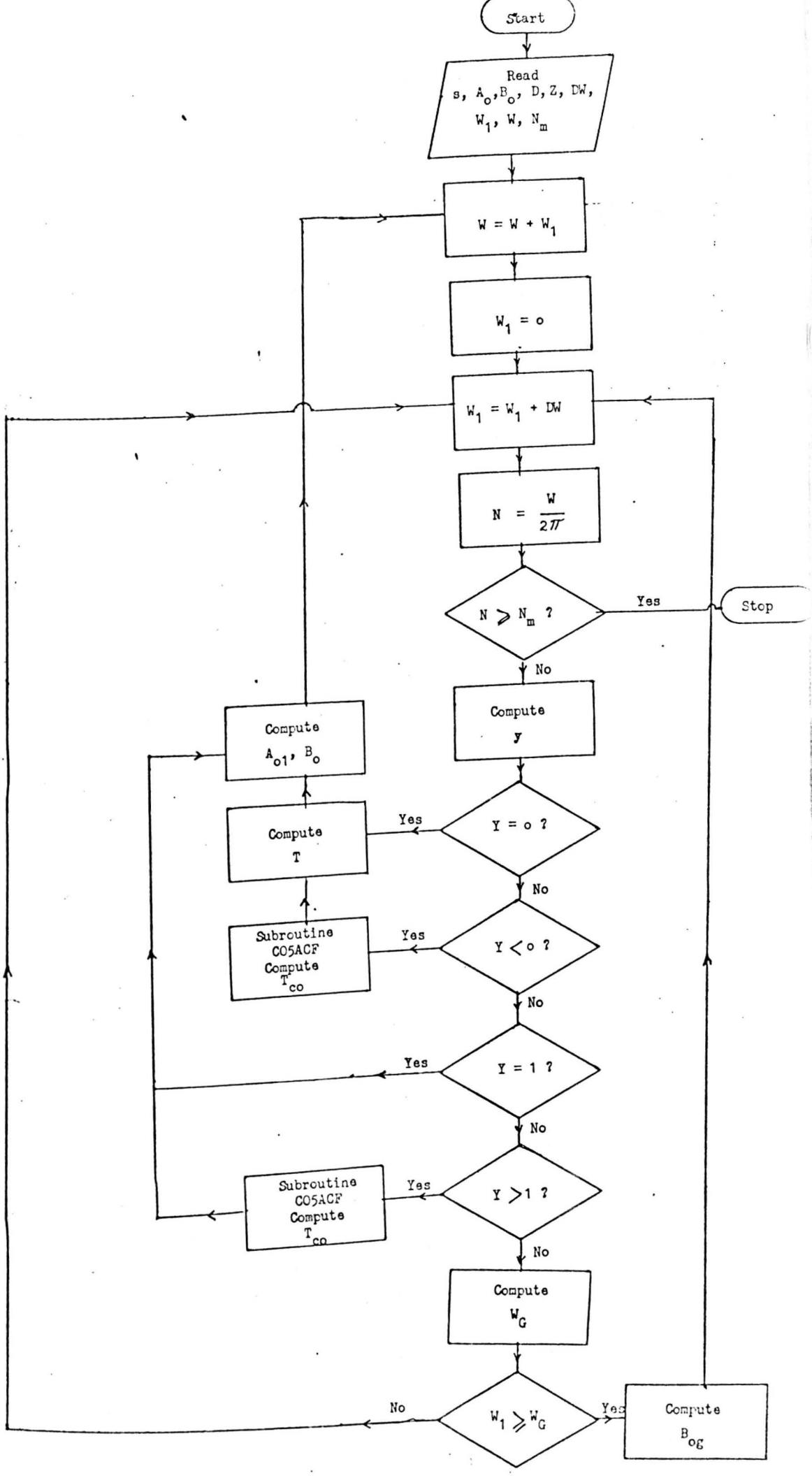

FIG. 3.2 FLOW CHART OF THE COMPUTER PROGRAM WITHOUT THE TIME OF IMPACT

3.3.1.1 Input Data to the Computer Program

Table (3.1) shows the input data to the computer program. The ultrasonic fuel injector has been designed with the following parameters (1):-

$y_x = 0.0025\text{mm}$, $y_w = 0.25\text{mm}$ and $f = 60$ KHz

In this analysis the following ranges of the parameters were used:

$y_x = 0.001 - 0.008\text{mm}$, $y_w = 0.1 - 0.8\text{mm}$ and

$f = 40$ KHz $- 80$ KHz .

According to these ranges, the ranges of the dimensionless groups were chosen:

$D = 0.1 - 0.005$ and $Z = 1 \times 10^{-6} - 5 \times 10^{-4}$

s was set up to 0 when the tip was moving up at $t = o$, and it was set up to π when the tip was moving down at $t = o$. It could be seen from the parameters that the acceleration of the tip was very high compared to the gravity acceleration for very small increment of time, so that the separation of the ball from the tip was assumed to occur at $t = o$.

According to the starting conditions which were mentioned in Section (3.2.1.2), the valves of A_o and B_o were as follows:

$A_o = 1$ and $B_o = o$, when the ball was moving up at $t = o$.

$A_o = 0$ and $B_o = 0$, when the ball was moving down at $t = o$.

ΔW was set up to 0.4 rad which was very small compared to the period of the tip motion, and could save a lot of computing time.

s (rad)	A_o	B_o	D	Z	W (rad)	W_1 (rad)	W (rad)	N_m (cycle)
π	0	0	0.1 - 0.005	$1 \times 10^{-6} - 5 \times 10^{-4}$	0.4	0	0	1000
0	1	0	0.1 - 0.005	$1 \times 10^{-6} - 5 \times 10^{-4}$	0.4	0	0	1000

TABLE (3.1). INPUT DATA TO THE COMPUTER PROGRAM WITHOUT THE TIME OF IMPACT

3.3.2 Computer Program With the Time of Impact

Fig. (3.3) shows the flow chart of this cimputer program. The computer program of Section (3.3.1) was modified by feeding w_o, σ, E, m, r and the time of impact euqation to the computer program. The input data to the computer program is shown in Table (3.2). The computer program is shown in appendix (3).

3.4 RESULTS AND DISCUSSIONS

3.4.1 The Ball Motion Without the Time of Impact

3.4.1.1 The Tip Moving Down at t = o.

Figs. (3.4- 3.7) show plots of the period (T) of the ball cycle versus the tip cycles (N), for D in the range 0.005 - 0.1 and $Z = 5 \times 10^{-4}$. These figs. show that the ball was not moving in a steady state. Some times the ball was moving with repeatable periods, but this repeatability disappeared again, figs. (3.6, 3.7). The reason for unsteady state motion was because the impact was with improper phase.

Also it can be seen from these figs. that when D was increased, T decreased. This is because the increase in D can be viewed as a decrease in the maximum gap (y_w) between the ball and the walls of the valve, and hence T is expected to decrease. Alternatively an increase in D might be due to the increase in the maximum amplitude (y_x) of the tip while keeping y_w constant, but since Z was constant, this increase would decrease the frequency of the tip (w_o) , but the maximum velocity of the tip increases. The velocity (v_{o1}) of the ball after the collision was dependent on the instantaneous velocity (v) of the tip, i.e., on the magnitude

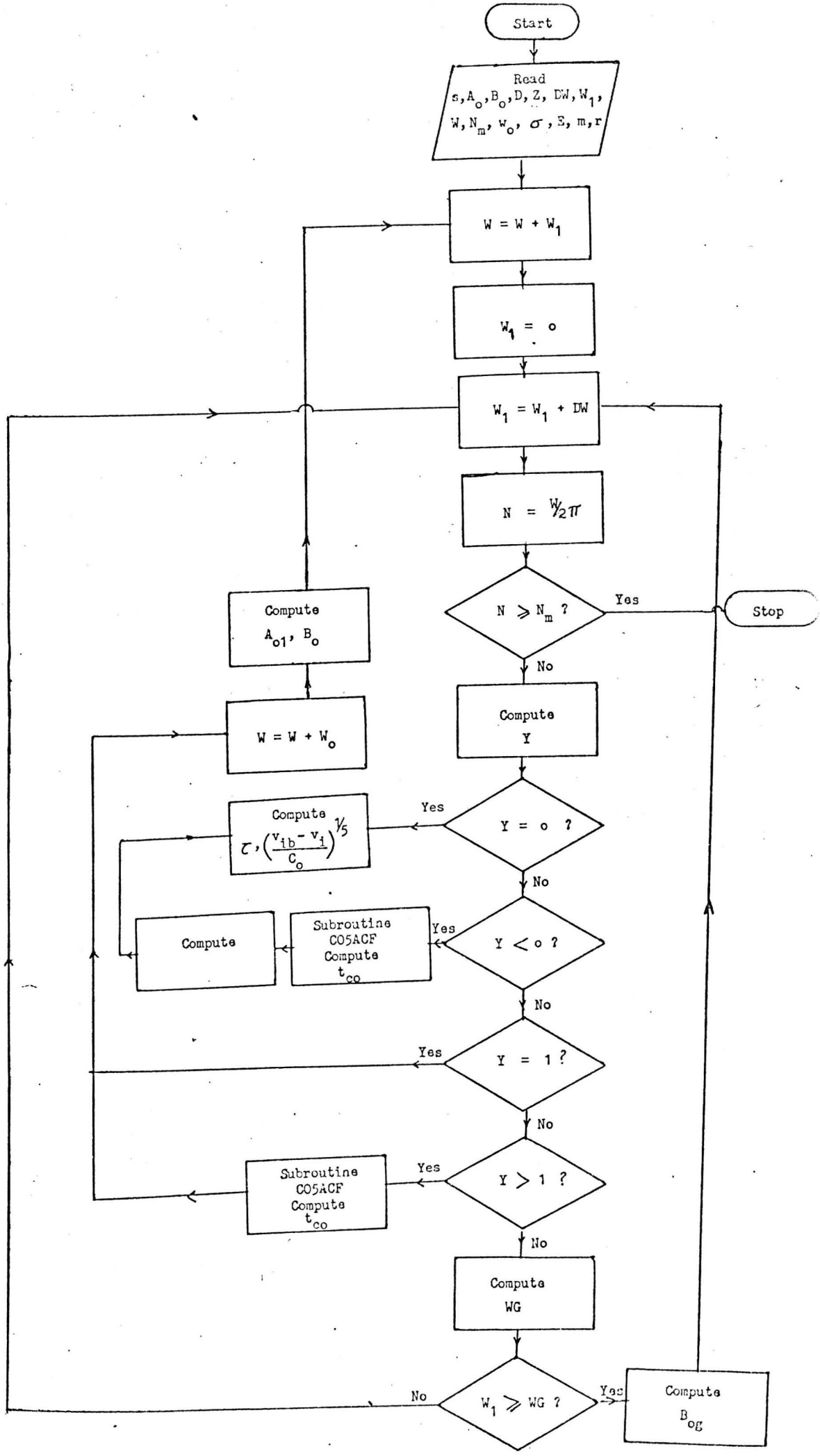

FIG. 3.3 FLOW CHART OF THE COMPUTER PROGRAM WITH THE TIME OF IMPACT

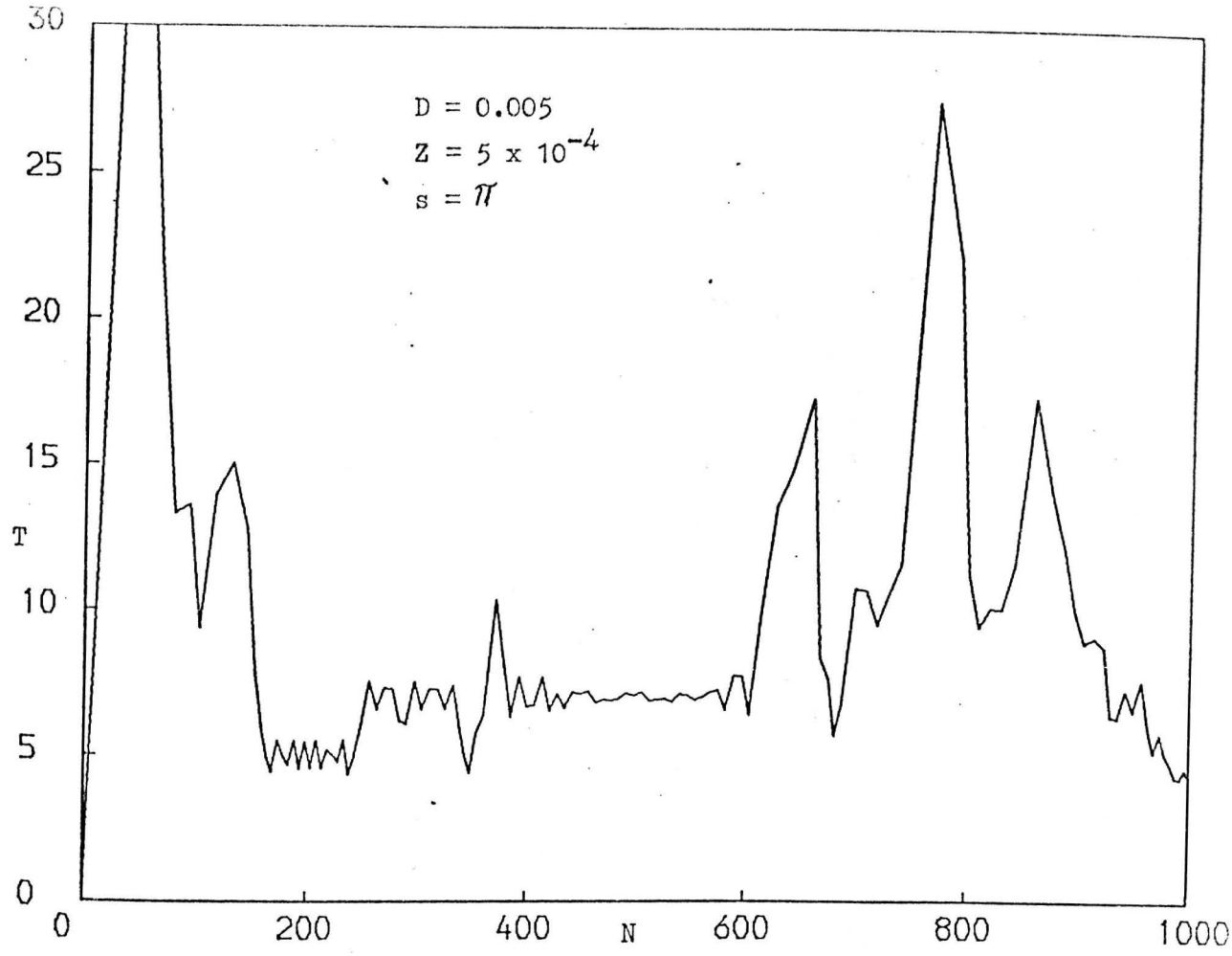

FIG. 3.4 PERIOD OF THE BALL CYCLE (IN TERM OF THE TIP CYCLES) - NUMBER OF THE TIP CYCLES RELATIONSHIP

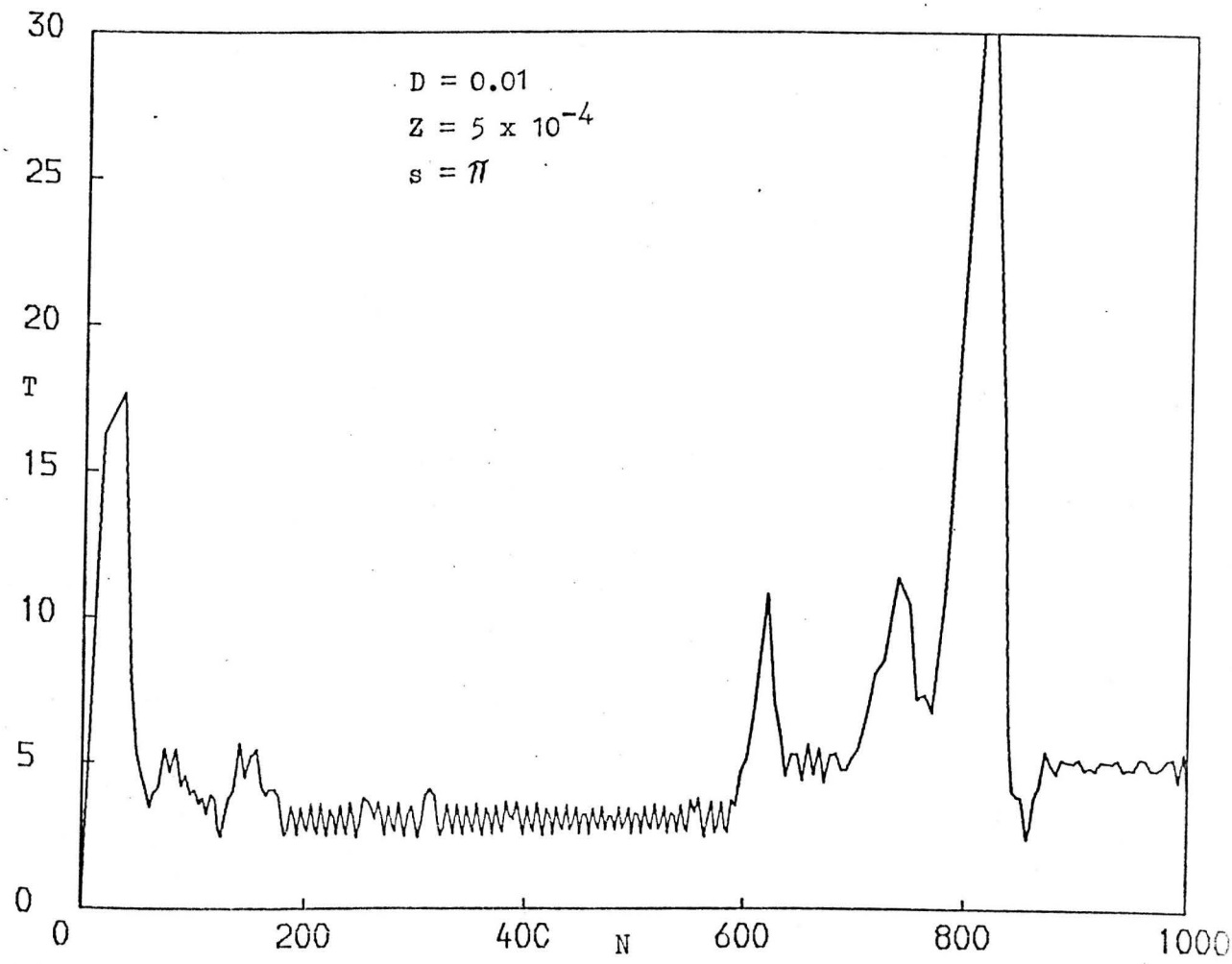

FIG. 3.5 PERIOD OF THE BALL CYCLE (IN TERM OF THE TIP CYCLES)- NUMBER OF THE TIP CYCLES RELATIONSHIP

s (rad)	A_o	B_o	D	Z	ΔW (rad)	W_1 (rad)	W (rad)	N_m (cycle)	w_o (rad)	σ	E (N/r^2)	m (kg)	r (mm)
π	0	0	0.1-0.005	1×10^{-6} - 5×10^{-4}	0.4	0	0	1000	2.5×10^{5} - 5×10^{5}	0.3	212×10^{9}	3×10^{-5}	1

TABLE (3.2). INPUT DATA TO THE COMPUTER PROGRAM WITH THE TIME OF IMPACT

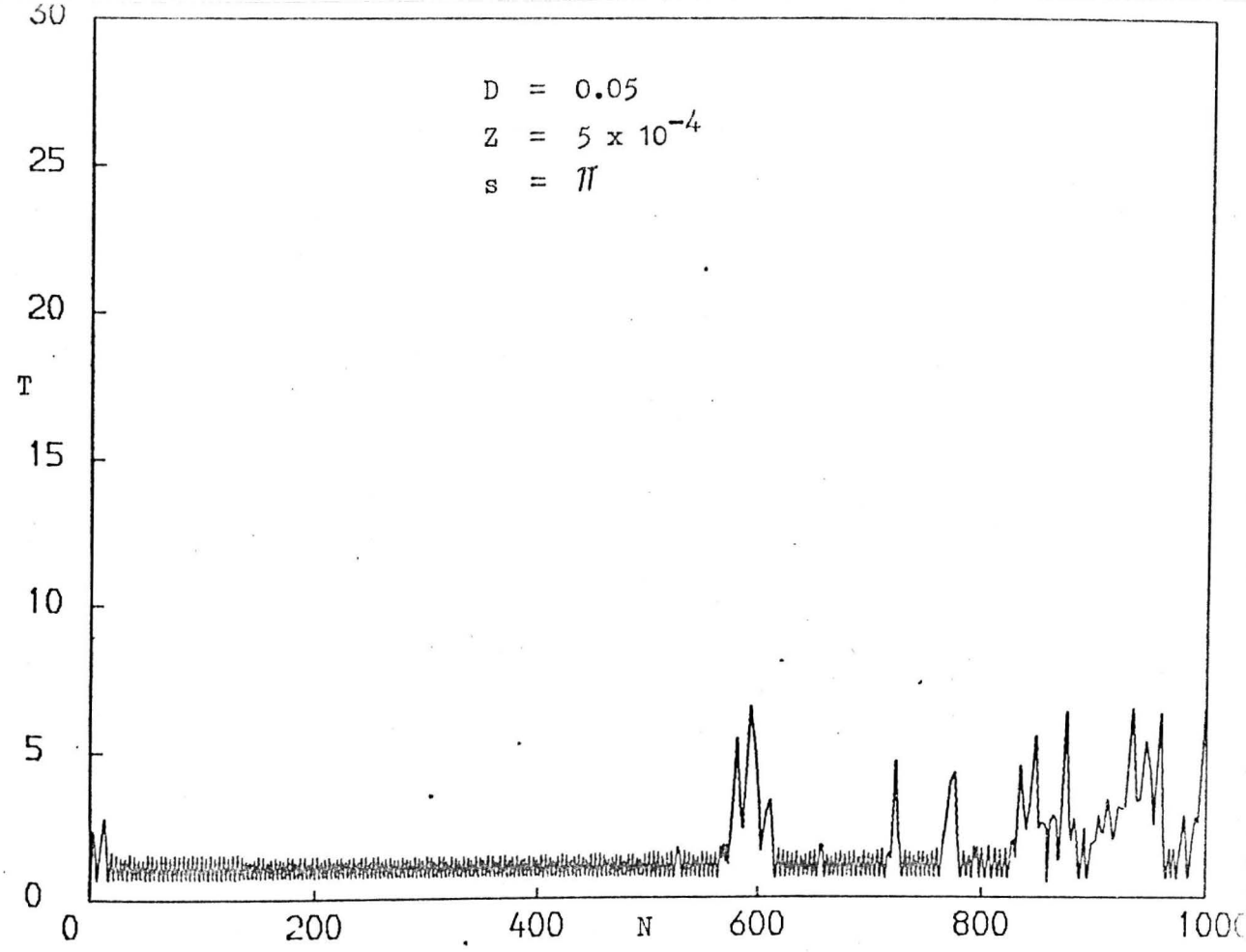

FIG. 3.6 PERIOD OF THE BALL CYCLE (IN TERM OF THE TIP CYCLES) - NUMBER OF THE TIP CYCLES RELATIONSHIP

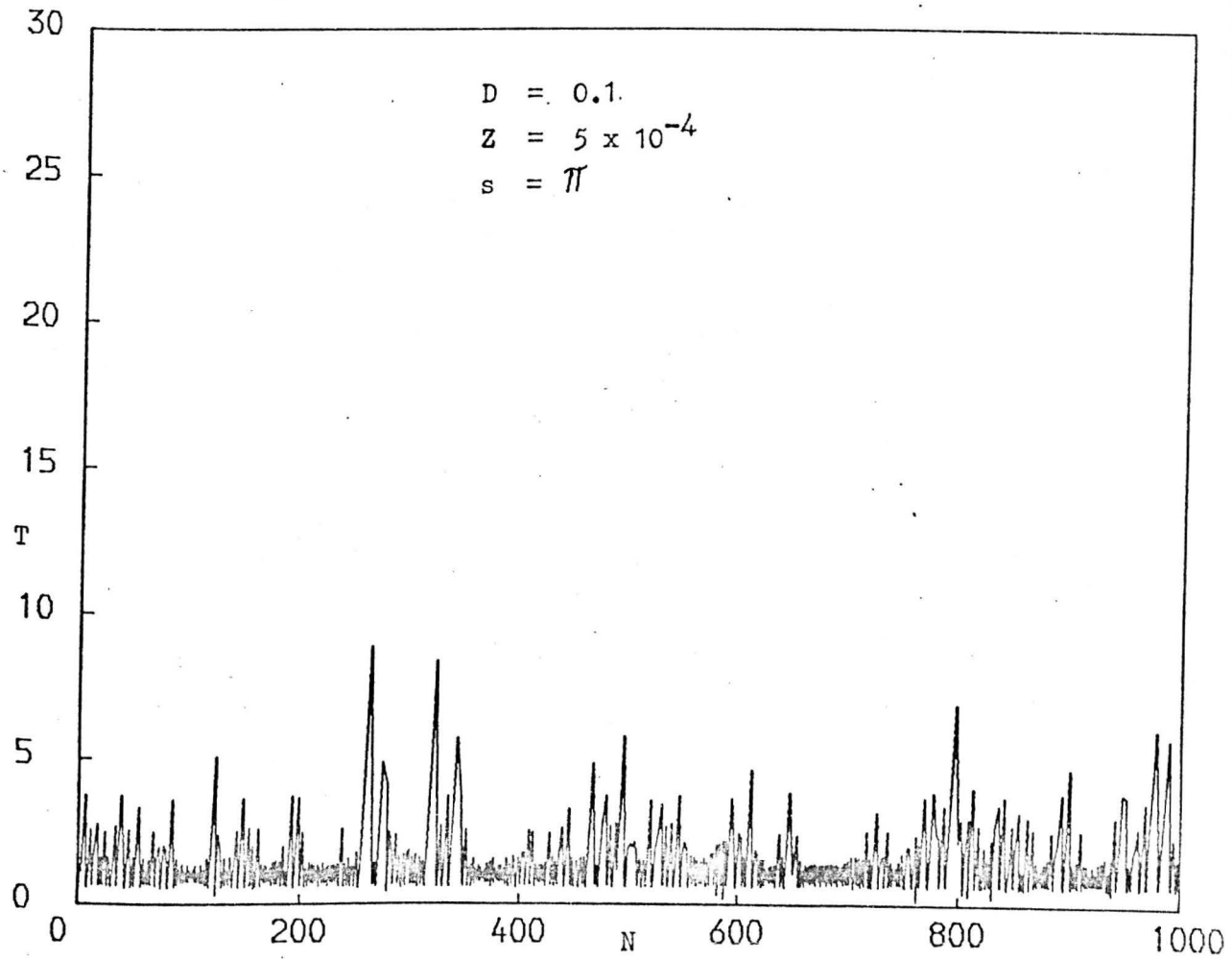

FIG. 3.7 PERIOD OF THE BALL CYCLE (IN TERM OF THE TIP CYCLES) - NUMBER OF THE TIP CYCLES RELATIONSHIP

of the velocity and the phase angle with which the ball hit the walls of the valve, and on the velocity (v_{ib}) of the ball before the collision. So the decrease in the period (T) when D was increased might not be due to the increase in y_x or due to the decrease in w_o.

These figs. show also that there was a more orderly pattern with increasing D.

Similar results were obtained for Z in the range $1 \times 10^{-6} - 5 \times 10^{-4}$.

Figs. (3.8-3.12) show the relationship between the ratio (A_{o1}) of the ball velocity (v_{o1}) after the collision with the lower wall of the valve to the maximum velocity of the tip, versus the tip cycles (N), for D range 0.001 - 0.1 and $Z = 5 \times 10^{-4}$. It can be seen from these figs. that A_{o1} was changing randomly with the increase of D. An increase of D can arise due to the decrease of the maximum gap (y_w) between the ball and the walls which would change the phase angles in which the ball hit the walls of the valve. Also an increase in D can arise from an increase in the maximum velocity of the tip with constant Z and this would change the phase angles with which the ball hit the walls of the valve. Similar results were obtained for Z in the range $1 \times 10^{-6} - 5 \times 10^{-4}$.

Figs. (3.13- 3.18) show plots of the period (T) versus the tip cycles (N), for D = 0.01 and Z range $1 \times 10^{-6} - 5 \times 10^{-4}$. These figs show that when Z was increased for constant D, the periods (T) were changed randomly. The explanation of this is that an increase in Z can be due to a decrease of the tip frequency (w_o) whilst keeping the maximum

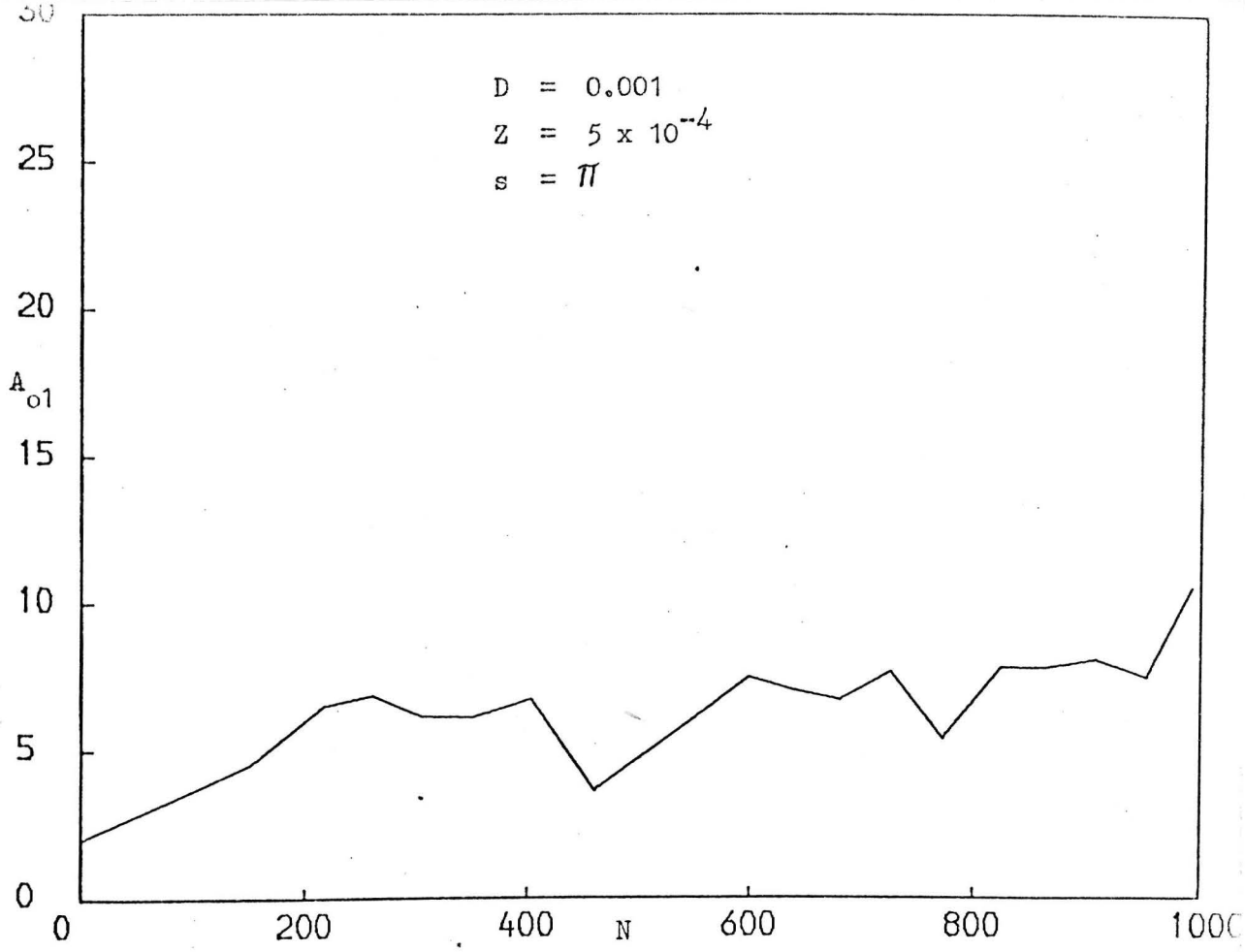

FIG. 3.8 RATIO OF THE BALL VELOCITY AFTER THE COLLISION WITH THE LOWER WALL TO THE MAXIMUM VELOCITY OF THE TIP - NUMBER OF THE TIP CYCLES RELATIONSHIP

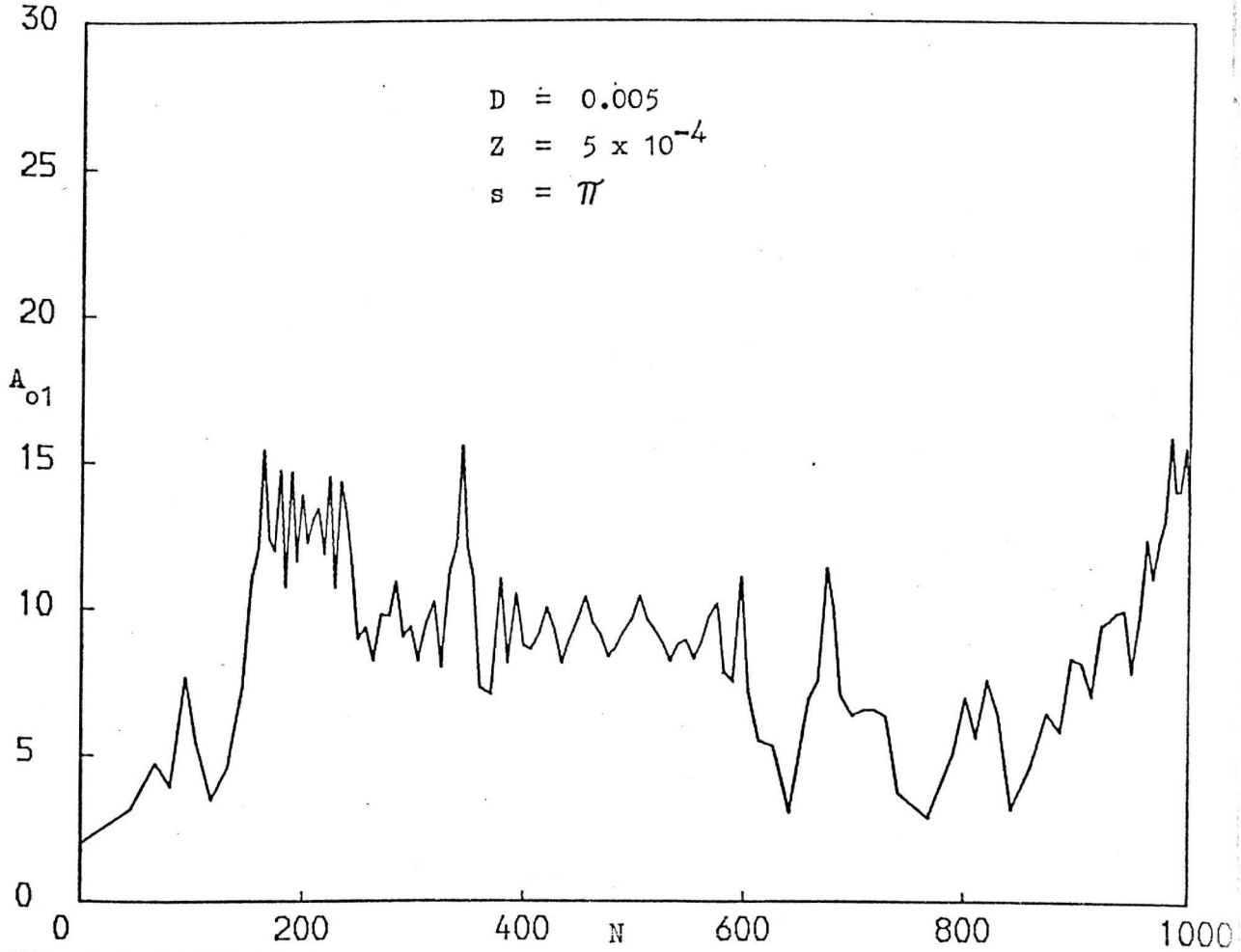

FIG. 3.9 RATIO OF THE BALL VELOCITY AFTER THE COLLISION WITH THE LOWER WALL TO THE MAXIMUM VELOCITY OF THE TIP - NUMBER OF THE TIP CYCLES RELATIONSHIP

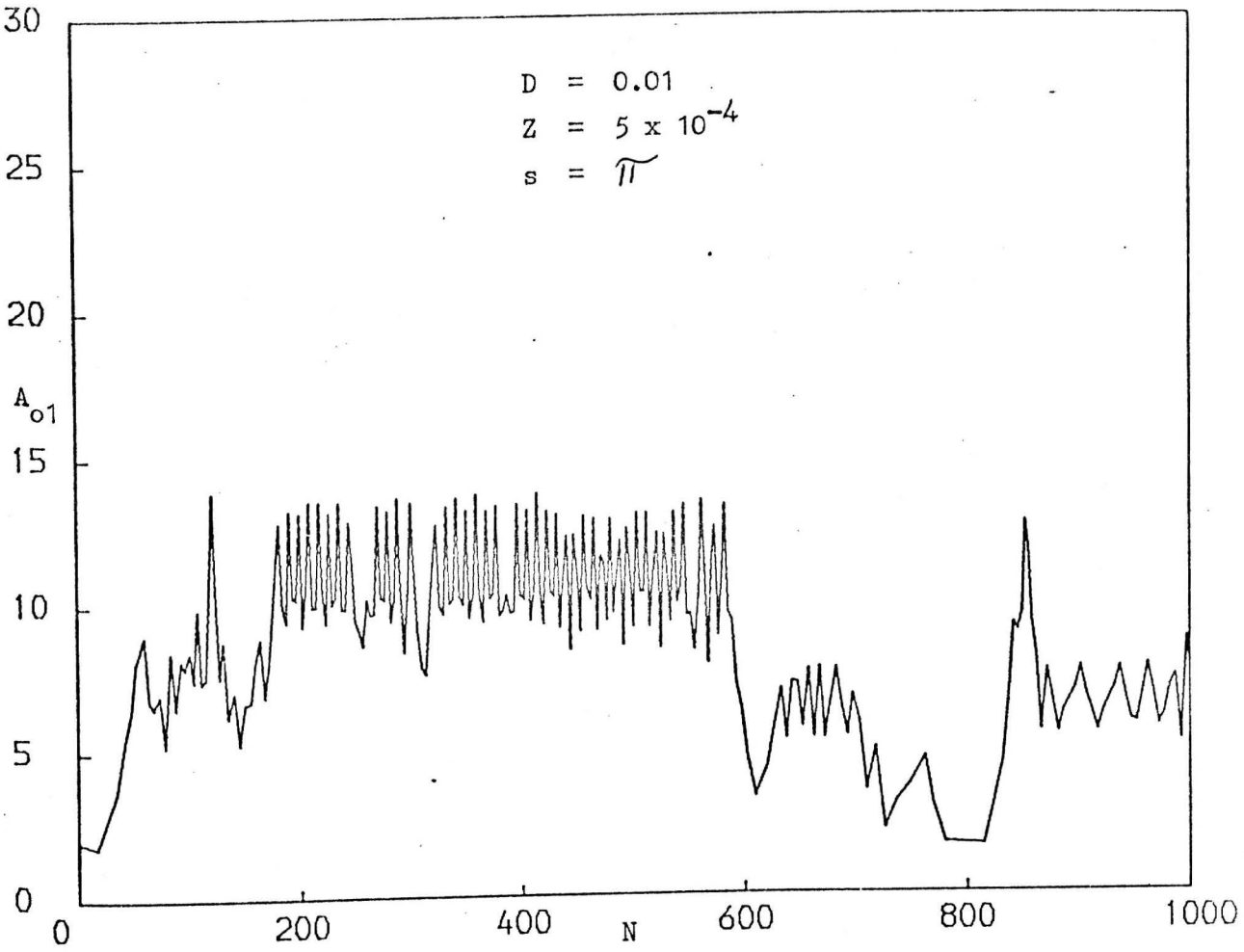

FIG. 3.10 RATIO OF THE BALL VELOCITY AFTER THE COLLISION WITH THE LOWER WALL TO THE MAXIMUM TIP VELOCITY - NUMBER OF THE TIP CYCLES RELATIONSHIP

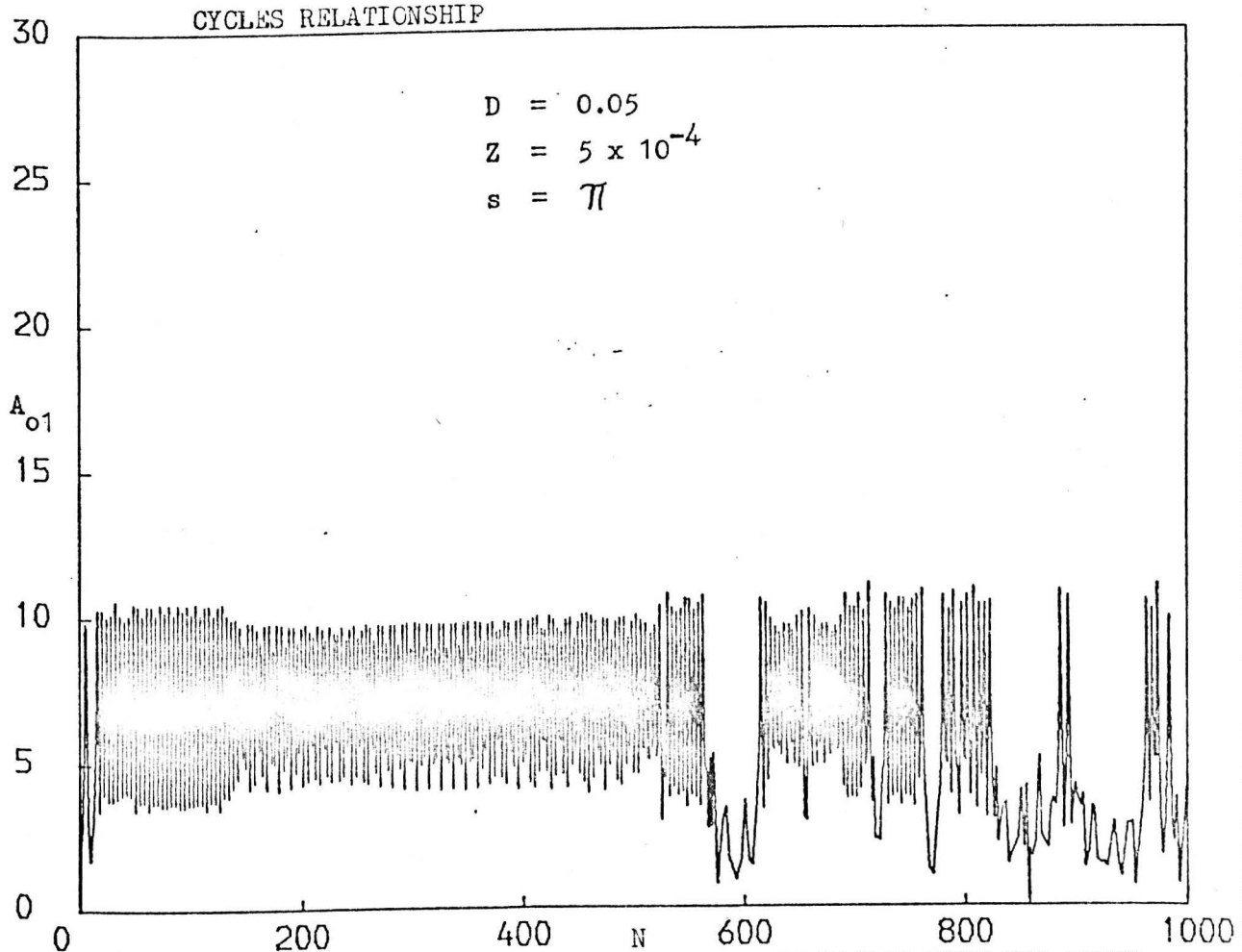

FIG. 3.11 RATIO OF THE BALL VELOCITY AFTER THE COLLISION WITH THE LOWER WALL TO THE MAXIMUM TIP VELOCITY - NUMBER OF THE TIP CYCLES RELATIONSHIP

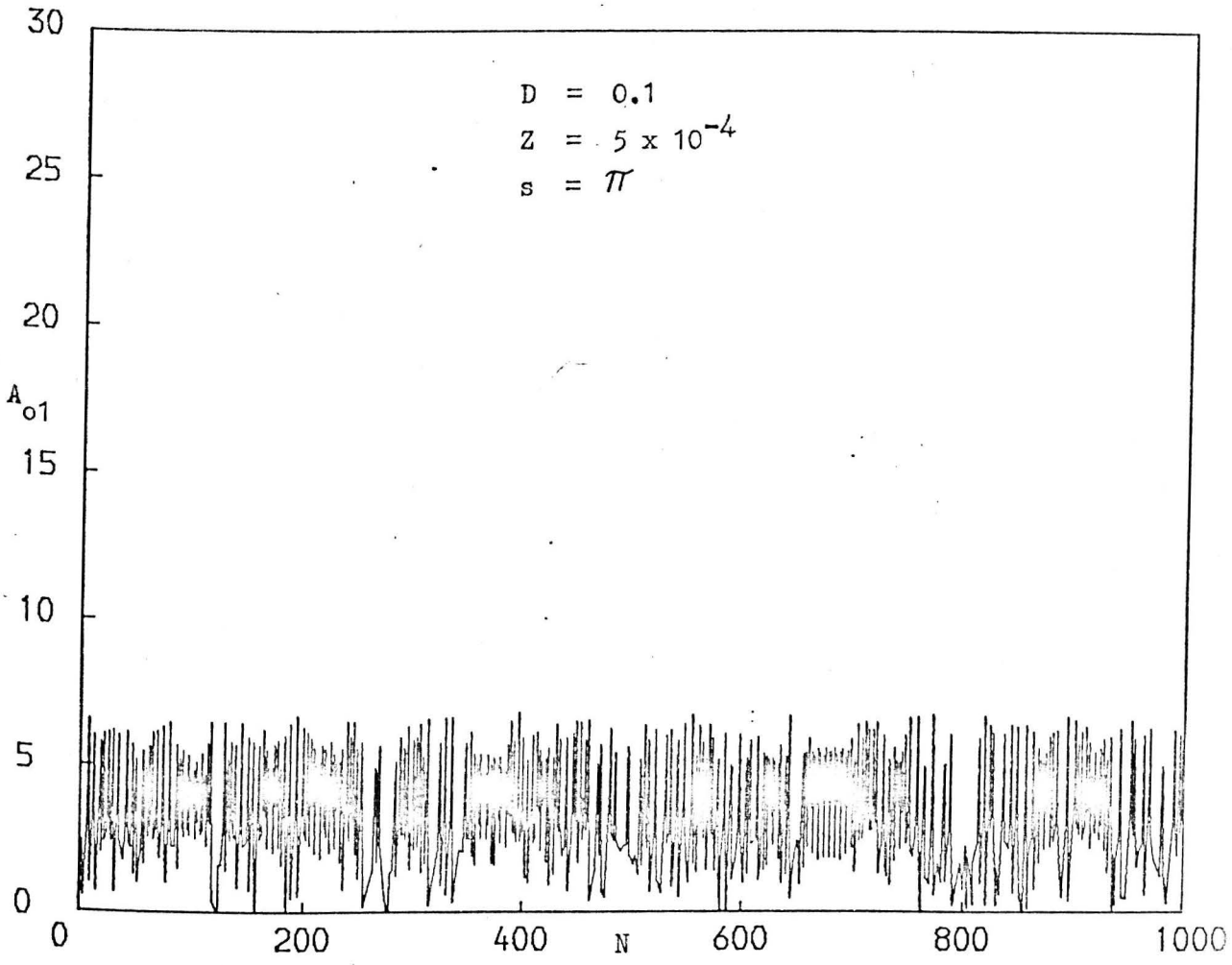

FIG. 3.12 RATIO OF THE BALL VELOCITY AFTER THE COLLISION WITH THE LOWER WALL TO THE MAXIMUM VELOCITY OF THE TIP - NUMBER OF THE TIP CYCLES RELATIONSHIP

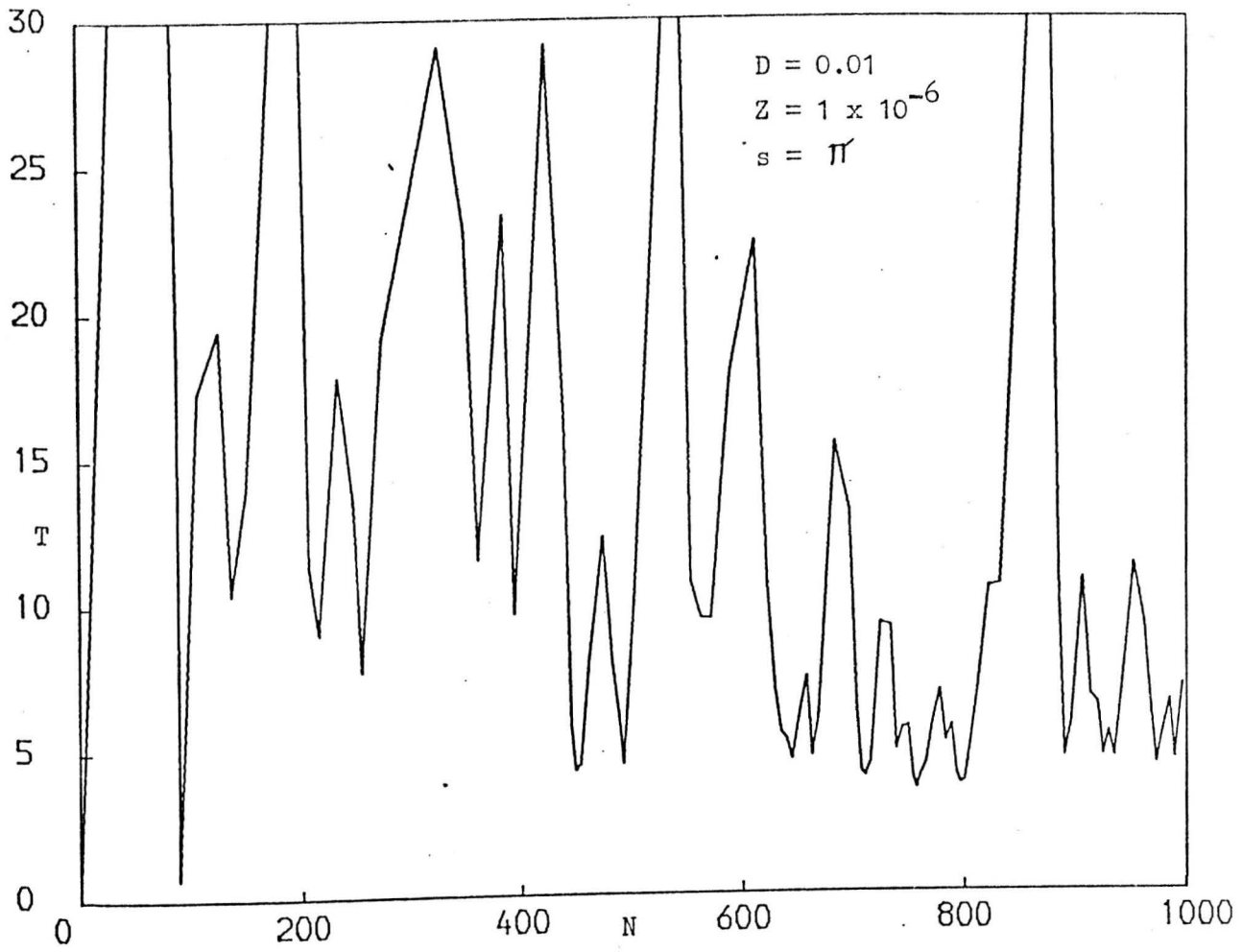

FIG. 3.13 PERIOD OF THE BALL CYCLE (IN TERM OF THE TIP CYCLES) - NUMBER OF THE TIP CYCLES RELATIONSHIP

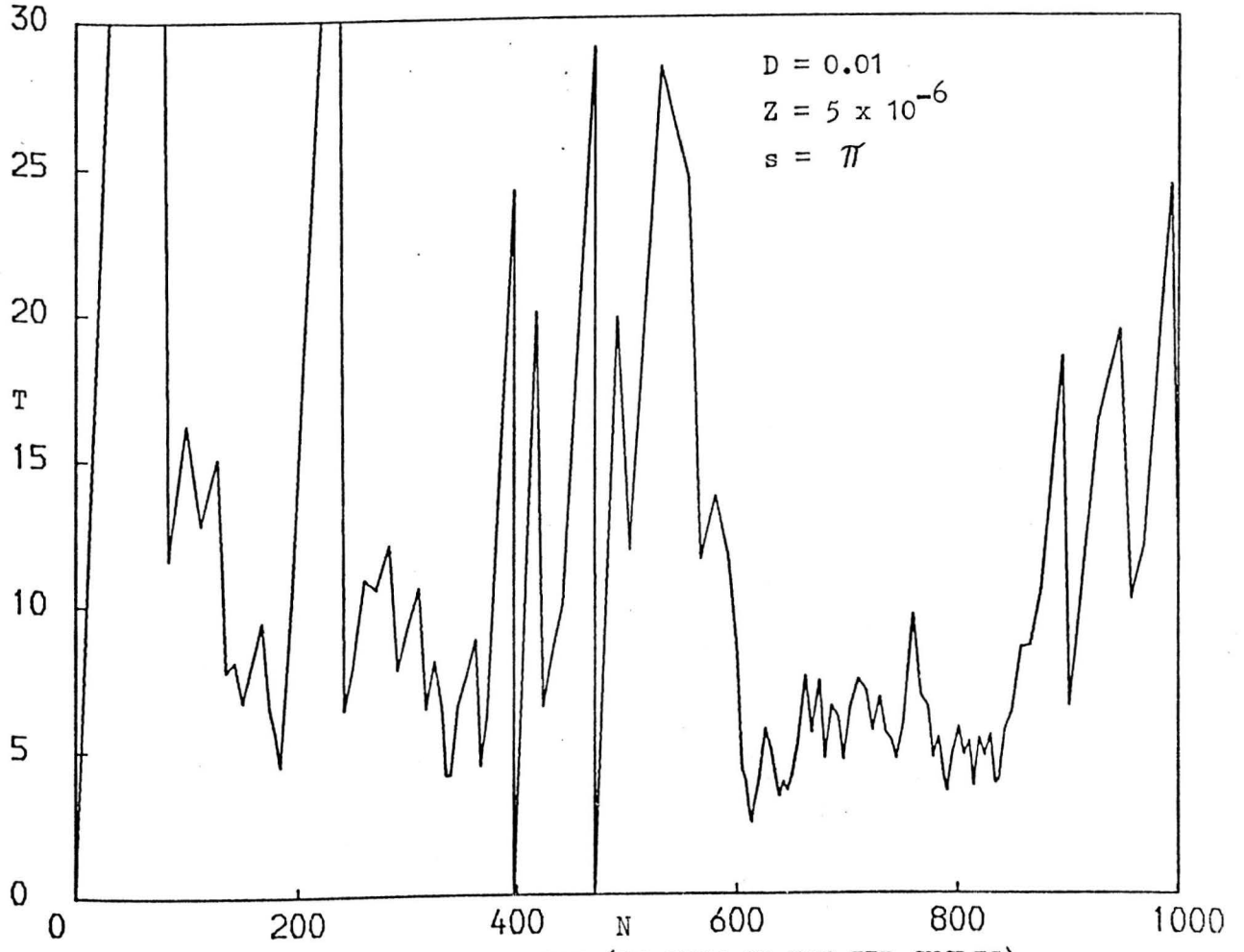

FIG. 3.14 PERIOD OF THE BALL CYCLE (IN TERM OF THE TIP CYCLES) - NUMBER OF THE TIP CYCLES RELATIONSHIP

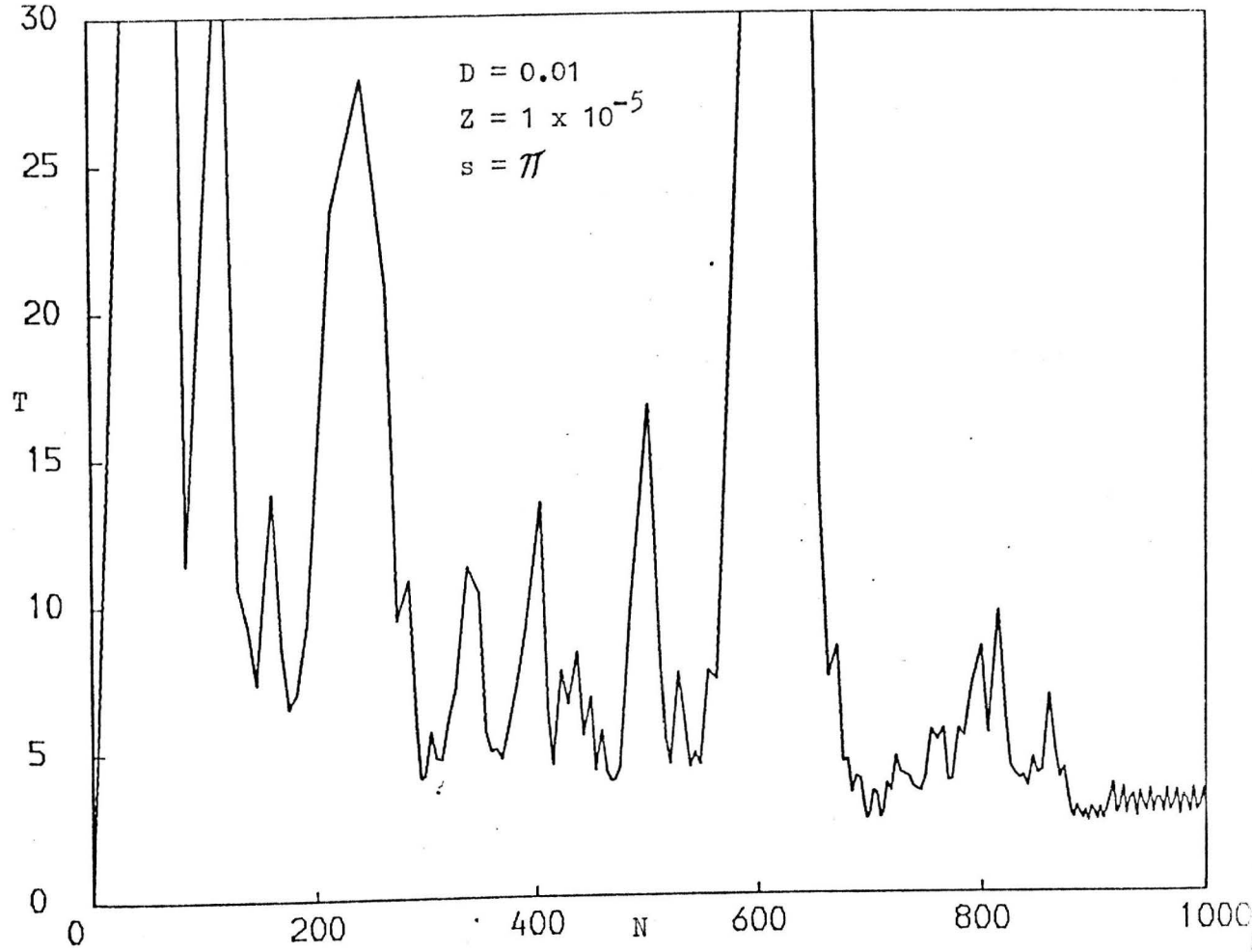

FIG. 3.15 PERIOD OF THE BALL CYCLE (IN TERM OF THE TIP CYCLES) - NUMBER OF THE TIP CYCLES RELATIONSHIP

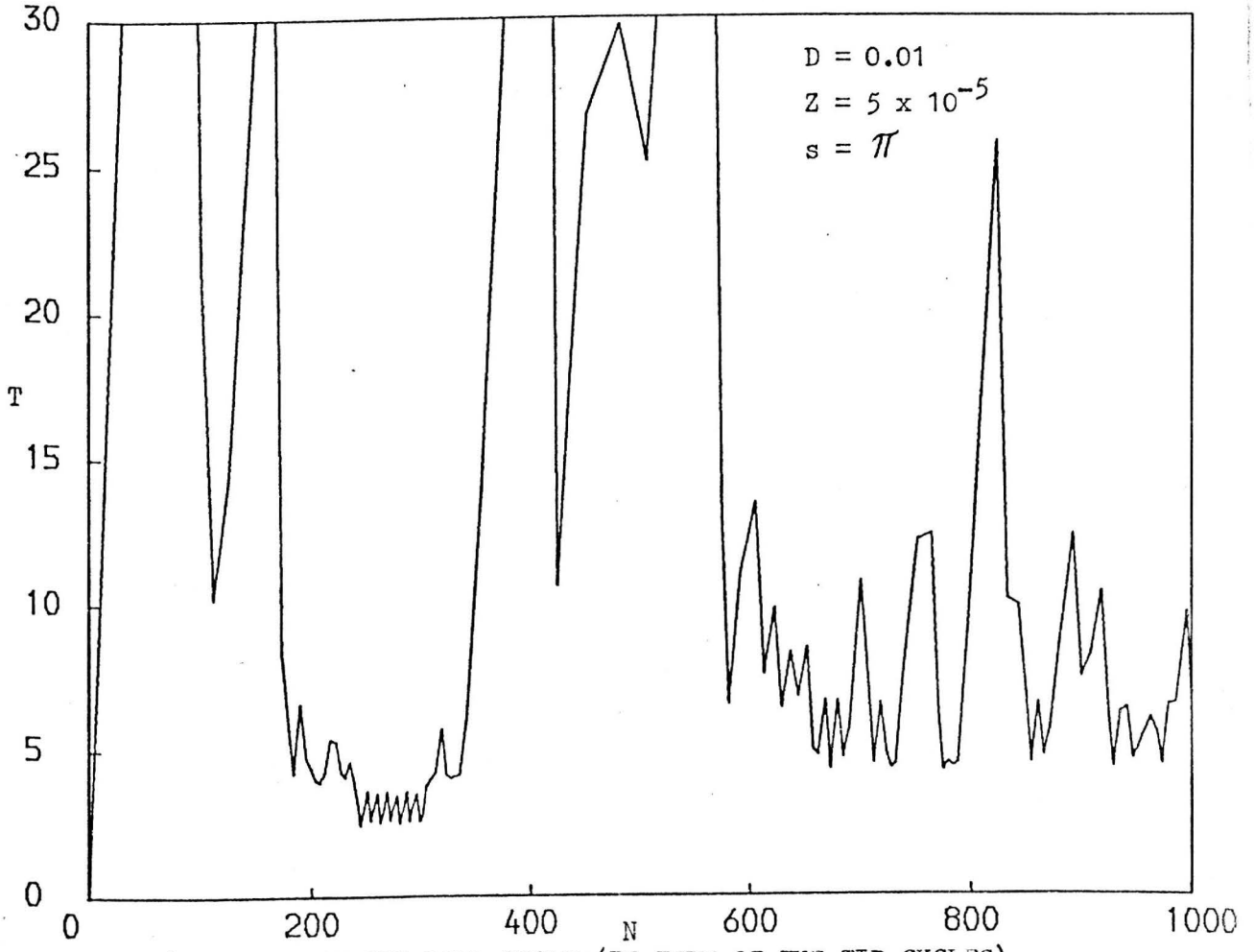

FIG. 3.16 PERIOD OF THE BALL CYCLE (IN TERM OF THE TIP CYCLES) - NUMBER OF THE TIP CYCLES RELATIONSHIP

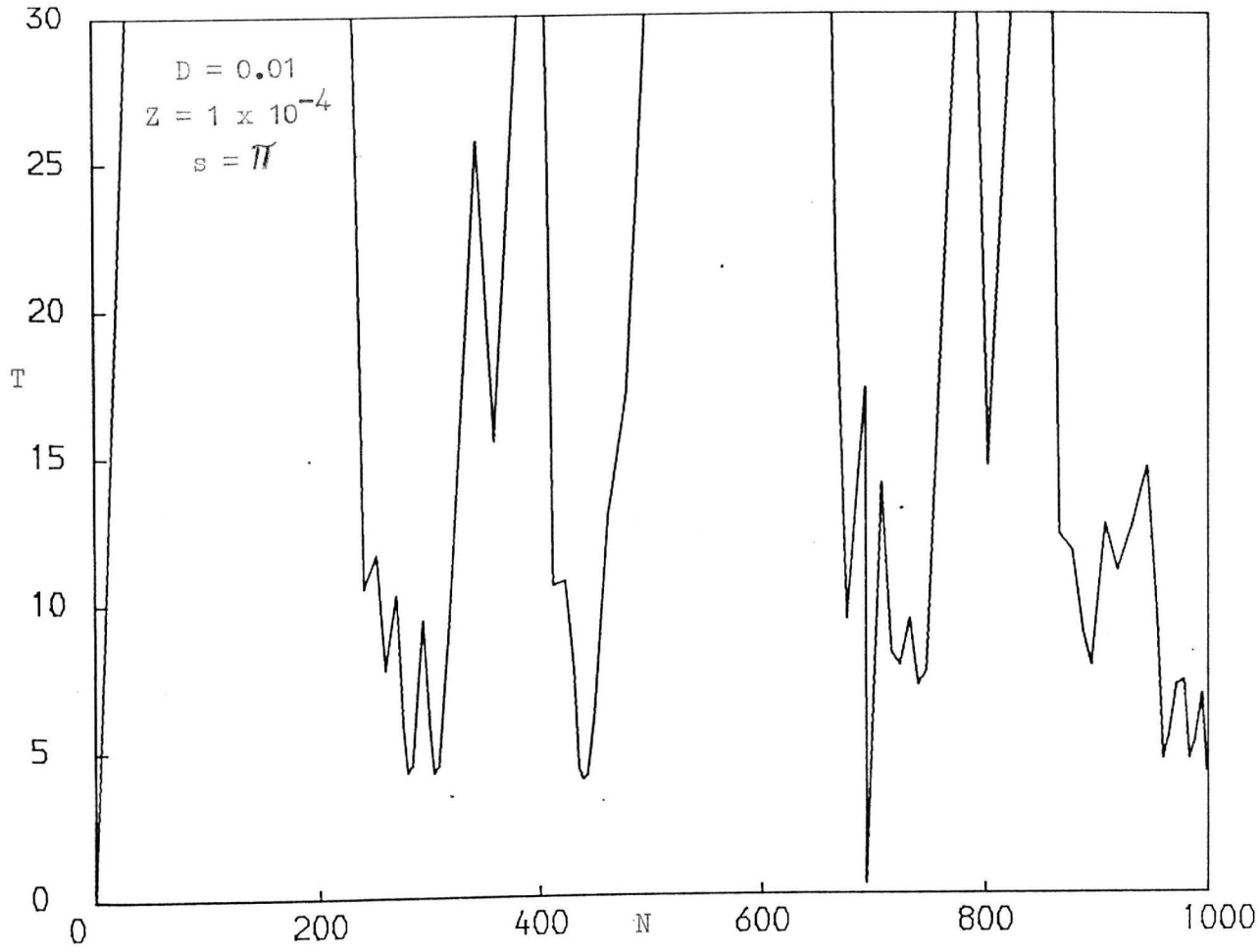

FIG. 3.17 PERIOD OF THE BALL CYCLE (IN TERM OF THE TIP CYCLES) - NUMBER OF THE TIP CYCLES RELATIONSHIP

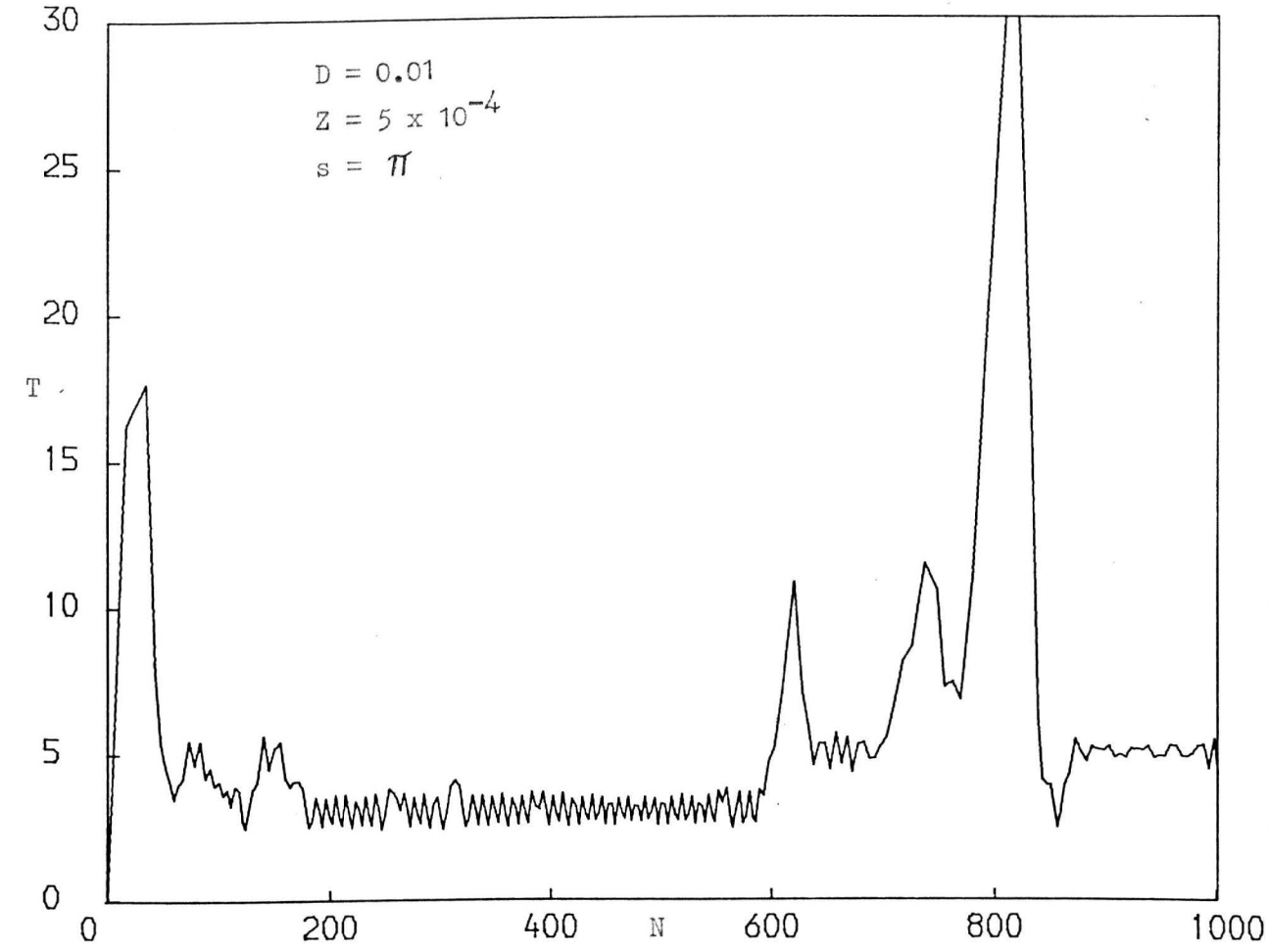

FIG. 3.18 PERIOD OF THE BALL CYCLE (IN TERM OF THE TIP CYCLES) - NUMBER OF THE TIP CYCLES RELATIONSHIP

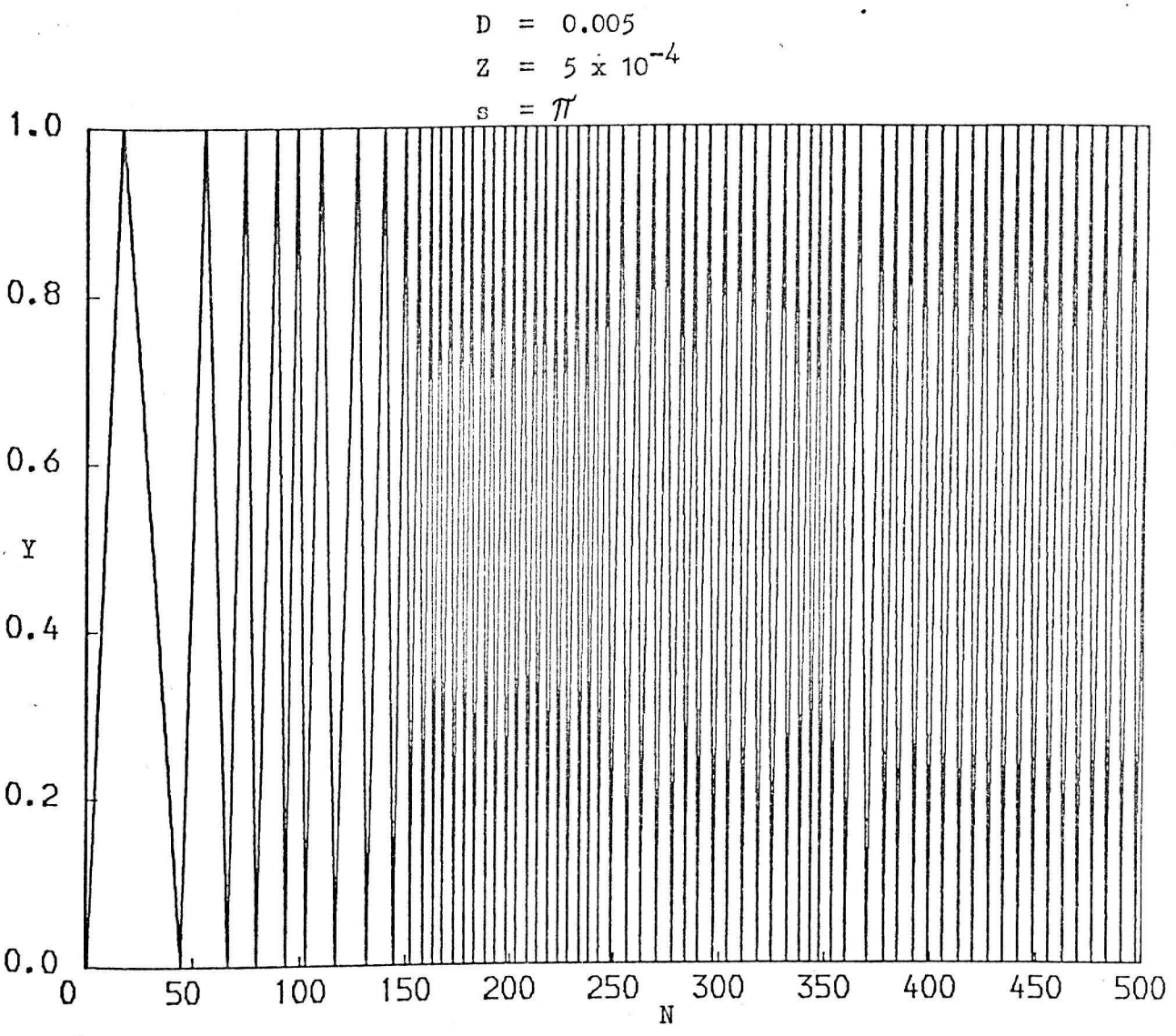

FIG. 3.19 RATIO OF THE GAP BETWEEN THE BALL AND THE LOWER WALL TO THE MAXIMUM GAP - NUMBER OF THE TIP CYCLES RELATIONSHIP

amplitude (y_x) of the tip and the maximum gap (y_w) between the ball and the walls of the valve constant. This would decrease the maximum velocity of the tip. Also an increase in Z can be due to a decrease in y_x whilst keeping w_o constant and decreasing y_w. The decrease in the maximum velocity of the tip would change the phase angles with which the ball hit the walls of the valve.

Similar results were obtained for D in the range 0.005 - 0.1. The relationship between the ratio (Y) of the gap (y) between the ball and the lower wall of the valve to the maximum gap (y_w) versus the tip cycles (N) for D = 0.005 and Z = 5×10^{-4} is shown in fig. (3.19). This fig. shows that the effect of gravity could not reverse the direction of the ball. Also this fig. shows that the ball could reach the top wall from the first cycle.

Similar results were obtained for D in the range 0.005 - 0.1 and Z in the range 1×10^{-6} - 5×10^{-4}.

3.4.1.2 The Tip Moving Up at t = o.

Fig. (3.20) shows plot of the period (T) of the ball cycle versus the tip cycles (N), for D = 0.05 and Z = 5×10^{-4}. It can be seen from this plot that the ball was also moving in random motion, and the ball moved some times in repeatable periods, but this repeatability disappeared again. It can be deduced from the results that the change in the initial condition of the tip could change the motion of the ball, but the effects of D and Z remained the same (see fig. (3.6)). Similar results were obtained for D in the range 0.005 - 0.1 and Z in the range 1×10^{-6} - 5×10^{-4}.

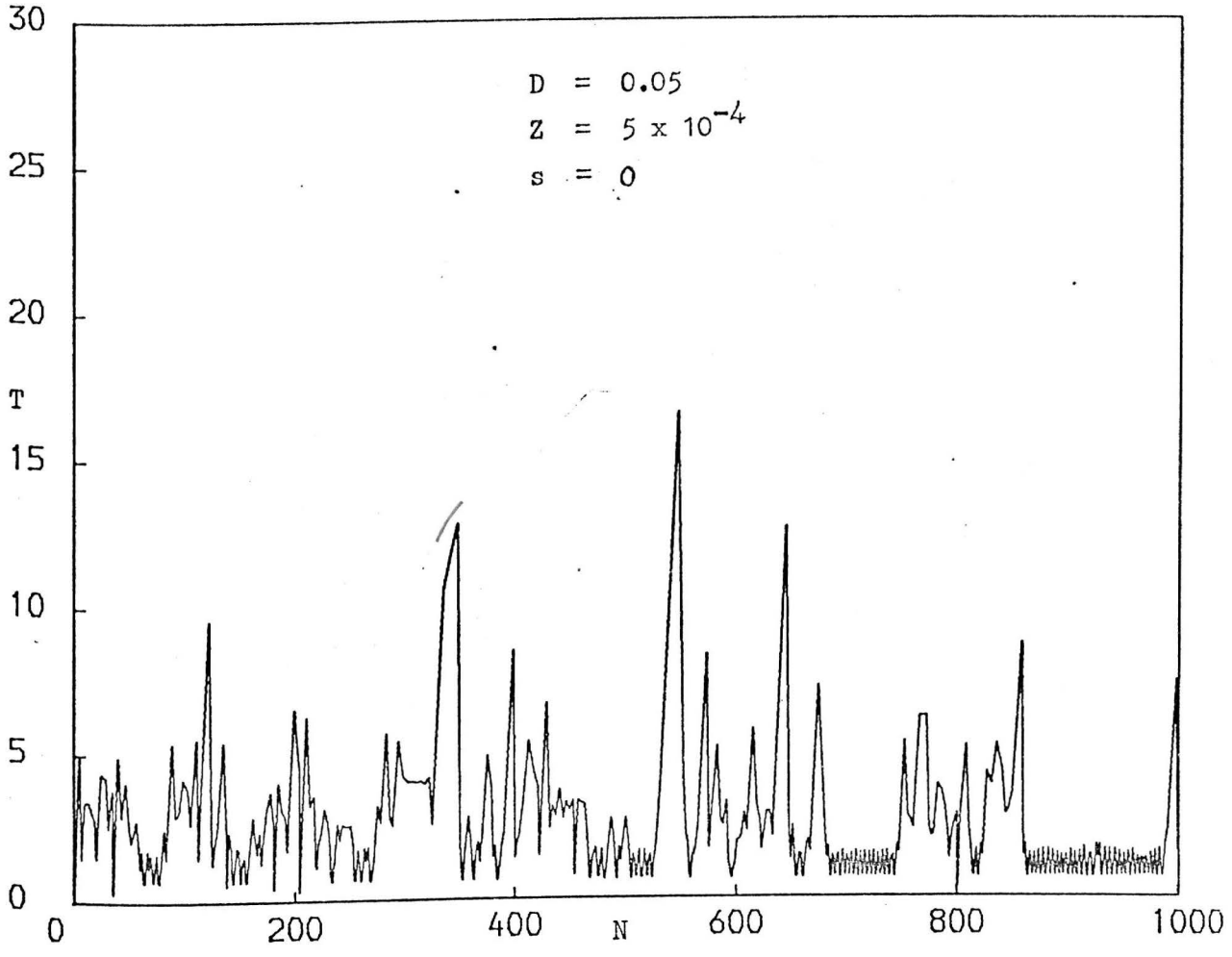

FIG. 3.20 PERIOD OF THE BALL CYCLE (IN TERM OF THE TIP CYCLES) - NUMBER OF THE TIP CYCLES RELATIONSHIP

3.4.2 The Time of Impact

The relationship between the time (τ) of impact and the time (t) is shown in fig. (3.21), for $w_o = 5 \times 10^5$ rad, D = 0.01 and $Z = 5 \times 10^{-6}$. This fig. shows that the time (τ) of impact was less than 10×10^{-6} s .

Similar results were obtained for w_o range 2.5×10^5 rad - 5×10^5 rad, D range 0.005 - 0.1 and Z range 1×10^{-6} - 5×10^{-4}. Since the length of the injector horn was 30 mm, the elastic wave took 12×10^{-6} s to return to the contact area, and hence the impact terminated before the first elastic wave returned to the contact area. This is one of the limits of applying Hertz theory of impact. Fig. (3.22) shows plot of the ratio $\left(\frac{v_{ib} - v_i}{c_o}\right)^{1/5}$ of the relative velocity before the impact to the sonic velocity in the steel raised to the power one-fifth versus the time (t), for $w_o = 2.5 \times 10^5$ rad, D = 0.01 and $Z = 2 \times 10^{-5}$. This fig. shows that the maximum value of $\left(\frac{v_{ib} - v_i}{c_o}\right)^{1/5}$ was 0.36.

Similar results were obtained for w_o in the range 2.5×10^5 rad - 5×10^5 rad, D in the range 0.005 - 0.1 and Z in the range 1×10^{-6} - 5×10^{-4}. Hunter (5) has found that when the ratio was equal 0.17 the experimental value of the coefficient of restitution was significantly lower than the theoretical estimate by Hertz theory. From this it can be deduced that the values of $\left(\frac{v_{ib} - v_i}{c_o}\right)^{1/5}$ were not satisfying the limits of Hertz theory, and hence Hertz theory was not used in predicting the time of impact.

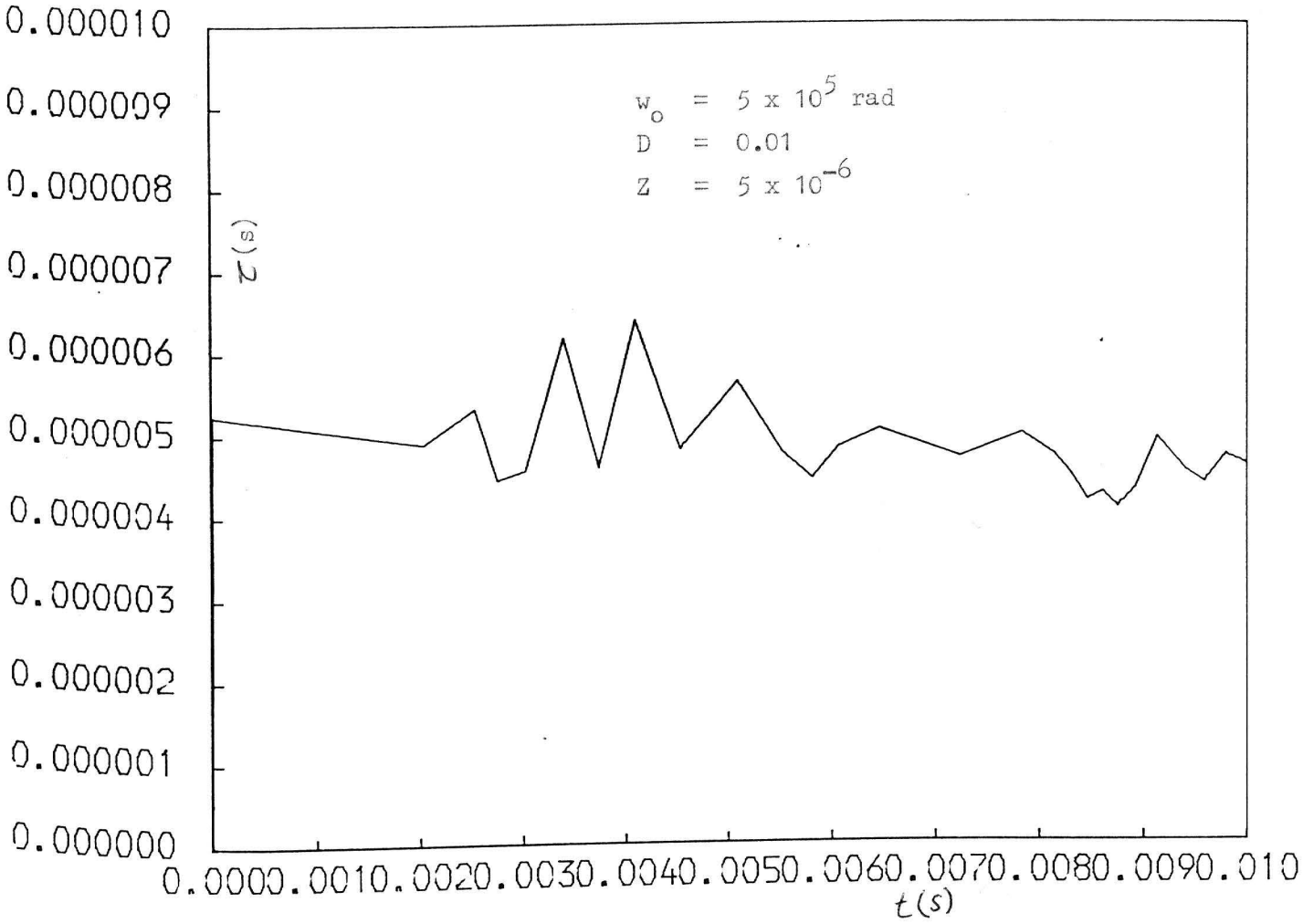

FIG. 3.21 TIME OF IMPACT - TIME RELATIONSHIP

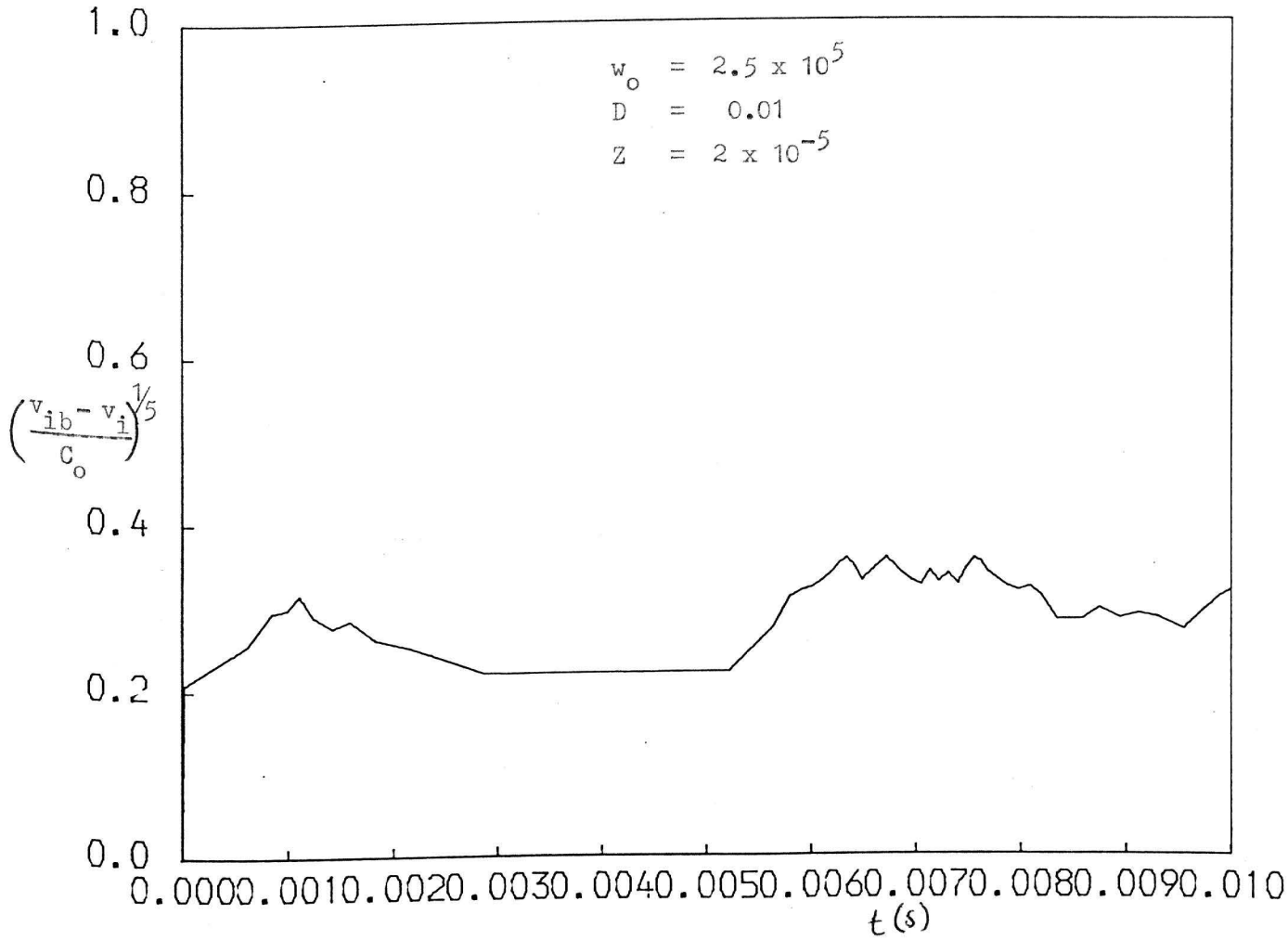

FIG. 3.22 RELATIVE VELOCITY BEFORE THE COLLISION - TIME RELATIONSHIP

Since the velocity of impact was very high and the ball collided with the walls of the valve all round, the time of impact was expected to be very small compared to the period of the ball cycle. Therefore the time of impact was not considered in this analysis.

Chapter Four

MEASURING THE MOTION OF A BALL IN A LARGE MODEL OF THE INJECTOR TIP WITHOUT FLUID RESISTANCE

4.1 INTRODUCTION

This chapter is devoted to measuring the ball motion in a large model of the injector valve without any liquid resistance. The purpose of this measurement was to check the results of the theoretical analysis of the ball motion which was described in Chapter 3, and to get an understanding of the ball motion between two vibrating walls. Details concerning the test apparatus and procedure, and the test results and discussions are given below.

4.2 TEST APPARATUS AND PROCEDURE

Fig. (4.1) shows the layout of the test apparatus. Fig. (4.2) shows the photograph of the test apparatus. A ball is fixed inside an LVDT transducer which is itself vibrated.

Ball movement is measured by LVDT output.

LVDT body movement is measured by a proximity transducer.

The linear variable differential transformer (LVDT) (Schaevitz Engineering, type 100 M.S.L.) served as a model of the valve of the injector. A 3 mm. steel ball was put in the hole of the LVDT transducer, and the two ends of the hole were blocked by two 3 mm. steel bars. The gap in which the ball moved was controlled by the distance between the ends of these bars inside the transducer. The lower bar was fixed inside the transducer and the ball rested on the bar before the test was started. The upper bar was marked with 1 mm. marks and was a tight fit into the bore of the transducer. Before starting the test the upper bar was fixed in one position inside the

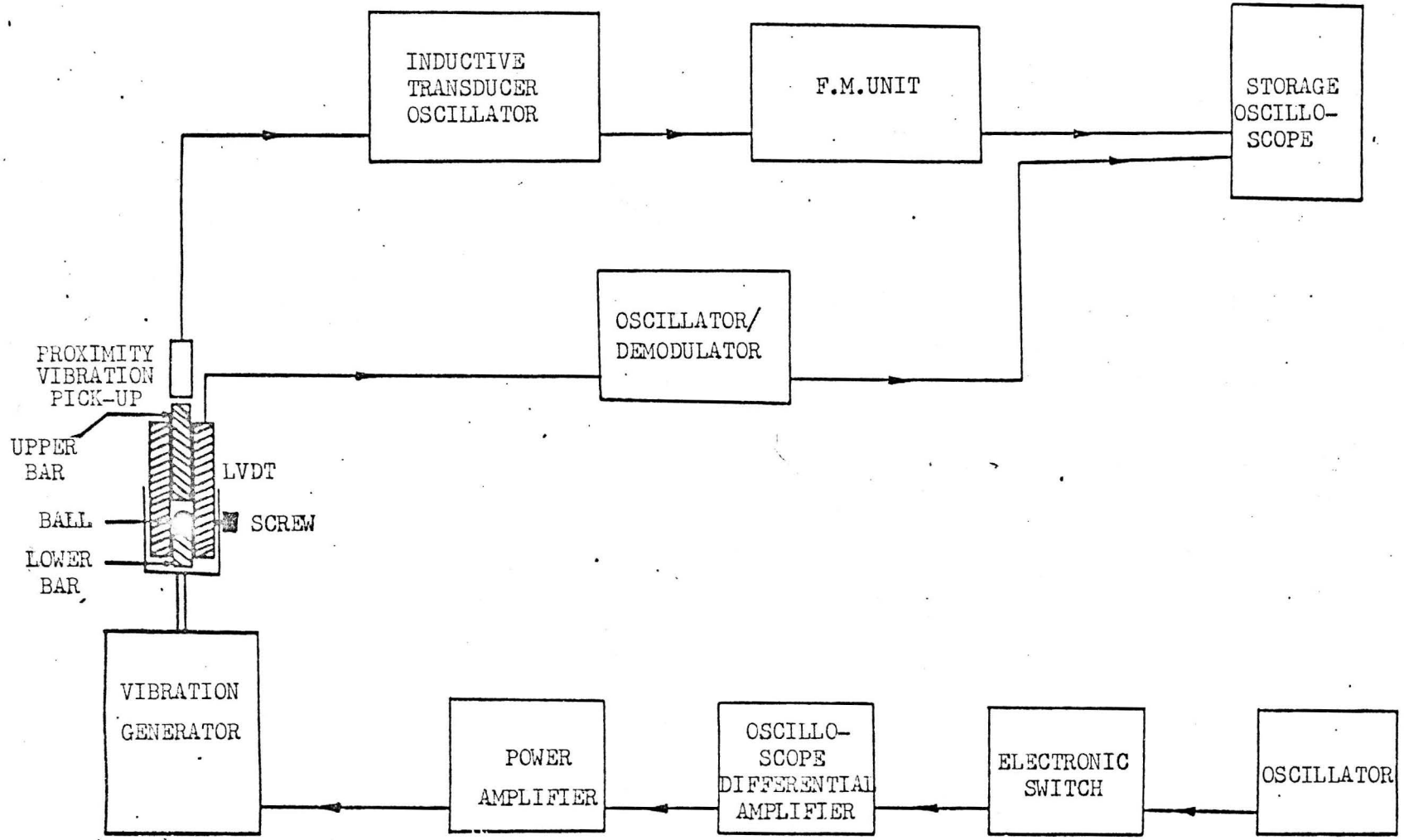

FIG. 4.1 LAYOUT OF THE APPARATUS

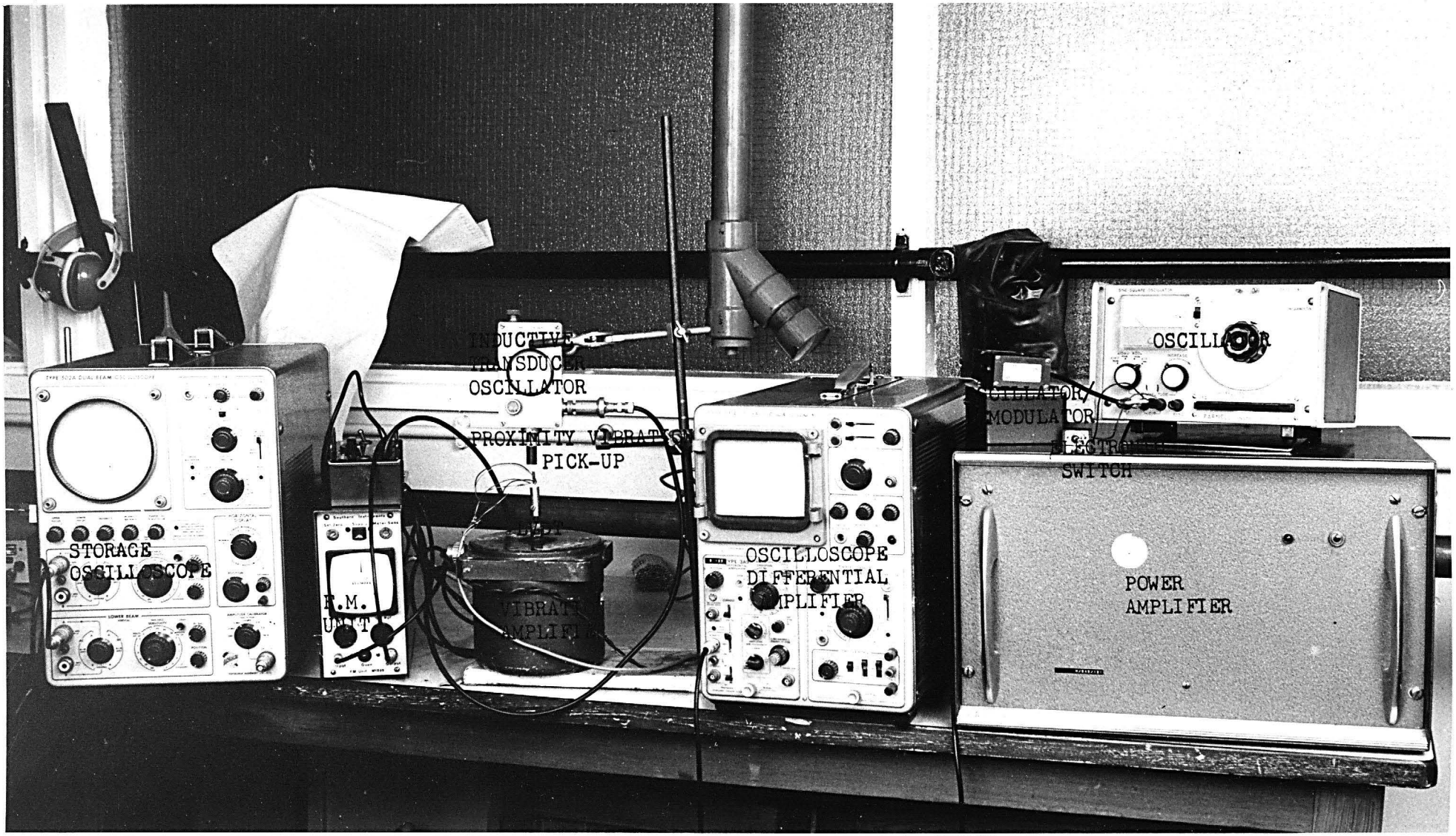

FIG. 4.2 APPARATUS FOR MEASURING BALL MOTION

transducer, and hence the maximum gap in which the ball moved was fixed. The LVDT was connected to the oscillator/demodulator (R.D.P. Electronics Ltd., type D7). The power was supplied to the transducer by the oscillator section. The output signal (which was an amplitude-modulated wave) was restored to the form of the original displacement by the demodulator. The output of the oscillator/demodulator (which was fed to the storage oscilloscope), represented the motion of the ball. The period of the ball cycle was measured from this signal. The LVDT transducer was secured to the driving spindle of a vibration generator (Goodmans, type V.50 Mk. 1). The vibration generator was connected to a power amplifier (Goodmans, type 50 VA) which amplified the driving current from an oscillator (Farnell Sine-Square, type LFM2). The oscillator was connected to the power amplifier through a special electronic switch and an oscilloscope. The amplified oscilloscope input signal was available as an output which was connected to the power amplifier. This not only provided gain but permitted the output signal to be phase inverted relative to the input. The electronic switch received the continuous signal from the Farnell oscillator and gave no output until the input signal was rising through zero. Thus, in combination with the oscilloscope amplifier, this permitted the initial phase of the oscillation to be controlled to either 0 or 180° on a sine wave. The frequency and the amplitude of the oscillator signal were controlled by the manual controls of the oscillator. The amplitude and frequency of the oscillatory motion of the LVDT transducer was controlled by the oscillator signal. The motion was measured by a proximity vibration pick-up (Southern Instruments Ltd, type G211A.199) which was connected to the inductive transducer

oscillator (Southern Instruments Ltd., type M.1822). The output of this transducer was fed to F.M unit (type M. 1800) whose output was fed to the storage oscilloscope, representing the motion of the LVDT transducer. The maximum amplitude of the LVDT body was measured from this signal.

Before starting the test the output signal of the F.M. Unit on the oscilloscope was calibrated by turning the dial of the proximity vibration pick-up by the screw at the top of the transducer, and measuring the change in the voltage on the oscilloscope. Also before starting the test the initial phase of the oscillation, the frequency and the amplitude of the LVDT transducer were fixed. To start the test the electronic switch was turned on.

Since it was difficult to compare the theoretical results of Chapter 3 with the experimental results of this Chapter when the ball was moving in random motion, the measurements were done when the ball was moving in steady state motion. Therefore if the ball was not moving in steady state, the electronic switch was turned off, the frequency and the amplitude of the LVDT transducer were then changed. The electronic switch was turned on again. This process was repeated until the ball moved in a steady state motion. If the steady state motion of the ball was not obtained, the electronic switch was turned off and the gap in which the ball moved was changed. The electronic switch was turned on again. This process was repeated until the ball moved in steady state motion. When the steady state condition was obtained, the following readings were taken:

1. The frequency of the LVDT transducer body.
2. The maximum amplitude of the LVDT transducer body.
3. The period of the ball cycle.

4.3 RESULTS AND DISCUSSIONS

Figs. (4.3-4.8) show photographs of the ball motion signal and LVDT transducer motion signal on the oscilloscope for different values of maximum amplitude of the LVDT transducer, frequency of LVDT transducer, initial phase and the gap in which the ball was moving. Figs. (4.3-4.5) show that the ball was moving in steady state motion. The reason for the steady state motion is because the ball was colliding with the upper and lower walls in proper phase. It can be seen from these figs. that the time of impact was very small compared to the period of the cycle, because the relative velocity before the collision was very high.

Figs. (4.6-4.7) show that the ball had double impacts with the lower wall. Multiple impact phenomenon also have been found by M. A. Veluswami (10) who studied the motion of a ball between two oscillated plates. This phenomenon is due to a rapid change in the phase at impact when the wall catches up with the ball after the first impact and strikes it again. It can be seen from these figs. that the time of impact was significant compared to figs. (4.3-4.5). M. A. Veluswami (10) has also found that when the multiple impacts occurred, the time of impact increased. He has explained this result as due to the low velocity of impact. This agrees with Hertzian impact theory and the observation that low ball velocity is a prerequisite for double impact.

Fig. (4.8) shows that the time of impact was significant compared to the period of the ball cycle. It can be seen from Figs. (4.3-4.8) that the frequency of the ball was approximately the same as the excitation frequency. M. A. Veluswami (10) has found that the ball was moving at the excitation frequency in

BALL MOTION
0.5mm/Div - 5 ms/Div

LVDT MOTION
0.6mm/Div - 5 ms/Div

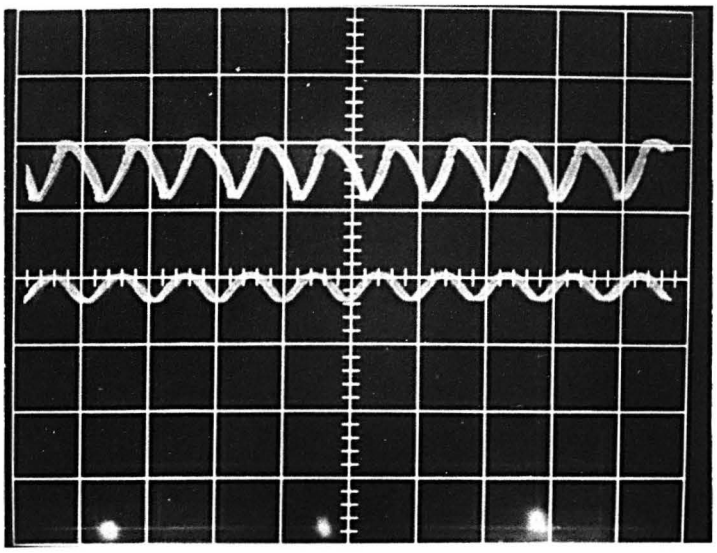

FIG. 4.3 - PHOTOGRAPH OF THE BALL MOTION SIGNAL AND OF THE LDVT MOTION SIGNAL
f = 190 Hz, y_x = 0.254 mm, y_w = 0.4 mm.

BALL MOTION
0.8 mm/Div- 5 ms/Div

LVDT MOTION
0.6 mm/Div- 5 ms/Div

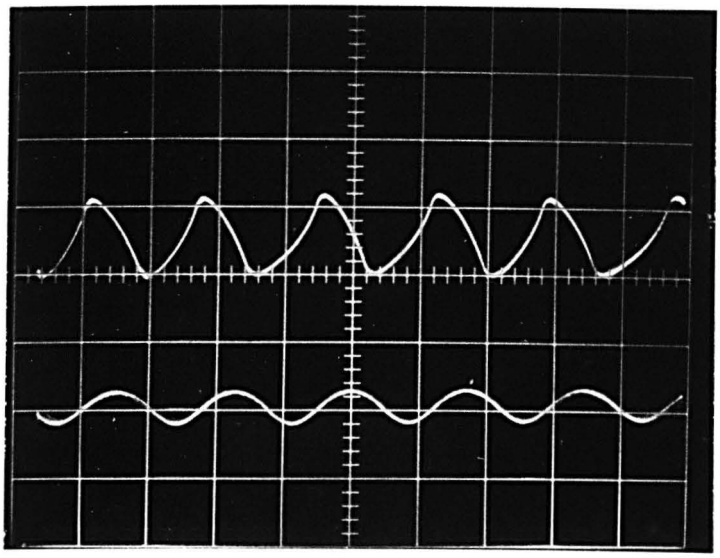

FIG. 4.4 - PHOTOGRAPH OF THE BALL MOTION SIGNAL AND FOR THE LVDT MOTION SIGNAL
f = 100 Hz, y_x = 0.254 mm, y_w = 1 mm.

BALL MOTION
0.8 mm/Div - 5 ms/Div

LVDT MOTION
0.16 mm/Div - 5 ms/Div

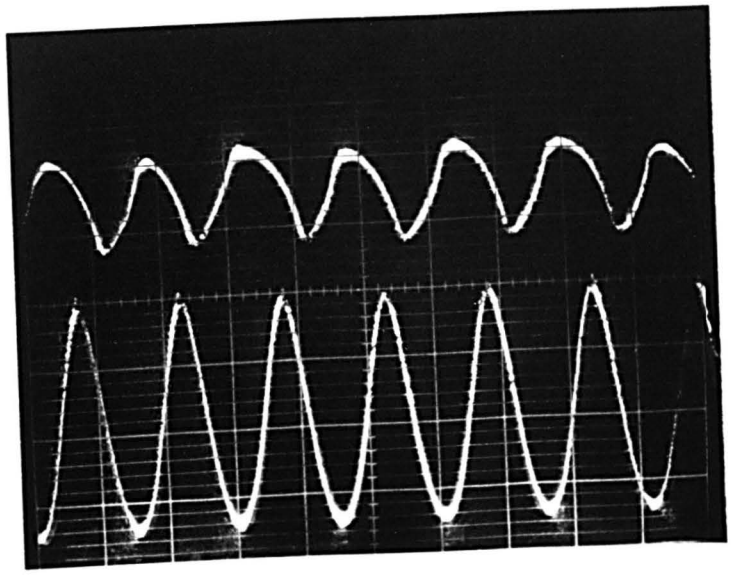

FIG. 4.5 - PHOTOGRAPH OF THE BALL MOTION SIGNAL AND OF THE LVDT MOTION SIGNAL
f = 120 Hz, y_x = 0.54 mm, y_w = 1 mm.

BALL MOTION
0.5 mm/Div - 5 ms/Div

LVDT MOTION
0.8 mm/Div - 5 ms/Div

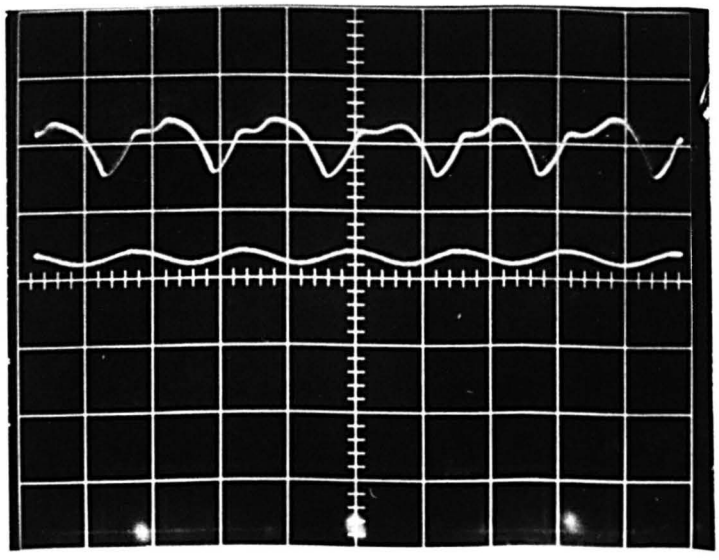

FIG. 4.6 - PHOTOGRAPH OF THE BALL MOTION SIGNAL AND OF THE LVDT MOTION SIGNAL
f = 114 Hz, y_x = 0.163 mm, y_w = 0.4 mm.

BALL MOTION
0.5 mm/Div - 5 ms/Div

LVDT MOTION
0.8 mm/Div - 5 ms/Div

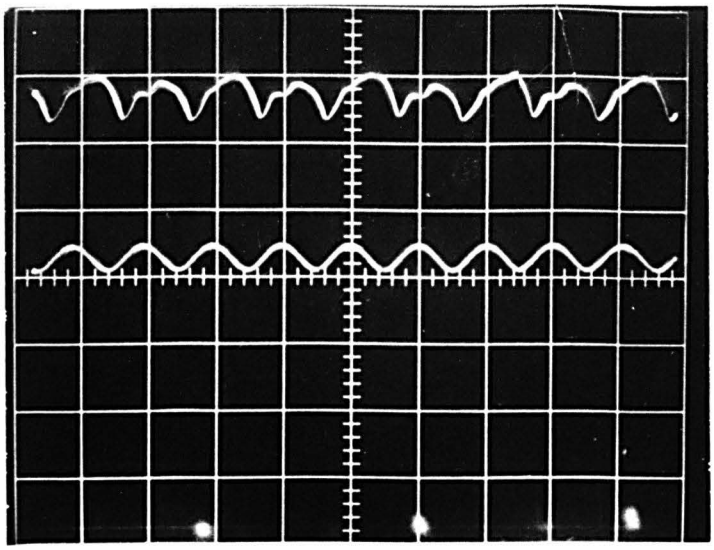

FIG. 4.7 - PHOTOGRAPH OF THE BALL MOTION SIGNAL AND OF THE LVDT MOTION SIGNAL
f = 179 Hz, y_x = 0.326 mm, y_w = 0.3 mm.

BALL MOTION
0.5 mm/Div - 5 ms/Div

LVDT MOTION
0.5 mm/Div - 5 ms/Div

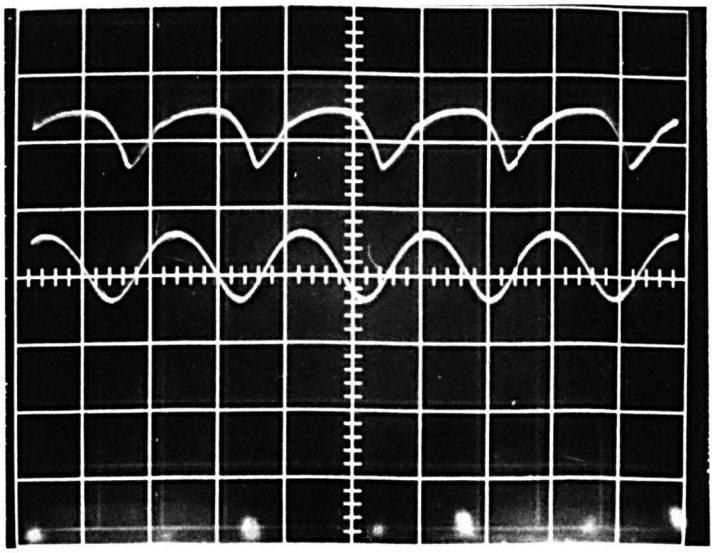

FIG. 4.8 - PHOTOGRAPH OF THE BALL MOTION SIGNAL AND OF THE LVDT MOTION SIGNAL
f = 98 Hz, y_x = 0.5 mm, y_w = 0.45 mm.

D	Z	Period (actual experimental) (sec)	Impact Time (sec)	Period (modified experimental) (sec)	Period (theoretical) (sec)	Initial Phase (experimental)	Initial Phase (theoretical)
0.18	0.1379	8×10^{-3}	0	8×10^{-3}	7.2×10^{-3}	up	up
0.41	0.1172	8.3×10^{-3}	3.8×10^{-3}	4.5×10^{-3}	4×10^{-3}	up	up
0.54	0.032	7.5×10^{-3}	0	7.5×10^{-3}	6.8×10^{-3}	down	down
0.637	0.027	5×10^{-3}	0	5×10^{-3}	4.7×10^{-3}	down	down
1.086	0.0237	5×10^{-3}	2.7	2.3×10^{-3}	1.7×10^{-3}	up	up
1.225	0.0527	9.6×10^{-3}	4.4×10^{-3}	5.2×10^{-3}	5×10^{-3}	down	down

TABLE 4.1 - COMPARISON BETWEEN THE EXPERIMENTAL AND THE THEORETICAL RESULTS

steady state. The experimental values of the maximum amplitude of the LDVT transducer, the frequency of the LVDT transducer and the maximum gap in which the ball moved for each initial phase angle were fed into the computer program (which was described in Chapter 3) as D and Z parameters (also defined in Chapter 3). The results of the computer program were checked with the experimental results.

Table (4.1) shows comparison between the values of the period of the ball cycle theoretically and experimentally for different values of D and Z for each initial phase angle. Since the time of impact was not considered in the analysis of Chapter 3, it was subtracted from the experimental value of the period of the ball cycle. The time of impact is also shown on the table.

Chapter Five

MEASUREMENT OF THE AMPLITUDE OF THE ULTRASONIC FUEL INJECTOR TIP BY LASER ANEMOMETRY

5.1 INTRODUCTION

In the theoretical analysis of the ball motion which has been described in Chapter 3, the injector tip was assumed moving sinusoidally. To predict the equation of the injector tip motion and to find the effects of the fluid flow from the injector and the inertia of the injector body on the tip motion, the tip motion has been measured.

Grubb, Milsom and Abram (1) have measured the amplitude of the tip by using a microscope. Their results were not accurate because the amplitude of the tip was too small and the frequency was too high to allow accurate measurement by this method. Also, they could only measure steady-state amplitudes and not transients.

A capacitive measuring technique was also used by (1). The principle on which this method operated was the variation in capacitance of a parallel plate capacitor as the plate separation was changed. The injector was examined without atomisation but it was filled with the fuel. The amplitude of the tip was deduced to be 2.6×10^{-3} mm, and the motion could be seen to build up slowly to the final amplitude when the injector was energised, and this build up was seen to take place over several milliseconds.

In this investigation a laser technique has been employed in measuring the tip motion to get accurate results. The measurement has been done with and without atomisation, and the effects of the supply pressure and the pulse width on tip motion has been studied.

The details of test apparatus, test program, test procedure, results and discussions are given below.

5.2 TEST APPARATUS

The test apparatus consisted of injector equipment and laser equipments.

Fig. (5.1) shows the photograph for the apparatus.

5.2.1 Injector Equipment

Fig. (5.2) shows the layout of the injector equipments. The injector (type EX4) which is described in Chapter 2 was fixed rigidly above a small tank which was filled with kerosine. The kerosine was delivered from the tank to the injector by a pump (Lucas) of 120 psi. maximum pressure. The supply pressure of the kerosine to the injector was controlled by a regulator (Norgren) and measured by pressure gauge (Hamworthy Engineering). A filter (Fram, type C1191) was used in filtering the kerosine before it was delivered to the injector. The pulse width during which the injector was switched on, was controlled by an oscillator (Farnell Sine-Square, type LFM2) and was of 50% duty cycle. The frequency of the oscillator, which was equal $\frac{1}{2 \text{ pulse width}}$ was read on a Counter-Timer (Racal, type SA535).

5.2.2 Laser Equipments

Fig. (5.3) shows the layout of the laser equipment. The laser anemometer (DISA, type 55L) is a system for scientific measurements of local flow velocity. The DISA laser Doppler Anemometer possesses advantages in flow measurement, and its performance data ensures a

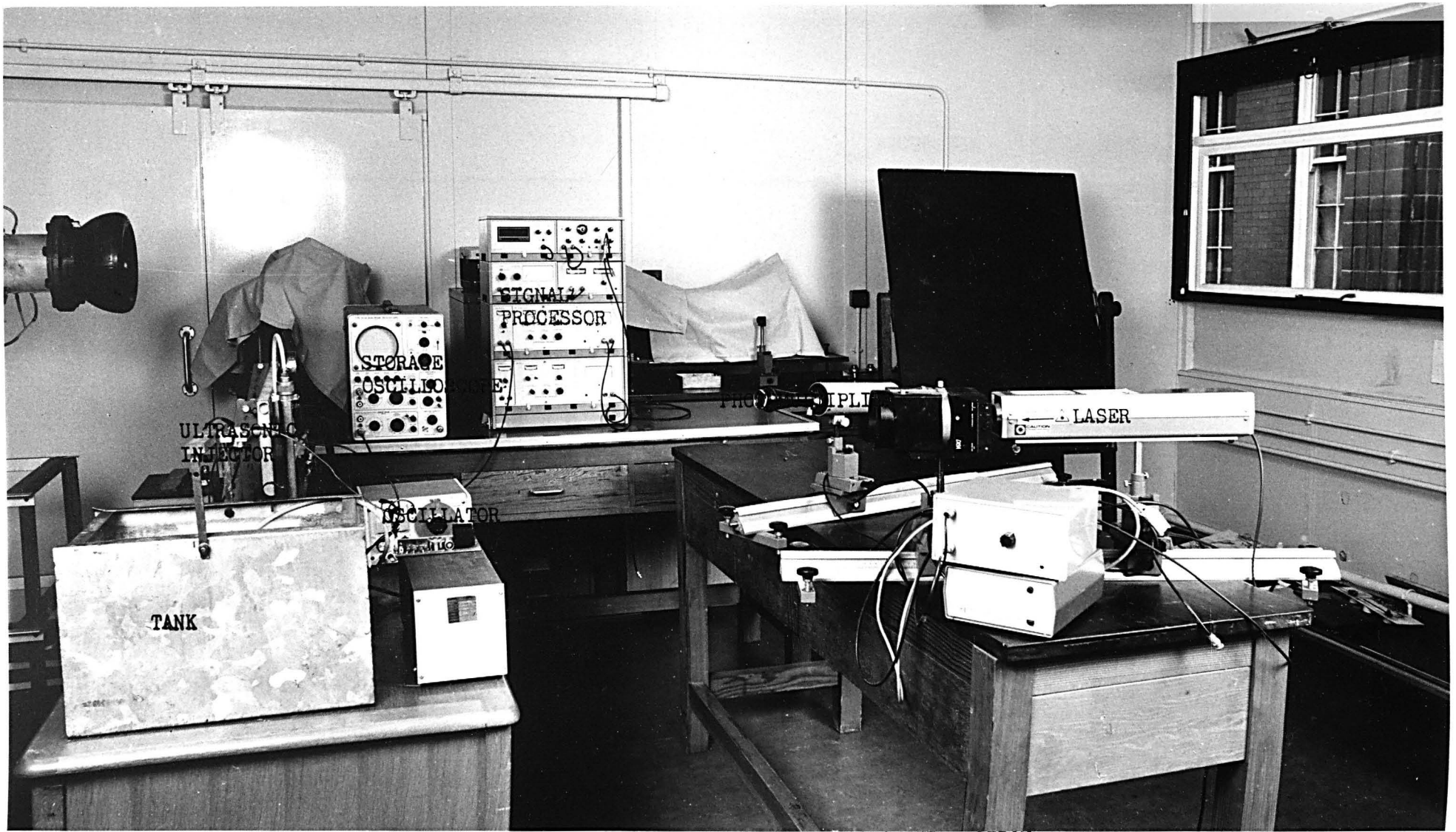

FIG. 5.1 APPARATUS FOR MEASURING INJECTOR TIP MOTION

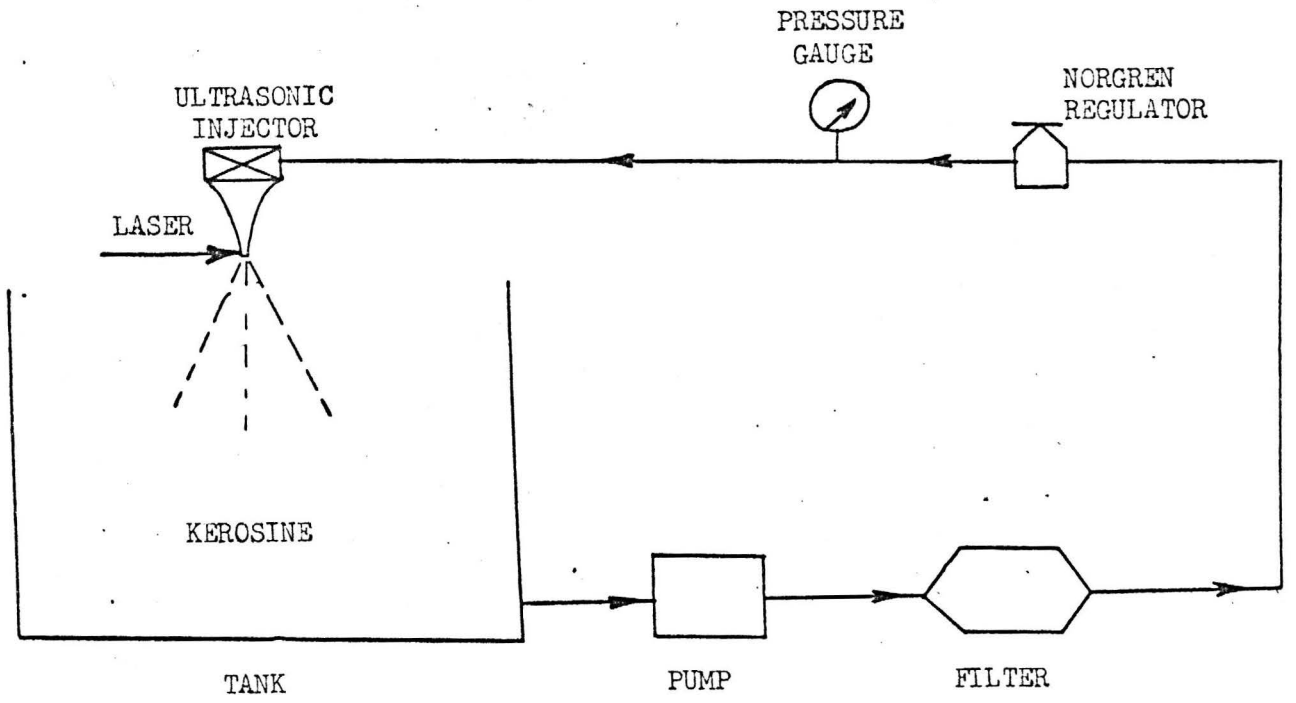

FIG. 5.2 LAYOUT OF THE INJECTOR EQUIPMENT

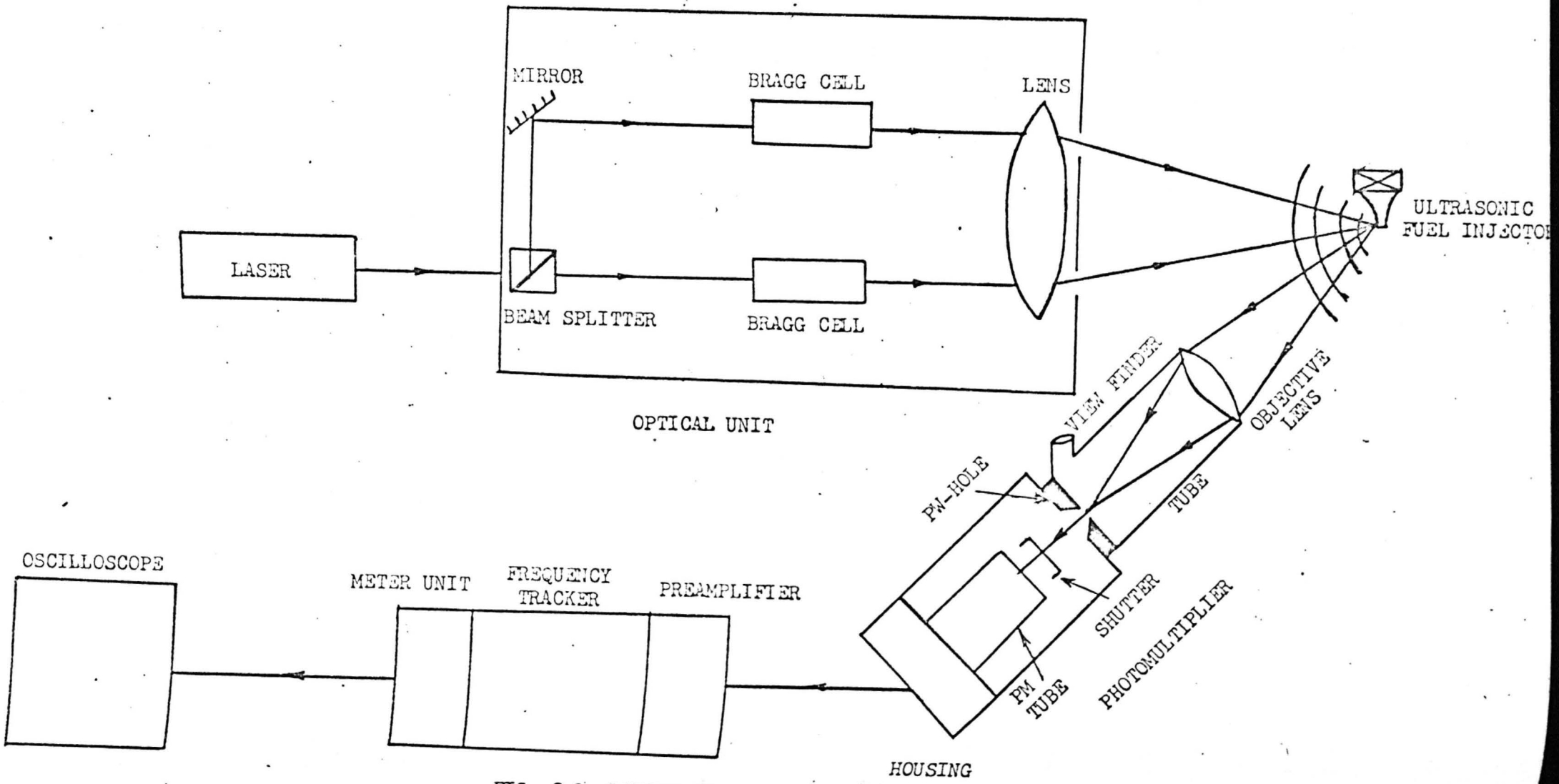

FIG. 5.3 LAYOUT OF THE LASER EQUIPMENT

high order of accuracy in velocity measurements (11).

The detail of the laser equipment was described in (11). The instrument comprised 5 mW He-Ne laser, integrated optical unit, high voltage supply, photomultiplier mounted on optical bench, and electronic frequency tracker for continuous tracking of the Doppler frequency. The laser equipment was set up in such a way that the beam was directed on the tip of the injector. The optical unit (type 55L01) was operated in differential Doppler mode on backward scattered light. In this mode two beams of equal intensity were intersected on the tip of the injector. The beam intersection angle (θ) was set up to 4.77 degrees. The optical unit comprised beam splitter, mirror, Bragg cells and lens.

The optical bench constituted a rigid base for mounting of the laser head, optical unit, and photomultiplier. The photomultiplier (type 55L10) was used to detect the Doppler shifted light scattered from the point of the measurement. The photomultiplier comprised PM tube, shutter, pin-hole, view finder, tube and objective lens. High voltage supply (type 55L15) was used to supply a continuously adjustable DC voltage for the photomultiplier. Voltage indication was provided by a front-panel meter. Another front-panel meter read PM-tube anode current.

The signal processor (type 55L20) improved the signal-to-noise ratio of the Doppler signal and converted the frequency (f_D) into an analog voltage. It comprised preamplifier, frequency tracker unit, and meter unit. The preamplifier had level selectors and a front-panel meter to indicate signal level. The anode current of the high voltage supply was connected to the input of the preamplifier.

The frequency tracker had controls for tuning (manual and automatic), IF level, set level, threshold level, IF bandwidth, Doppler frequency range, and the dropout detector which had OUT/IN switch and a front-panel-meter which read relative duration of signal dropouts (0 to 100%).

The meter unit indicated Doppler frequency, corresponding to the injector tip velocity. The two output sockets are in parallel and carry the instantaneous analog output voltage.

5.3 TEST PROGRAM

In each test the maximum instantaneous Doppler frequency was measured for each pulse width and for each supply pressure. The tests with atomisation were done for pulse width range 1 - 6 ms, and for supply pressure range 5 - 60 psi. One test was done for pulse width 0.5 - 50 ms, and for 40 psi. pressure supply. The test without atomisation was done for 1 - 6 ms pulse width.

5.4 TEST PROCEDURE

The supply pressure to the injector was fixed to a specific value. The pulse width in which the injector was switched on was also fixed to specific value.

The shift frequency was fixed to 7.5 MHz. The SET LEVEL knob of the preamplifier was adjusted until the PREAMP LEVEL meter was set at the red marker (90).

The TUNING selector switch was set to MANUAL, and the TUNING knob was turned fully clockwise. The SET LEVEL knob of the frequency tracker was set to the middle position. The ADJUST

THRESHOLD knob was also set to the middle position. The IF BANDWIDTH selector was set at 2% of FREQUENCY RANGE. The FREQUENCY RANGE selector was set to 15 MHz.

The DROP-OUT DETECTOR was switched to IN. The TUNNEL knob was turned slowly counter-clockwise until the IF LEVEL meter indicated a peak showing that the filter was tuned in to the signal. The DOPPLER FREQUENCY meter showed the corresponding Doppler frequency of the signal. The SET LEVEL of the frequency tracker was adjusted until the IF LEVEL meter was set at the red marker (90) indicating that the signal was of good quality. The TUNING selector switch was set to AUTOMATIC. The frequency tracker then automatically was locked on to the Doppler signal frequency. The IF BANDWIDTH selector was changed from 2% until the signal on the oscilloscope which represented the Doppler frequency remained constant. It was found that the difference between 4% and 8% was very small, so that the BANDWIDTH selector was set to 4%.

The analog output voltage was set to 10 volts. The time knob of the oscilloscope was adjusted until the sinusoidal signal appeared on the oscilloscope. A typical signal is shown in fig. (5.5). This shows clearly the transient motion of the tip in response to a square-wave drive to the crystal drive circuit. Only for longer pulse widths the tip velocity (and amplitude) will reach a steady state. Its peak above the zero line represented maximum instantaneous Doppler frequency which was proportional (for constant tip frequency) to the instantaneous maximum amplitude of the tip. This value of the maximum instantaneous Doppler frequency was recorded and then the pulse width was changed to another value.

The same procedure was repeated again until the data for the required pulse width range was obtained. The supply pressure then was changed to another value, and the same procedure was repeated again until the data for the required supply pressure range was obtained. The maximum instantaneous Doppler frequency without atomisation was measured by switching off the pump which supplied the kerosine to the injector, and changing the pulse width for the required range. Photographs of the signal on the oscilloscope were taken during the test.

5.5 MEASUREMENT ANALYSIS OF THE LASER OUTPUT

The maximum velocity of the injector tip was calculated from the following formula (11):

$$V_T = \frac{f_{DM} \lambda}{2 \sin \theta/2} \qquad (5.1)$$

where V_T represents maximum velocity of the injector tip, f_{DM} maximum instantaneous Doppler frequency, λ beam wave length and θ beam intersection angle.

The maximum amplitude of the injector tip (y_x) was calculated from the following equation:

$$V_T = 2\pi f y_x \qquad (5.2)$$

$$\text{i.e.} \quad y_x = \frac{V_T}{2\pi f} \qquad (5.3)$$

where f represents frequency of the injector, y_x maximum amplitude of the injector tip.

5.6 TEST RESULTS AND DISCUSSIONS

Fig. (5.4) shows the relationship between the maximum amplitude of the injector tip (y_x) with the pulse width (p_w) for supply pressure range 5 - 60 psi. This fig. also shows the relationship without atomisation. It can be seen from this fig. that the maximum amplitude of the tip built up to the steady state value after 5 ms. This is due to the inertia effect of the ultrasonic injector body. Also this fig. shows that for each pulse width the increase in the supply pressure reduced the magnitude of the maximum amplitude. This is because the increase in the supply pressure would increase the flow per pulse, i.e., the damping factor would increase and so that the maximum amplitude would decrease. For this reason it can be seen from this fig. that the decrease in the maximum amplitude due to the increase of the fluid pressure increased when the pulse width was increased.

This fig. shows that there was a large difference between the maximum amplitude at 5 psi (which is near enough to zero) and the maximum amplitude without atomisation. This is because without atomisation the channels of the injector were empty of fluid, but in the case of 5 psi the channels were full of fluid and a small flow was very influential on the value of the maximum amplitude.

This fig. also shows that the maximum amplitude was not affected by the increase of the supply pressure above 40 psi. This is probably because the flow per pulse was not affected by the increase of the supply pressure above 40 psi. The damping effect of the fluid flow on the maximum amplitude of the injector tip was very clear when the maximum amplitude with atomisation was compared with the maximum

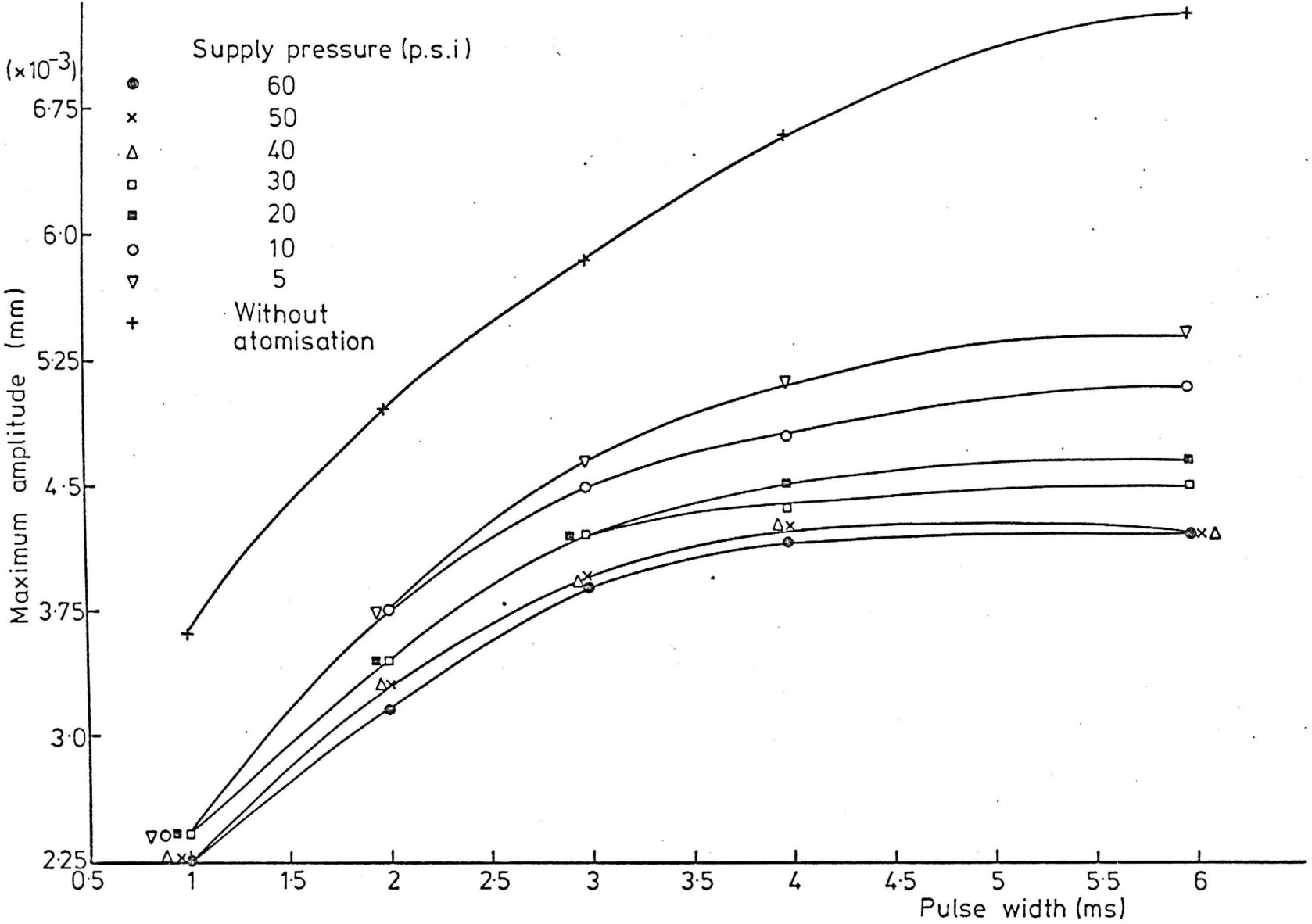

FIG. 5-4 INJECTOR TIP MAXIMUM AMPLITUDE – PULSE WIDTH RELATIONSHIP FOR VARIOUS SUPPLY PRESSURES AND FOR WITHOUT ATOMISATION

amplitude without atomisation.

Fig. (5.5) shows a photograph of the signal of the tip motion without atomisation. This photograph shows the build up in the tip motion when the injector was on and the decay in the motion when the injector was off. The decay in the motion was 2 ms.

Figs. (5.6 - 5.7) shows photographs of the signal of the tip motion with atomisation for 1 ms pulse width and 40 psi supply pressure and for 3 ms pulse width and 60 psi supply pressure respectively. These photographs show that the decay in the motion of the tip was approximately 1.5 ms. The difference in the time of the decay between the case without atomisation and the case with atomisation is due to the damping effect of the fluid.

Figs. (5.8 - 5.9) show photographs of the expanded signals of the tip motion at maximum amplitude with atomisation, for 3 ms pulse width and for 5 psi and 60 psi supply pressure respectively. Fig. (5.10) shows a photograph of the expanded signal of the tip motion without atomisation for 3 ms pulse width. The damping effect of the fluid on the maximum amplitude of the tip was shown clearly from comparing these photographs. It can be seen from these photographs that the injector was moving at 60 KHz frequency. Fig. (5.11) represents a plot between the maximum amplitude of the tip versus the pulse width for 40 psi supply pressure. It can be seen from this fig. that when the pulse width was less than 0.5 ms the maximum amplitude fluctuated. This is probably because the injector was switched on while the tip motion was decaying. When the electrical signal was in phase with this decaying motion of the injector tip, the maximum amplitude increased, and if it was not in

0.3×10^{-3} mm/Div

1 ms/Div

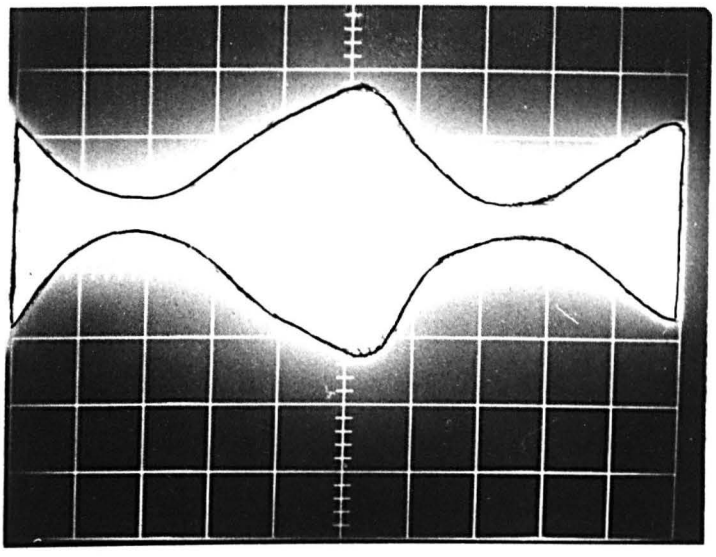

FIG. 5.5 - PHOTOGRAPH OF THE LASER SIGNAL

PW = 3 ms, WITHOUT ATOMISATION

0.3×10^{-3} mm/Div

0.5 ms/Div

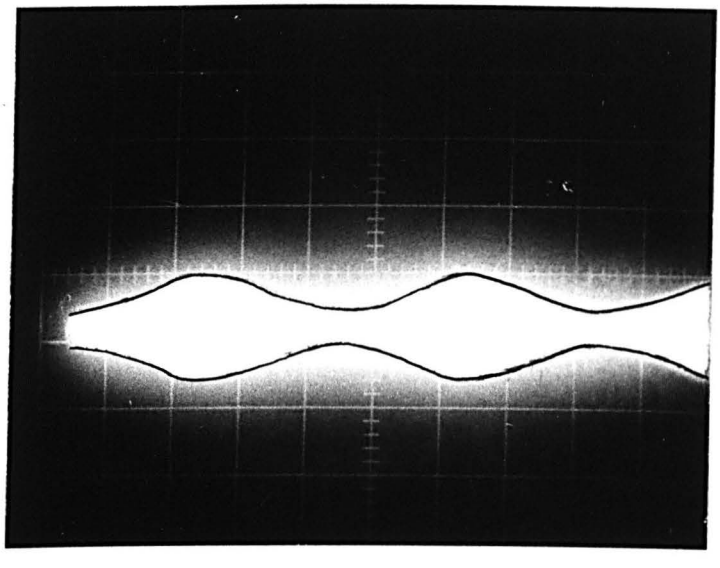

FIG. 5.6 - PHOTOGRAPH OF THE LASER SIGNAL

PW - 1 ms, P_v = 40 psi.

0.3×10^{-3} mm/Div

0.5 ms/Div

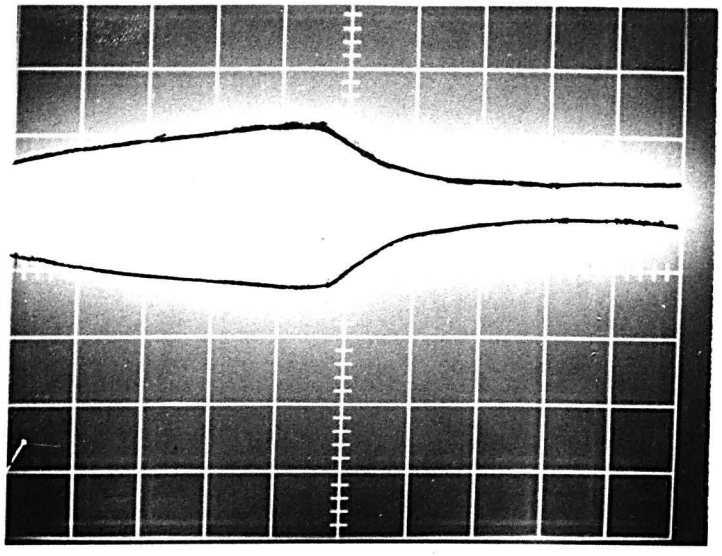

FIG. 5.7 - PHOTOGRAPH OF THE LASER SIGNAL

PW = 3 ms, P_v = 60 psi.

0.3×10^{-3} mm/Div

10 μs/Div

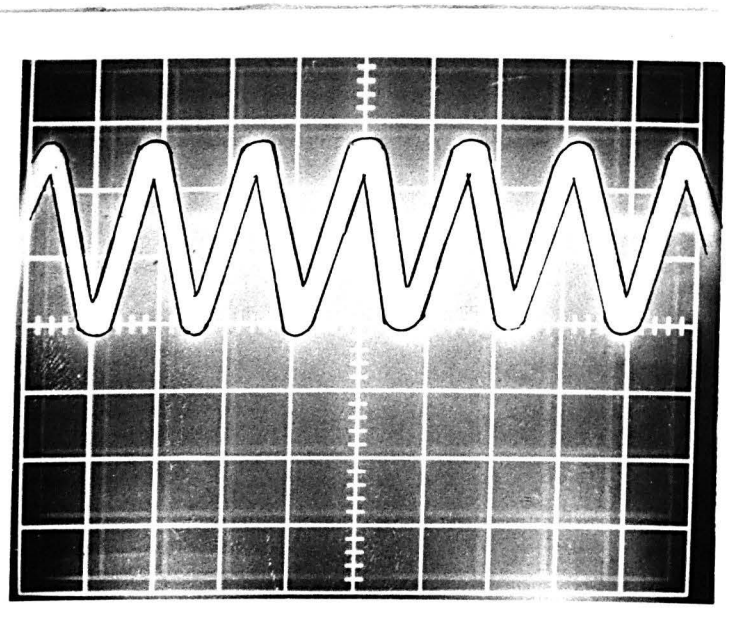

FIG. 5.8 - PHOTOGRAPH OF THE LASER SIGNAL

PW = 3 ms, P_v = 5 psi.

0.3 mm/Div

10 μs/Div

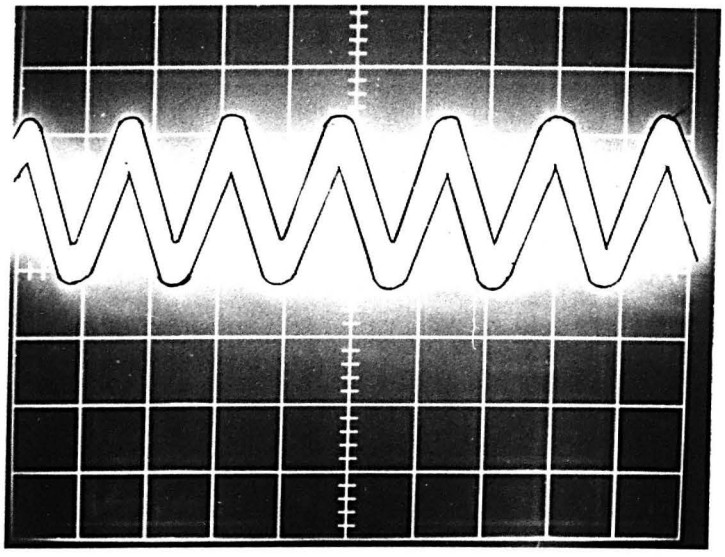

FIG. 5.9 - PHOTOGRAPH OF THE LASER SIGNAL

PW = 3 ms, P_v = 60 psi.

0.3 mm/Div

10 μs/Div

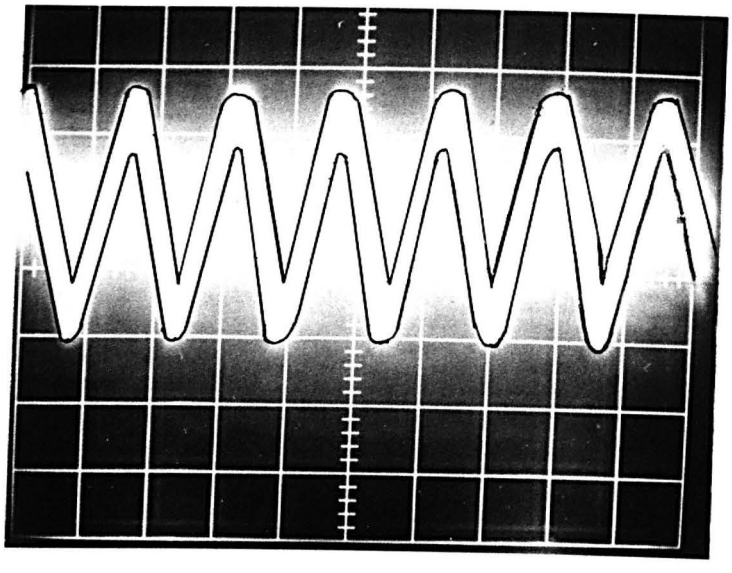

FIG. 5.10 - PHOTOGRAPH OF THE LASER SIGNAL

PW = 3 ms, WITHOUT ATOMISATION.

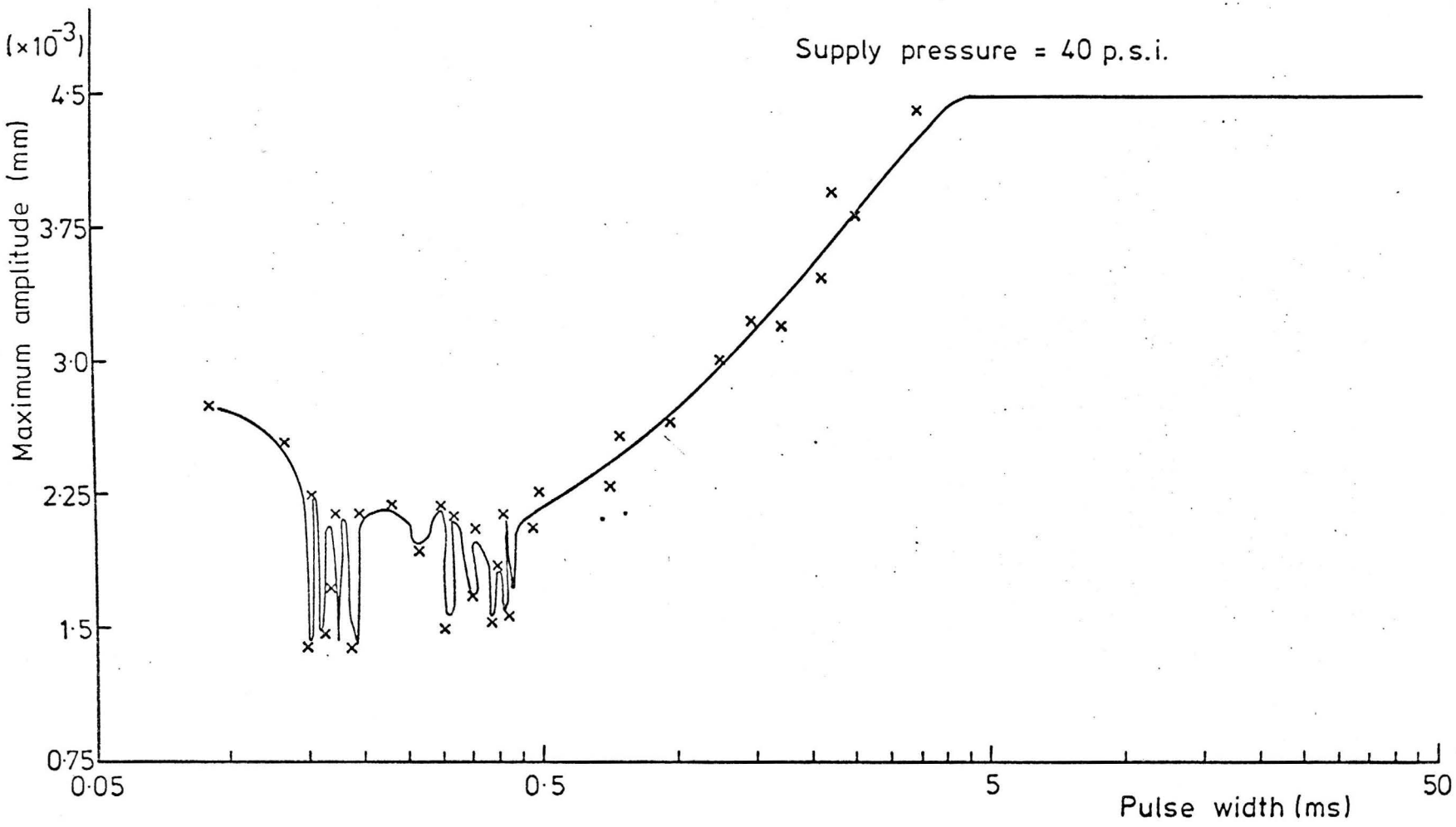

FIG. 5-11 INJECTOR TIP MAXIMUM AMPLITUDE – PULSE WIDTH RELATIONSHIP

phase (or even in anti-phase) with the motion of the injector tip, the maximum amplitude decreased. Also these fluctuations might arise because the pulse width was very small, so that the crystal drive circuit could not follow the electrical signal. When the pulse width was increased more than 5 ms the maximum amplitude of the tip increased continuously to a constant maximum amplitude after 5 ms.

Chapter Six

THEORETICAL ANALYSIS OF THE BALL MOTION WITHOUT FLUID RESISTANCE BY USING LASER DATA

6.1 INTRODUCTION

Since the motion of the injector tip has been measured in Chapter 5, the ball motion in the injector valve could be predicted by using this experimental data in the theoretical analysis which was described in Chapter 3.

This chapter describes such a theoretical analysis. The details of theory, computer program and results and discussions are given below.

6.2 THEORY

6.2.1 Injector Tip Motion

6.2.1.1 Equations of the Injector Tip Motion

From the results of the tip motion measurements by using laser technique, it was found that the tip was moving in a transient to steady state resonance.

The following equation represented the motion of the tip from a fixed datum which was assumed to be the line passing through the seat of the ball at t = o (12)

$$y_1 = B\, e^{-\gamma t/2} \cos(w_d t + \beta) + y_x \cos(w_o t - \delta) \qquad (6.1)$$

Where

$$w_d = (w_n^2 - \frac{\gamma^2}{4})^{\frac{1}{2}} \qquad (6.2)$$

and

$$\tan \delta = \frac{\gamma w_o}{W_n^2 - w_o^2} \qquad (6.3)$$

where B represents a constant, γ parameter of damped vibration, t time at any instance during the pulse, w_d damped natural frequency, β initial phase angle of the free motion, y_x maximum amplitude of the tip, w_o frequency of the tip, δ initial phase angle of the steady-state motion, W_n tip natural frequency.

At resonance:

$$W_n = w_o$$

and hence

$$\delta = \frac{\pi}{2} .$$

By substituting the value of δ in eqn. (6.1), it becomes:

$$y_1 = B\, e^{-\gamma t/2} \cos(w_d t + \beta) + y_x \cos(w_o t - \frac{\pi}{2}) . \qquad (6.4)$$

It was assumed that $y_1 = o$ at $t = o$. For this conditions, eqn. (6.4) becomes:

$$0 = B \cos(\beta) ,$$

therefore

$$\beta = \frac{\pi}{2} .$$

By substituting the value of β in eqn. (6.4) it becomes:

$$y_1 = B\, e^{-\gamma t/2} \cos(w_d t + \frac{\pi}{2}) + y_x \cos(w_o t - \frac{\pi}{2}) . \qquad (6.5)$$

The equation of velocity of the tip was obtained from the derivative of y_1 with respect to t :

$$\frac{d y_1}{dt} = v = -\frac{\gamma}{2} B e^{-\gamma t/2} \cos(w_d t + \frac{\pi}{2}) - B e^{-\gamma t/2}$$

$$w_d \sin(w_d t + \frac{\pi}{2}) - y_x w_o \sin(w_o t - \frac{\pi}{2}). \qquad (6.6)$$

Also it was assumed that $\frac{d y_1}{dt} = 0$ at $t = 0$. For this condition, eqn. (6.6) becomes:

$$o = - B w_d + y_x w_o.$$

Therefore:

$$B = y_w \frac{w_o}{w_d} .$$

By substituting the value of B in eqns. (6.5) and (6.6) we have respectively:

$$y_1 = \frac{w_o}{w_d} y_x e^{-\gamma t/2} \cos(w_d t + \frac{\pi}{2}) + y_x \cos(w_o t - \frac{\pi}{2}) \qquad (6.7)$$

$$v = -\frac{\gamma w_o}{2 w_d} y_x e^{-\gamma t/2} \cos(w_d t + \frac{\pi}{2}) - y_x w_o e^{-\gamma t/2} \sin(w_d t + \frac{\pi}{2})$$

$$- y_x w_o \sin(w_o t - \frac{\pi}{2}) \qquad (6.8)$$

The equation of the acceleration of the injector tip was obtained from the derivative of v with respect to t :

$$\frac{dv}{dt} = a = \frac{\gamma^2 w_o}{4 w_d} y_x e^{-\gamma t/2} \cos(w_d t + \frac{\pi}{2}) + \frac{\gamma}{2} y_x w_o e^{-\gamma t/2}$$

$$\sin(w_d t + \frac{\pi}{2}) + \frac{\gamma}{2} y_x w_o e^{-\gamma t/2} \sin(w_d t + \frac{\pi}{2}) - y_x w_o$$

$$e^{-\gamma t/2}\ w_d \cos(w_d t + \frac{\pi}{2}) - y_x w_o^2 \cos(w_o t - \frac{\pi}{2}) . \quad (6.9)$$

6.2.1.2 Starting Condition of the Injector Tip Motion

To control the starting condition of the injector tip motion, the initial phase angle (s) was added to the equations of motion. Hence eqns. (6.7), (6.8) and (6.9) become respectively:

$$y_1 = \frac{w_o}{w_d} y_x e^{-\gamma t/2} \cos(w_d t + \frac{\pi}{2} + s) + y_x \cos(w_o t - \frac{\pi}{2} + s) , \quad (6.10)$$

$$v = -\frac{\gamma w_o}{2 w_d} y_x e^{-\gamma t/2} \cos(w_d t + \frac{\pi}{2} + s) - y_x w_o e^{-\gamma t/2} \sin(w_d t + \frac{\pi}{2} + s) - y_x w_o \sin(w_o t - \frac{\pi}{2} + s), \quad (6.11)$$

and

$$a = \frac{\gamma^2 w_o}{4 w_d} y_x e^{-\gamma t/2} \cos(w_d t + \frac{\pi}{2} + s) + \frac{\gamma}{2} y_x w_o e^{-\gamma t/2} \sin(w_d t + \frac{\pi}{2} + s) + \frac{\gamma}{2} y_x w_o e^{-\gamma t/2} \sin(w_d t + \frac{\pi}{2} + s) - y_x w_o e^{-\gamma t/2} w_d \cos(w_d t + \frac{\pi}{2} + s) - y_x w_o^2 \cos(w_o t - \frac{\pi}{2} + s) . \quad (6.12)$$

Two starting conditions were assumed:

1. The tip was moving down at $t = o$, i.e., $s = \pi$.
2. The tip was moving up at $t = o$, i.e., $s = o$.

6.2.2 Motion of the Ball

6.2.2.1 Equations of the Ball Motion

The assumptions about the ball motion which were made in Chapter 3, were also assumed in this analysis except for the starting condition of the ball.

Eqn. (3.2) was used to compute the position of the ball from the same datum as the tip.

$$y_2 = g\, t_1^2/2 + v_o\, t_1 + y_o \qquad (6.13)$$

where g represents gravity of accelerations, t_1 time at any instance between two successive impacts, v_o initial ball velocity and y_o initial position of the ball.

Eqn. (3.8) was used to compute the velocity of the ball at any instance between two successive collisions:

$$v_b = -g\, t_1 + v_o \,. \qquad (6.14)$$

6.2.2.2 Starting Conditions of the Ball Motion

The assumed starting conditions of the ball motion was that the ball separated from the seat with the same velocity as the injector tip when the injector tip was moving up with negative acceleration less than the gravitational acceleration, or the ball separated with the same velocity as the injector tip when the injector tip was moving down with positive acceleration greater than the gravitational acceleration, i.e. separation occurred when:

$$a > g \text{ (when the tip was moving down)} \,, \qquad (6.15)$$

or

$a < -g$ (when the tip was moving up).

6.2.2.3 Equation of the Gap Between the Ball and the Seat

Equation (3.3) was used to compute the gap between the ball and the seat:

$$y = y_2 - y_1 \quad . \tag{6.16}$$

i.e.,

$$y = g\, t_1^2/2 + v_o\, t_1 + y_o - \frac{w_o}{w_d}\, y_x\, e^{-\gamma t/2} \cos(w_d\, t + \frac{\pi}{2} + s)$$

$$- y_x \cos(w_o\, t - \frac{\pi}{2} + s). \tag{6.17}$$

6.2.2.4 Collision Between the Ball and the Walls of the Valve

The assumptions made in Chapter 3 concerning the collision between the ball and the walls of the valve (see section (3.2.2.4)) were also assumed in this analysis. The time of impact was assumed to be negligible. Eqn. (3.6) was used to compute the velocity of the ball after the collision (v_{o1}):

$$v_{o1} = 2v_f - v_{ib} \tag{6.18}$$

where

$v_f = v_i = v$ at the time of impact,

and

$v_{iv} = v_b$ at the time of impact.

By substituting eqn. (6.11) for v and eqn. (6.14) for v_b in eqn. (6.18) we have:

$$v_{o1} = -\frac{\gamma w_o}{w_d} y_x e^{-\gamma t/2} \cos(w_d t + \frac{\pi}{2} + s) - 2y_x$$

$$w_o e^{-\gamma t/2} \sin(w_d t + \frac{\pi}{2} + s) - 2y_x w_o$$

$$\sin(w_o t - \frac{\pi}{2} + s) + g t_1 - v_o \qquad (6.19)$$

6.2.3 Dimensional Expressions

The dimensionless groups derived in Chapter 3 can be used to obtain dimensionless form of eqns. (6.10), (6.11), (6.15), (6.17) and (6.19), respectively:

$$Y_1 = D W_m \cos(W/W_m + \frac{\pi}{2} + s) e^{-W G_m/2} + D \cos(w - \frac{\pi}{2} + s) . \qquad (6.20)$$

where

$$Y_1 = \frac{y_1}{y_w}, \quad D = \frac{y_x}{y_w}, \quad W_m = \frac{w_o}{w_d}, \quad W = w_o t \text{ and } G_m = \frac{\gamma}{w_o} .$$

$$A = G_m^2 W_m \cos(W/W_m + \frac{\pi}{2} + s) e^{-W G_m/2} + 2 G_m$$

$$\sin(W/W_m + \frac{\pi}{2} + s) e^{-W G_m/2} - \cos(W/W_m + \frac{\pi}{2} + s)$$

$$e^{-W G_m/2} W_m^{-1} - \cos(W - \frac{\pi}{2} + s). \qquad (6.21)$$

where $A = \frac{\nu}{y_x w_o}$.

$$Y = D(-Z W_{1/2}^2 + A_o W_1 + B_o - W_m \cos(W/W_m + \frac{\pi}{2} + s)$$

$$e^{-W G_m/2} - \cos(W - \frac{\pi}{2} + s)) \qquad (6.22)$$

where $Y = \frac{y}{y_w}$, $Z = \frac{g}{y_x \cdot w_o^2}$, $A_o = \frac{v_o}{y_x \cdot w_o^2}$, $W_1 = t_1 w_o$

and $B_o = \frac{y_o}{y_w}$.

$$A_{o1} = -2\ G_m\ W_m \cos(W/W_m + \frac{\pi}{2} + s)\ e^{-W\ G_m/2} - 2$$

$$\sin(W/W_m + \frac{\pi}{2} + s)\ e^{-W\ G_m/2} - 2 \sin(W - \frac{\pi}{2} + s) + Z\ W_1 - A_o \ . \qquad (6.23)$$

Where $A_{o1} = \frac{v_{o1}}{y_x \cdot w_o}$.

$$A > Z$$

$$A < -Z \qquad (6.24)$$

where $A = \frac{v}{y_x \cdot w_o}$.

6.2.4 Checking of Equation (6.20)

Eqn. (6.20) has been checked by substituting the values of G_m and W_m which was computed from the laser results, and plotting y_1/y_x versus the pulse width, (see fig. (6.1)). It can be seen from this fig. that the injector tip built up to a steady state motion after approximately 5 ms. It can be deduced from this fig. that eqn. (6.20) represented well the motion of the injector tip.

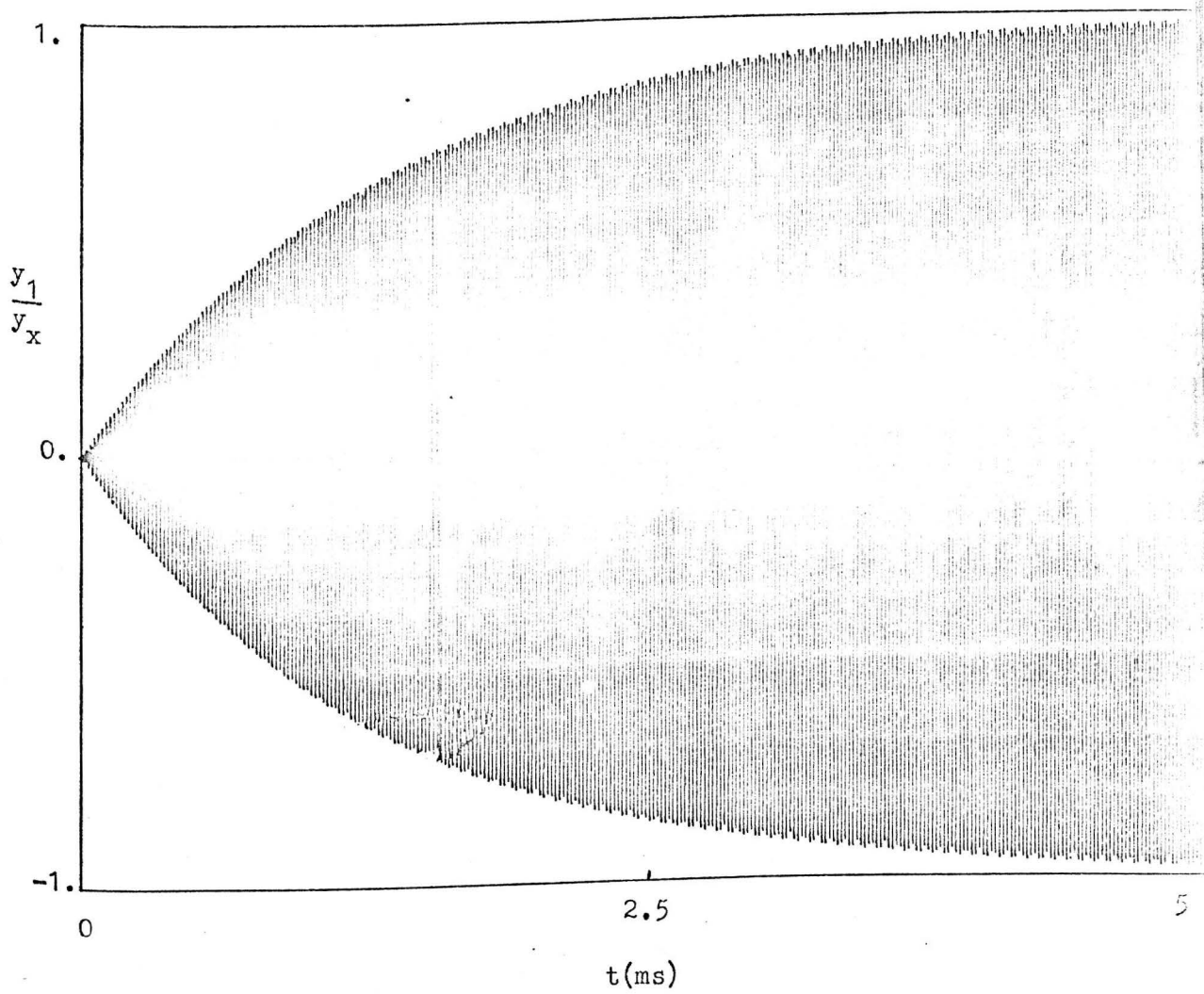

FIG. 6.1 RATIO OF THE MOTION OF THE TP TO THE MAXIMUM AMPLITUDE OF THE TIP - TIME RELATIONSHIP

6.3 COMPUTER PROGRAM

Fig. (6.2) shows the flow chart of the computer program. Fortran language was used in the 1906 Computer at Sheffield University. The flow chart was the same as the flow chart of Chapter 3 (fig. (3.2)) except for the separation problem.

The subroutine C05ACF was used to compute the value (W_s) of W at which separation occurred. The subroutine was based on the bisection method.

The computer program is given in Appendix (4).

S	D	Z	D_w	W	N_m	G_m	W_m	W_1
0	0.001 - 0.1	1×10^{-6} 5×10^{-4}	0.4	0	1000	0.00112	1	0
π	0.001 - 0.1	1×10^{-6} 5×10^{-4}	0.4	0	1000	0.00112	1	0

TABLE (6.1) INPUT DATA TO THE COMPUTER PROGRAM

6.3.1 Input Data to the Computer Program

The input data to the computer program is shown in Table (6.1).

It can be seen from the laser results (which were described in Chapter 5) that the range of the maximum amplitude of the injector tip (y_x) was 4.2×10^{-3} mm - 7.5×10^{-3} mm, when the tip was moving at a frequency of 60 KHz. In this analysis the maximum gap (y_w) between the ball and the walls of the cavity was chosen in the range of 0.1 mm - 0.8 mm. According to these ranges, the ranges of the dimensionless groups D and Z were respectively:

0.001 - 0.1 and $1 \times 10^{-6} - 5 \times 10^{-4}$.

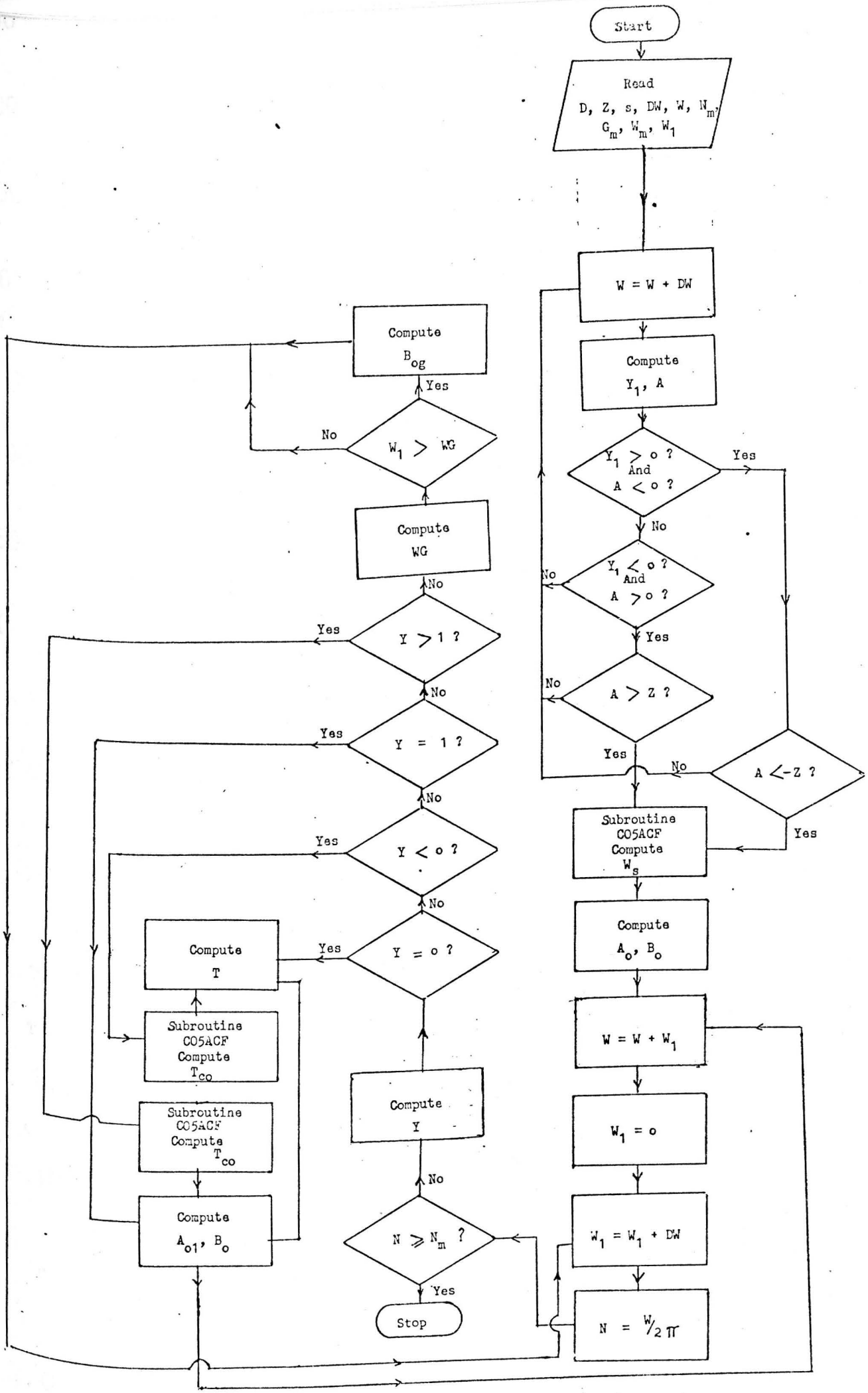

FIG. 6.2 FLOW CHART OF THE COMPUTER PROGRAM OF THE BALL MOTION

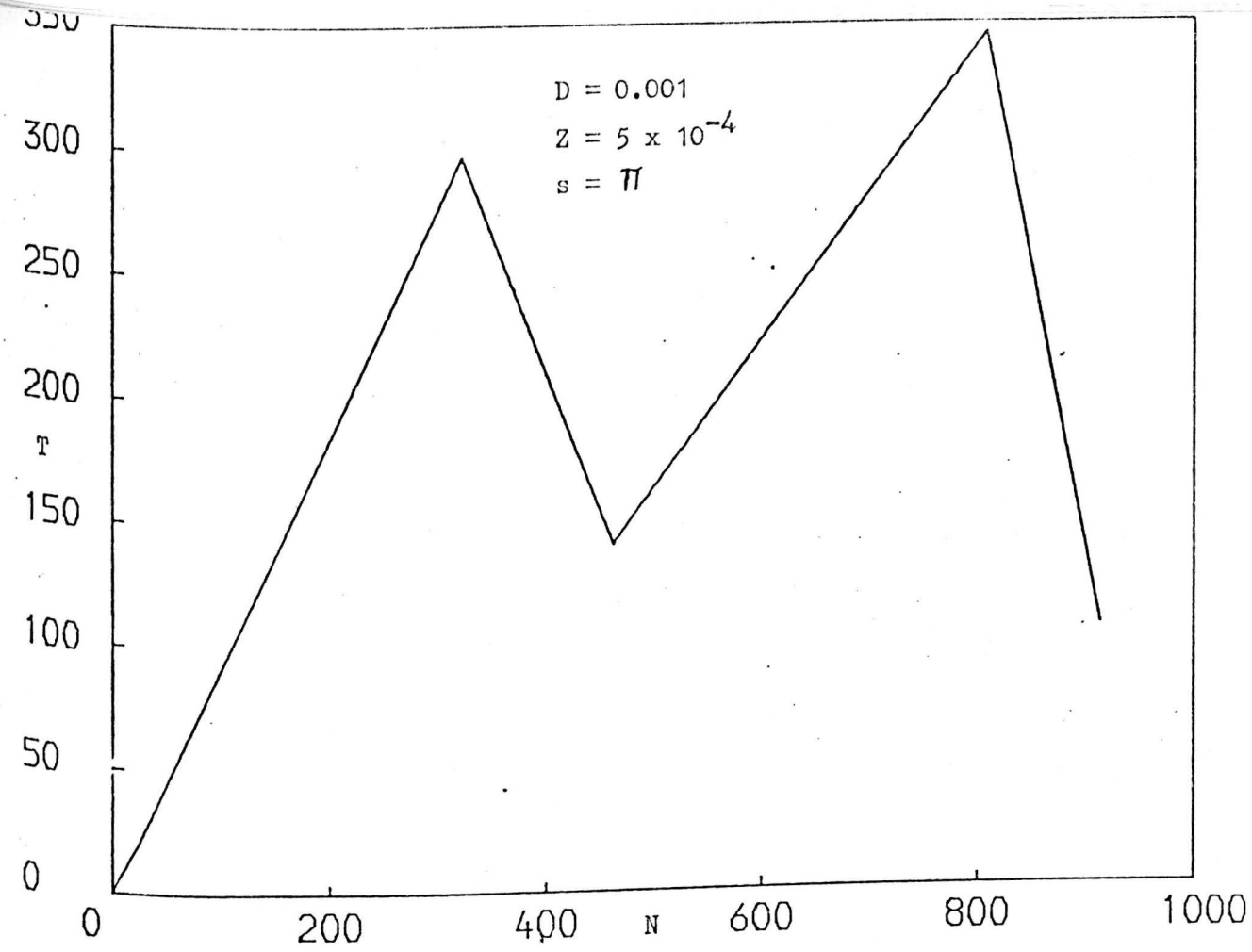

FIG. 6.3 PERIOD OF THE BALL CYCLE (IN TERM OF THE TIP CYCLE) - NUMBER OF THE TIP CYCLES RELATIONSHIP

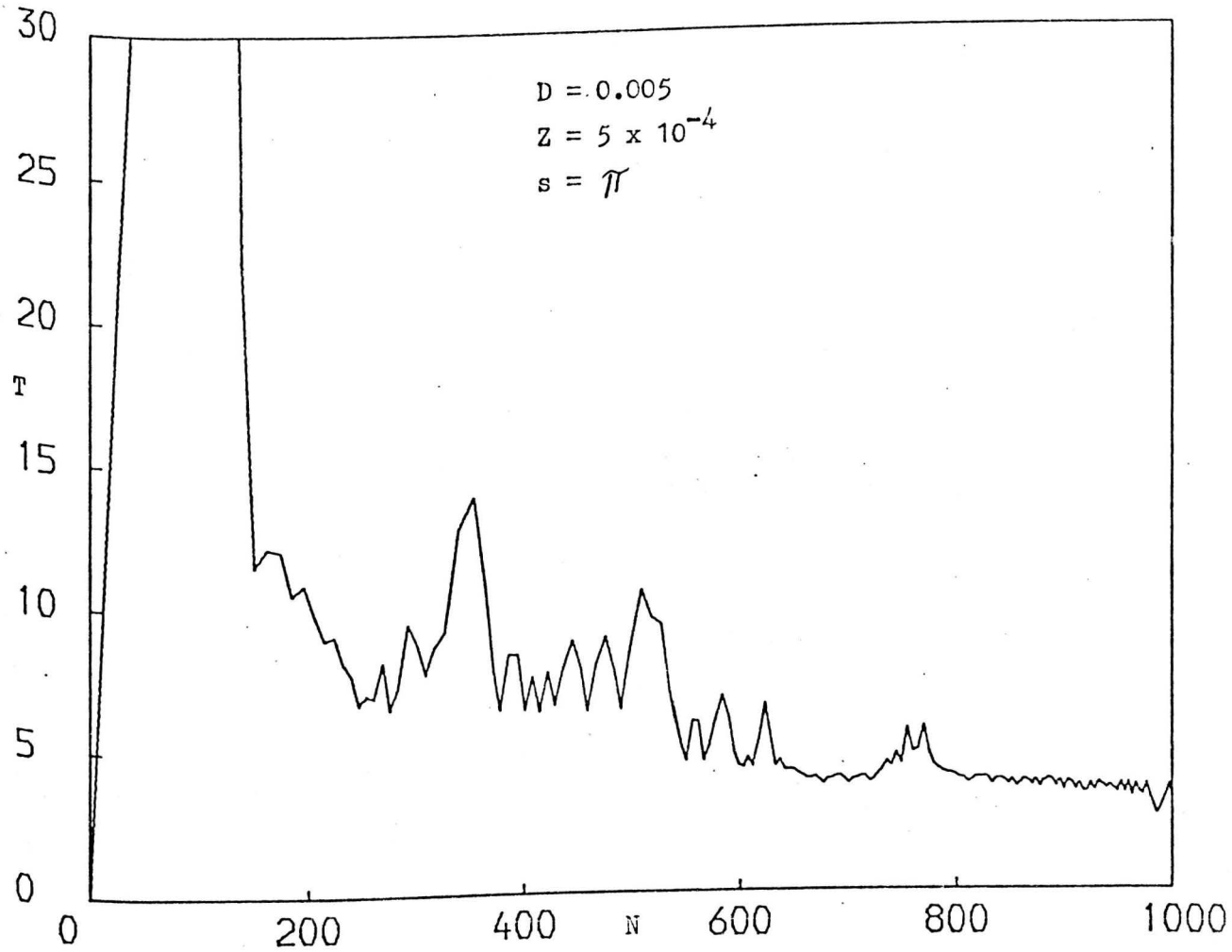

FIG. 6.4 PERIOD OF THE BALL CYCLE (IN TERM OF THE TIP CYCLES) - NUMBER OF THE TIP CYCLES RELATIONSHIP

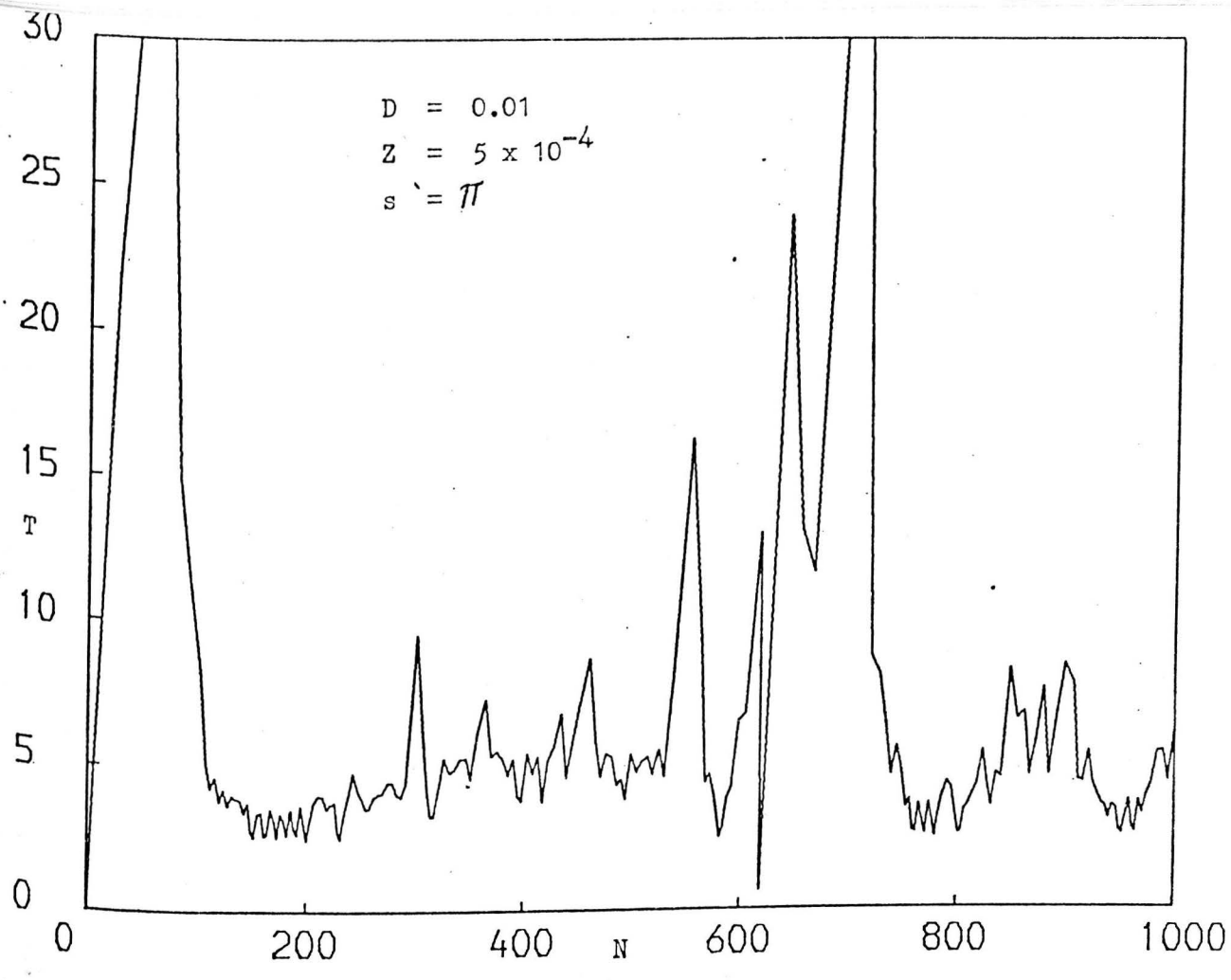

FIG. 6.5 PERIOD OF THE BALL CYCLE (IN TERM OF THE TIP CYCLES) - NUMBER OF THE TIP CYCLES RELATIONSHIP

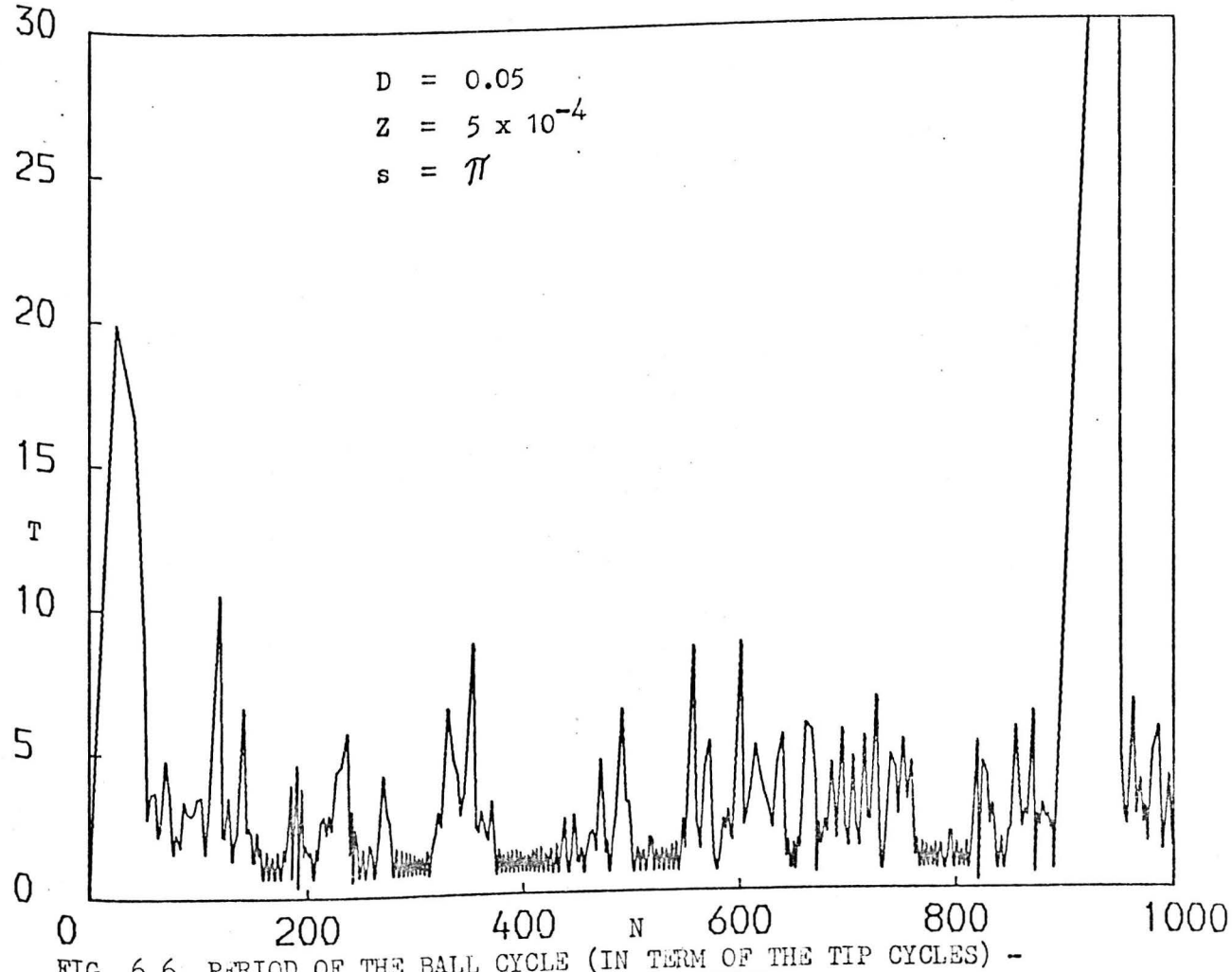

FIG. 6.6 PERIOD OF THE BALL CYCLE (IN TERM OF THE TIP CYCLES) - NUMBER OF THE TIP CYCLES RELATIONSHIP

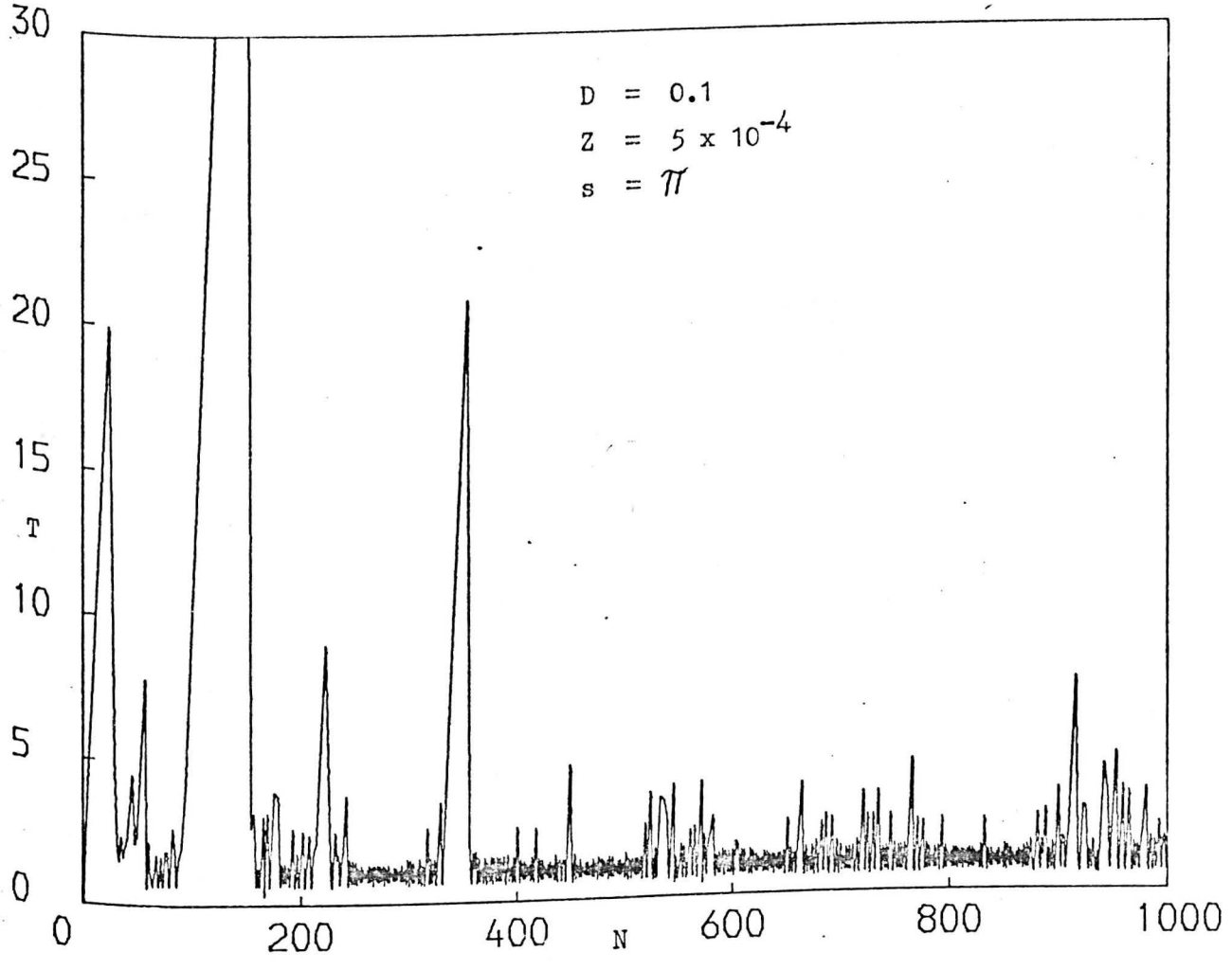

FIG. 6.7 PERIOD OF THE BALL CYCLE (IN TERMS OF THE TIP CYCLES) - NUMBER OF THE TIP CYCLES RELATIONSHIP

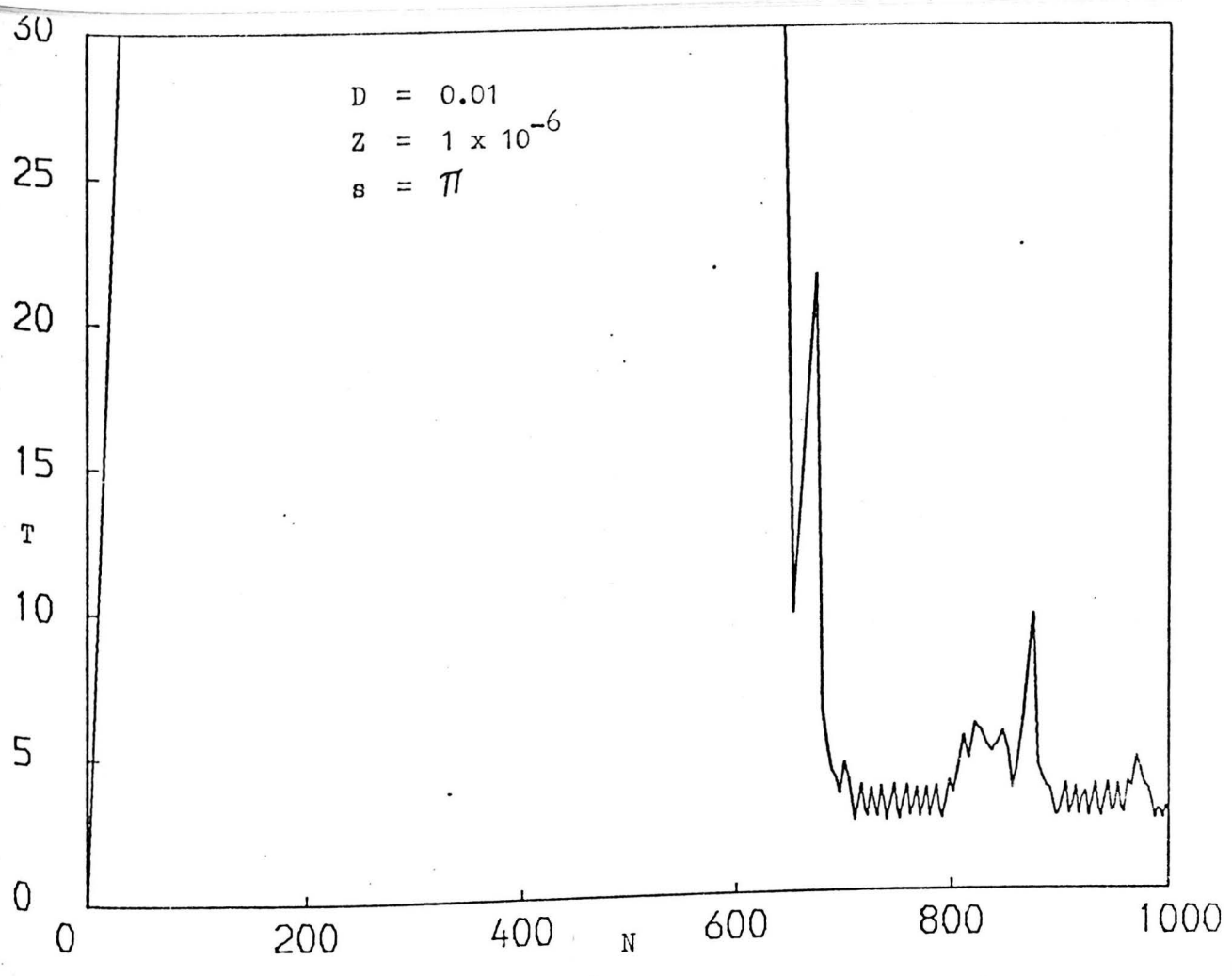

FIG. 6.8 PERIOD OF THE BALL CYCLE (IN TERMS OF THE TIP CYCLES) - NUMBER OF THE TIP CYCLES RELATIONSHIP

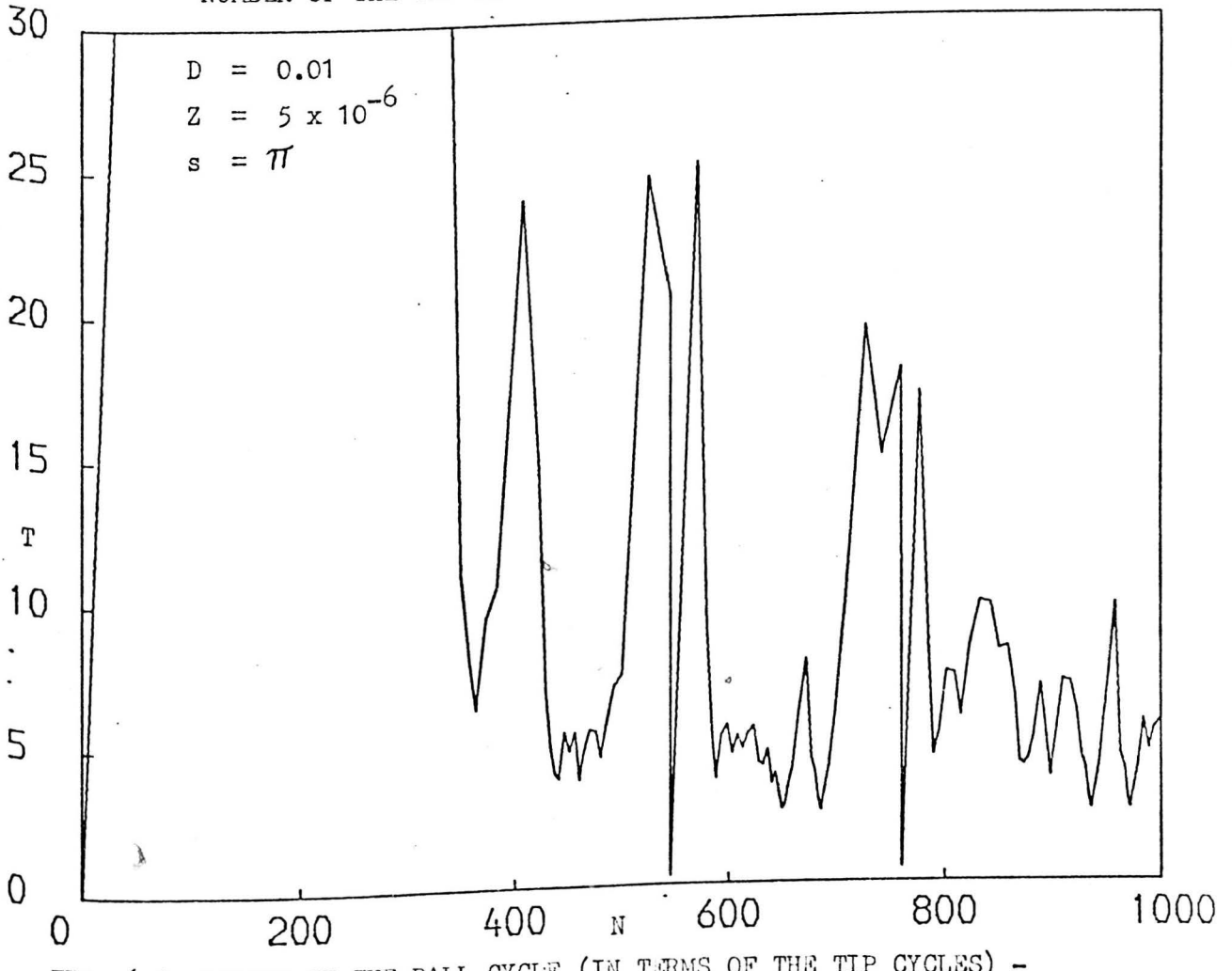

FIG. 6.9 PERIOD OF THE BALL CYCLE (IN TERMS OF THE TIP CYCLES) - NUMBER OF THE TIP CYCLES RELATIONSHIP

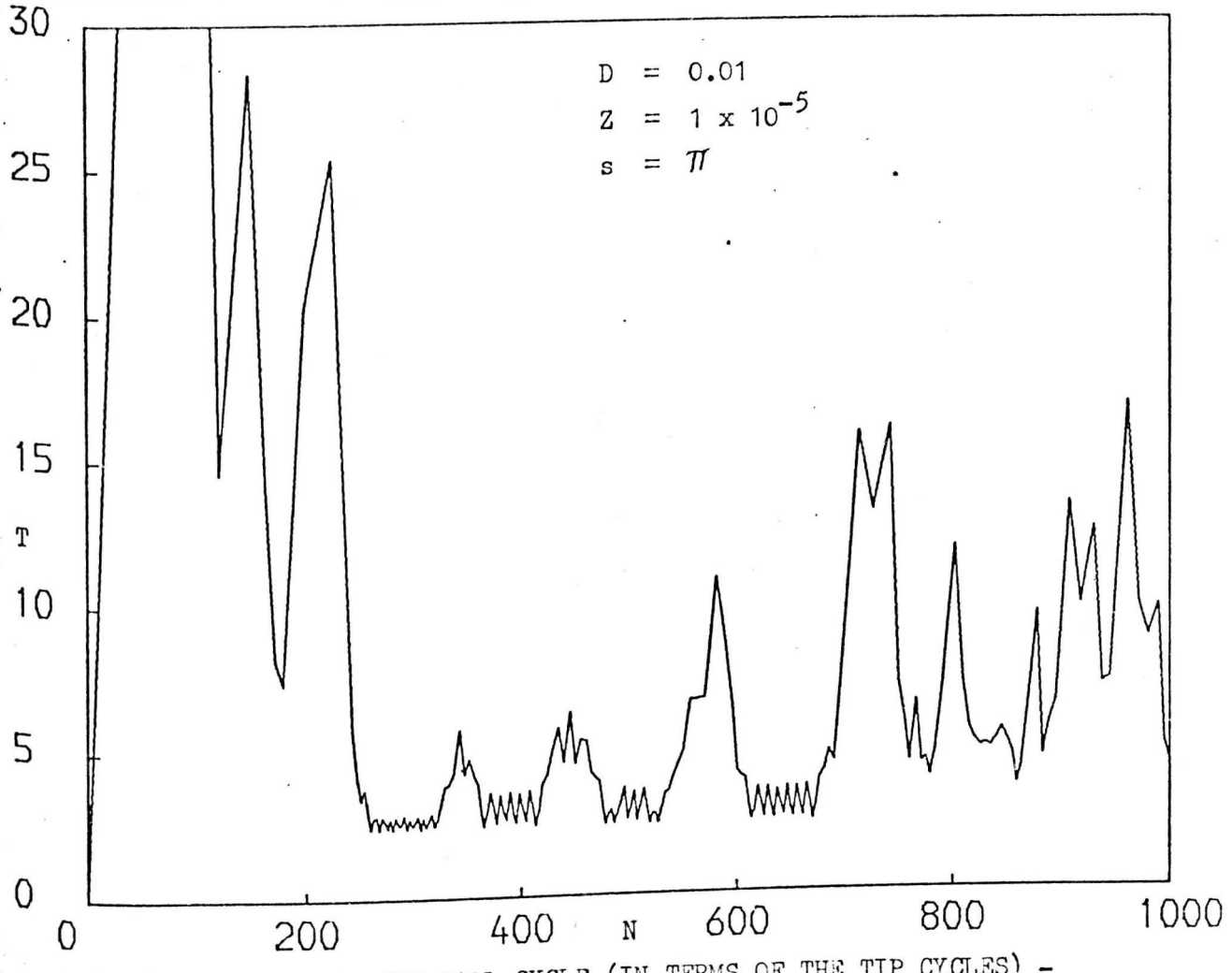

FIG. 6.10 PERIOD OF THE BAIL CYCLE (IN TERMS OF THE TIP CYCLES) - NUMBER OF THE TIP CYCLES RELATIONSHIP

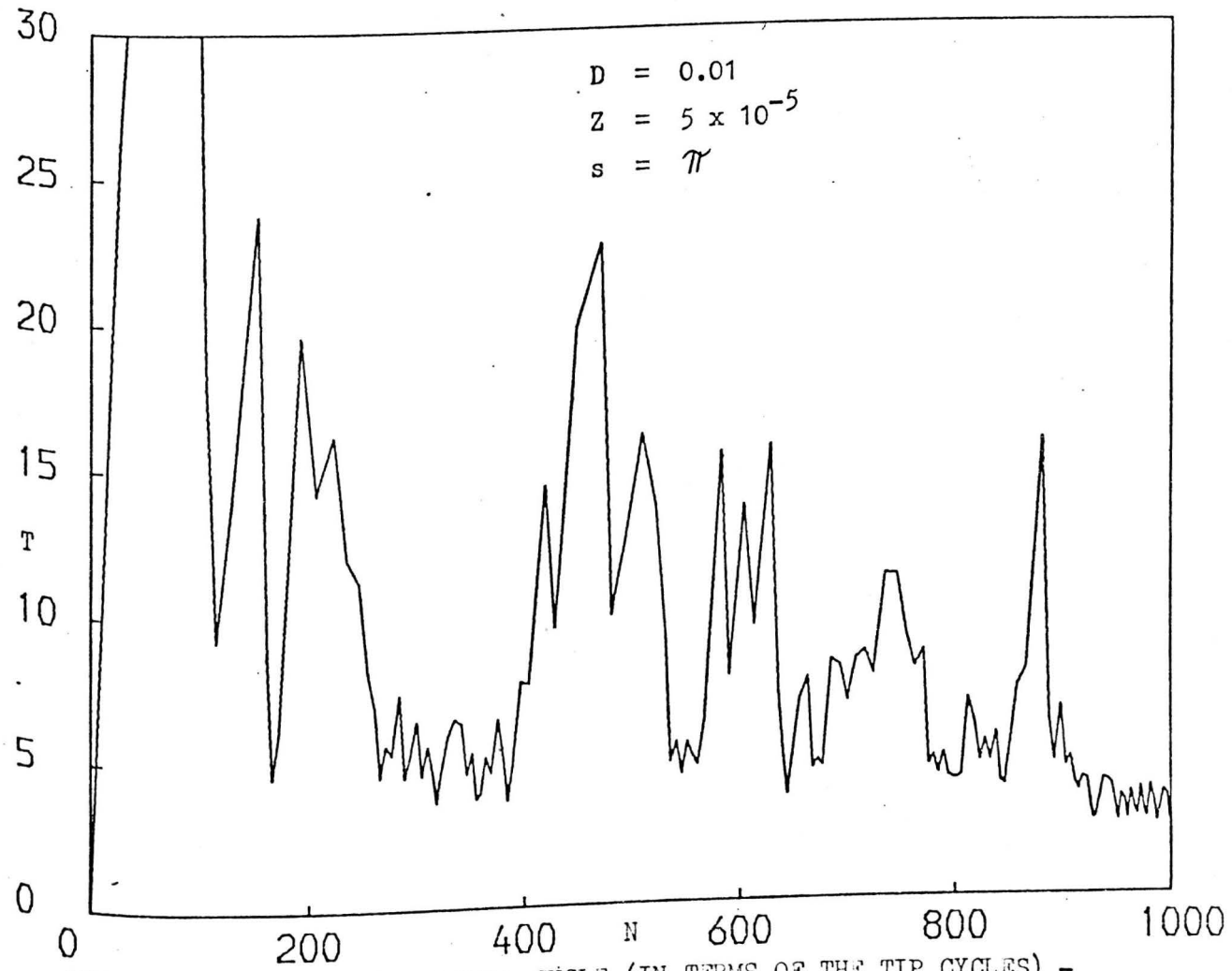

FIG. 6.11 PERIOD OF THE BALL CYCLE (IN TERMS OF THE TIP CYCLES) - NUMBER OF THE TIP CYCLES RELATIONSHIP

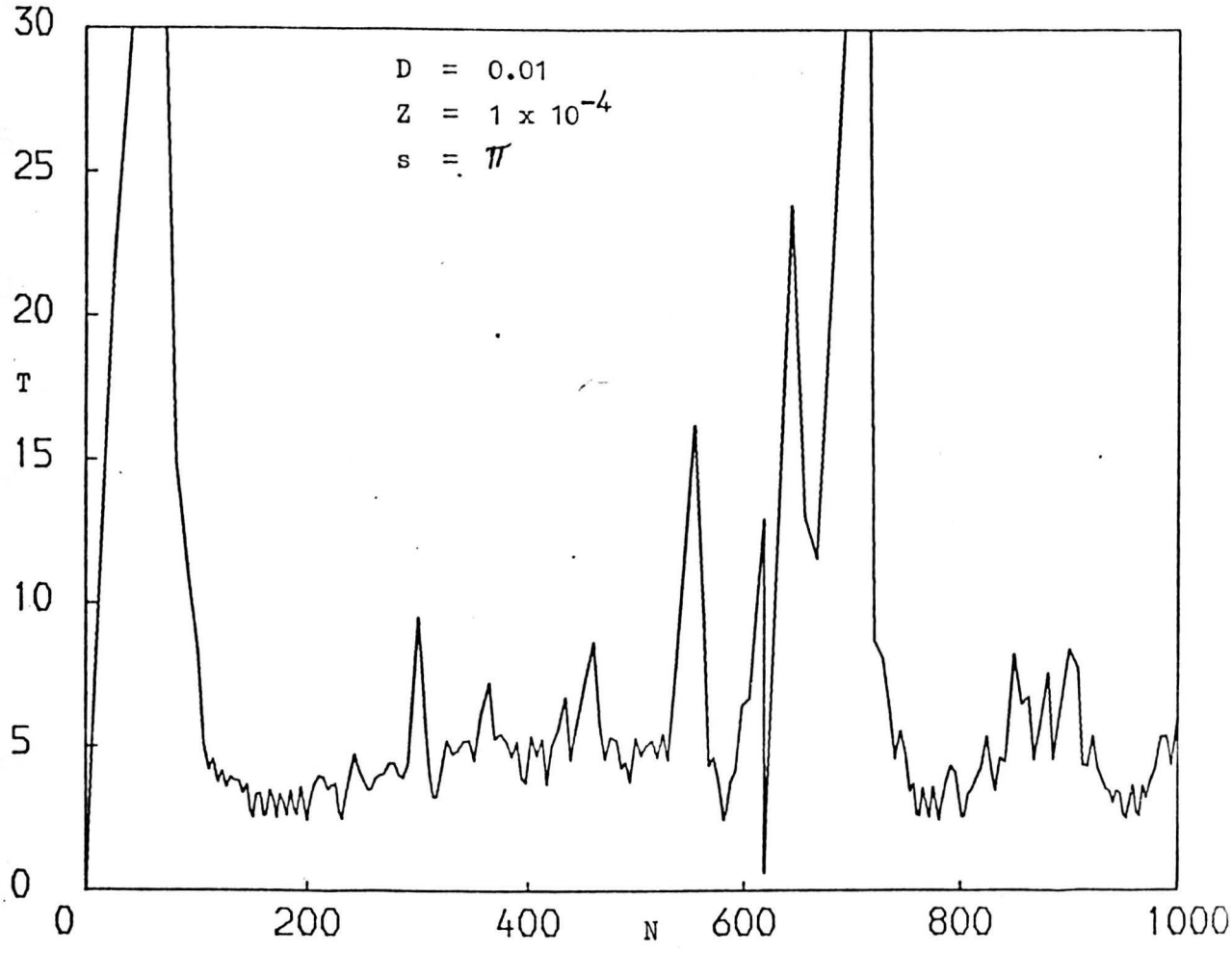

FIG. 6.12 PERIOD OF THE BALL CYCLE (IN TERMS OF THE TIP CYCLES) - NUMBER OF THE TIP CYCLES RELATIONSHIP

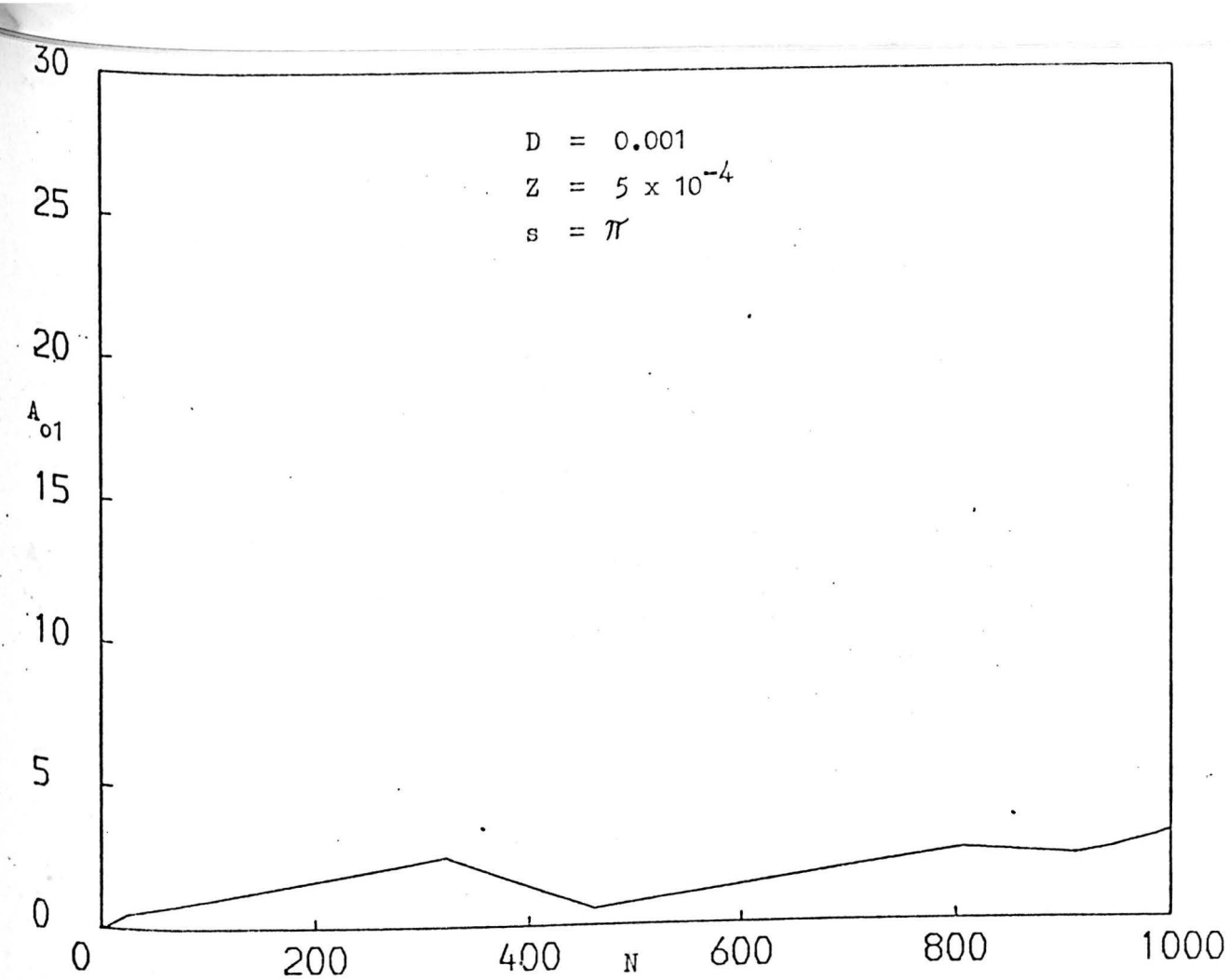

FIG. 6.13 RATIO OF THE BALL VELOCITY AFTER THE COLLISION WITH THE LOWER WALL TO THE MAXIMUM TIP VELOCITY - NUMBER OF THE TIP CYCLES RELATIONSHIP

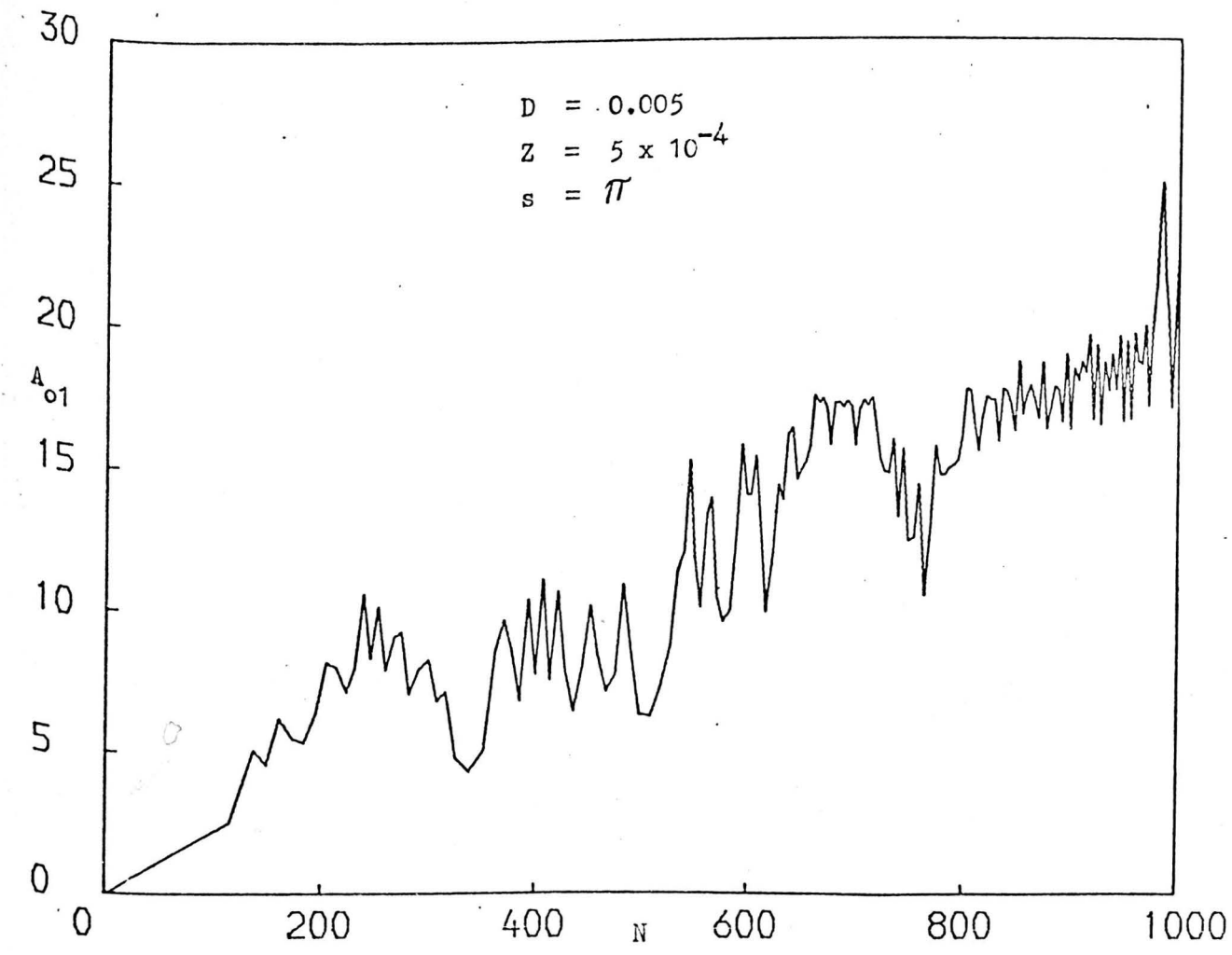

FIG. 6.14 RATIO OF THE BALL VELOCITY AFTER THE COLLISION WITH THE LOWER WALL TO THE MAXIMUM TIP VELOCITY - NUMBER OF THE TIP CYCLES RELATIONSHIP

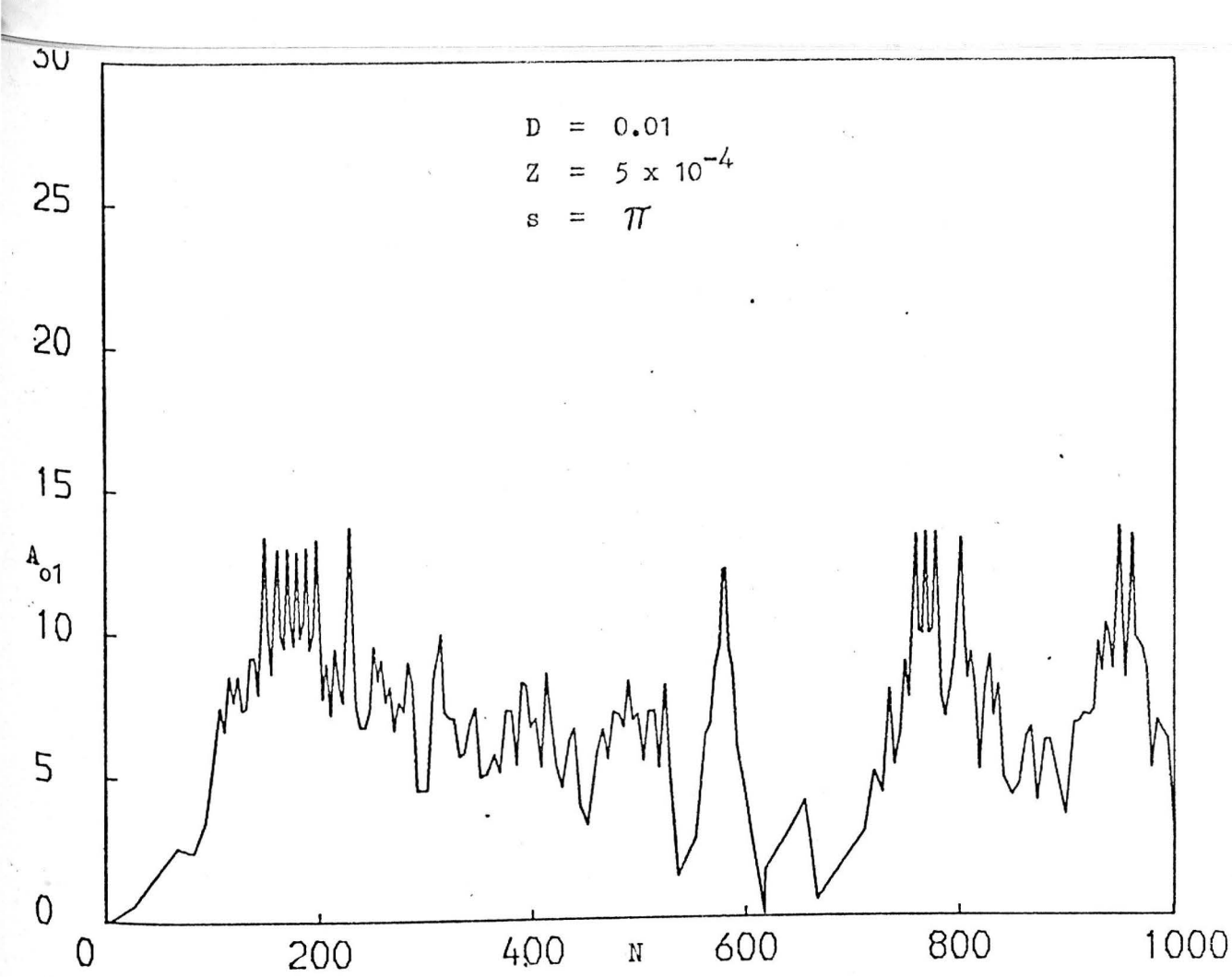

FIG. 6.15 RATIO OF THE BALL VELOCITY AFTER THE COLLISION WITH THE LOWER WALL TO THE MAXIMUM TIP VELOCITY - NUMBER OF THE TIP CYCLES RELATIONSHIP

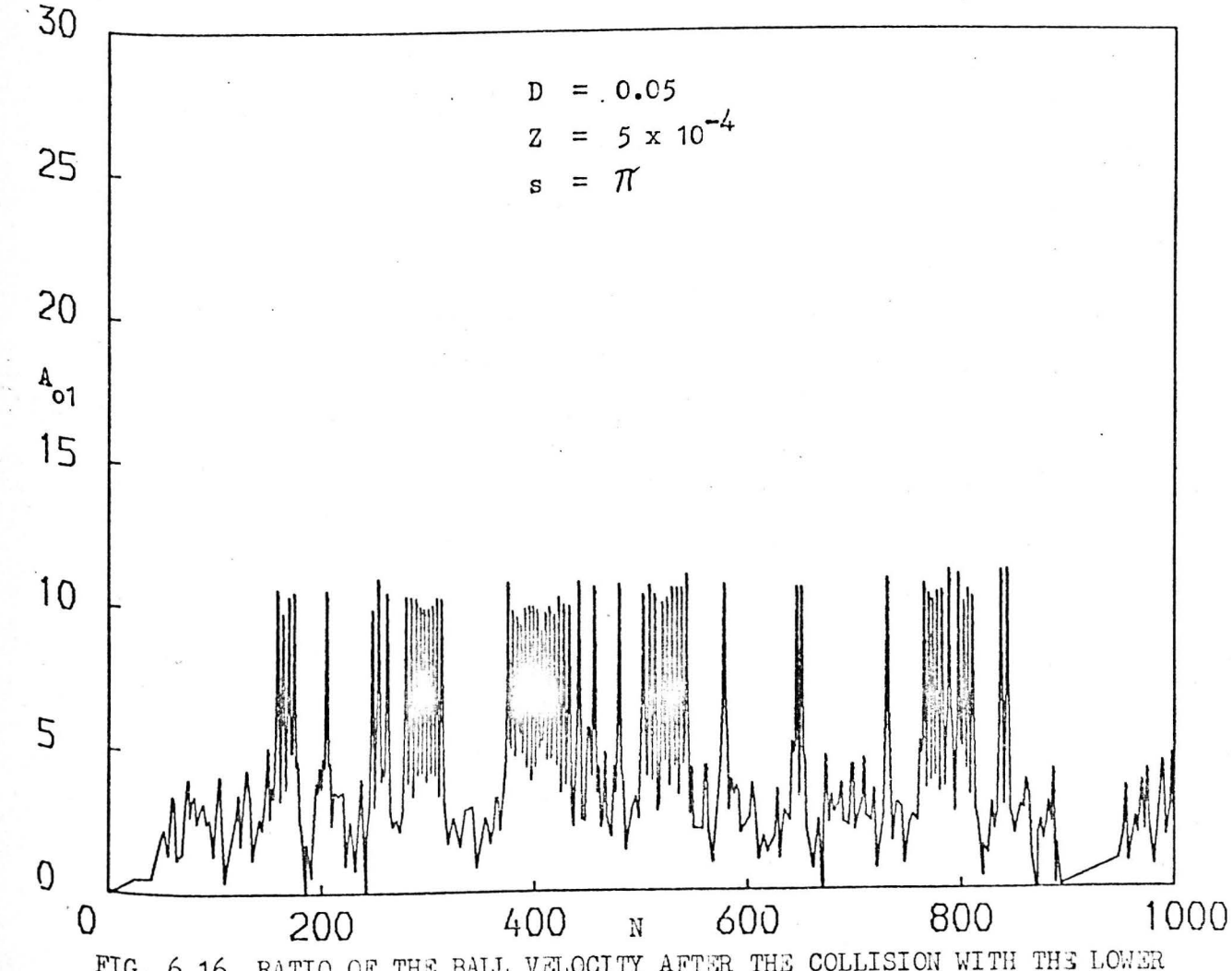

FIG. 6.16 RATIO OF THE BALL VELOCITY AFTER THE COLLISION WITH THE LOWER WALL TO THE MAXIMUM TIP VELOCITY - NUMBER OF THE TIP CYCLES RELATIONSHIP

6.4 RESULTS AND DISCUSSIONS

6.4.1 The Tip Moving Down at t = o

Figs. (6.3- 6.7) show plots of the period (T) of the ball cycle versus the tip cycles (N), for D in the range 0.001 - 0.1 and $Z = 5 \times 10^{-4}$. These figs. show that the ball was not in steady state motion. As mentioned in Chapter 3 (see section (3.4.1.1)), the reason for the unsteady state motion was that the impact occurred with improper phase.

These figs. also show that sometimes the ball was moving with repeatable periods, but this repeatability disappeared again, Figs. (6.6, 6.7).

It can be seen from these figs. that when D was increased, T increased. Also, as mentioned in Chapter 3, (see section (3.4.1.1)), the reason for this phenomenon was because the increase in D can be viewed as a decrease in the maximum gap (y_w) between the ball and the walls of the valves and hence T is expected to decrease.

These figs. also show that there was a more orderly pattern with increasing D.

Similar results were obtained for Z in the range 1×10^{-6} - 5×10^{-4}. The effect of increasing Z while keeping D constant is shown in figs. (6.8 - 6.12). These figs. show the T- N relationship for D = 0.01 and Z in the range 1×10^{-6} - 1×10^{-4}. These plots show that when Z was increased for constant D, the periods (T) were changed randomly.

Similar results were obtained for D in the range 0.001 - 0.1. Figs. (6.13 - 6.17) show the relationship between the ratio (A_{o1})

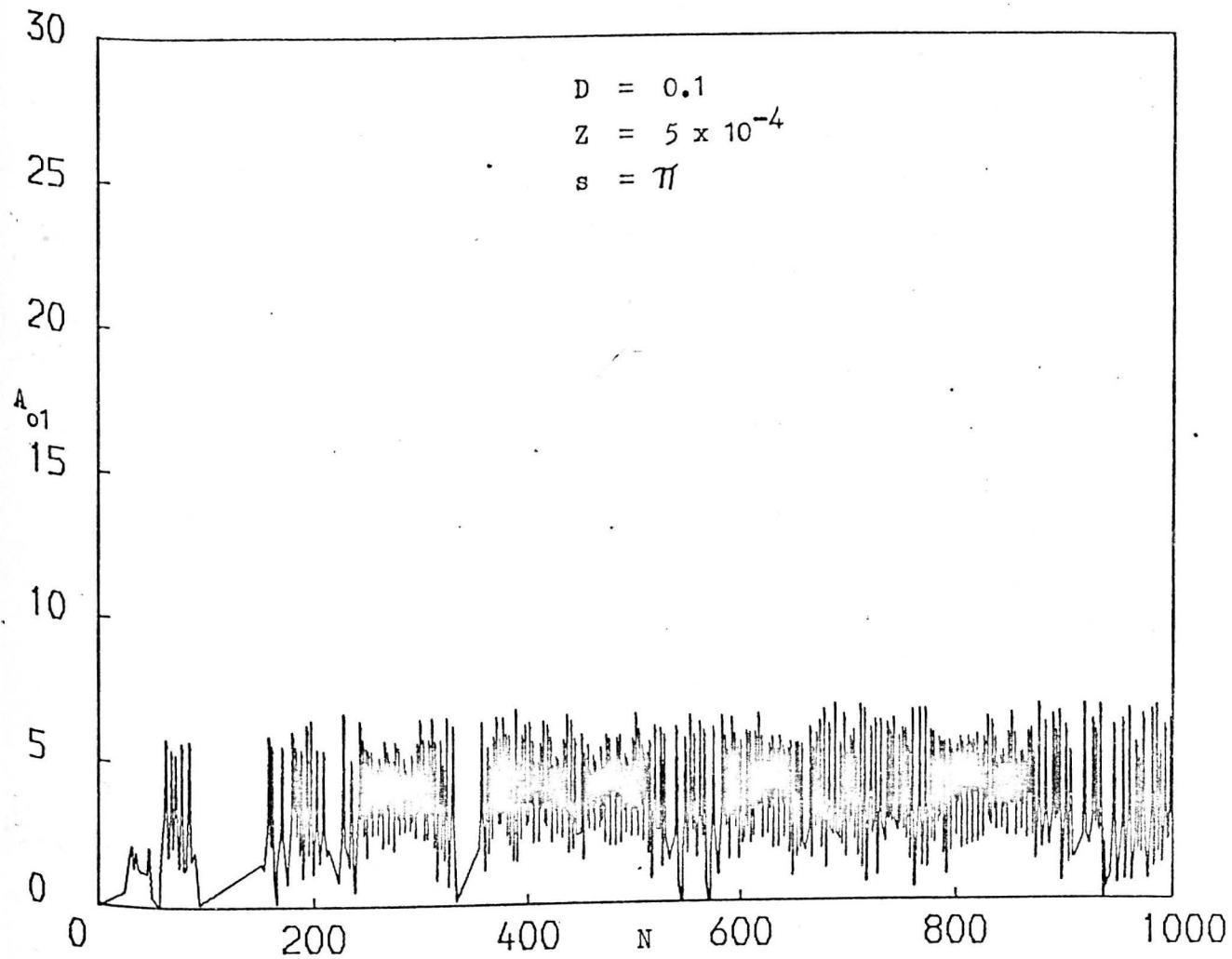

FIG. 6.17 RATIO OF THE BALL VELOCITY AFTER THE COLLISION WITH THE LOWER WALL TO THE MAXIMUM TIP VELOCITY - NUMBER OF THE TIP CYCLES RELATIONSHIP

of the ball velocity (v_{o1}) after the collision with the lower wall of the valve to the maximum velocity of the tip, versus the tip cycles (N), for a D range of 0.001 - 0.1 and Z = 5×10^{-4}. As found in Chapter 3 (see section (3.4.1.1)), A_{o1} was changing randomly with the increase of D. It can be seen from fig. (6.14) that A_{o1} increased with increasing N. Comparing this fig. with fig. (6.4), it can be seen that the period of the ball cycle was inversely proportional to the velocity of the ball after the collision with the lower wall, and then inversely proportional to the number of the tip cycles. The increase of the velocity at the ball after the collision is an attractive phenomenon. This phenomenon is good for response (i.e., the ball comes back to the seat as soon as the injector is switched off) but might be bad for wear.

Similar results were obtained for a Z range of 1×10^{-6} - 5×10^{-4}. Fig. (6.18) is a plot of the ratio (Y) of the gap (y) between the ball and the lower wall of the valve to the maximum gap (y_w) versus the tip cycles (N) for D = 0.005 and Z = 5×10^{-4}. This plot shows that the ball could not reach the top wall of the valve in the first cycle. This is because at the instance of separation of the ball from the tip, the velocity of the tip was very small (the tip motion built up in 5 ms).

It can be seen from this fig. that the time of the first cycle was significant compared to that of the remaining cycles.

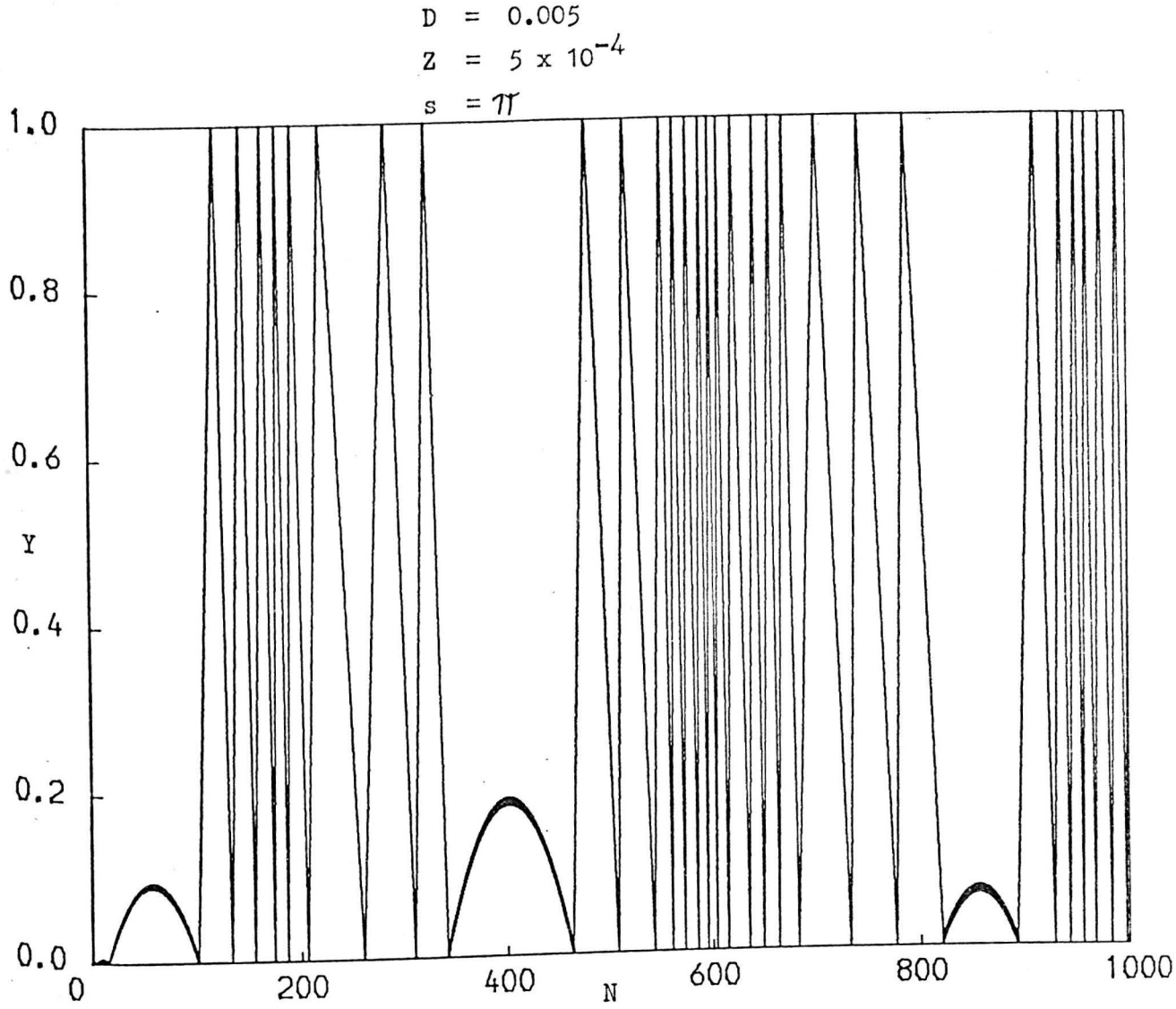

FIG. 6.18 RATIO OF THE GAP BETWEEN THE BALL AND THE LOWER WALL TO THE MAXIMUM GAP - NUMBER OF THE TIP CYCLES RELATIONSHIP

6.4.2 The Tip Moving Up at t = o

Fig. (6.19) is a plot of the period (T) of the ball cycle versus the tip cycles (N), for D = 0.05 and Z = 5×10^{-4}. This plot shows that the ball was again moving in unsteady state motion. It can be deduced from this plot that a change in the initial condition of the tip could change the motion of the ball, but the general features of the results remained the same, (see fig. (6.5)).

Similar results were obtained for D range 0.001 - 0.1 and Z range 1×10^{-6} - 5×10^{-4}.

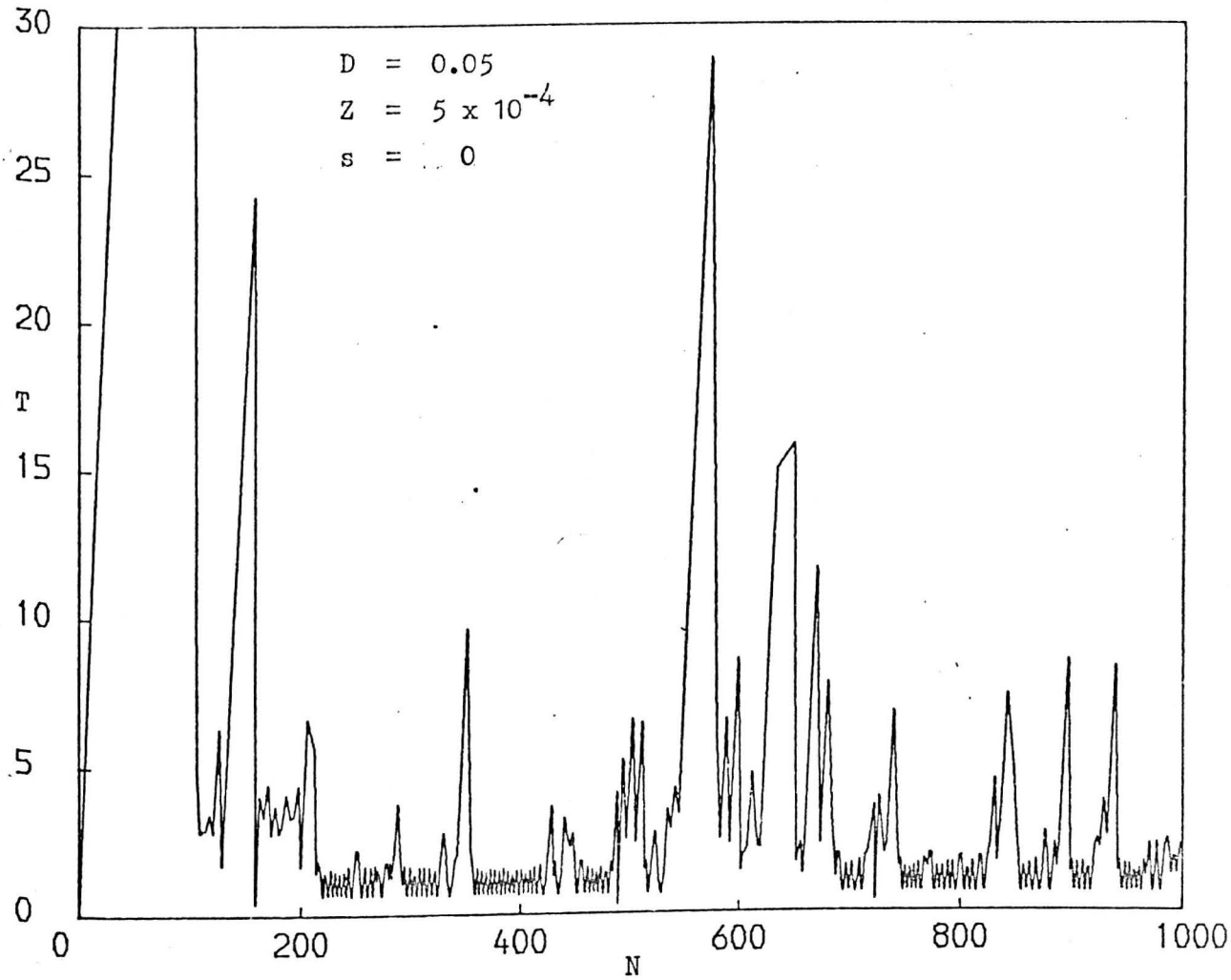

FIG. 6.19 PERIOD OF THE BALL (IN TERM OF THE TIP CYCLES) - NUMBER OF THE TIP CYCLES RELATIONSHIP

Chapter Seven

MODEL TESTS OF FLOW RATES AND BALL FLOW FORCE

7.1 INTRODUCTION

Measuring the flow force on the ball, the total flow rate and the inlet ports flow rates of the injector valve for each position of the ball is important in understanding the behaviour of the injector. The theoretical analysis of the ball motion which was described in Chapter 3 and in Chapter 6 was carried out without any fluid resistance. Knowledge of the fluid resistance is important in studying the actual behaviour of the ball.

Since the dimensions of the injector valve were too small to take these measurements accurately on the valve itself, a scale model to the injector valve should be constructed and the results of the measurements should be scaled to the injector valve.

This chapter describes the measurements of the flow force on the ball, the total flow rate and the inlet ports flow rates for each position of the ball, in a scale model of the injector valve.

The details of test apparatus, procedure and program, analysis of the results and discussions are given below.

7.2 TEST APPARATUS

Fig. (7.1) shows a photograph of the test apparatus used, while the layout is given in fig. (7.2). The test apparatus consisted of a model for the injector valve, instruments for measuring the static pressure at each inlet to the model, the flow rate at each inlet to the model and the liquid forces on the ball,

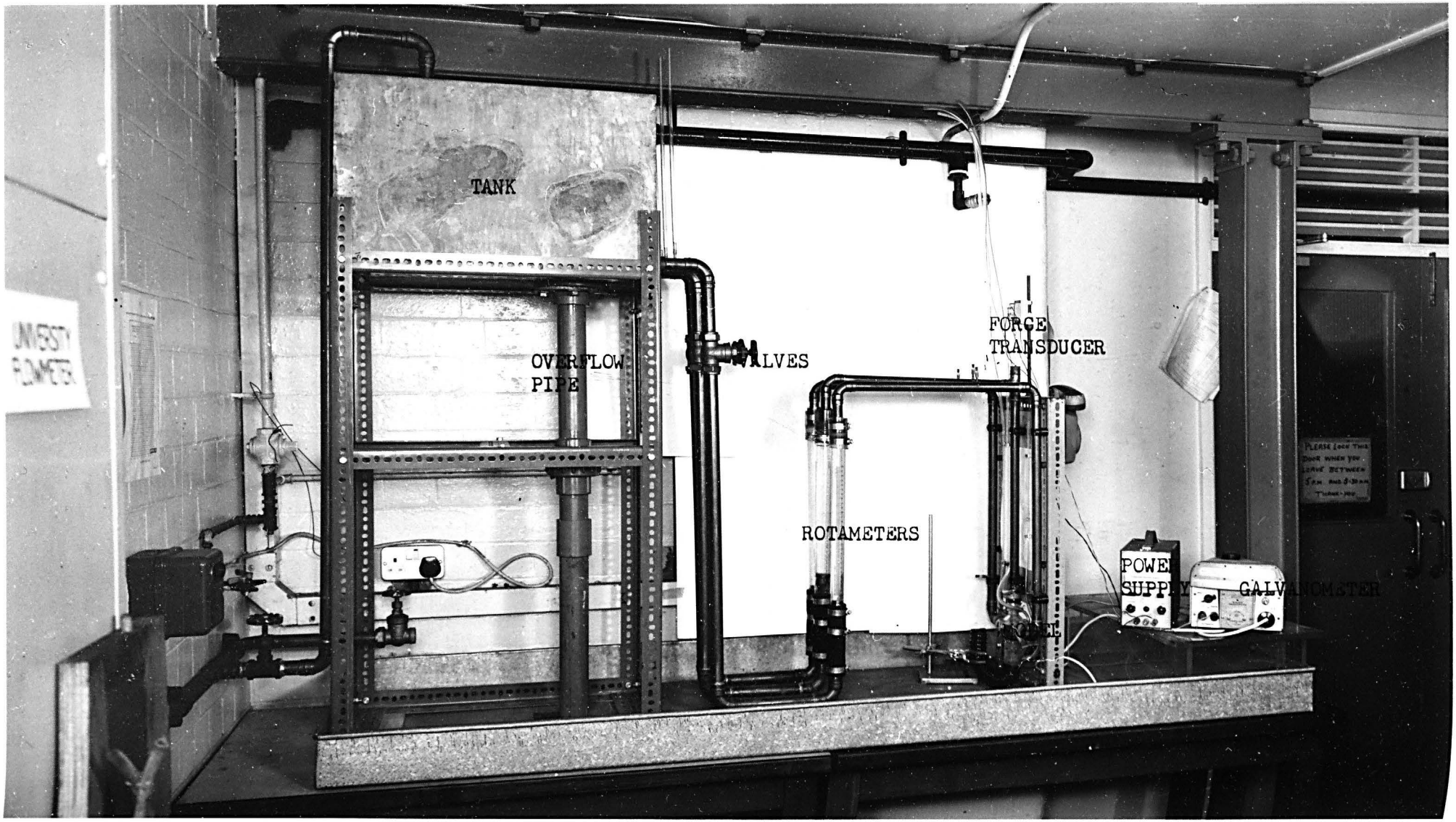

FIG. 7.1 APPARATUS FOR MEASURING FLOW FORCE AND FLOW RATES

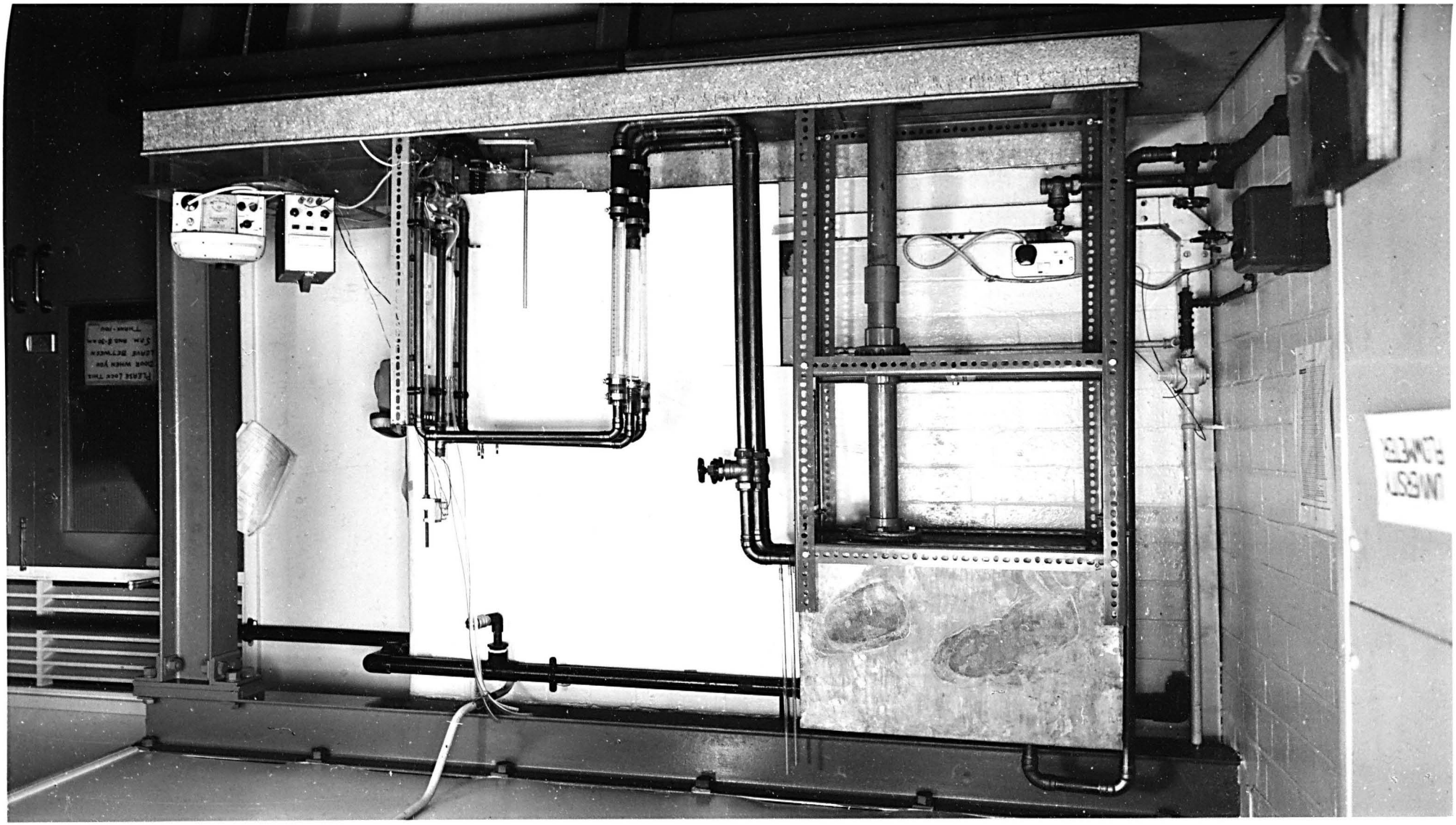

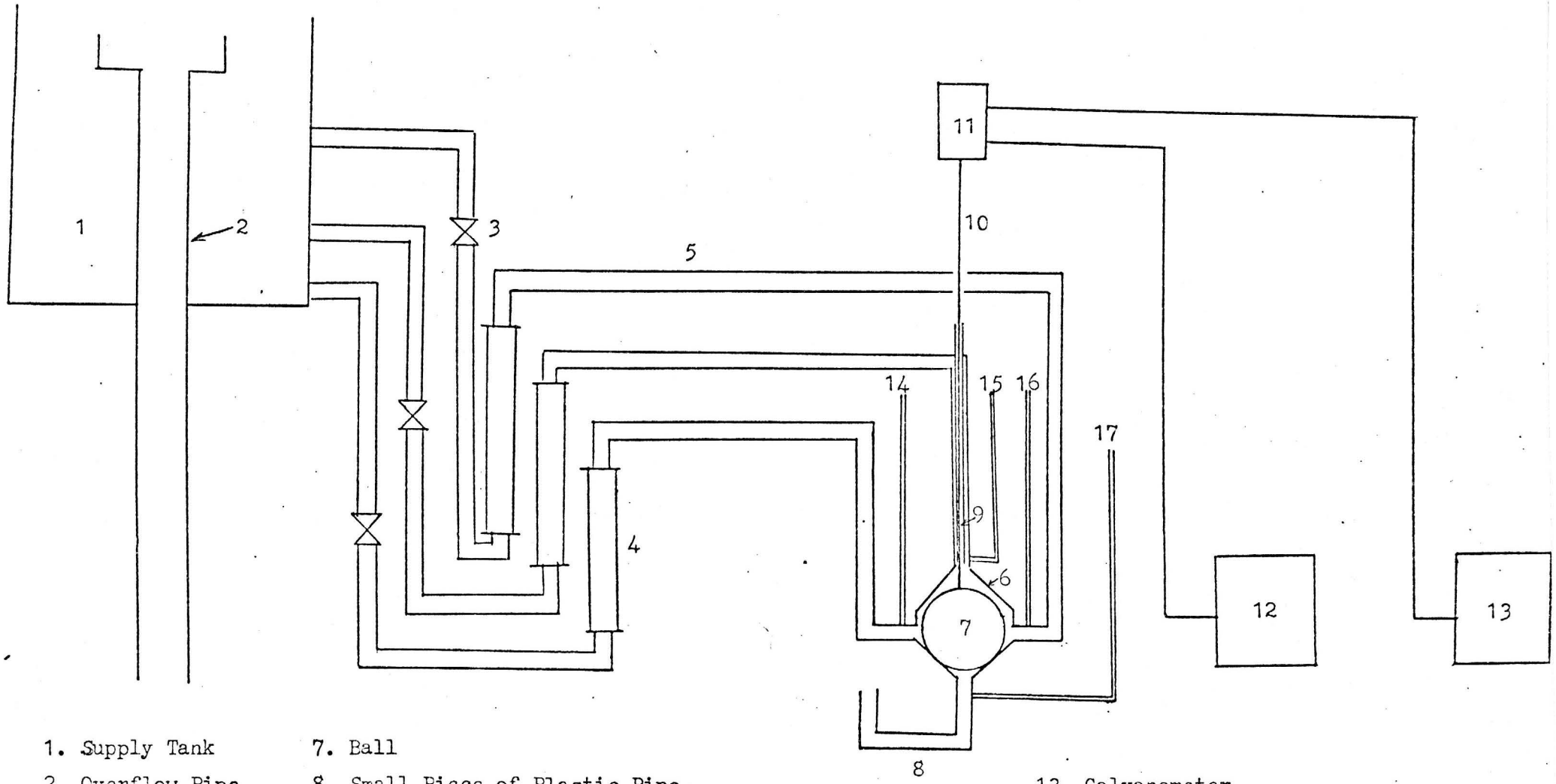

1. Supply Tank
2. Overflow Pipe
3. Valve
4. Rotameter
5. Pipe
6. Model
7. Ball
8. Small Piece of Plastic Pipe
9. Fine Tube
10. String
11. Force Transducer
12. Power Supply
13. Galvanometer
14. Vertical Manometer
15. Vertical Manometer
16. Vertical Manometer
17. Vertical Manometer

FIG. 7.2 LAYOUT OF THE APPARATUS

a supply tank, pipes and valves.

Fig. (7.3) shows a photograph of the model, and the layout is given in fig. (7.4).

The model was made geometrically similar to the injector valve and the scale factor was 20.6:1. The boundaries of the model were made from Perspex and from two parts. The upper part contained the top inlet and the lower part contained the two side inlets. The two parts were connected by screws. The ball of the model was made from a hard wood.

Since the forces which acted on the flow of the injector valve were viscous, pressure and inertia forces, Reynolds numbers (Re) of the two flows were kept the same to satisfy the condition of the dynamic similarity. By using the equality of Re of the two flows, it was found that with the scale factor 20.6, the water was a suitable fluid for measuring the flow velocities in the model corresponding to the range of the flow velocities in the injector valve (when the fluid of the injector valve was Gasoline of 0.718 specific gravity).

Each inlet of the model was connected to the supply tank by a Brass pipe.

Since the supply pressure at each side inlet of the injector valve was equal, this condition was also applied to the model by making the size and the length of the pipes connecting the side inlets to the supply tank equal, i.e., the loss in the total head due to the friction was the same in each pipe.

The flow rate for each inlet was measured by a rotameter (Rotameter Manufacturing Co.) placed between the inlet and the supply tank, and controlled by a valve (Gate Valve) placed between the

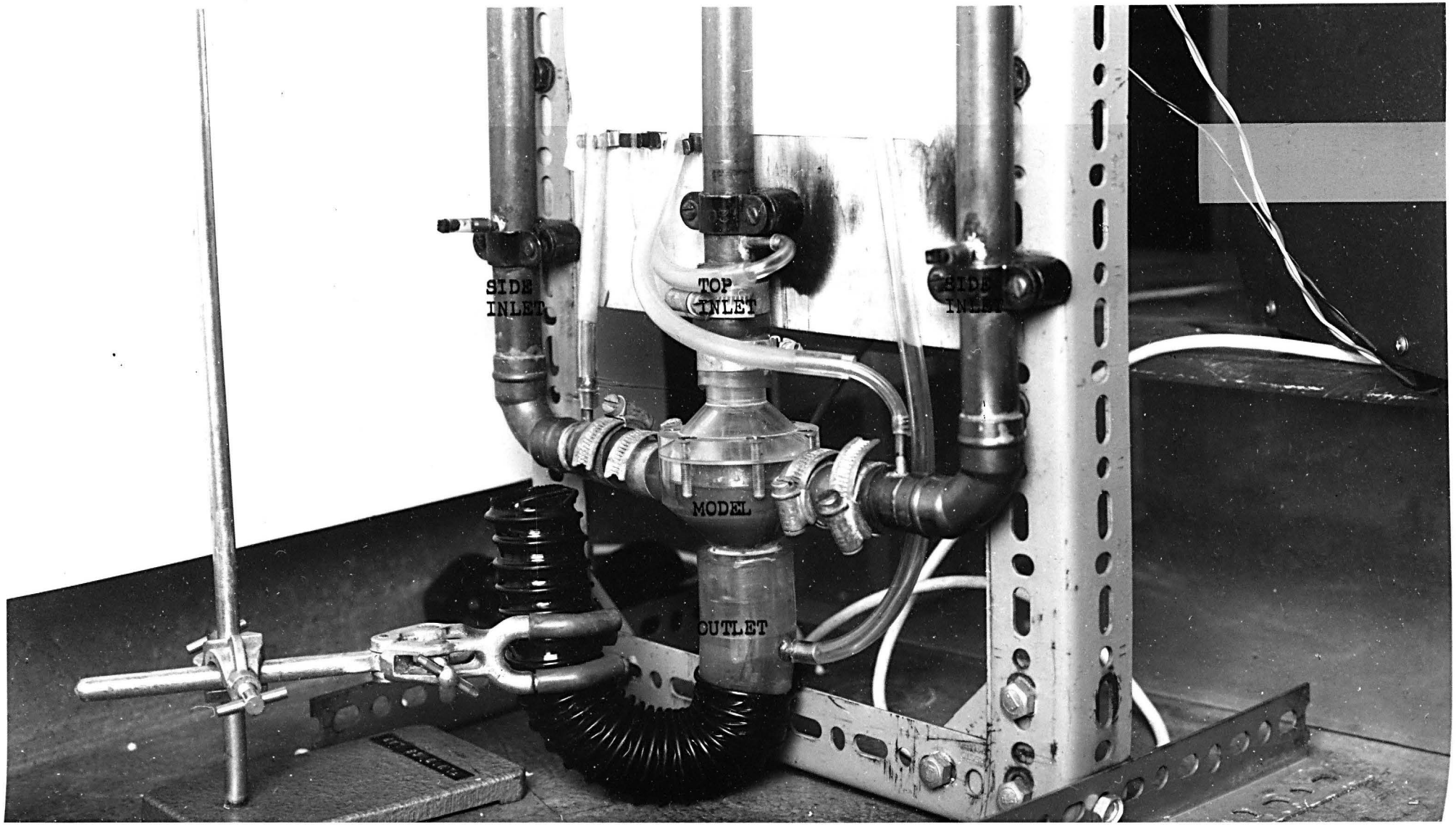

FIG. 7.3 MODEL OF THE INJECTOR VALVE

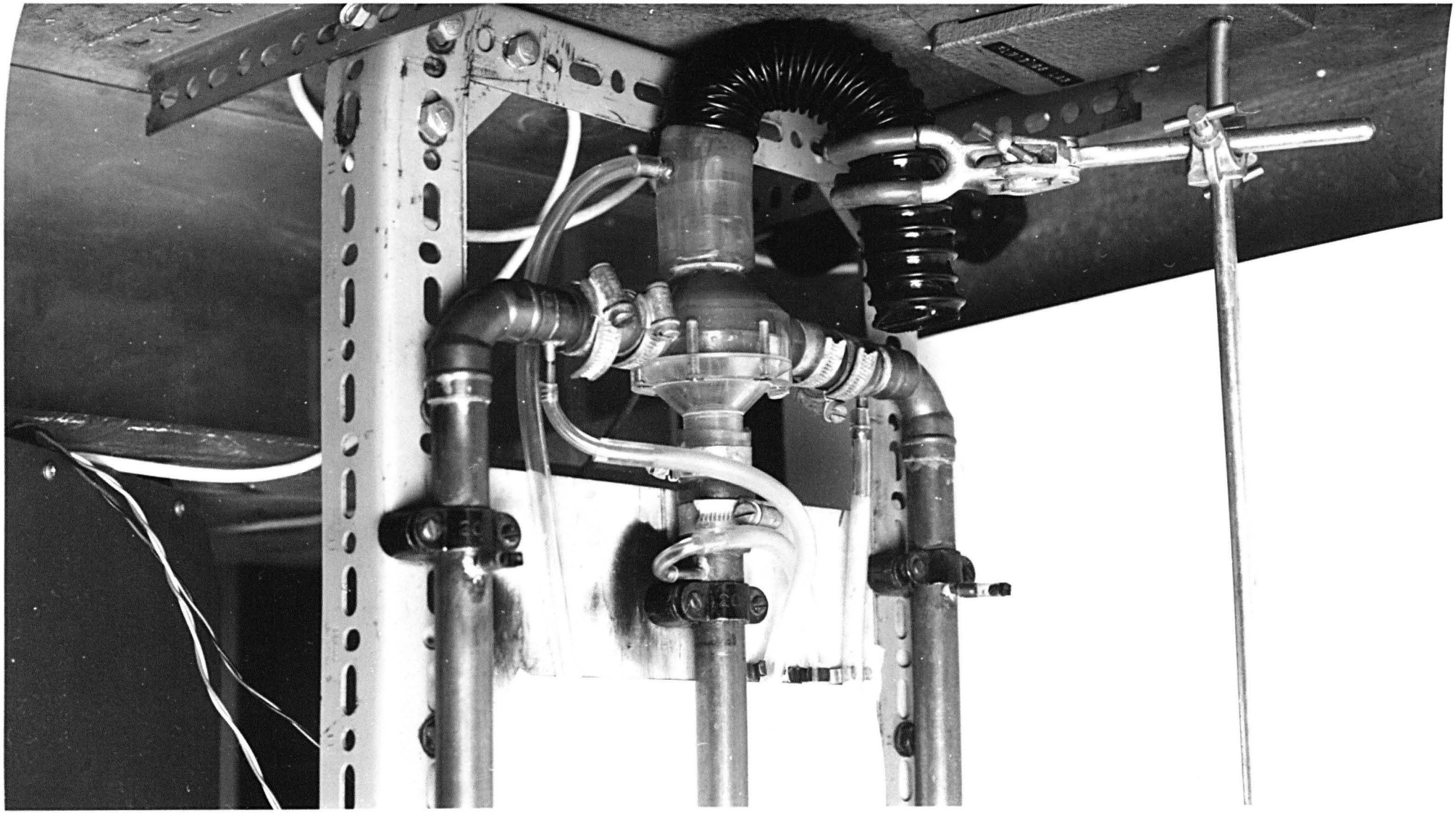

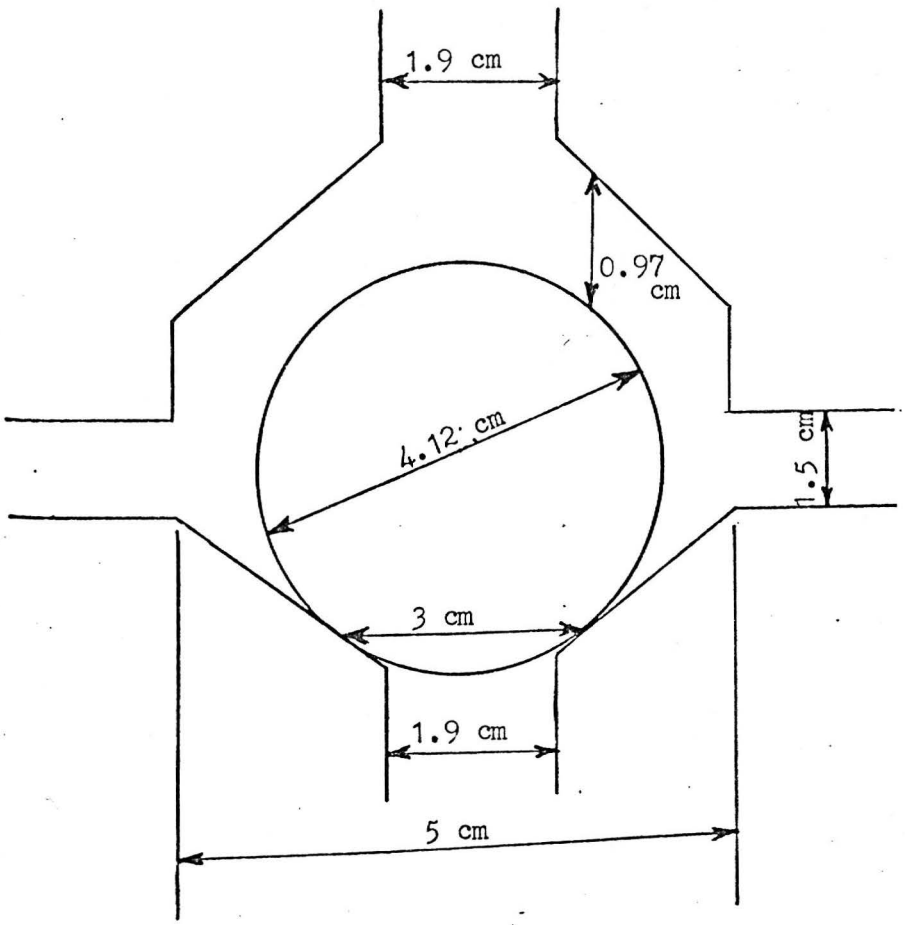

FIG. 7.4 LAYOUT OF THE MODEL

rotameter and the supply tank. The water was delivered to the supply tank by a pump from another large tank. The level of the water in the supply tank was kept constant during the measurements by an overflow pipe placed in the supply tank.

A pressure tap was placed at each inlet of the model for measuring the static pressure by a vertical manometer. Another pressure tap was placed at the outlet of the model for measuring the static pressure by a vertical manometer. A small piece of plastic pipe was connected to the outlet of the model to avoid the entrance of the air to the model during the measurements.

The ball was connected to the force transducer (Pye Ether, type VF1) by a strong string passing through fine tube. The other end of the ball was connected to a small piece of a brass bar passing through a guide to keep the centre of the ball always on the vertical centre line of the model.

The force transducer was fixed rigidly on a plate which could be positioned anywhere along the length of a screw bar. This was achieved by means of two nuts and a spring.

The electric power was supplied to the force transducer by power supply (Farnell, type E30/2). The output of the force transducer was read on galvanometer (W. G. Pye & Co. Ltd.).

7.3 TEST PROGRAM

In each test the flow force on the ball, the flow rates of the inlets and the static pressure at each inlet and at the outlet were measured. The range of the total flow rate from the model was $0-40\ {}^{l}/_{m}$. These measurements were done for one position of the

ball in the model. When the measurements were done, the position of the ball was then changed and the test was repeated.

7.4 TEST PROCEDURE

Before starting the test the Rotameters were calibrated by collecting the weighing water. Also the force transducer was calibrated by putting weights on the ball which was connected by a wire to the force transducer and reading the corresponding voltage on the galvanometer. To start the test the ball was fixed at the upper wall of the model. The position of the force transducer was read by a ruler fixed on a screw bar. This position of the transducer was considered as the zero position of the ball. The ball was then moved 1 mm from the upper wall of the model. At this position the indicator of the Galvanometer was fixed at the zero number on the scale. This position of the indicator represented zero fluid forces on the ball.

The valves were then opened until all the air escaped from the model and from the pipes.

Since the supply (total) pressure at each inlet of the injector valve was equal, and the flow rate from each side inlet was equal, these conditions were also applied for the model. The flow rate from each side inlet of the model was kept identical for each flow rate from the top inlet of the model. The flow velocity of each inlet of the model was then calculated. By measuring the static pressure at each inlet, the supply pressure at each inlet of the model was calculated. When the supply pressure at each inlet of the model was not the same, the flow rates were changed and the

procedure was repeated again until the supply pressure at each inlet of the model became identical. Then the readings from the Rotameter of each inlet, from the manometer at each inlet, from the manometer at the outlet and from the Galvanometer were taken. The flow rates of each inlet of the model were then changed and the same procedure was repeated again.

The ball was then positioned at 2 mm from the upper wall of the model. The same procedure was repeated until the measurements were taken for all the positions of the ball in the model.

7.5 MEASURING ANALYSIS OF THE EXPERIMENTAL DATA

In the following analysis it is assumed that the ball of the injector valve was in a similar position of that of the model, but with zero velocity.

The flow rate from the top inlet of the injector valve was calculated from the following equations:

$$R_{ev} = R_{em} , \qquad (7.1)$$

i.e.,

$$\frac{V_{vt}\ D_v}{\nu_v} = \frac{V_{mt}\ D_m}{\nu_m} .$$

where R_{ev} represents the Reynoldsnumber of the injector valve, R_{em} the Reynoldsnumber of the model, V_{vt} flow velocity at the top inlet of the valve, D_v diameter of the ball of the valve, ν_v kinematic viscosity of the liquid in the valve, V_{mt} flow velocity at the top inlet of the model, D_m diameter of the ball of the model

and ν_m kinematic viscosity of the liquid in the model.

Therefore

$$V_{vt} = V_{mt} \frac{D_m}{D_v} \frac{\nu_v}{\nu_m} \tag{7.2}$$

But

$$Q_{vt} = A_{vt} V_{vt} , \tag{7.3}$$

and

$$Q_{mt} = A_{mt} V_{mt} \tag{7.4}$$

where Q_{vt} represents flow rate at the top inlet of the valve, A_{vt} area of the top inlet of the valve, Q_{mt} flow rate at the top inlet of the model and A_{mt} area of the top inlet of the model.

Therefore

$$Q_{vt} = Q_{mt} \frac{A_{vt}}{A_{mt}} \frac{D_m}{D_v} \frac{\nu_v}{\nu_m} \tag{7.5}$$

But

$$A_{vt} = \pi \frac{d_{vt}^2}{4} , \quad \text{and}$$

$$A_{mt} = \pi \frac{d_{mt}^2}{4}$$

where d_{vt} represents the diameter of the top inlet of the valve and d_{mt} the diameter of the top inlet of the model.

And

$$\frac{d_{vt}}{d_{mt}} = \frac{D_m}{D_v}$$

Therefore

$$Q_{vt} = Q_{mt} \frac{d_{vt}}{d_{mt}} \frac{\nu_v}{\nu_m} \tag{7.6}$$

By the same procedure the side inlets flow rate (Q_{vs}) was calculated.

Since the Euler number for pressure loss must be identical for valve and model at the same Reynolds number, the supply pressure (P_{vt}) at the top inlet of the valve can be found as follows:

$$\frac{P_{vt} - p^*_{vo}}{\frac{1}{2} \rho_v V^2_{vo}} = \frac{P_{mt} - p^*_{mo}}{\frac{1}{2} \rho_m V^2_{mo}} \tag{7.7}$$

where

$$P_{vt} = p_{vt} + \tfrac{1}{2} \rho_v V^2_{vt} + \rho_v g z_{vt} , \tag{7.8}$$

$$p^*_{vo} = p_{vo} + \rho_v g z_{vo} , \quad (p_{vo} = p_a = 0) , \tag{7.9}$$

$$P_{mt} = p_{mt} + \tfrac{1}{2} \rho_m V^2_{mt} + \rho_m g z_{mt} \tag{7.10}$$

and

$$p^*_{mo} = p_{mo} + \rho_m g z_{mo} \tag{7.11}$$

P_{vt} represents supply pressure at the top inlet of the valve, p^*_{vo} piezometric pressure at the outlet of the valve, P_{mt} supply pressure at the top inlet of the model, p^*_{mo} piezometric pressure at the outlet of the model, V_{vo} velocity at the outlet of the

valve, V_{mo} velocity at the outlet of the model, p_{vt} static pressure at the top inlet of the valve, g gravitational acceleration, z_{vt} height of the top inlet of the valve from the datum, p_{vo} static pressure at the outlet of the valve, p_a atmospheric pressure, z_{vo} height of the outlet of the valve from the datum, p_{mt} static pressure at the top inlet of the model, z_{mt} height of the top inlet of the model from the datum, p_{mo} static pressure at the outlet of the model and z_{mo} height of the outlet of the model from the datum.

Therefore

$$P_{vt} = P_{mt} - p^*_{mo} \frac{\rho_v}{\rho_m} \left(\frac{V_{vo}}{V_{mo}}\right)^2 + p^*_{vo} \qquad (7.12)$$

Since the energy of the flow at the outlet of the injector valve was not used again for the valve and dissipated in the atmosphere, the pressure at the outlet of the valve was assumed static, and the same assumption was made for the model.

Since the flow force coefficient must be identical for valve and model at the same Reynolds number, the flow force (F_{vf}) on the ball of the valve can be found as follows:-

$$\frac{F_{vf}}{\frac{1}{2} \rho_v D_v^2 V_{vt}^2} = \frac{F_{mf}}{\frac{1}{2} \rho_m D_m^2 V_{mt}^2} \qquad (7.13)$$

i.e.

$$F_{vf} = F_{mf} \frac{\rho_v}{\rho_m} \left(\frac{D_v}{D_m}\right)^2 \left(\frac{V_{vt}}{V_{mt}}\right)^2 \qquad (7.14)$$

where F_{vf} represents flow force on the ball of the valve and F_{mf} flow force on the ball of the model.

The force transducer measured the net forces (F_e) on the ball, i.e., the flow force (positive in downward direction) minus the buoyancy force (F_{mb}) (negative in upward direction)

$$F_e = F_{mf} - F_{mb} \tag{7.15}$$

i.e.,

$$F_{mf} = F_e + F_{mb} .$$

7.6 RESULTS AND DISCUSSIONS

Figs. (7.5- 7.9) show the scaled relationship between the total flow rate from the injector valve (Q_{vT}), the side inlets flow rate (Q_{vs}) and the top inlet flow rate (Q_{vt}) with the supply pressure (P_v) of range 5-- 60 psi for various positions of the ball in the injector valve. These figs. show that when p_v was increased, Q_{vT}, Q_{vs} and Q_{vt} increased very nearly as the square root of pressure.

Figs. (7.10- 7.12) represent plots of Q_{vT}, Q_{vs} and Q_{vt} versus the position (y) of the ball from the seat, for P_v range 20- 60 psi. These figs. show that when the ball was lifted from the seat for 0.14 mm, Q_{vT}, Q_{vs} and Q_{vt} increased. This is because in this region the resistance (R_4) due to the area under the ball (see fig. (7.13)) was the main variable resistance to the flow. When the ball was lifted from the seat, R_4 increased and hence the flow rates increased.

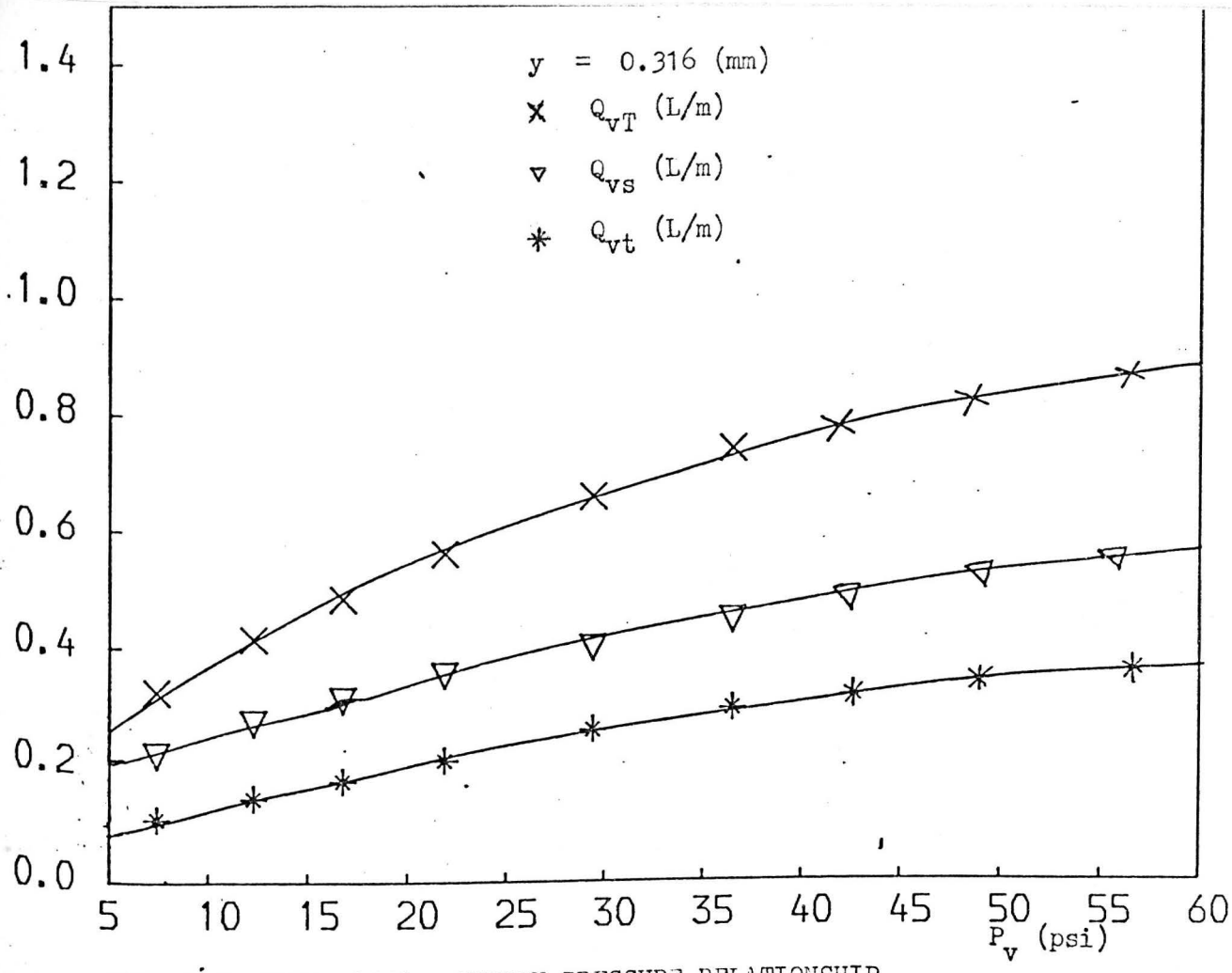

FIG. 7.5 FLOW RATES - SUPPLY PRESSURE RELATIONSHIP

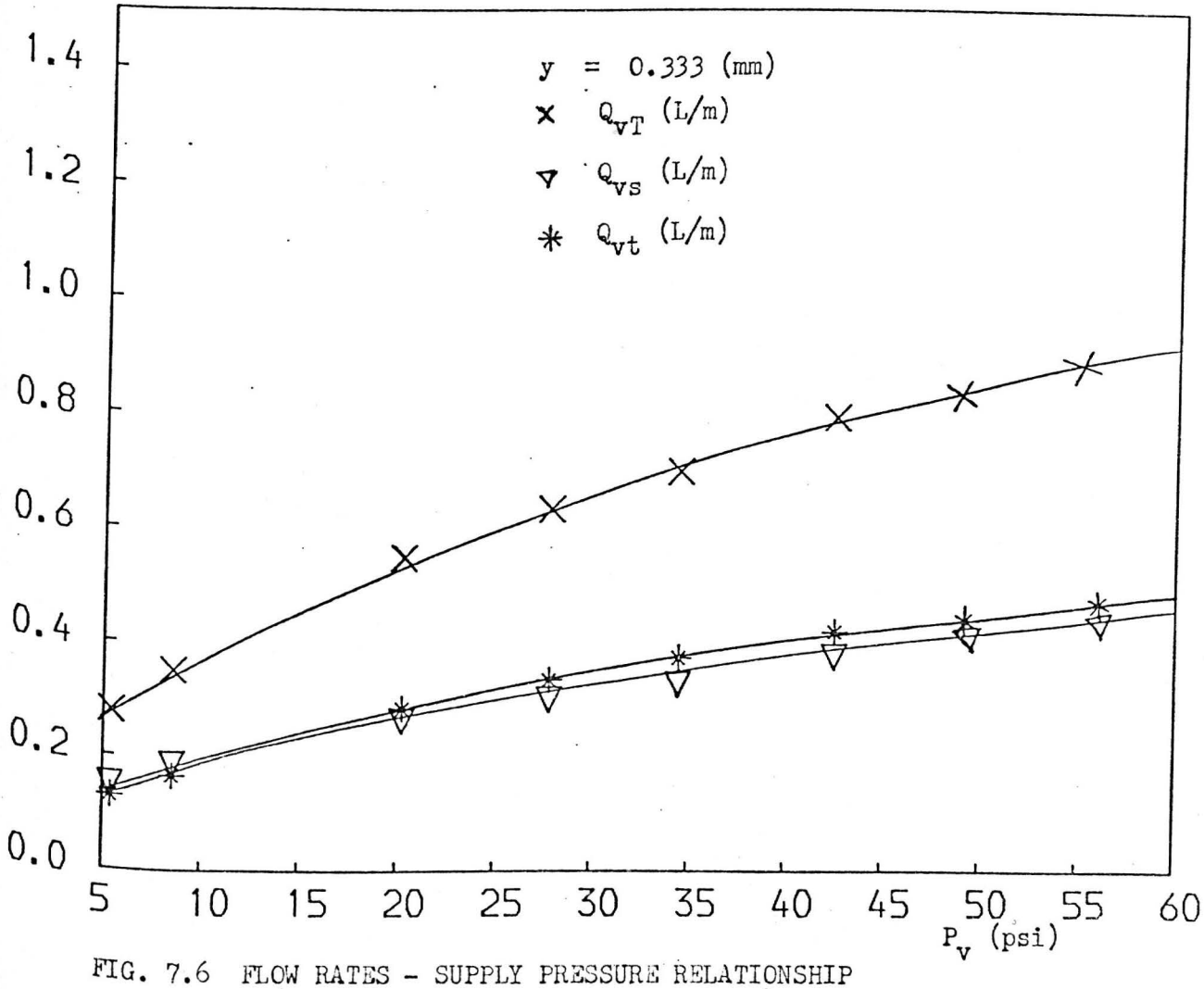

FIG. 7.6 FLOW RATES - SUPPLY PRESSURE RELATIONSHIP

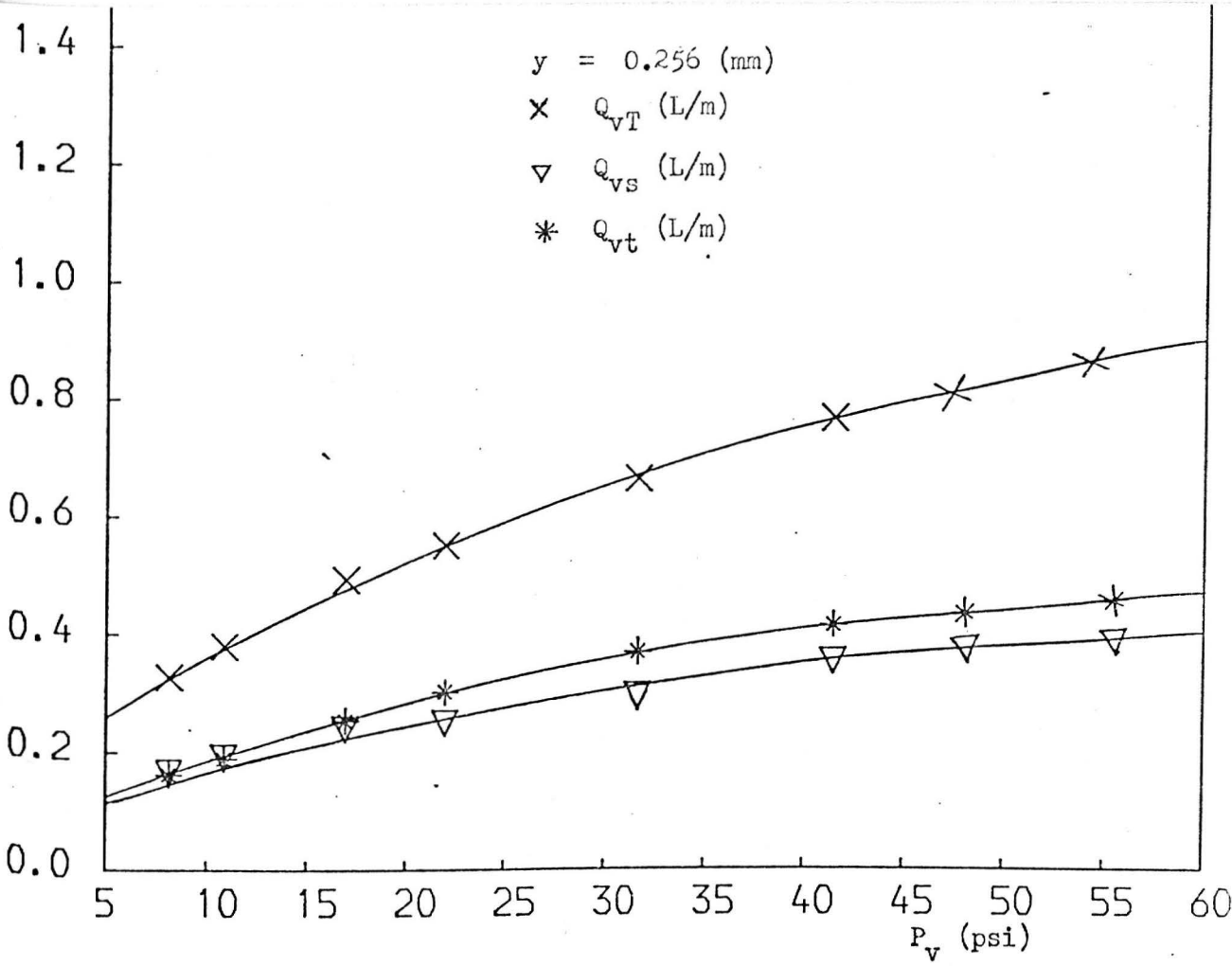

FIG. 7.7 FLOW RATES - SUPPLY PRESSURE RELATIONSHIP

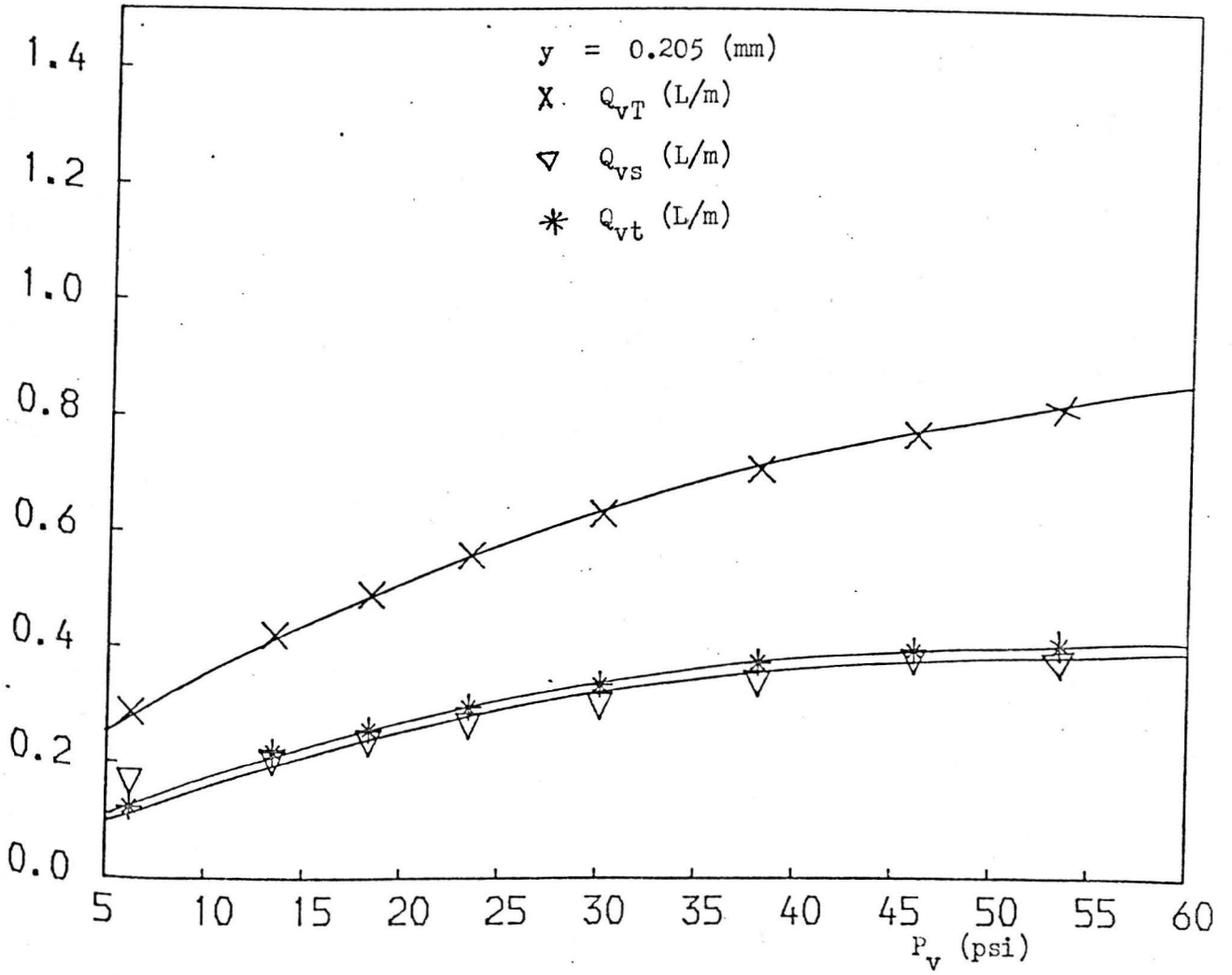

FIG. 7.8 FLOW RATES - SUPPLY PRESSURE RELATIONSHIP

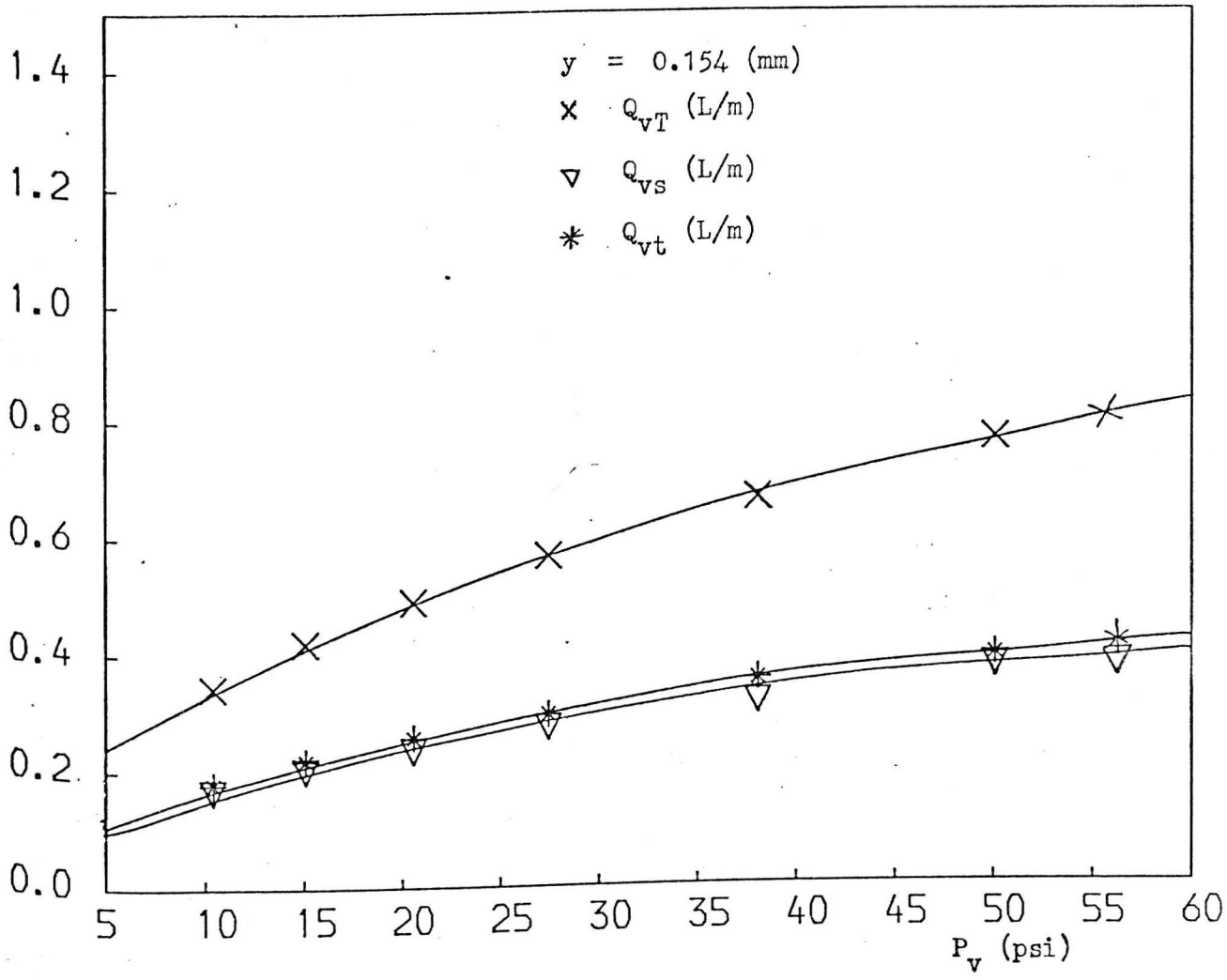

FIG. 7.9 FLOW RATES - SUPPLY PRESSURE RELATIONSHIP

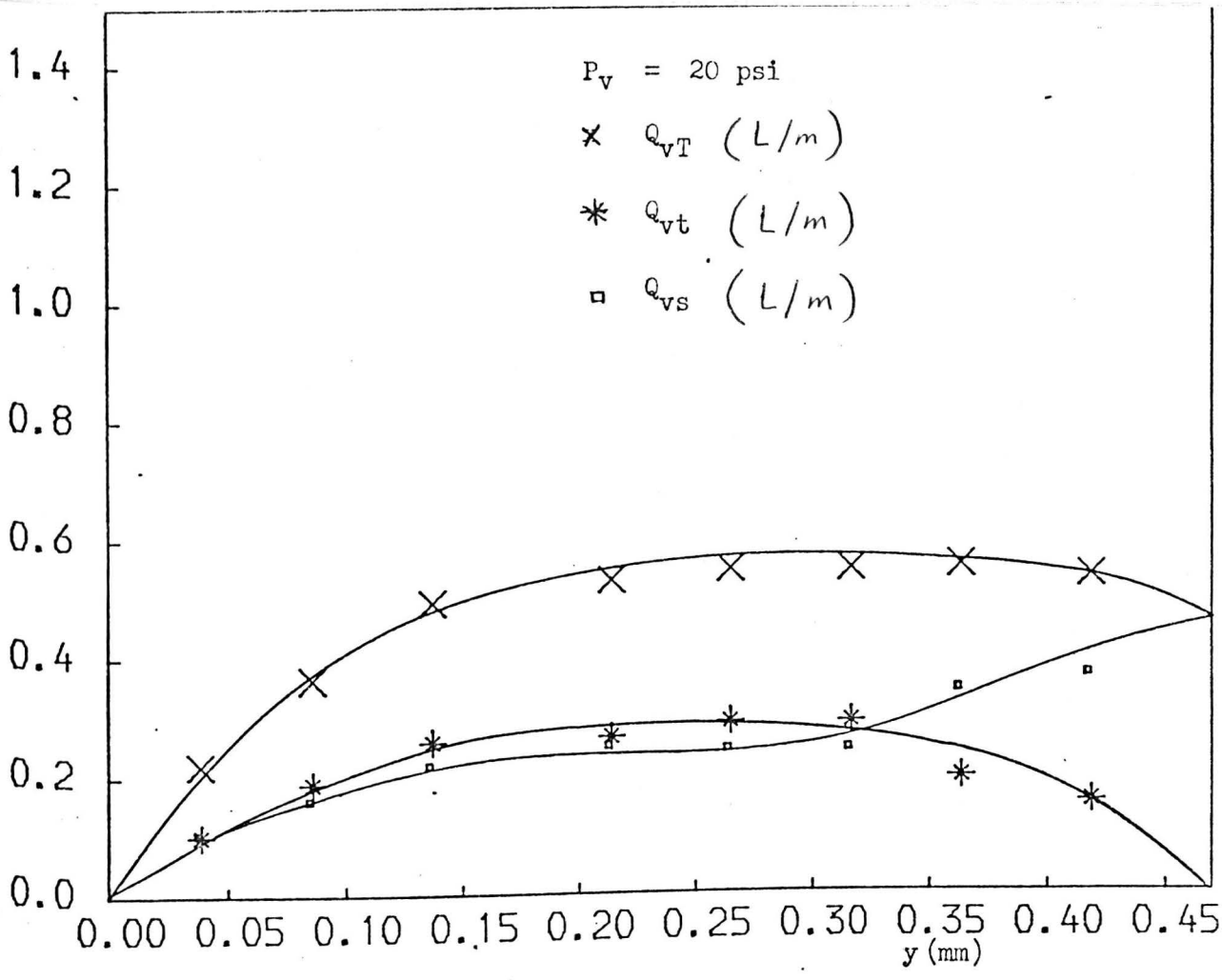

FIG. 7.10 FLOW RATES - POSITION OF THE BALL FROM THE SEAT RELATIONSHIP

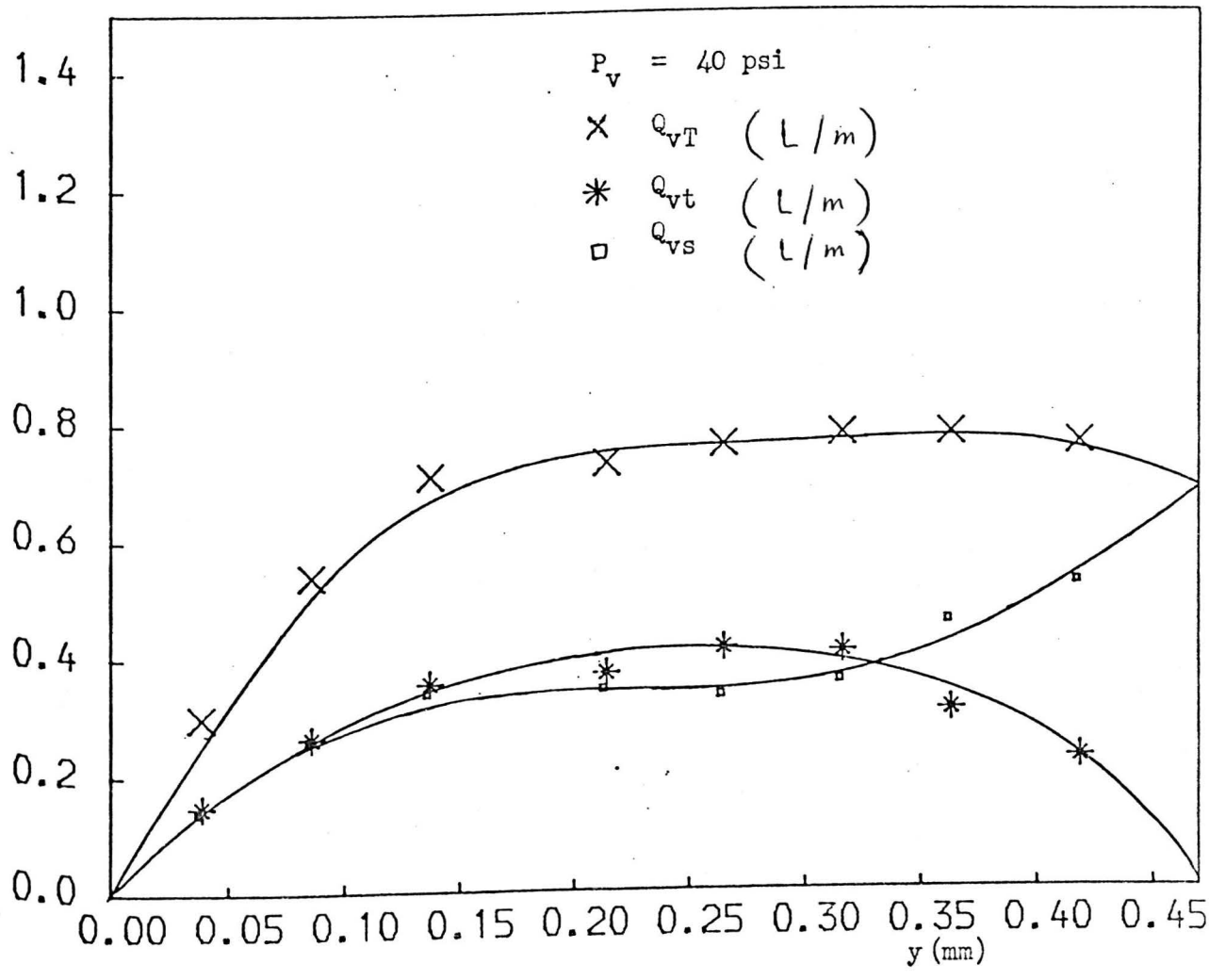

FIG. 7.11 FLOW RATES - POSITION OF THE BALL FROM THE SEAT RELATIONSHIP

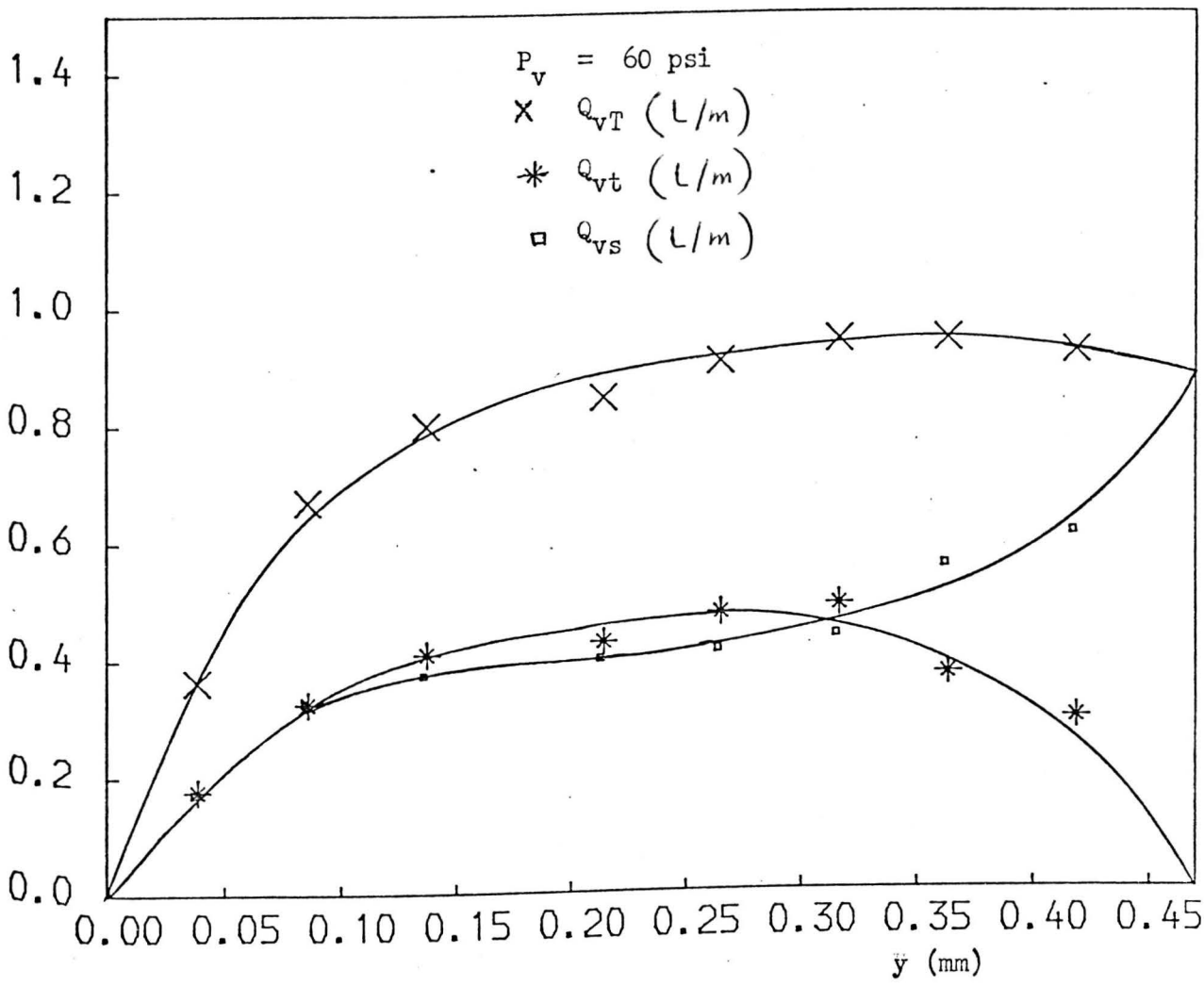

FIG. 7.12 FLOW RATES - POSITION OF THE BALL FROM THE SEAT RELATIONSHIP

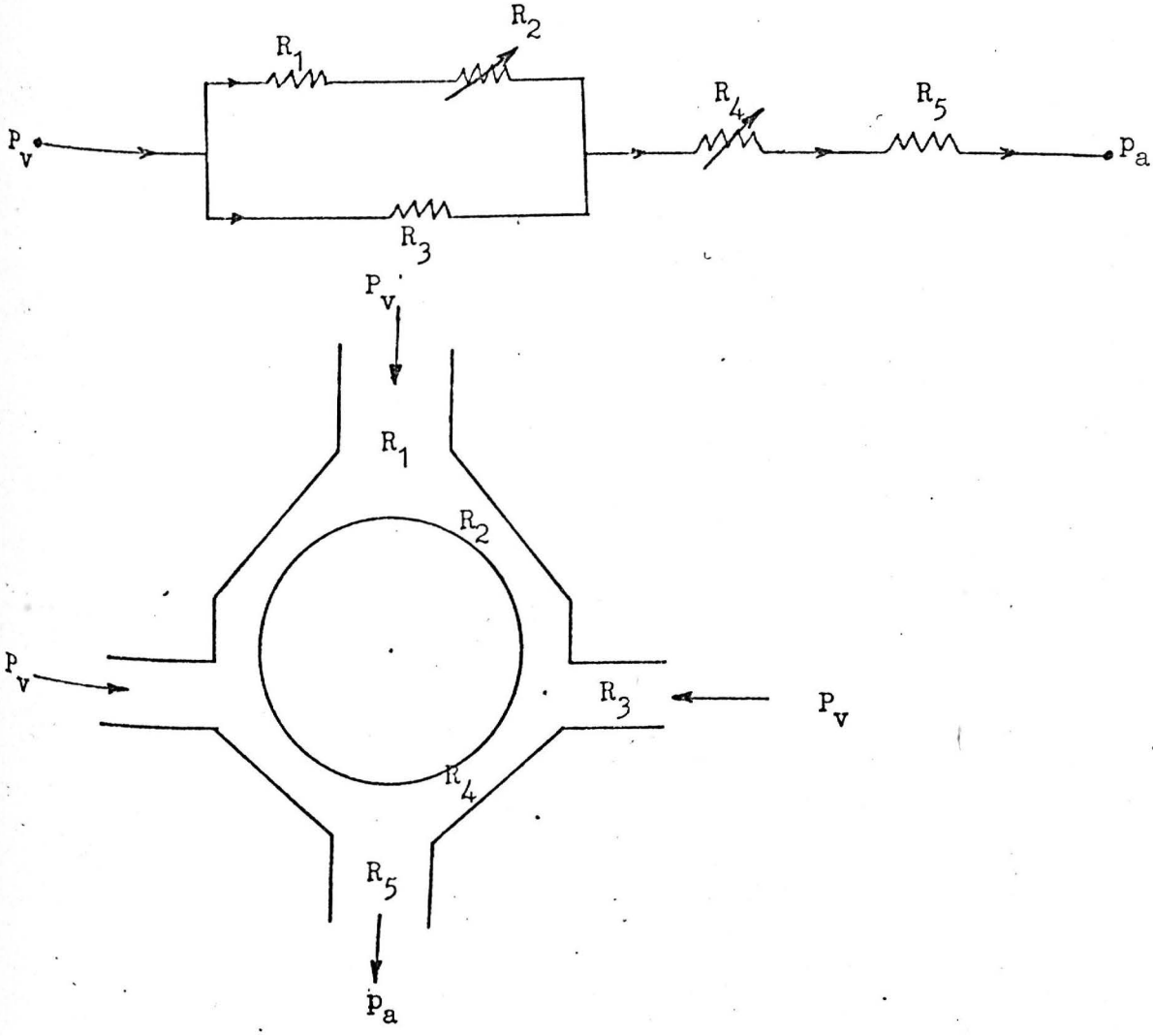

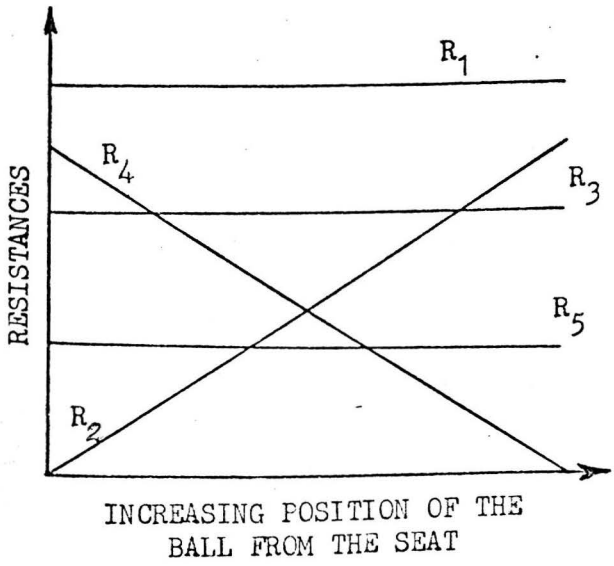

FIG. 7.13 ELECTRICAL ANALOGY

These figs. also show that when the ball was lifted until $y = 0.32$ mm, Q_{vT}, Q_{vs} and Q_{vt} remained approximately constant. This is because when the ball was lifted the resistance (R_4) due to the area under the ball and the resistance (R_2) due to the area above the ball were approximately negligible. Hence Q_{vs} was proportional to the side inlets areas and Q_{vt} was also proportional to the top inlet area.

Also it can be seen from these figs. that when the ball was lifted until $y = 0.47$ mm, Q_{vt} decreased and became equal to zero at $y = 0.47$ mm. This is because when the ball was lifted R_2 increased, and hence Q_{vt} decreased and became equal to zero when R_2 became equal infinity at $y = 0.47$ mm. Also it can be seen in this region that when the ball was lifted Q_{vs} increased. The reason for this is that since the resistance (R_3) due to the area of the side inlets was in parallel with $R_1 + R_2$ and hence the ratio of Q_{vs} to Q_{vt} was proportional to the ratio of $R_2 + R_1$ to R_3. Also these figs. show that in this region Q_{vT} decreased when the ball was lifted. This is because the increase in R_2 when the ball was lifted caused an increase in the total resistance of the parallel circuit which was slightly significant compared to the resistance (R_5) due to the area of the outlet.

It can be seen from these figs. that when y was in 0.14 - 0.32 mm range, Q_{vt} was greater than Q_{vs} (even R_1 was greater than R_3). This is probably because the stagnation of the side inlets flow on the ball caused an increase in the exit pressure of these inlets, and hence the pressure drop across these inlets reduced and caused the decrease in Q_{vs}. The stagnation effect was

also expected on Q_{vt}, but the flow from the top inlet escaped sideways where there were no side inlets.

Fig. (7.14) shows plots of the flow force (F_{vf}) versus P_v for various positions of the ball in the valve, and for pressure range 5-60 psi. This fig. shows that F_{vf} increased when P_v was increased. This is because when P_v was increased, the static pressure at the upper half of the ball increased which caused the increase of F_{vf}.

Fig. (7.15) shows the relationship between F_{vf} with y, for P_v range 20 - 60 psi. This fig. shows that when the ball was lifted from the seat until $y = 0.08$ mm, the flow force on the ball (F_{vf}) increased. This is because when the ball was on the seat, F_{vf} was totally due to P_v force, but when the ball was lifted from the seat until $y = 0.08$ mm, F_{vf} was due to P_v force on the upper half of the ball and due to the static pressure force on the lower half of the ball which decreased in this region due to the increase of velocity there.

When the ball was lifted more until $y = 0.32$ mm, F_{vf} decreased. This is probably because in this region the static pressure force at the upper half of the ball decreased due to the increase in the flow velocity at the upper half of the ball when Q_{vt} increased. Also the pressure above the ball will be less than P_v due to losses in R_1.

When the ball was lifted more until $y = 0.47$ mm, F_{vf} increased. This is probably because at this region Q_{vt} decreased due to the increase in R_2, and hence the flow velocity at the upper half of the ball decreased and caused an increase in the static pressure.

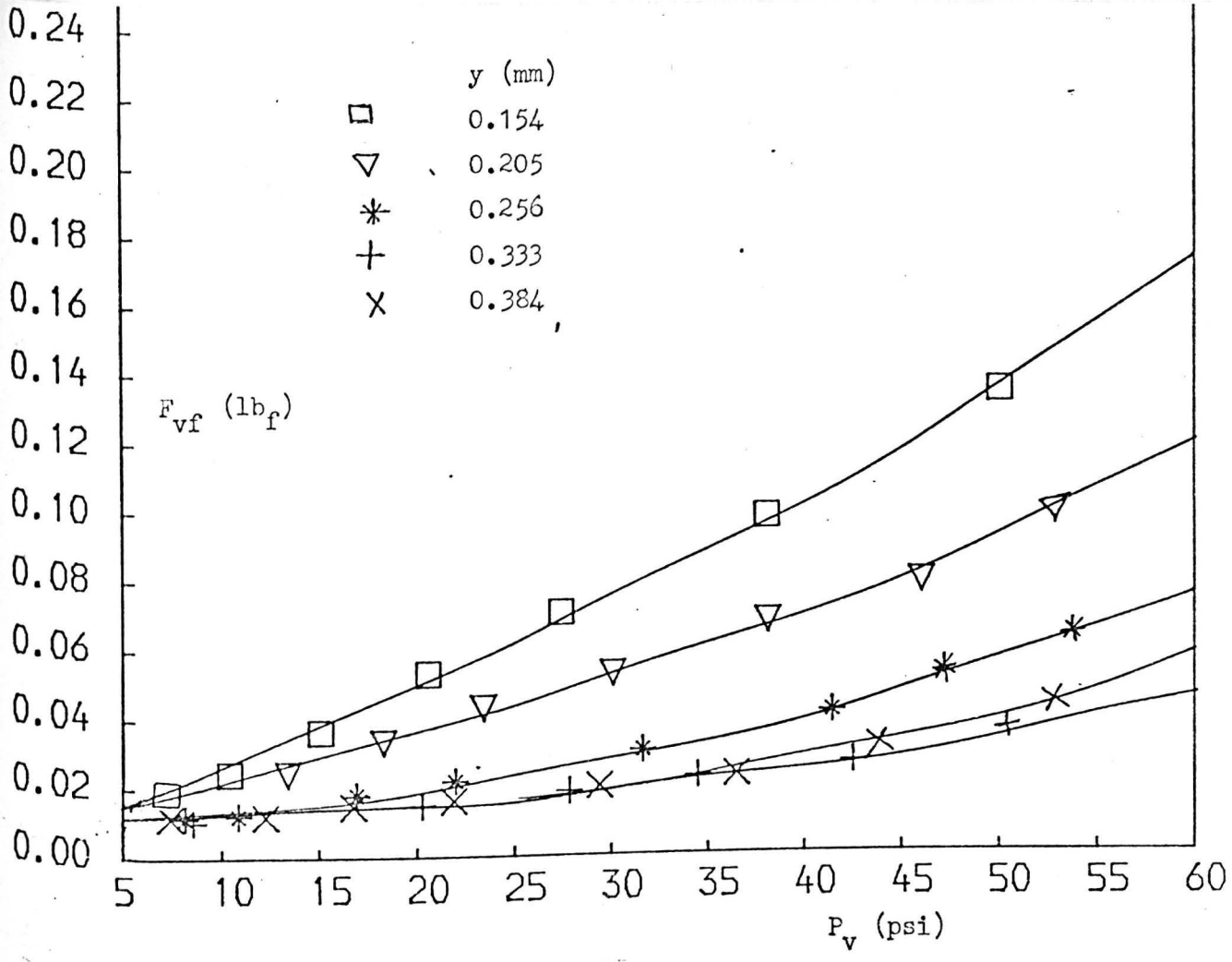

FIG. 7.14 FLOW FORCE - SUPPLY PRESSURE RELATIONSHIP

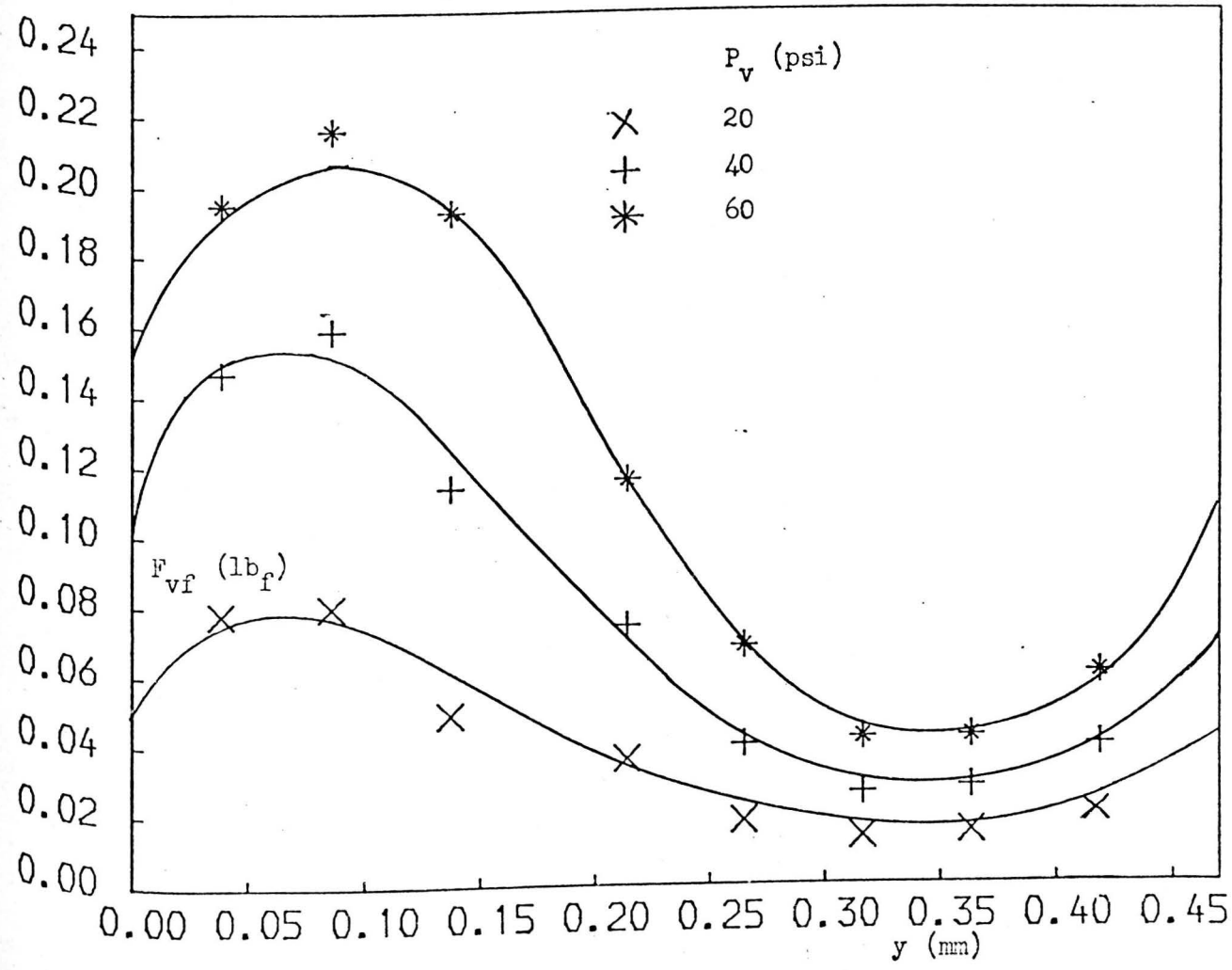

FIG. 7.15 FLOW FORCE - POSITION OF THE BALL FROM THE SEAT RELATIONSHIP

(which increased to P_v when Q_{vf} became equal to zero) at the upper half of the ball.

It was found from the calculations of the buoyancy and the gravity forces on the ball that the net force on the ball was always in downward direction. This would prevent the ball from staying stationary at any position between the upper and lower walls of the valve.

Chapter Eight

THEORETICAL STUDY OF THE BALL MOTION WITH LIQUID RESISTANCE, AND OF FLUID FLOW FROM THE INJECTOR VALVE

8.1 INTRODUCTION

In the theoretical analysis of the ball motion which was described in Chapter 3, it was assumed that the ball was moving without any fluid resistance. In this chapter the ball motion with fluid resistance was studied theoretically through a computer program. Consequently the fluid flow from the injector valve was also studied theoretically through a computer program.

Theory, computer programs and results and discussions are given below.

8.2 THEORY

8.2.1 Introduction

To simplify the analysis it was assumed that the ball was moving so slowly that it could be considered to have zero velocity relative to the flow velocity of the top inlet. This assumption would be examined from the results of the analysis. If the assumption was found to be wrong, the ball velocity would be modified in the analysis.

8.2.2 Analysis with Assumption of Zero Velocity of the Ball Relative to the Flow Velocity of the Top Inlet

8.2.2.1 Motion of the Injector Tip

8.2.2.1.1 Equations of Motion of the Injector Tip

Eqn. (6.10) of the motion of the injector tip was used in this analysis:

$$y_1 = y_x \frac{w_o}{w_d} e^{-\gamma t/2} \cos(w_d t + \frac{\pi}{2} + s) + y_x \cos(w_o t - \frac{\pi}{2} + s) \quad (8.1)$$

where y_1 represents the position of the injector tip from a fixed datum, y_x maximum amplitude of the tip, w_o frequency of the tip in radian, w_d damped natural frequency in radians, γ parameter of damped vibration, t time at any instance during the tip motion and s initial phase angle.

8.2.2.1.2 Assumptions on the Motion of the Injector Tip

The assumptions which were made on the tip motion in Chapter 6, were also assumed in this analysis.

It was found from the results of Chapter 6 that the effect of varying the initial condition of the injector tip had not any influence on the feature of the results. Hence the effect of varying the initial condition was not considered in this analysis. It was assumed in this analysis that the tip was moving up at $t = o$, i.e., $s = o$.

8.2.2.2 Motion of the Ball

8.2.2.2.1 Equation of Motion of the Ball

The following forces were assumed acting on the ball:

1. Flow force.
2. Buoyancy force.
3. Gravity force.
4. Inertia force.

Hence the equation of the forces acting on the ball was:

$$M \ddot{y}_2 = F_{vf} + F_{vb} - F_g \quad ,$$

or

$$\ddot{y}_2 = -F_{vf}/M + F_{vb}/M - F_g/M \quad , \qquad (8.2)$$

where

$$\ddot{y}_2 = \frac{d^2 y_2}{d t_1^2} \quad ,$$

$$M = m + \frac{4}{3} \left(\frac{D_v}{2}\right)^3 \rho_v \quad ,$$

$$F_b = \frac{4}{3} \left(\frac{D_v}{2}\right)^3 \rho_v \; g$$

and

$$F_g = mg \quad ,$$

where M represents mass (m) of the ball plus the added mass, $\ddot{y}_2$ acceleration of the ball, F_{vf} flow force on the ball, F_{vb} buoyancy force on the ball of the valve, F_g gravity force on the ball, t_1 time at any instance between two successive impacts, D_v diameter of the ball and ρ_v density of the liquid.

F_{vf} for various gaps (y) between the ball and the seat, for specific supply pressure was found from the measurements of Chapter 7. The equations of F_{vf} versus the gap (y) between the ball and the seat for specific supply pressures were represented in polynomials of Chebyshev-series form. The coefficients of each polynomial were computed by feeding the experimental data points of $F_{vf} - y$ to a subroutine stored in the library of the computer.

The degree of the polynomial which has given best curve fitting for the data points was found by plotting the polynomial of each

degree. The polynomial for each degree was evaluated by feeding the coefficients of the polynomial of each degree to another subroutine stored in the library of the computer.

It was found that the polynomial at degree 4 has given best curve fitting to the $F_{vf} - y$ data points.

Fig. (8.1) shows plot of $F_{vf} - y$ polynomial equation of degree 4 for 40 psi supply pressure. $F_{vf} - y$ equations was written in the following form:

$$F_{vf} = 0.5\ a_o + a_1\ \bar{y} + a_2\left[2\ (\bar{y})^2 - 1\right] + a_3\left[4\ (\bar{y})^3 - 3\ \bar{y}\right] + a_4 \left[8\ (\bar{y})^4 - 8\ (\bar{y})^2 + 1\right] . \qquad (8.3)$$

where

$$\bar{y} = \frac{2y - y_{max} - y_{min}}{y_{max} - y_{min}} , \qquad (8.4)$$

where

$$y = y_2 - y_1 \qquad (8.5)$$

where $\bar{y}$ represents the argument of the polynomial, y gap between the ball and the seat, y_{max} maximum value of y, y_{min} minimum value of y, y_2 position of the ball from a fixed datum and y_1 position of the tip from a fixed datum.

By substituting eqn. (8.1) in eqn. (8.5), we have

$$y = y_2 - y_x \frac{w_o}{w_d} e^{-\gamma t/2} \cos(w_d\ t + \frac{\pi}{2} + s) - y_x \cos(w_o\ t - \frac{\pi}{2} + s) \qquad (8.6)$$

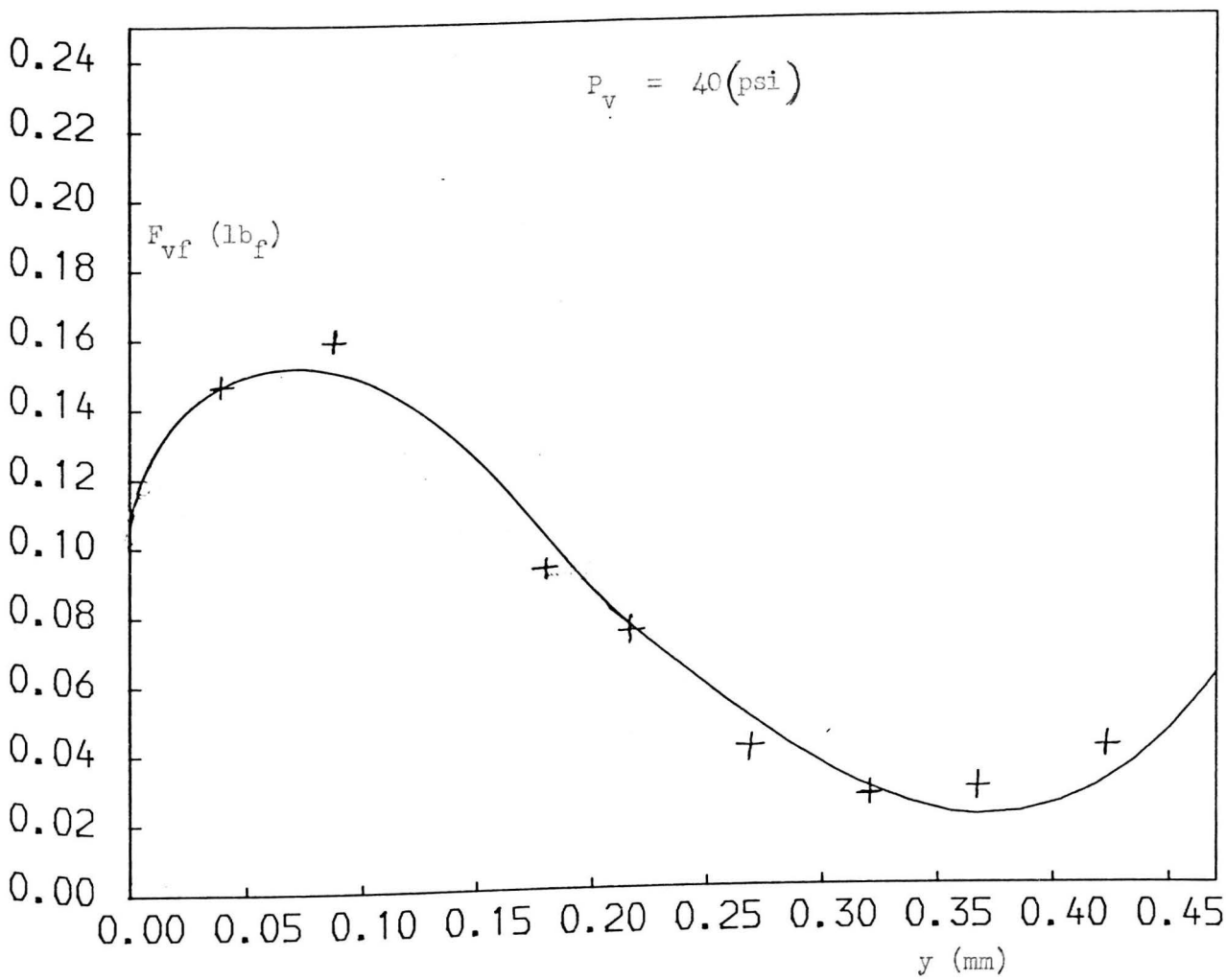

FIG. 8.1 FLOW FORCE - POSITION OF THE BALL FROM THE SEAT RELATIONSHIP

By substituting eqn. (8.6) in eqn. (8.4) we have:

$$\bar{y} = \frac{1}{y_{max} - y_{min}} \left[2y_2 - 2y_x \frac{w_o}{w_d} e^{-\gamma t/2} \cos(w_d t + \frac{\pi}{2} + s) \right.$$

$$\left. - 2y_x \cos(w_o t - \frac{\pi}{2} + s) - y_{max} - y_{min} \right] \qquad (8.7)$$

By substituting eqn. (8.7) into eqn. (8.3), and then substituting this result into eqn. (8.2), we have

$$\ddot{y}_2 = -\frac{1}{M} \left[0.5\, a_o + a_1 \left[\frac{1}{y_{max} - y_{min}} \left[2y_2 - 2y_x \frac{w_o}{w_d} e^{-\gamma t/2} \right. \right. \right.$$

$$\left. \cos(w_d t + \frac{\pi}{2} + s) - 2y_x \cos(w_o t - \frac{\pi}{2} + s) - y_{max} - y_{min} \right]$$

$$+ a_2 \left[2 \left[\frac{1}{y_{max} - y_{min}} \left[2y_2 - 2y_x \frac{w_o}{w_d} e^{-\gamma t/2} \right. \right. \right.$$

$$\left. \cos(w_d t + \frac{\pi}{2} + s) - 2y_x \cos(w_o t - \frac{\pi}{2} + s) - y_{max} - y_{min} \right] \Big]^2$$

$$- 1 \Big] + a_3 \left[4 \left[\frac{1}{y_{max} - y_{min}} \left[2y_2 - 2y_x \frac{w_o}{w_d} e^{-\gamma t/2} \right. \right. \right.$$

$$\left. \cos(w_d t + \frac{\pi}{2} + s) - 2y_x \cos(w_o t - \frac{\pi}{2} + s) - y_{max} - y_{min} \right] \Big]^3$$

$$- 3 \left[\frac{1}{y_{max} - y_{min}} \left[2y_2 - 2y_x \frac{w_o}{w_d} e^{-\gamma t/2} \cos(w_d t + \frac{\pi}{2} + s) \right. \right.$$

$$\left. \left. - 2y_x \cos(w_o t - \frac{\pi}{2} + s) - y_{max} - y_{min} \right] \right] \Big] + a_4 \left[\right.$$

$$8 \left[\frac{1}{y_{max} - y_{min}} \left[2y_2 - 2y_x \frac{w_o}{w_d} e^{-\gamma t/2} \cos(w_d t + \frac{\pi}{2} + s) \right. \right.$$

$$\left. - 2y_x \cos(w_o t - \frac{\pi}{2} + s) - y_{max} - y_{min} \right] \Big]^4 - 8$$

$$\left[\frac{1}{y_{max} - y_{min}} \left[2 y_2 - 2y_x \frac{w_o}{w_d} e^{-\gamma t/2} \cos(w_d t + \frac{\pi}{2} + s) - 2y_x \right.\right.$$

$$\left.\left. \cos(w_o t - \frac{\pi}{2} + s) - y_{max} - y_{min} \right]\right]^2 + 1 \Big] + F_{vb}/M - F_g/M$$

(8.8)

The value of y_2 and the velocity of the ball (v_b) for each increment of time between two successive impacts were computed by using Merson's form of the Runge-Kutta method through a subroutine stored in the library of the computer.

8.2.2.2.2 Starting Condition of the Ball Motion

The starting condition of the ball motion was assumed that the ball separated from the seat with the same velocity as the injector tip when the injector tip was moving upward with negative acceleration (a) less than the acceleration (g_1) of the ball due to the fluid and gravity forces, or the ball separated when the injector tip was moving downward with positive acceleration greater than the acceleration (g_1) of the ball due to the fluid and gravity forces, i.e., the separation occurred when:

$a < -g_1$ (when the tip was moving up)

or

$a > g_1$ (when the tip was moving down)

where a was computed from eqn. (6.12):

$$a = y_x \frac{\gamma^2 w_o}{4 w_d} e^{-\gamma t/2} \cos(w_d t + \frac{\pi}{2} + s) + \frac{\gamma}{2} y_x w_o e^{-\gamma t/2}$$

$$\sin(w_d\, t + \frac{\pi}{2} + s) + \frac{\gamma}{2}\, y_x\, w_o\, e^{-\gamma t/2} \sin(w_d\, t + \frac{\pi}{2} + s)$$

$$- y_x\, w_o\, e^{-\gamma t/2}\, w_d \cos(w_d\, t + \frac{\pi}{2} + s) - y_x\, w_o^2 \cos(w_o\, t - \frac{\pi}{2} + s) \,, \qquad (8.9)$$

and

$$g_1 = \frac{F_{vo}}{m} + g \,,$$

where F_{vo} represents flow force on the ball when it was on the seat.

8.2.2.2.3 Equation of the Gap Between the Ball and the Seat

Eqn (8.5) was used for computing the gap (y) between the ball and the seat:

$$y = y_2 - y_1 \qquad (8.10)$$

The value of y_2 was computed from eqn. (8.8) and the value of y_1 was computed from eqn. (8.1).

8.2.2.2.4 Collision Between the Ball and the Walls of the Valve

The assumptions of the collision between the ball and the walls of the valve which were described in Chapter 3 (see section (3.2.2.4)) were also assumed in this analysis.

Eqn. (3.6) was used for computing the velocity of the ball after the collision (v_{o1}):

$$v_{o1} = 2v_f - v_{ib} \qquad (8.11)$$

where

$v_f = v_i = v$ at instance of the impact,

and

$$v_{ib} = v_b \text{ at instance of the impact,}$$

where v_f represents velocity of the tip after the impact, v_i velocity of the tip before the impact, v velocity of the tip at any instance, v_{ib} velocity of the ball before the impact and v_b velocity of the ball at any instance between two successive collisions.

Eqn. (6.11) was used for computing v :

$$v = -y_x \frac{\gamma w_o}{2 w_d} e^{-\gamma t/2} \cos(w_d t + \frac{\pi}{2} + s) - y_x w_o e^{-\gamma t/2}$$

$$\sin(w_d t + \frac{\pi}{2} + s) - y_x w_o \sin(w_o t - \frac{\pi}{2} + s) \qquad (8.12)$$

Eqn. (3.8) was used for computing v_b :

$$v_b = -g t_1 + v_o \qquad (8.13)$$

where v_o represents initial ball velocity.

8.2.3 Analysis with Assumption of Finite Velocity of the Ball Relative to the Flow Velocity of the Top Inlet

8.2.3.1 Motion of the Injector Tip

8.2.3.1.1 Equation of Motion of the Injector Tip

Eqn. (6.10) of the motion of the injector tip was used in this analysis:

$$y_1 = y_x \frac{w_o}{w_d} e^{-\gamma t/2} \cos(w_d t + \frac{\pi}{2} + s) + y_x \cos(w_o t - \frac{\pi}{2} + s)$$

(8.14a)

The same assumptions which were made on the tip motion in Chapter 6, were also made in this analysis. The effect of varying the initial condition of the injector tip motion was not considered in this analysis. It was assumed in this analysis that the tip was moving up at $t = o$, i.e., $s = o$.

8.2.3.1.2 Equation of the Decay in the Motion of the Injector Tip

It was found from the laser measurements of the injector tip motion that the motion decayed for approximately 1.5 ms. The decay in the motion was represented by the following equation:

$$y_1 = y_x \, e^{-\alpha t/2} \cos(w_o \, t) \qquad (8.14b)$$

where α represents parameter of damped vibration. This equation was checked by plotting y/y_x versus t (fig.(8.2)). The value of α was obtained from the laser measurements. It can be seen from this fig. that the injector tip motion decayed for approximately 1.5 ms. It can be deduced from this fig. that eqn. (8.14b) represented well the decay in the motion of the injector tip.

8.2.3.2 The Relationship Between the Ball Velocity, the Pressure Drop Across the Valve of the Injector, and Flow Force on the Ball

Because the area of the three inlets (the two side inlets and the top inlet) of the injector valve were $\gg$ the area of the outlet or the area of the gap under the ball of the injector valve,

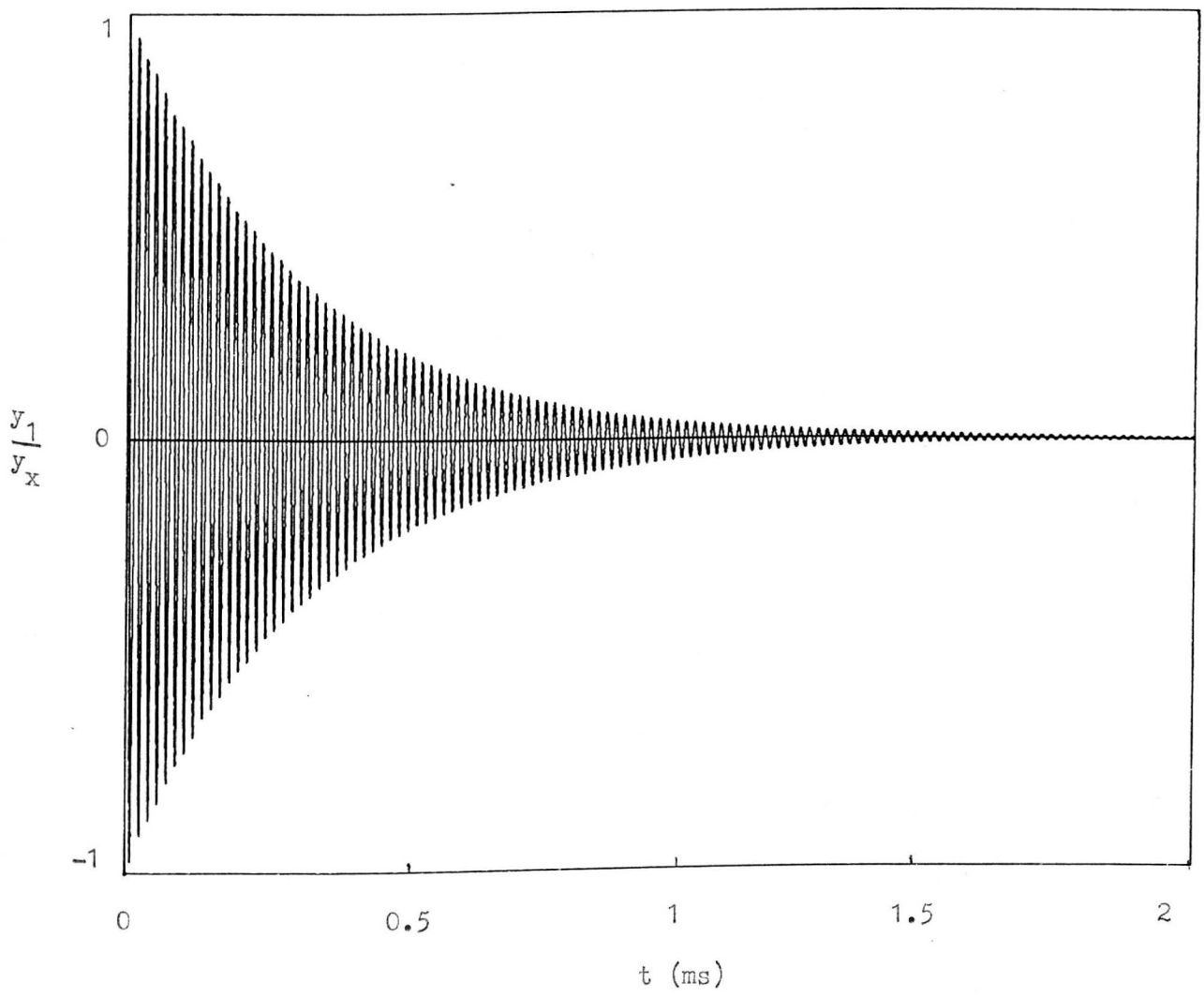

FIG. 8.2 RATIO OF THE TIP MOTION TO THE MAXIMUM AMPLITUDE OF THE TIP - TIME RELATIONSHIP

therefore the pressure drop across the three inlets was very small compared to the pressure drop across the outlet or the gap under the ball. Therefore if the top inlet was restricted due to the upward velocity of the ball and consequently the flow reduced from this inlet, the extra flow would come through the other two inlets with a very slightly higher pressure drop (but still very small). Hence the flow through the outlet or the gap would be the same approximately, i.e. unaffected by the restriction of one inlet hole. Thus, due to the upward ball velocity it could be assumed that:

$$E_v = \frac{P_{vt} - p^*_{vo}}{\frac{1}{2} \rho_v V^2_{vo}} = \phi R_{ev} \left(\frac{V_{vo} D_v}{\nu_v} \right) \qquad (8.15)$$

where E_v represents Euler number of the valve, P_{vt} supply pressure at the top inlet, p^*_{vo} piezometric pressure at the outlet of the valve, V_{vo} velocity of the flow at the outlet of the valve, R_{ev} Reynolds number based on the zero velocity of the ball of the valve and ν_v kinematic viscosity of the liquid in the valve. But the flow force on the ball of the injector valve was affected by the relative velocity between the ball and the flow of the top inlet. Thus, it could be assumed that:

$$C_{Dv} = \frac{F_{vf}}{\frac{1}{2} \rho_v D_v^2 v_r^2} = \phi \bar{R}_{ev} \left(\frac{v_r D_v}{\nu_v} \right) \qquad (8.16)$$

where C_{Dv} represents coefficient of drag of the valve, v_r relative velocity between the ball and the top inlet flow of the valve, $\bar{R}_{ev}$ Reynolds number of the valve based on the relative velocity between the ball and the flow of the top inlet.

It was assumed that the flow force on the ball was due to the flow of the top inlet.

Since the velocity of the ball of the model was zero, hence:

$$C_{Dm} = \frac{F_{mt}}{\frac{1}{2} \rho_v D_m^2 V_{mt}^2} = \phi R_{em}\left(\frac{V_{mt} D_m}{\nu_m} \right) \qquad (8.17)$$

where C_{Dm} represents coefficient of drag of the model, F_{mt} flow force on the ball of the model, ρ_m density of the liquid of the model, D_m diameter of the ball of the model, V_{mt} velocity of the flow at the top inlet of the model, R_{em} Reynolds number of the model and ν_m kinematic viscosity of the liquid in the model.

To apply the dynamic similarity between the model and the injector valve, the Reynolds number of the two systems should be identical:

$$R_{ev} = R_{em} \qquad (8.18)$$

Hence

$$C_{Dv} = C_{Dm} \qquad (8.19)$$

8.2.3.3 Motion of the Ball

8.2.3.3.1 Equation of the Ball Motion

The following forces were also assumed acting on the ball:

1. Flow force.
2. Buoyancy force.
3. Gravity force.
4. Inertia force.

Eqn. (8.2) of the acceleration of the ball was also used here:

$$\ddot{y}_2 = - F_{vf}/M + F_{vb}/M - F_g/M \cdot \qquad (8.20)$$

It was assumed that F_{vf} was constant for small increment of time.

By integrating eqn. (8.19), we have:

$$y_2 = \tfrac{1}{2} t_1^2 \left(- F_{vf}/M + F_{vb}/M - F_g/M\right) + v_o t + y_o \qquad (8.21)$$

where y_o represents initial position of the ball from a fixed datum.

The velocity (v_b) of the ball was found from the derivative of eqn. (8.20) with respect to t_1:

$$v_b = t_1 \left(- F_{vf}/M + F_{vb}/M - F_g/M\right) + v_o \cdot \qquad (8.21)$$

8.2.3.3.2 Starting Conditions of the Ball Motion

The same assumption of the starting conditionsof the ball motion of the analysis of zero ball velocity relative to the flow velocity of the top inlet, (see section (8.2.2.2.2)), was also assumed here, i.e., the separation of the ball from the seat occurred when:

$a < - g_1$ (when the tip was moving up),

or

$a > g_1$ (when the tip was moving down)

where

a was computed from eqn. (6.12):

$$a = y_x \frac{\gamma^2 w_o}{4 w_d} e^{-\gamma t/2} \cos(w_d t + \frac{\pi}{2} + s) + \frac{\gamma}{2} y_x w_o e^{-\gamma t/2}$$

$$\sin(w_d t + \frac{\pi}{2} + s) + \frac{\gamma}{2} y_x w_o e^{-\gamma t/2} \sin(w_d t + \frac{\pi}{2} + s)$$

$$- y_x w_o e^{-\gamma t/2} w_d \cos(w_d t + \frac{\pi}{2} + s) - y_x w_o^2$$

$$\cos(w_o t - \frac{\pi}{2} + s) \qquad (8.23)$$

and

$$g_1 = F_{vo}/m + g \quad .$$

8.2.3.3.3 Equation of the Gap Between the Ball and the Seat

Eqn. (8.5) was used for computing the gap between the ball and the seat (y) :

$$y = y_2 - y_1 \qquad (8.24)$$

The value of y_2 was computed from eqn. (8.21), and the value of y_1 was computed from eqn. (8.14a) or (8.14b).

8.2.3.3.4 The Collision Between the Ball and the Walls of the Valve

The assumptions of the collision between the ball and the walls of the valve which were described in Chapter 3, were also assumed in this analysis. Eqn. (3.6) was used for computing the velocity of the ball after the collision (v_{o1}) :

$$v_{o1} = 2v_f - v_{ib} \qquad (8.25)$$

where

$$v_f = v_i = v \quad \text{at the time of impact,}$$

and

$$v_{ib} = v_b \quad \text{at the time of impact.}$$

Eqn. (6.11) was used for computing v :

$$v = -y_x \frac{\gamma w_o}{2 w_d} e^{-\gamma t/2} \cos(w_d t + \frac{\pi}{2} + s) - y_x w_o e^{-\gamma t/2} \sin(w_d t + \frac{\pi}{2} + s) - y_x w_o \sin(w_o t - \frac{\pi}{2} + s) \quad (8.26)$$

Eqn. (3.8) was used for computing v_b :

$$v_b = -g t_1 + v_o \quad (8.27)$$

8.2.3.3.5 Evaluating of y for Each Increment of Time

The following procedure was used for evaluating y for each increment of time:

a) From the results of Chapter 7, the equation of

$$C_{Dm}\left(\frac{F_{mf}}{\frac{1}{2}\rho_m D_m^2 V_{mt}^2}\right) - R_{em}\left(\frac{V_{mt} D_m}{\nu_m}\right) \quad \text{for different gaps}$$

between the ball and the seat in the model was evaluated. The method of evaluating $C_{Dm} - R_{em}$ eqn. was the same as the method of evaluating $F_{vf} - y$ eqn. (which was described in section (8.2.2.2.1)).

Since $C_{Dv} = C_{Dm}$ (eqn. (8.18)), and $\bar{R}_{ev} = R_{em}$ (eqn. (8.19)), hence eqn. $C_{Dv} - R_{ev}$ for different scaled gaps between the ball and seat in the model was obtained.

b) Also from the results of Chapter 7, the equation of $Q_{vt} - y$ for specific supply pressure was evaluated. The method of evaluating $Q_{vt} - y$ eqn. was the same as the method of evaluating $F_{vf} - y$ eqn. (see section (8.2.2.2.1)). Fig. (8.3) shows a plot of $Q_{vt} - y$ for supply pressure 40 psi.

c) For the first increment of time after the separation of the ball from the seat, the values y_2 and v_b were calculated from eqns. (8.21) and (8.27) respectively. The flow force on the ball was assumed equal to the supply pressure force (F_{vo}) when the ball was on the seat. It was assumed that $v_o = v$ and $y_o = y_1$ at the moment of the separation. The value of y was then computed.

d) The value of Q_{vt} was computed by substituting the value of y in $Q_{vt} - y$ eqn. The value of V_{vt} was then computed.

e) The value of the relative velocity (v_r) between the ball and the flow of the top inlet was then computed.

f) The value of $\bar{R}_{ev}$ was then computed.

g) By substituting the value of $\bar{R}_{ev}$ in $C_{Dv} - \bar{R}_{ev}$ eqn. of the different gaps between the ball and the seat, $C_{Dv} - y$ points were obtained. The value of C_{Dv} was then computed by interpolation for the value of y. The interpolation was done by using a subroutine stored in the library of the computer.

h) The value of F_{vf} was then computed.

i) The same procedure was repeated again for the next increment of time. The value of F_{vf} was assumed constant during the increment.

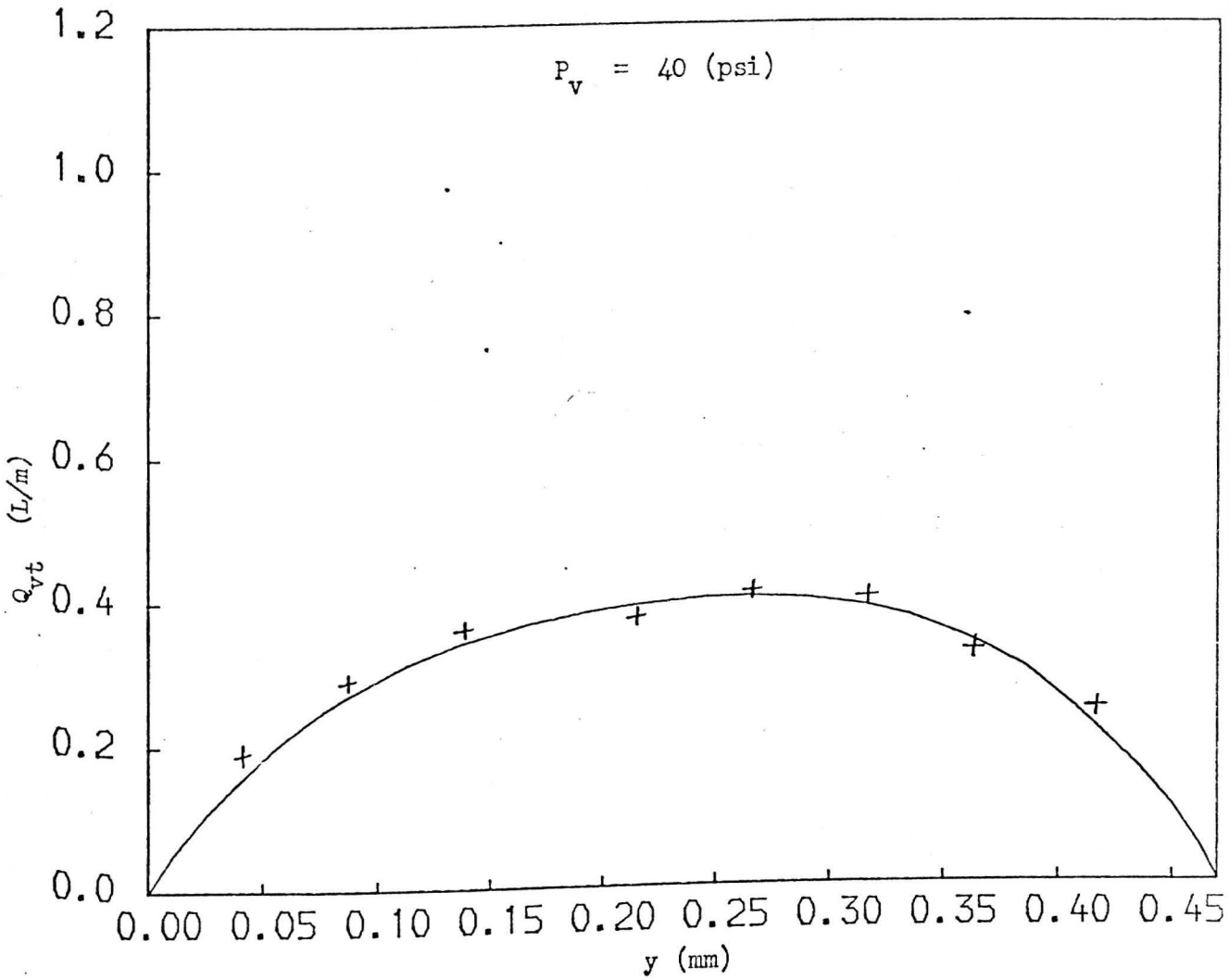

FIG. 8.3 TOP INLET FLOW RATE - POSITION OF THE BALL FROM THE SEAT RELATIONSHIP

8.2.3.4 Computing the Flow from the Injector Valve

8.2.3.4.1 Computing the Total Flow Rate for Each Increment of Time

The following procedure was done for computing the total flow rate for each increment of time:

a) From the results of Chapter 7, the equation of $Q_{vT} - y$ for specific supply pressure was evaluated. The method of evaluating $Q_{vT} - y$ eqn. was the same as the method of evaluating $F_{vf} - y$ eqn. (which was described in section (8.2.2.2.1)). Fig. (8.4) shows a plot of $Q_{vT} - y$ for supply pressure 40 psi.

b) The value of Q_{vT} for each increment of time was computed by substituting the value of y (which was computed in the same procedure of section (8.2.3.3.5)) in eqn. $Q_{vT} - y$.

8.2.3.4.2 Computing the Total Flow for Each Increment of Time

The total flow (Q_{vN}) for each increment of time was computed by multiplying the value of Q_{vT} (which was computed by the same procedure as section (8.2.3.4.1)) by the value of the increment of time.

8.3 COMPUTER PROGRAMS

Fortran language was used in 1906 Computer - Sheffield University.

8.3.1 Computer Programs of the First Analysis

8.3.1.1 Computer Program for Evaluating the Degree of the Polynomial

Fig. (8.5) shows the flow chart of the computer program. Subroutine E02ADF was used for computing the coefficients of the

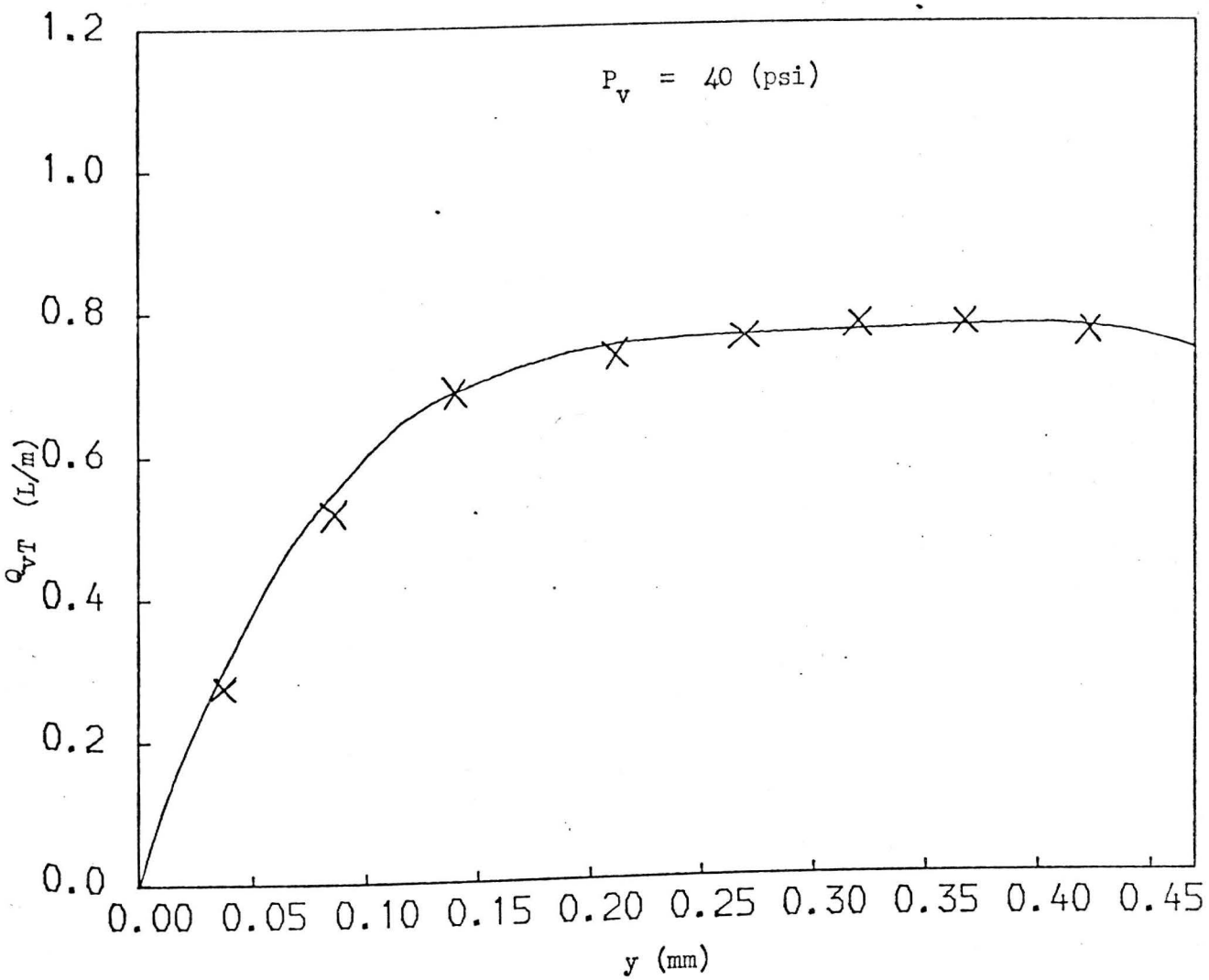

FIG. 8.4 TOTAL FLOW RATE - POSITION OF THE BALL FROM THE SEAT RELATIONSHIP

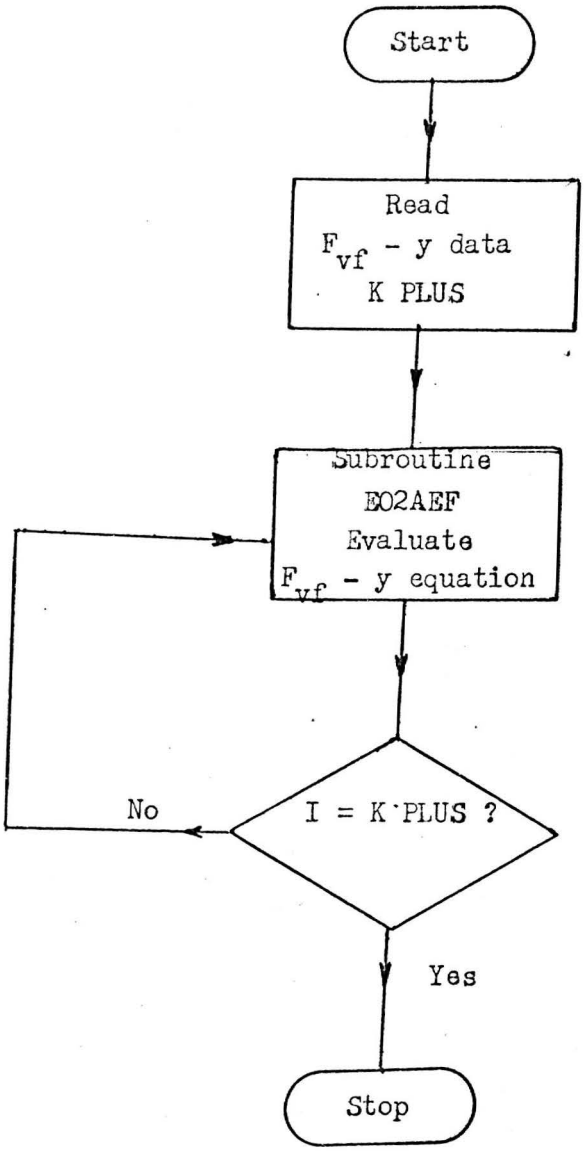

FIG. 8.5 FLOW CHART OF THE COMPUTER PROGRAM FOR EVALUATING THE DEGREE OF THE POLYNOMIAL

$F_{vf} - y$ equation. This subroutine computed weighted least-squares polynomial approximations to the data points. Subroutine E02AEF was used for evaluating the $F_{vf} - y$ equation for each degree. This subroutine evaluated the polynomial from its Chebyshev-series representation. The computer program is shown in Appendix 5.

8.3.3.1.2 Computer Program of the Ball Motion

Fig. (8.6) shows the flow chart of the computer program.

The input data to the computer program is shown on Table (8.1). Subroutine E02ADF was used for computing the coefficients of the $F_{vf} - y$ equation. This subroutine computed weighted least-square polynomial approximations to the data points. Subroutine C05ACF was used to find the value of time in which the ball separated from the seat. Bisection method was used. Subroutine D02ABF was used for evaluating the value of y_2 at each increment of time (dt). Merson's form of Runge-Kutta method was used. The time (tco) between two successive collisions was computed by interpolation at $y = o$, and at $y = y_w$ (the conditions of the collision). Also the velocity of the ball before the collision was computed by the interpolation at $y = o$, or at $y = y_w$.

The computer program is shown in appendix (6).

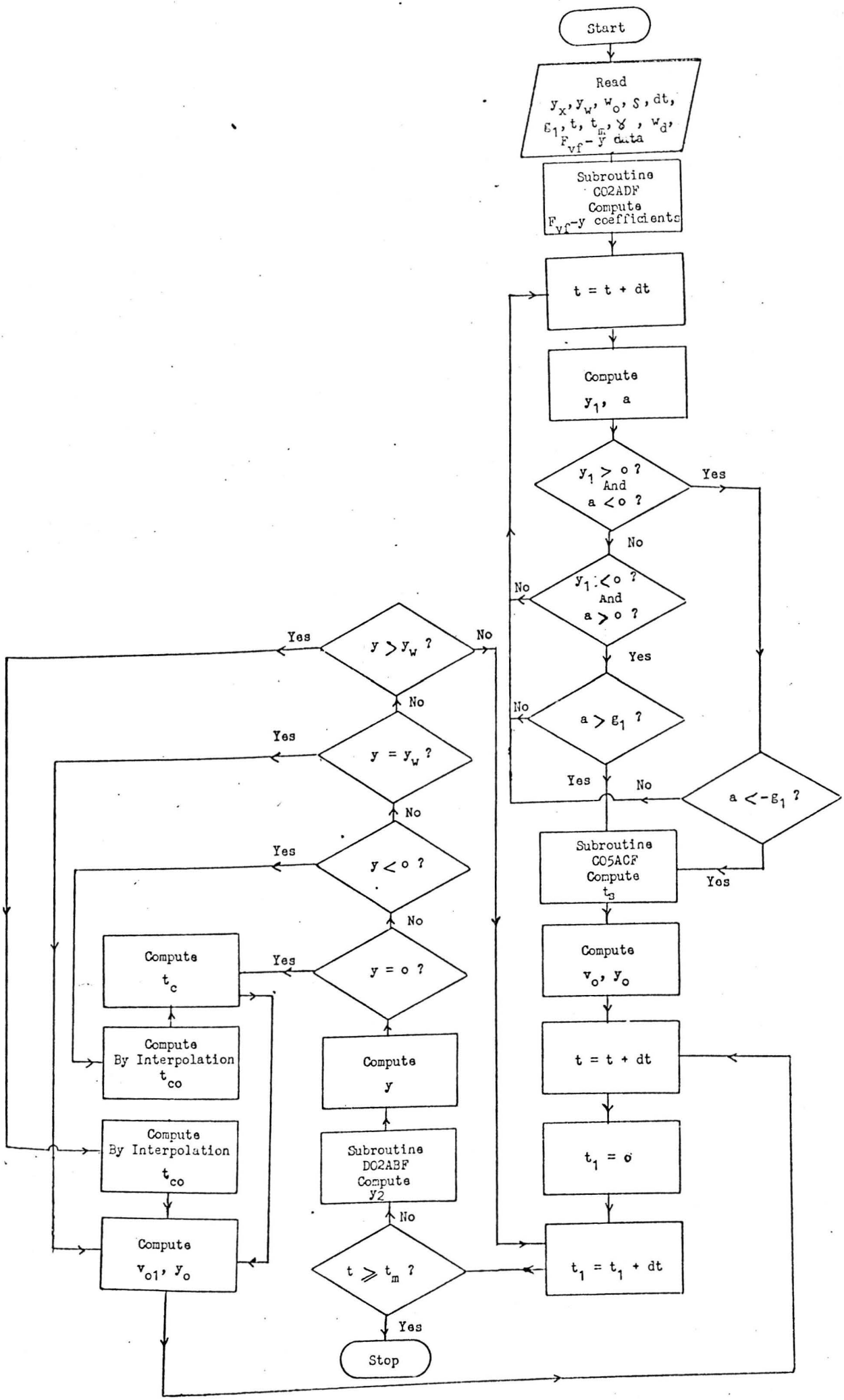

FIG. 8.6 FLOW CHART OF THE COMPUTER PROGRAM OF THE BALL MOTION

Supply Pressure (psi)	y_x (mm)	y_w (mm)	w_o (rad)	s rad	dt (s)	g_1 mm/s^2	t (s)	tm (s)	γ (rad)	w_d (rad)	$F_{vf} - y$ data
20	4.65×10^{-3}	0.47	3.76×10^{5}	0	1×10^{-6}	6.6×10^{6}	0	5×10^{-3}	414	3.76×10^{5}	From Chapter 7
40	4.23×10^{-3}	0.47	3.76×10^{5}	0	1×10^{-6}	1.3×10^{7}	0	5×10^{-3}	414	3.76×10^{5}	From Chapter 7
60	4.23×10^{-3}	0.47	3.76×10^{5}	0	1×10^{-6}	1.9×10^{7}	0	5×10^{-3}	414	3.76×10^{5}	From Chapter 7

TABLE 8.1 INPUT DATA TO THE COMPUTER PROGRAM

8.3.2 Computer Programs of the Second Analysis

8.3.2.1 Computer Program of the Ball Motion

The flow chart of the computer program is shown in fig. (8.7). The input data to the computer program is shown in table (8.2). Subroutine E02ADF was used for computing the coefficients of the $C_{Dm} - R_{em}$ eqn. for the different gaps between the ball and the seat in the model.

Subroutine E02ADF was used for computing the coefficients of the $Q_{vt} - y$ eqn. This subroutine computed weighted least-square polynomial approximation to the data points.

Subroutine C05ACF was used to compute the time (t) in which the ball separated from the seat. Bisection method was used.

Subroutine E02AEF was used for evaluating C_{Dv} from $C_{Dv} - \bar{R}_{ev}$ eqn. This subroutine evaluated the polynomial from its Chebyshev-series representation.

Subroutine E01ADF was used to interpolate at a given value of y from $C_{Dv} - y$ points. Aitken's technique of successive linear interpolation was used. The time (tco) between two successive collisions was computed by the interpolation at $y = o$, or at $y = y_w$ (the condition of the collision). Also the velocity of the ball before the collision was computed by the interpolation at $y = o$, or at $y = y_w$.

The computer program is shown in appendix (7).

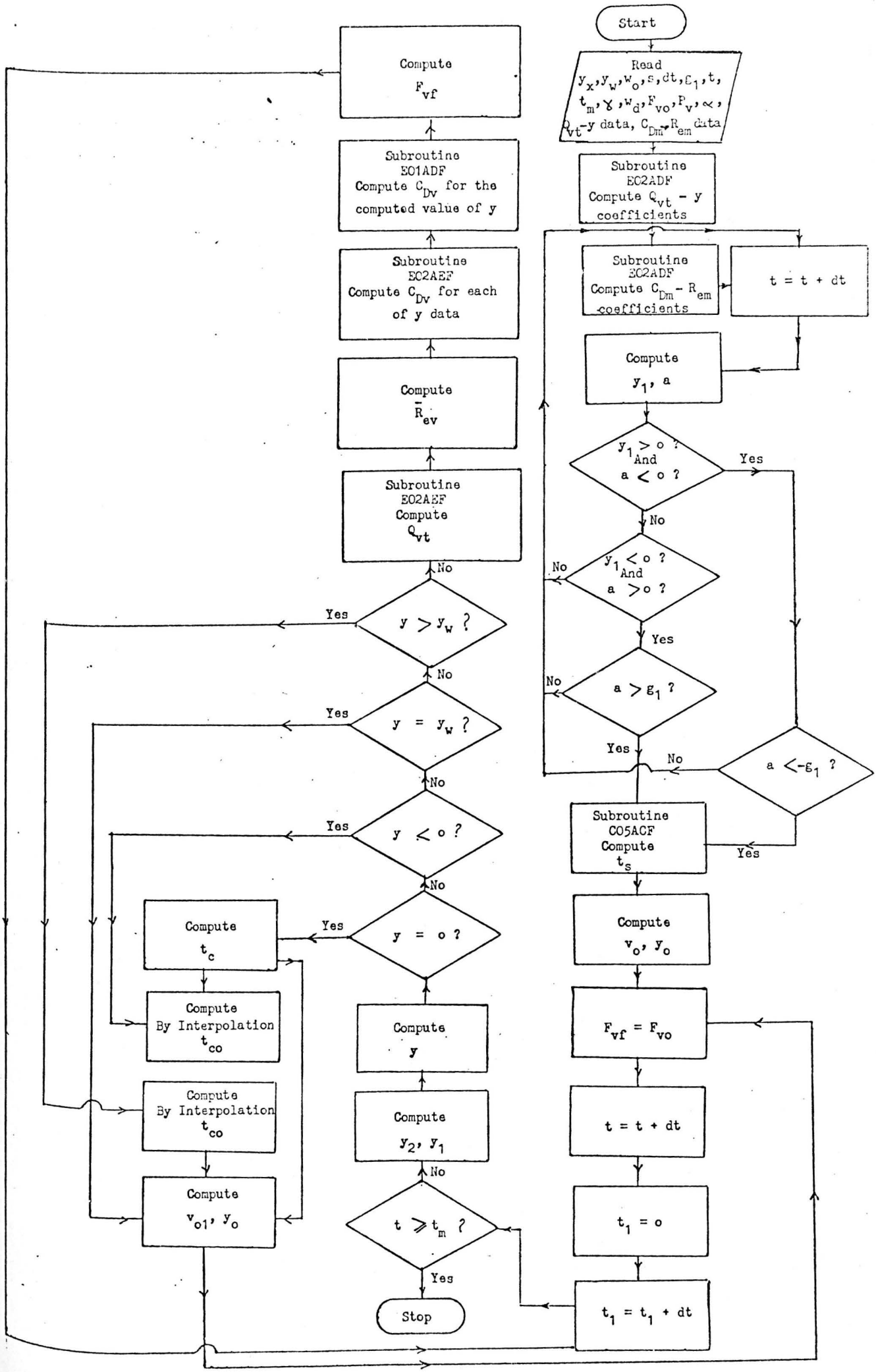

FIG.8.7. FLOW CHART OF THE COMPUTER PROGRAM OF THE BALL MOTION

Supply Pressure (psi)	y_x (mm)	y_w (mm)	w_o (rad)	s (rad)	dt (s)	g_1 (mm/s^2)	t (s)	tm (s)	γ (rad)	w_d (rad)	Q_{vm} - y data	C_{Dm}-R_{em} data	F_{vo} (N)	α (rad)
20	4.65×10^{3}	0.47	3.76×10^{5}	0	1×10^{-6}	6.6×10^{6}	0	5×10^{-3}	4.14×10^{2}	3.76×10^{5}	From Chapter 7	From Chapter 7	0.221	1.3×10^{3}
40	4.23×10^{3}	0.47	3.76×10^{5}	0	1×10^{-6}	1.3×10^{7}	0	5×10^{-3}	4.14×10^{2}	3.76×10^{5}	From Chapter 7	From Chapter 7	0.442	1.3×10^{3}
60	4.23×10^{3}	0.47	3.76×10^{5}	0	1×10^{-6}	1.9×10^{7}	0	5×10^{-3}	4.14×10^{2}	3.76×10^{5}	From Chapter 7	From Chapter 7	0.663	1.3×10^{3}

TABLE 8.2 INPUT DATA TO THE COMPUTER PROGRAM OF THE BALL MOTION

8.3.2.2 Computer Program of the Flow From the Injector Valve

Fig. (8.8) shows the flow chart of the computer program. The flow chart was mainly the same of section (8.3.2.1).

Q_{vT} - y data points were obtained from Chapter 7. Subroutine E01ADF was used to interpolate at a given value of y from Q_{vT} - y points. Aitken's technique of successive linear interpolation was used. The computer program is shown in Appendix 8.

8.4 RESULTS AND DISCUSSIONS

8.4.1 Analysis with the Assumption of Zero Velocity of the Ball Relative to the Flow Velocity of the Top Inlet

Figs. (8.9 - 8.11) shows the relationship between the velocity of the ball (v_b) with the time (t) for injector tip frequency (f) 60 KHz, maximum amplitude (y_x) of the injector tip , 0.00465 mm, 0.00423 mm and 0.00423 mm respectively, maximum gap (y_w) between the ball and the seat 0.47 mm and supply pressure p_v 20 psi, 40 psi and 60 psi respectively. These figs. show that when the ball left the seat, its velocity decreased with the time between the two walls of the injector valve. The decrease in the velocity was due to the effect of the fluid forces on the motion of the ball. The shape of the decrease of the velocity with the time was similar to the shape of the F_{vf} - y curve. This similarity has given support to the accuracy of the computer program. Also when the ball left the upper wall of the injector valve, its velocity increased (in the negative direction) with the time between the two walls of the injector valve. The shape of the decrease of the velocity with the time was also similar to the shape of the F_{vf} - y curve.

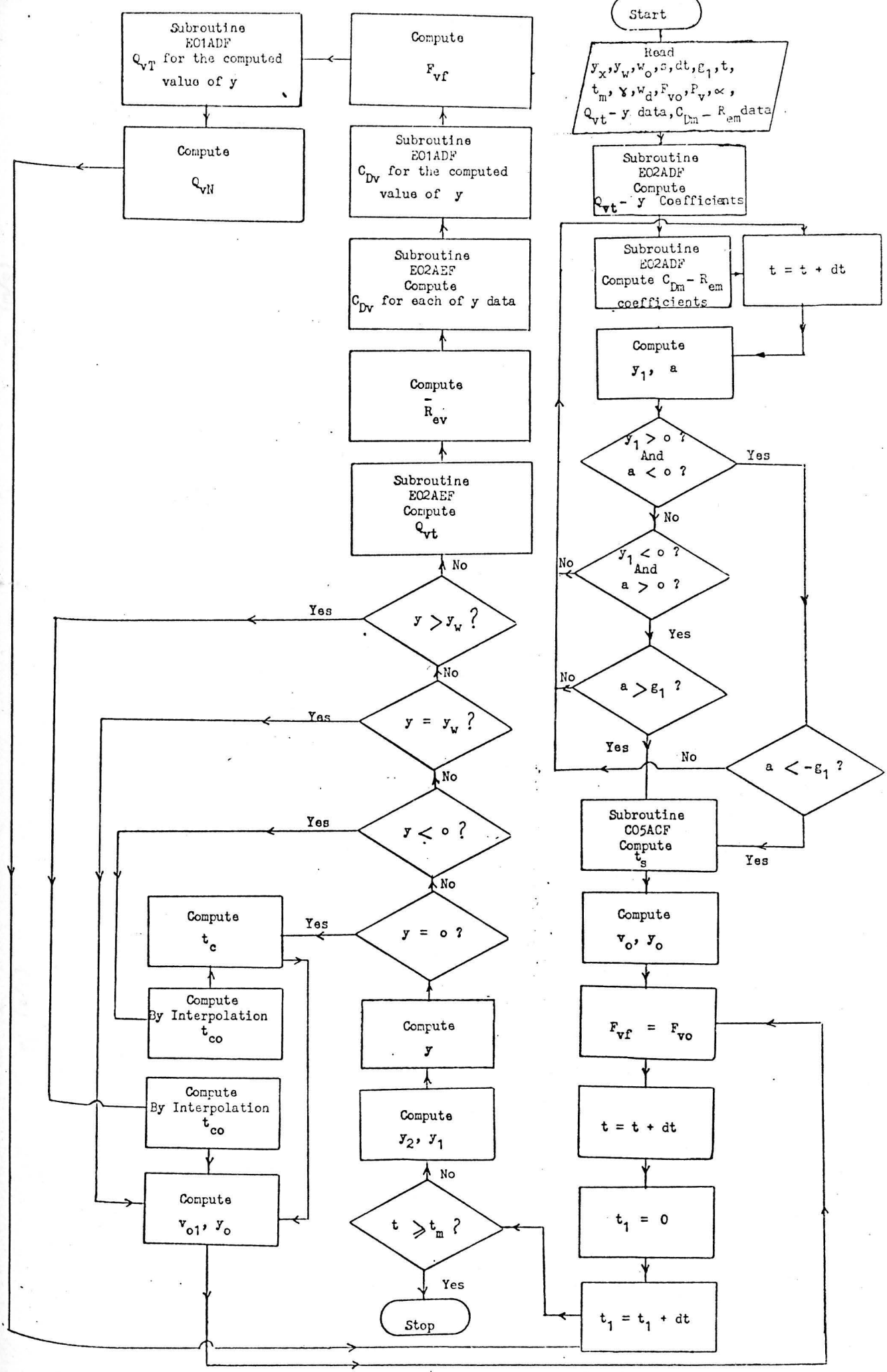

FIG.8.8. FLOW CHART OF THE COMPUTER PROGRAM OF THE FLOW

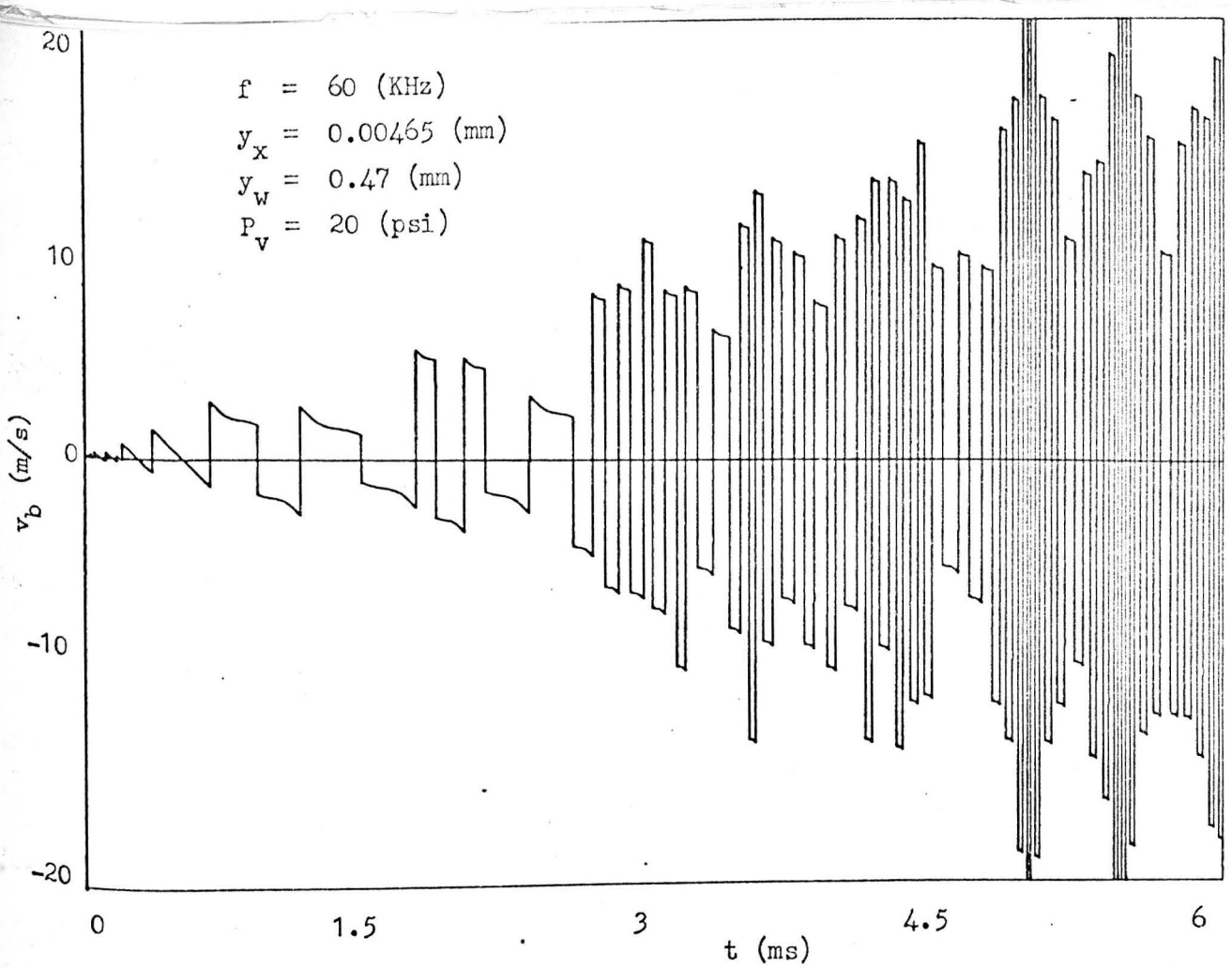

FIG. 8.9 BALL VELOCITY - TIME RELATIONSHIP

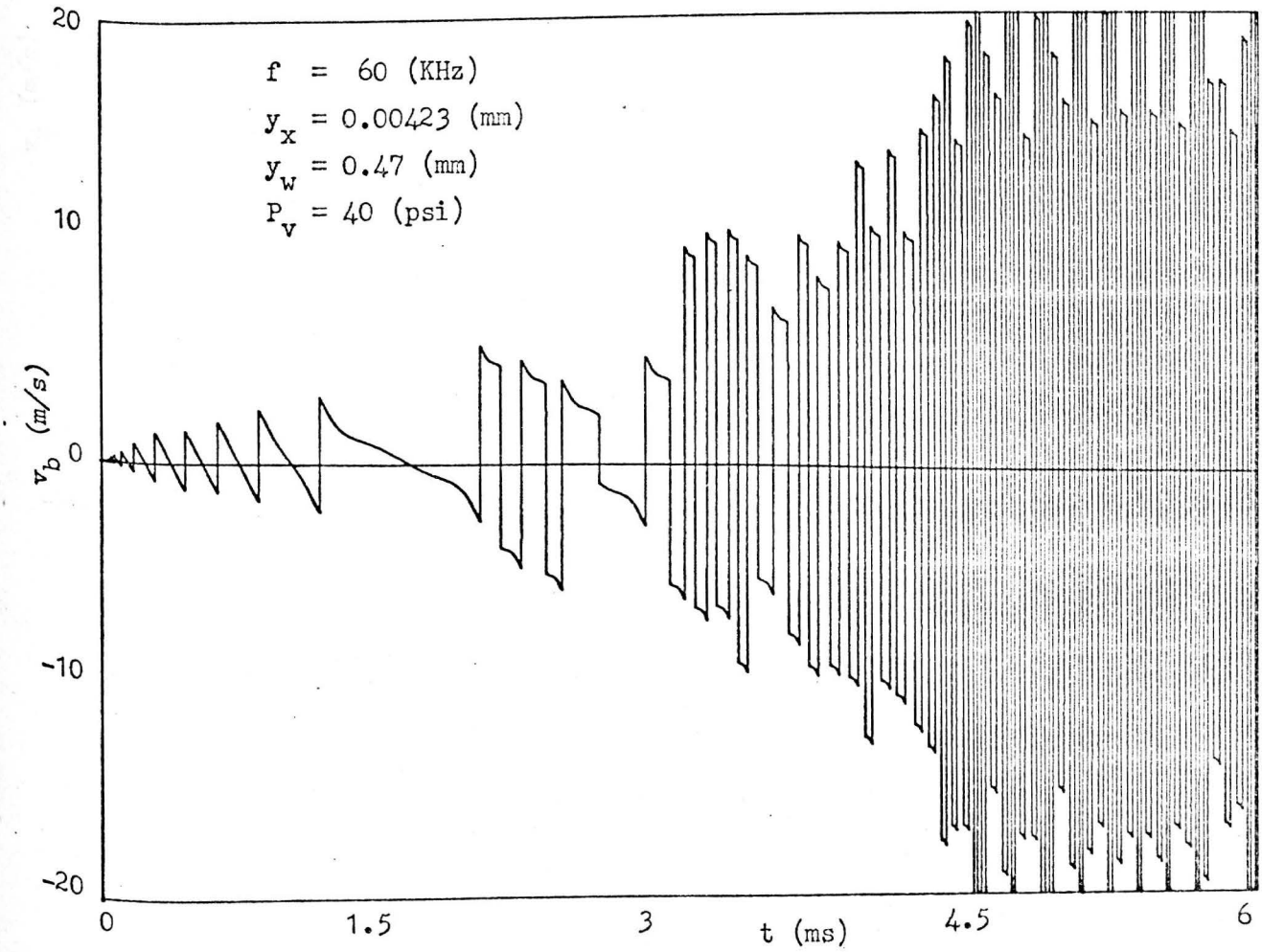

FIG. 8.10 BALL VELOCITY - TIME RELATIONSHIP

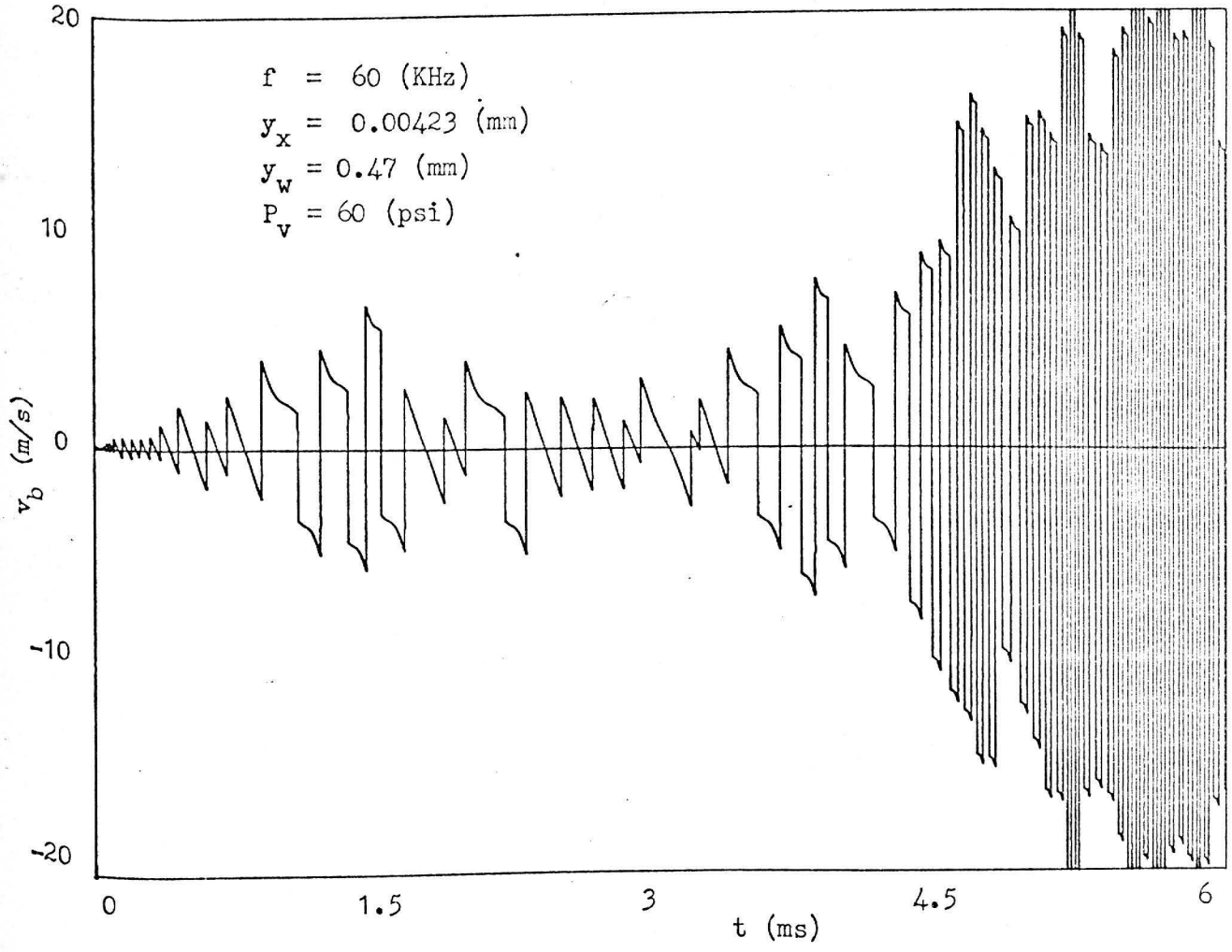

FIG. 8.11 BALL VELOCITY - TIME-RELATIONSHIP

It can be seen from these figs. that the velocity of the ball was significant compared with the flow velocity at the top inlet (the flow velocity at the top inlet was of order 12m/sec). Hence the assumption of zero velocity of the ball relative to the flow velocity of the top inlet was not accurate.

8.4.2 Analysis with the Assumption of Finite Velocity of the Ball Relative to the Flow Velocity of the Top Inlet

8.4.2.1 Motion of the Ball

Figs. (8.12 - 8.14) show the relationship between the ratio (Y) of the gap between the ball and the seat to the maximum gap between the ball and the seat with the time (t), for injector tip frequency (f) 60 KHz, maximum amplitude of the injector tip (y_x) 0.00465 mm, 0.00423 mm and 0.00423 mm respectively, maximum gap between the ball and the seat (y_w) 0.47 mm and supply pressure (p_v) 20 psi, 40 pso and 60 psi respectively.

Fig. (8.12) shows that the ball could reach the upper wall of the injector valve after 0.0008 s from switching on the injector. The ball could reach the upper wall often after 0.0015 s. The reason of the build up in the motion of the ball was due to the effect of the build up in the motion of the injector tip (from the laser results, the tip motion built up in 5 ms) and the effect of the fluid forces on the ball.

Also it can be seen from this fig. that the fluid forces on the ball forced the ball to come back to the seat many times after the build up of the motion of the ball. This is because in these cases the ball had low velocities after the collision with the seat.

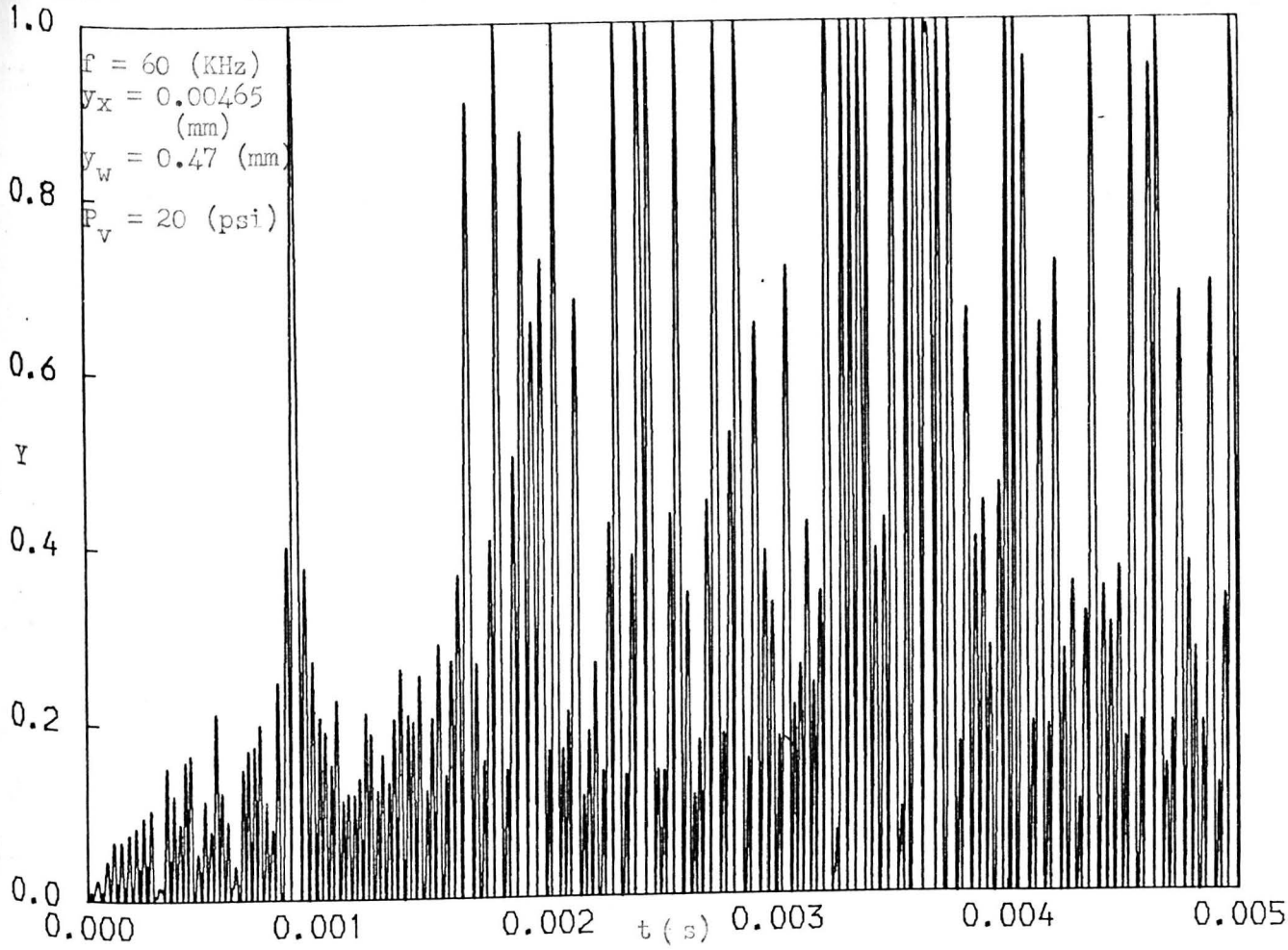

FIG. 8.12 RATIO OF THE GAP BETWEEN THE BALL AND THE SEAT TO THE MAXIMUM GAP - TIME RELATIONSHIP

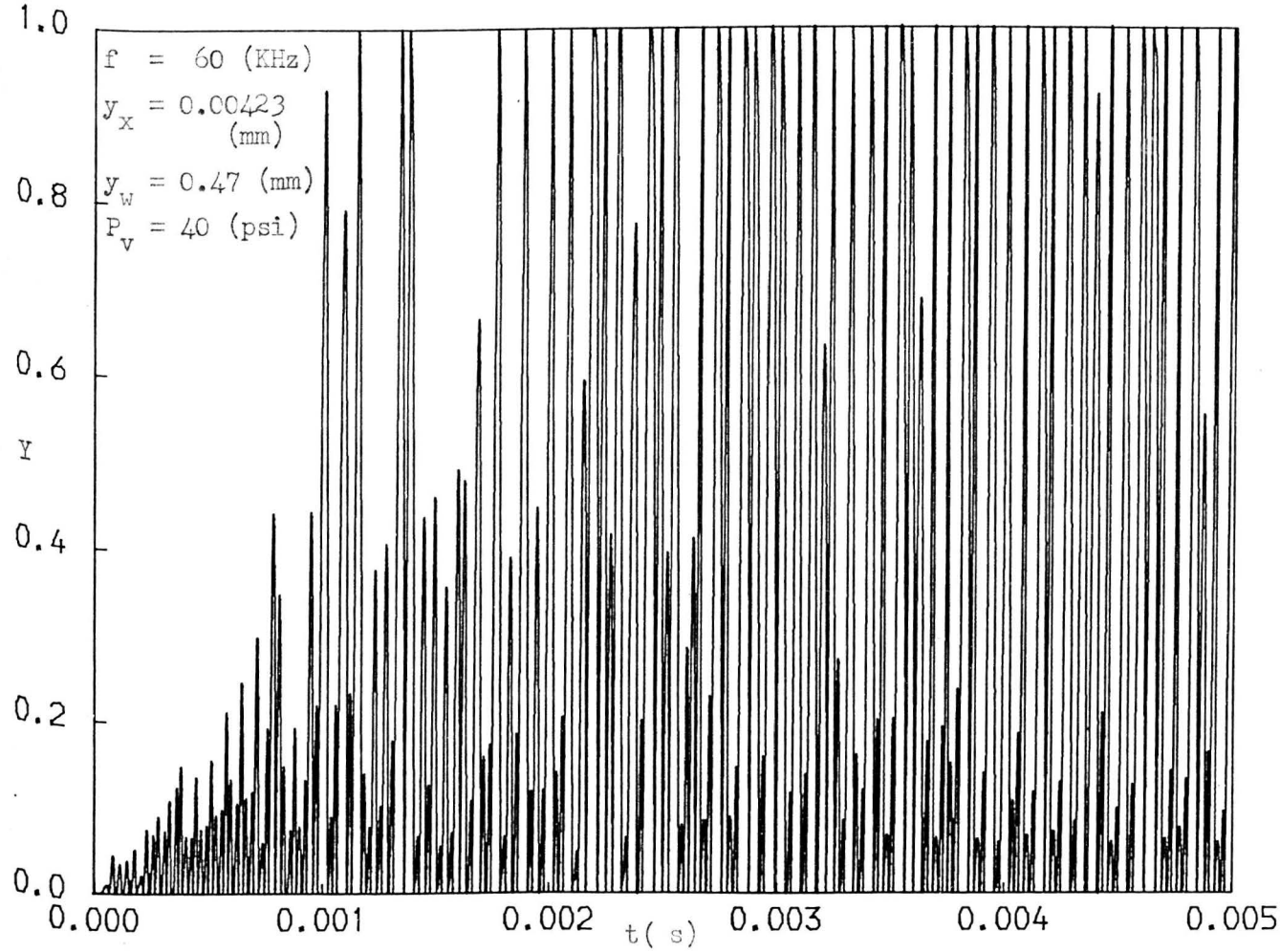

FIG. 8.13 RATIO OF THE GAP BETWEEN THE BALL AND THE SEAT TO THE MAXIMUM GAP - TIME RELATIONSHIP

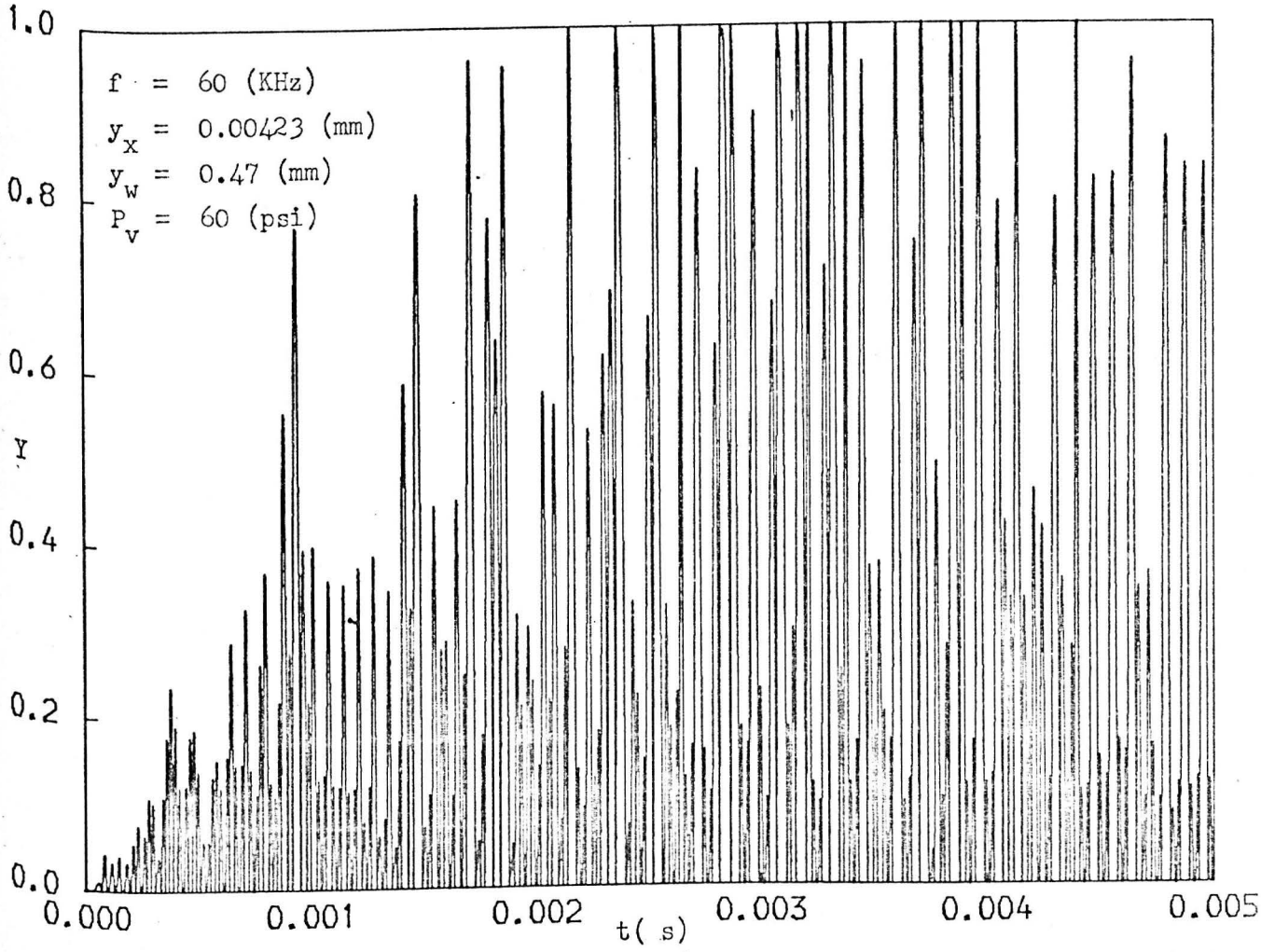

FIG. 8.14 RATIO OF THE GAP BETWEEN THE BALL AND THE SEAT TO THE MAXIMUM GAP - TIME RELATIONSHIP

Fig. (8.13) shows that the ball could reach the upper wall of the valve after 0.0011 s from switching on the injector. The ball could reach the upper wall often after 0.0015 s.

Fig. (8.14) shows that the ball could reach the upper wall of the injector valve after 0.002 s from switching on the injector valve.

It can be seen from these figs. that when the supply pressure was increased from 20 psi to 40 psi, the time of the build up in the motion of the ball was identical. But when the supply pressure was increased from 40 psi to 60 psi, the time of the build up was greater. This is because the increase in the supply pressure could decrease the amplitude of the ball, but in the same time the increase in the supply pressure might change the phase in which the ball hit the seat.

The relationship between the velocity (v_b) of the ball with t, for f = 60 KHz, y_x = 0.00423 mm, y_w = 0.47 mm and P_v = 40 psi is shown in fig. (8.15). This fig. shows how the velocity of the ball changes due to the effect of the fluid force on the ball. This fig. also shows that the shape of the change in the velocity of the ball due to the effect of the fluid force was similar to the F_{vf} - y curve. This similarity has given support to the accuracy of the computer program. Similar ball velocity-time relationship was obtained for supply pressure 20 psi and 60 psi. Fig. (8.16) shows the relationship between the time of each ball cycle (tc) with t, for f = 60 KHz, y_x = 0.00423 mm, y_w = 0.47 mm and P_v = 40 psi. This fig. shows that the ball was moving in random frequency.

The effect of the decay in the motion of the injector tip after

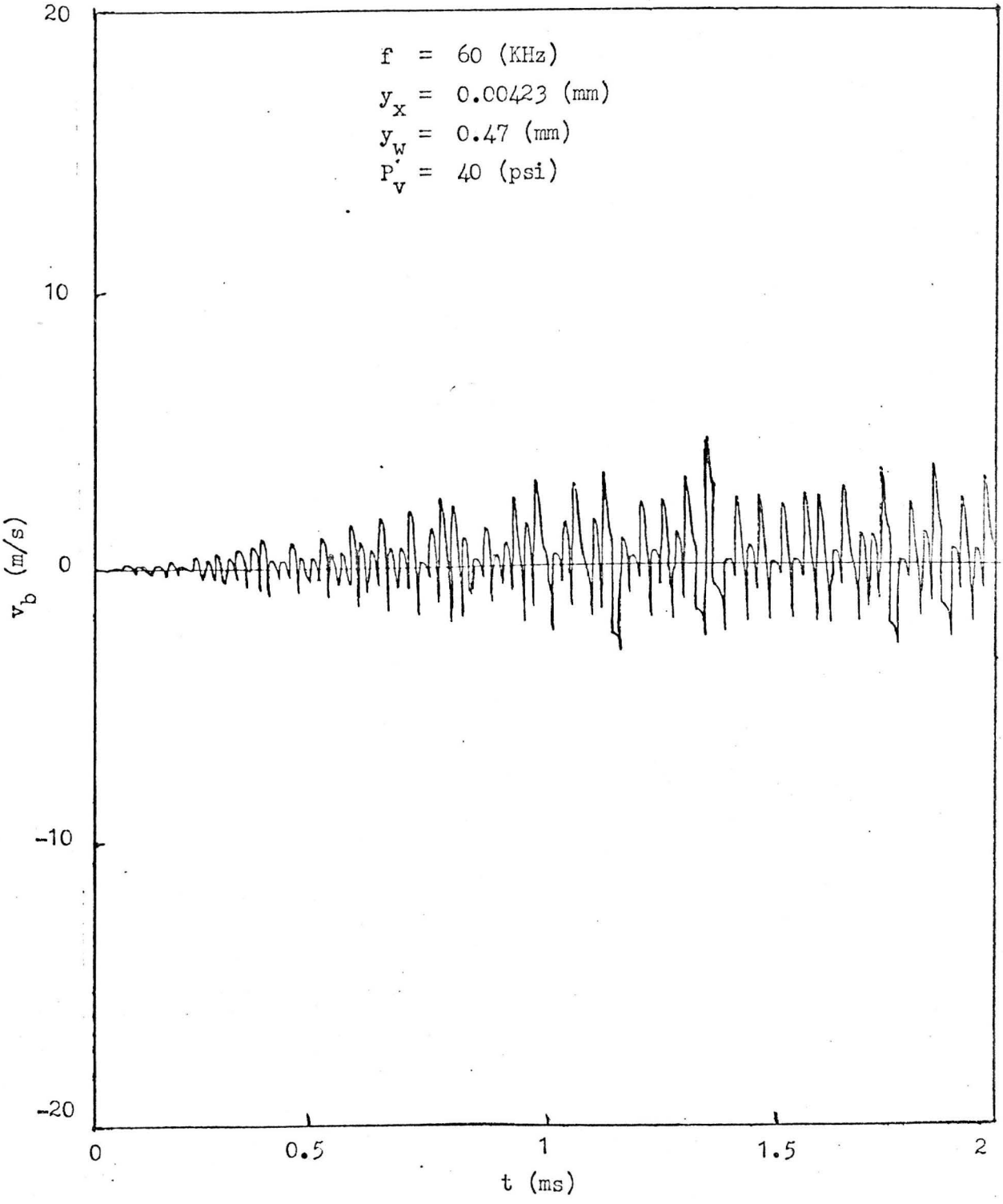

FIG. 8.15 BALL VELOCITY - TIME RELATIONSHIP

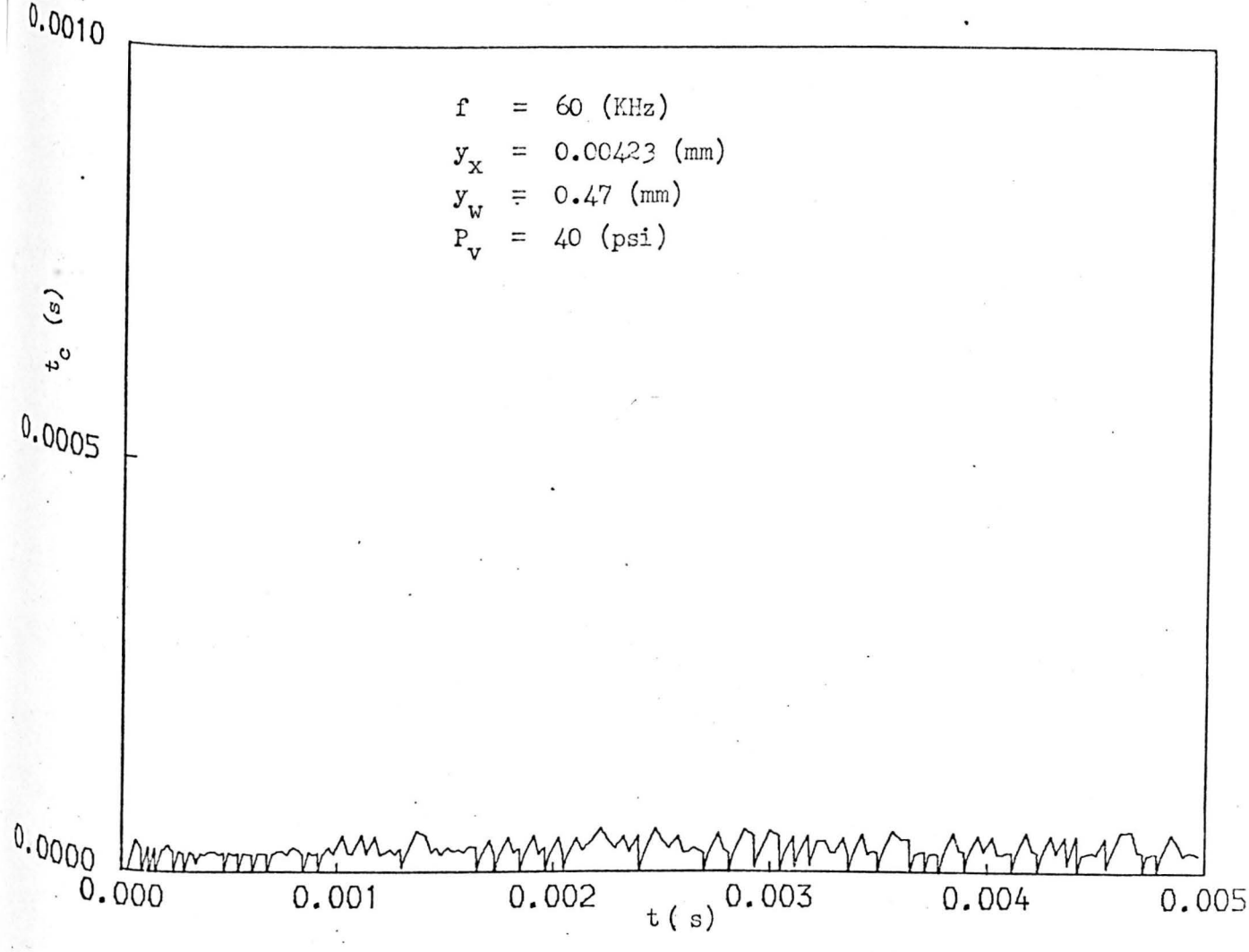

FIG. 8.16 TIME OF THE BALL CYCLE - TIME RELATIONSHIP

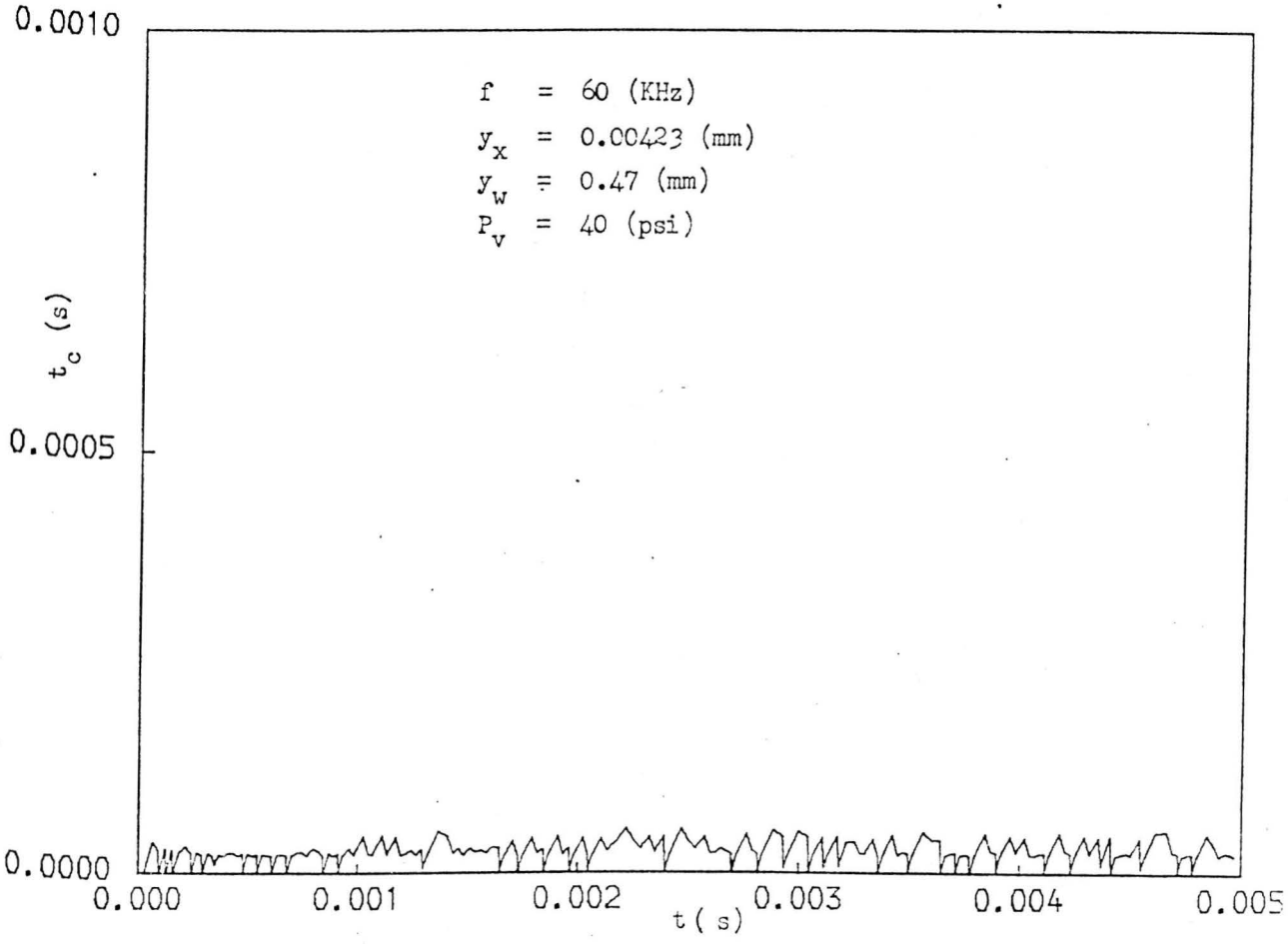

FIG. 8.16 TIME OF THE BALL CYCLE - TIME RELATIONSHIP

switching off the injector on the ball motion is shown in fig. (8.17). This fig. shows the relationship between the ratio (Y) of the gap between the ball and the seat to the maximum gap between the ball and the seat with t, for f = 60 KHz, y_x = 0.00423 mm, y_w = 0.47 mm and P_v = 40 psi. It can be seen from this fig. that the ball could reach the upper wall of the injector valve often in the first millisecond after switching off the injector (the injector was switched off at t = 5 ms). The motion of the ball then decayed to the zero in approximately 2 ms. This fig. shows that the time of decay in the ball motion was 1.5 ms more than the time of decay in the tip motion, due to the continuity in the motion of the ball.

8.4.2.2 Flow from the Injector Valve

8.4.2.2.1 Flow Rate

Figs. (8.18- 8.20) show total flow rate (Q_{vT}) from the injector valve - time (t) relationship, for f = KHz, y_x = 0.00465 mm, 0.00423 mm and 0.00423 mm respectively; y_w = 0.47 and P_v = 20 psi, 40 psi, and 60 psi respectively. These figs. show that the total flow rate has built up to 80% of the maximum value after approximately 0.5 ms from switching on the injector. This is because the total flow rate built up to the maximum value after 30% of the maximum gap between the ball and the seat.

The effect of the decay in the ball motion after switching off the injector on the total flow rate is shown in Fig. (8.21). This fig. represents the relationship between the total flow rate

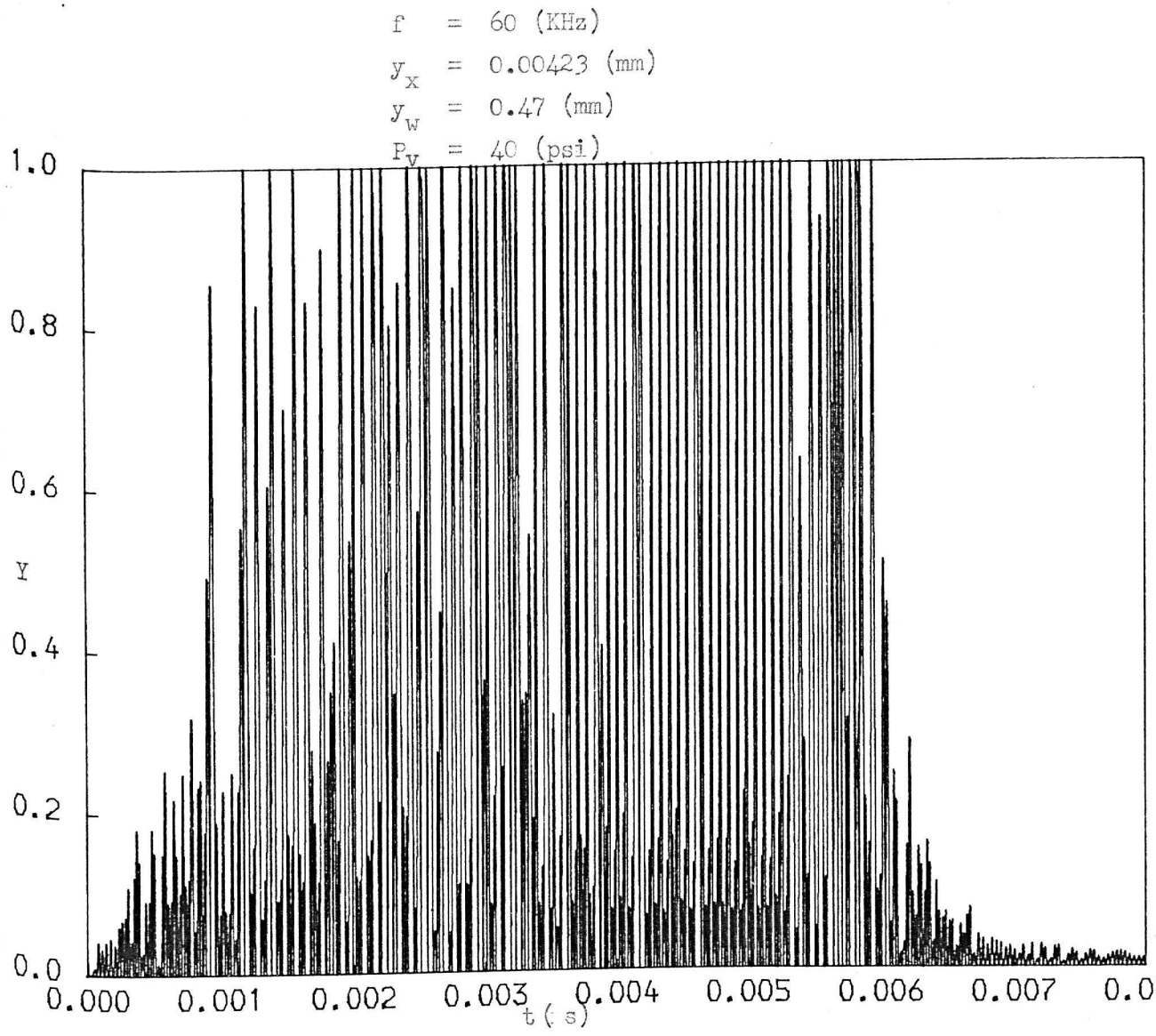

FIG. 8.17 RATIO OF THE GAP BETWEEN THE BALL AND THE SEAT TO THE MAXIMUM GAP - TIME RELATIONSHIP

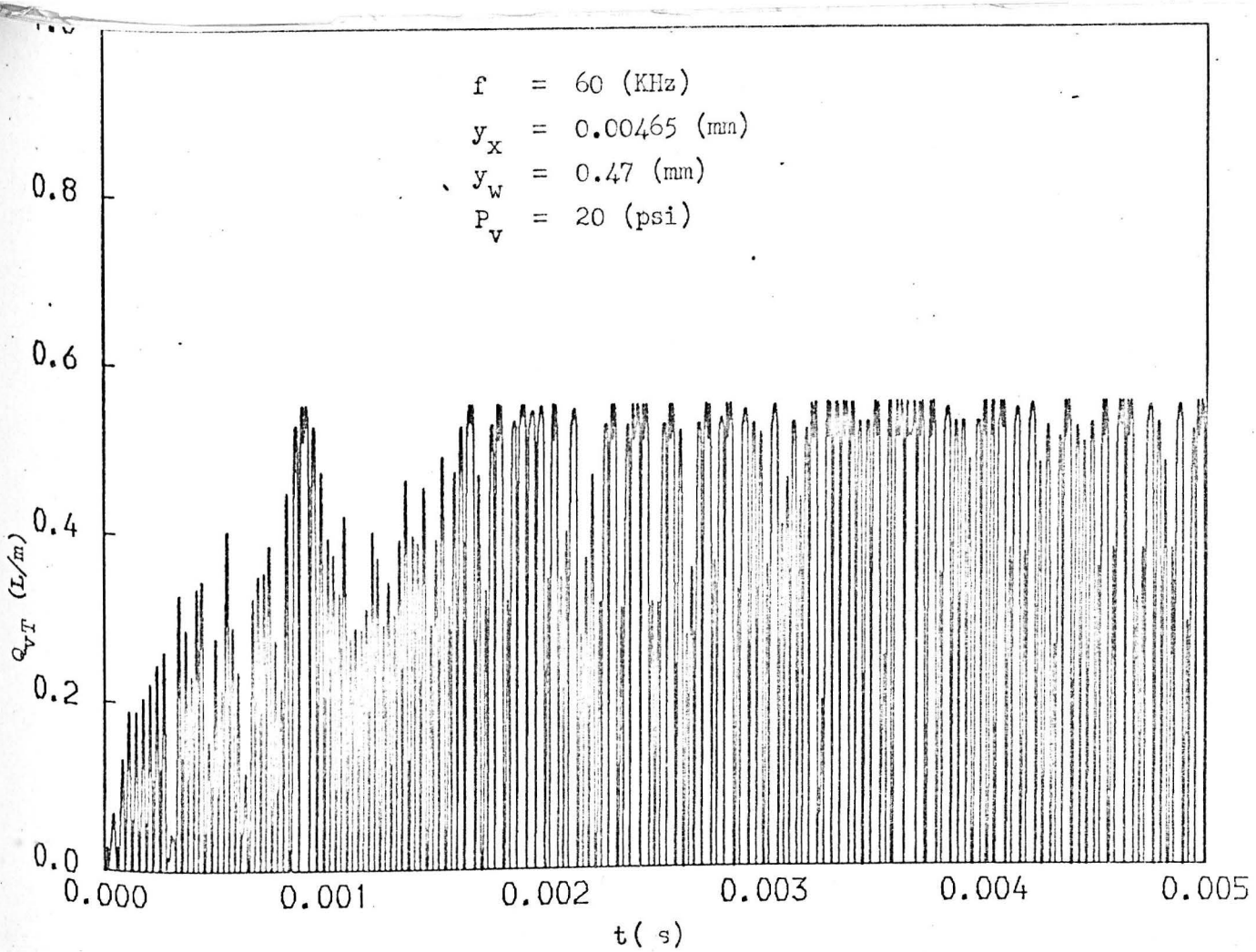

FIG. 8.18 TOTAL FLOW RATE - TIME RELATIONSHIP

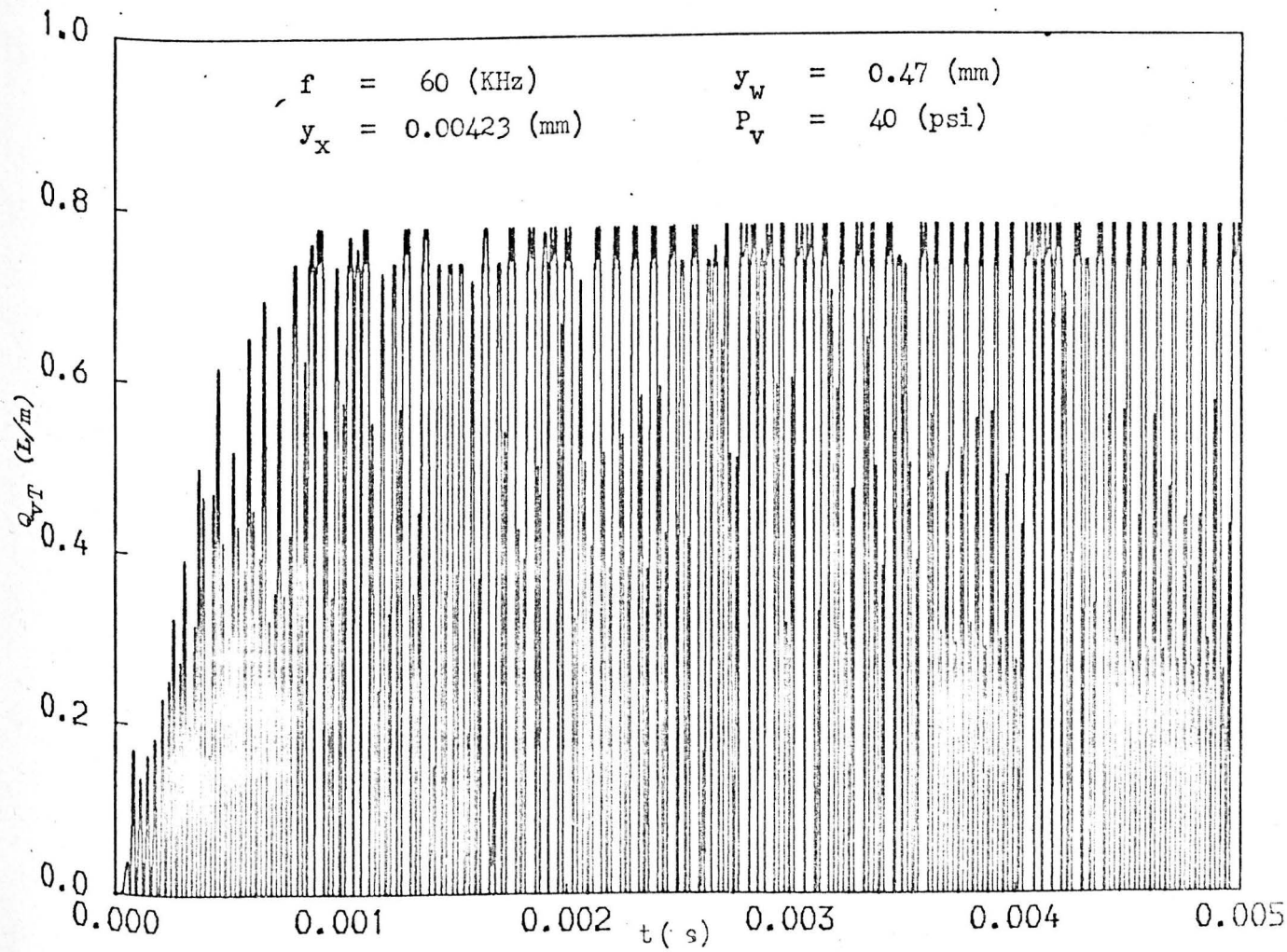

FIG. 8.19 TOTAL FLOW RATE - TIME RELATIONSHIP

$f = 60$ (KHz)

$y_x = 0.00423$ (mm)

$y_w = 0.47$ (mm)

$P_v = 60$ (psi)

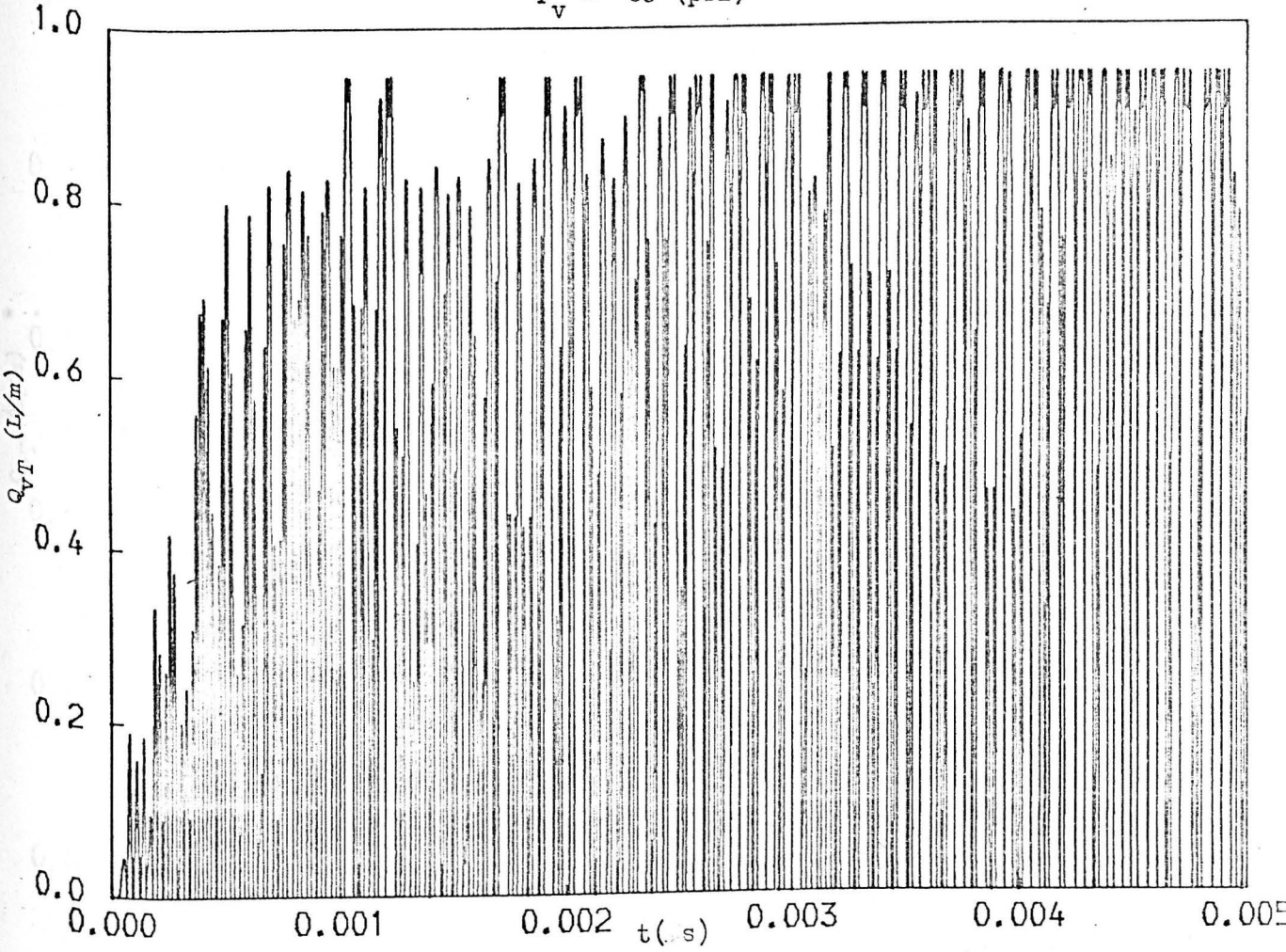

FIG. 8.20 TOTAL FLOW RATE - TIME RELATIONSHIP

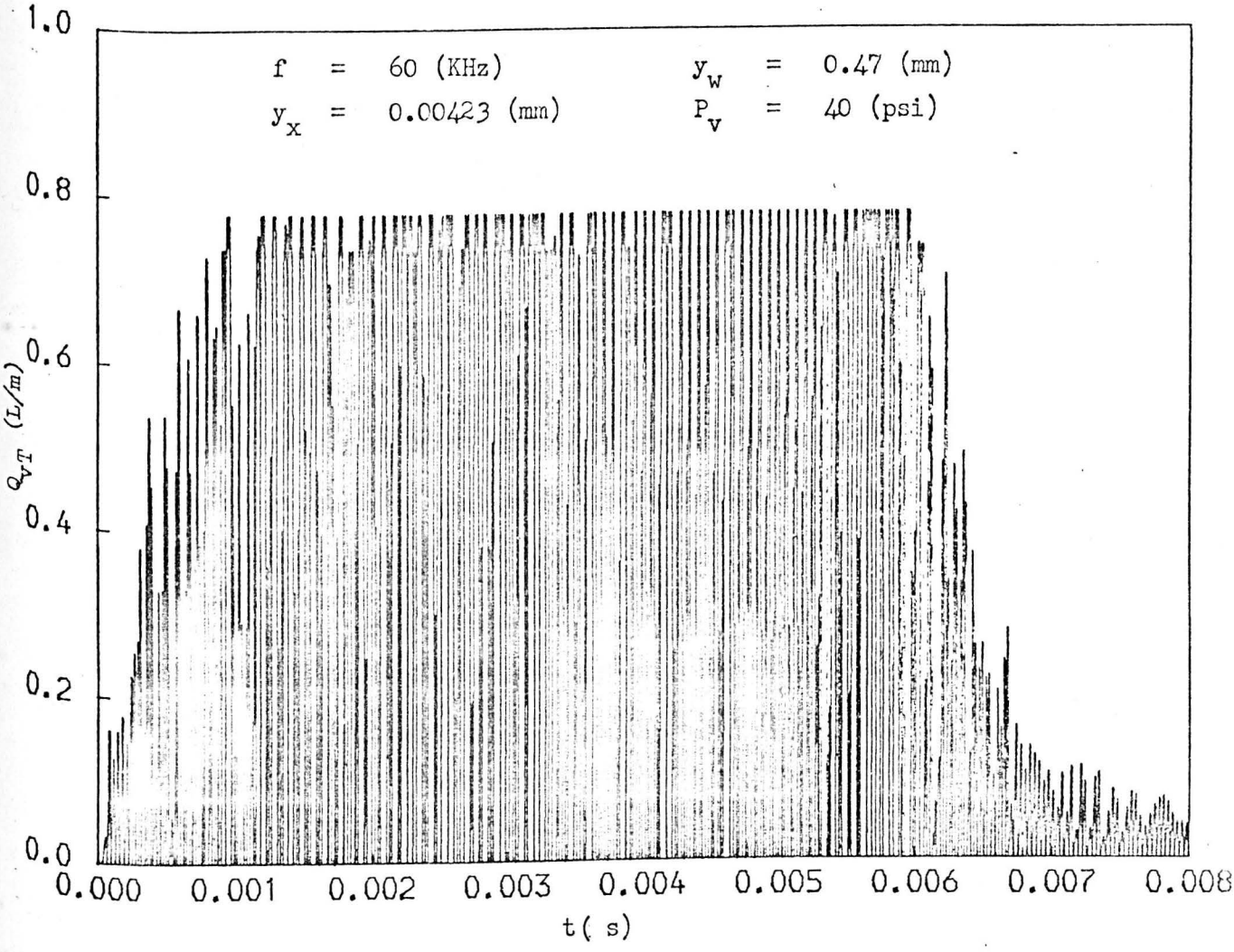

FIG. 8.21 TOTAL FLOW RATE - TIME RELATIONSHIP

from the injector valve with the time for $f = 60$ KHz, $y_x = 0.00423$ mm and $P_v = 40$ psi. This fig. shows that the total flow rate could reach the maximum value after the first millisecond after switching off the injector (the injector was switched off at $t = 5$ ms). The total flow rate was then delayed to zero for approximately two milliseconds.

8.4.2.2.2 Total Flow

Fig. (8.22) shows the total flow (Q_{vN}) - time (t) relationship for $f = 60$ KHz, $y_x = 0.00465$ mm, 0.00423 mm and 0.00423 mm respectively, $y_w = 0.47$ mm and $P_v = 20$ psi, 40 psi and 60 psi respectively. This fig. shows that for supply pressure 20 psi the change of the total flow with time (total flow rate) became constant after approximately 1.5 ms from switching on the injector. This is because the total flow rate built up to the maximum value in 1.5 ms (see fig. (8.18)). Also this is because the total flow rate built up to the maximum value in a very small gap between the ball and the seat. For the same reason this fig. shows that the total flow rate of supply pressure 40 psi and 60 psi became constant after 1.5 ms and 2 ms respectively (see figs. (8.19) and (8.20)). Comparing these plots shows that the total flow was identical in the rime range 0 - 0.5 ms. The reason for this is because when the supply pressure increased the total flow rate increased but in the mean time the amplitude of the ball was reduced due to the effect of the increase of the flow force. The effect of the increase of the supply pressure on the ball amplitude was important in this time range because the velocity of

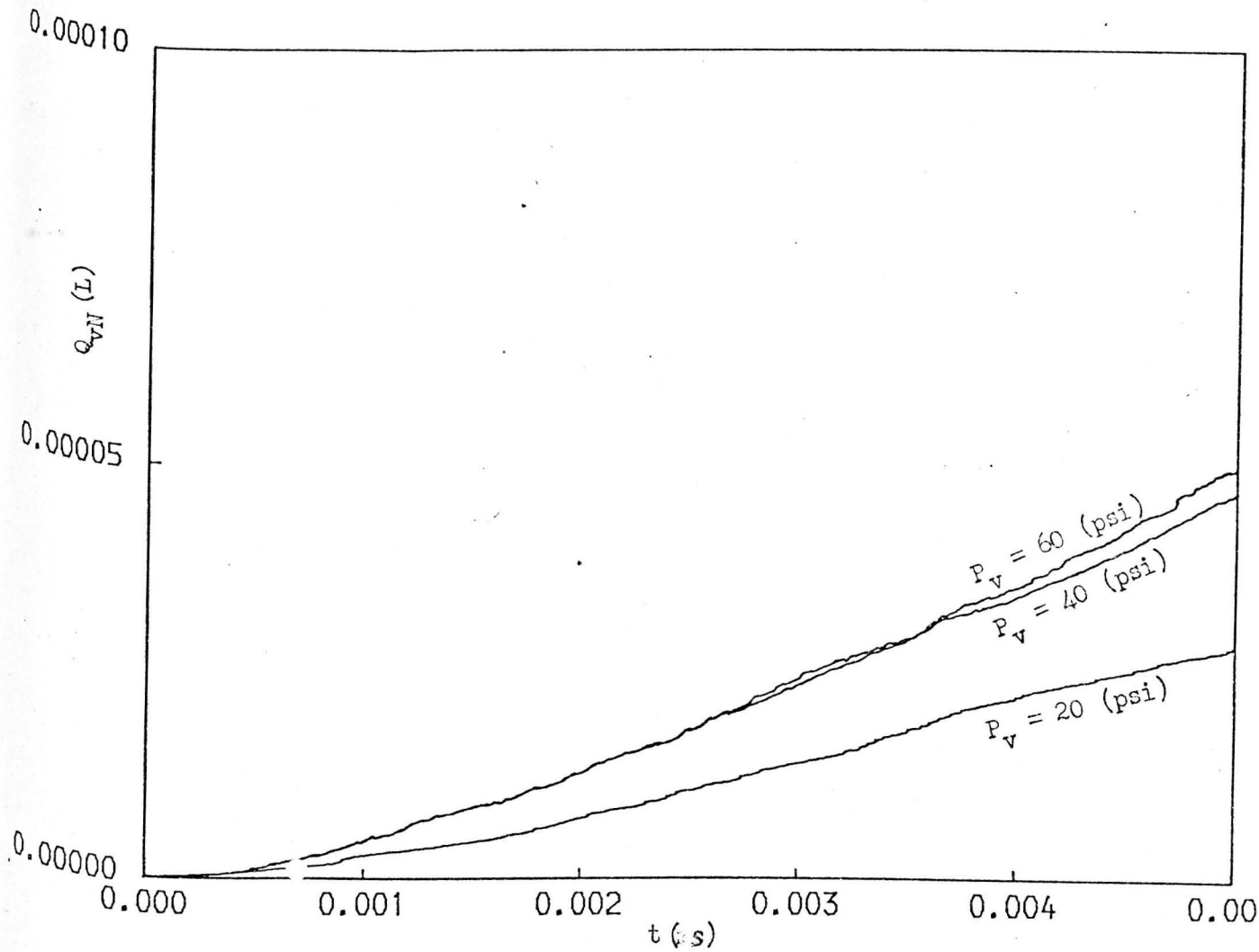

FIG. 8.22 TOTAL FLOW - TIME RELATIONSHIP

the ball after the collision with the seat was very small. Also this fig . show that when the supply pressure increased from 20 psi to 40 psi, the total flow rate increased. The explanation of this is because the increase in the flow rate due to the increase of the supply pressure was greater than the decrease in the total flow rate due to the decrease in the amplitude of the ball due to the increase of the supply pressure. It can be seen from the fig. that when the supply pressure increased from 40 psi to 60 psi, the total flow rate remained almost identical. This is because the increase of the flow rate due to the increase of the supply pressure was approximately identical with the decrease in the flow rate due to the decrease in the ball amplitude due to the increase of the supply pressure. Experimental evidence of this theoretically predicted phenomenon is included in Chapter 11. Also this fig . show that the average flow rate (total flow/time) was approximately equal to 60% of the peak flow rate (which is shown in figs. (8.18 - 8.20)) for pressures below the pressure at which the flow is the maximum. It can also be seen from this fig. that the total flow was fluctuating due to the random frequency of the ball.

Chapter Nine

MODEL TESTS OF FLOW RATES AND BALL FLOW FORCE FOR DIFFERENT GEOMETRIES OF THE INJECTOR VALVE

9.1 INTRODUCTION

Studying the effect of the geometry of the injector valve on the flow force on the ball and on the flow rates should give better understanding of the behaviour of the injector and lead to its improvement.

In this chapter the flow force on the ball, the total flow rate and the inlet flow rates for each position of the ball were measured in five scale models of different geometries of the injector valve.

The final section is concerned with estimating theoretically the flow rate and the flow force on the ball at small lift in all the models using a simple theory. These estimates are compared with the measurements.

The details of the test apparatus, test procedure, test program, analysis of the experimental data and results and discussions are given below.

9.2 TEST APPARATUS

Fig. (9.1) shows a photograph of the test apparatus used, while the layout is given in fig. (9.2).

The apparatus consisted of a model of the injector valve, a perspex tank, instruments for measuring the static pressure at the top inlet and at the outlet of the model, the flow rate from the model and the flow force on the ball.

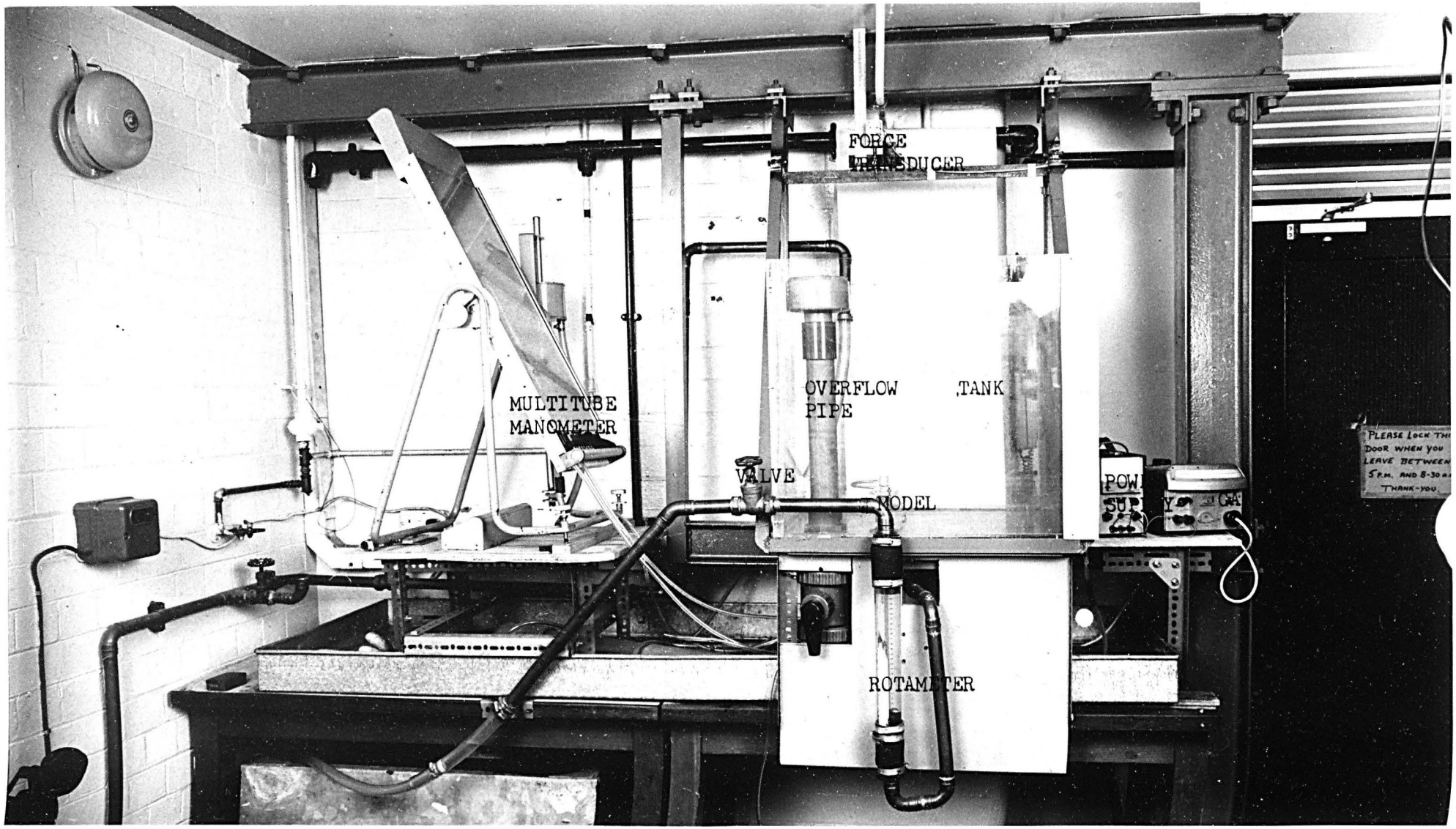

FIG. 9.1 APPARATUS FOR MEASURING FLOW FORCE AND FLOW RATES

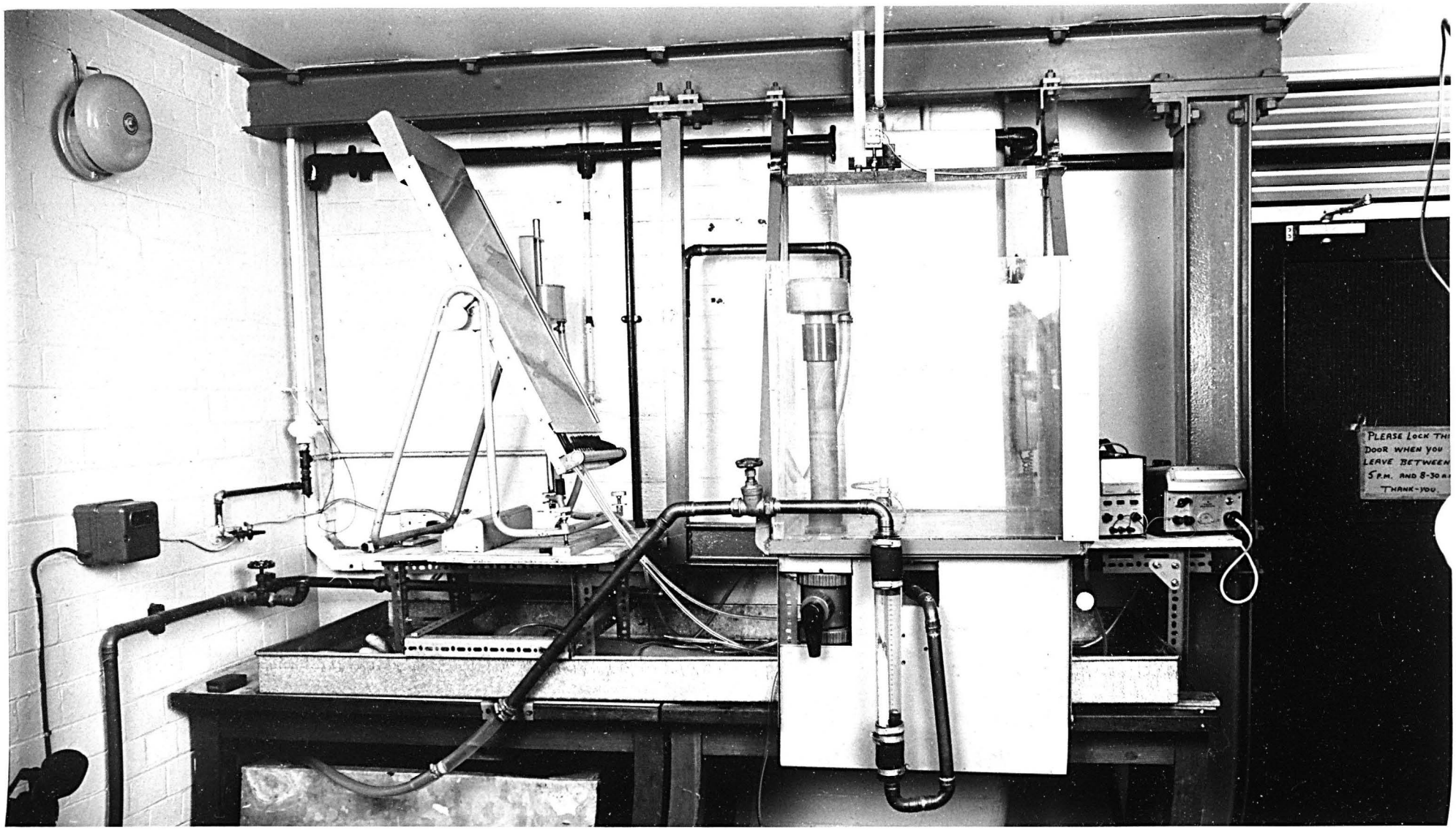
PLEASE LOCK THI
DOOR WHEN YOU
LEAVE BETWEEN
5 P.M. AND 8-30 A.
THANK-YOU.

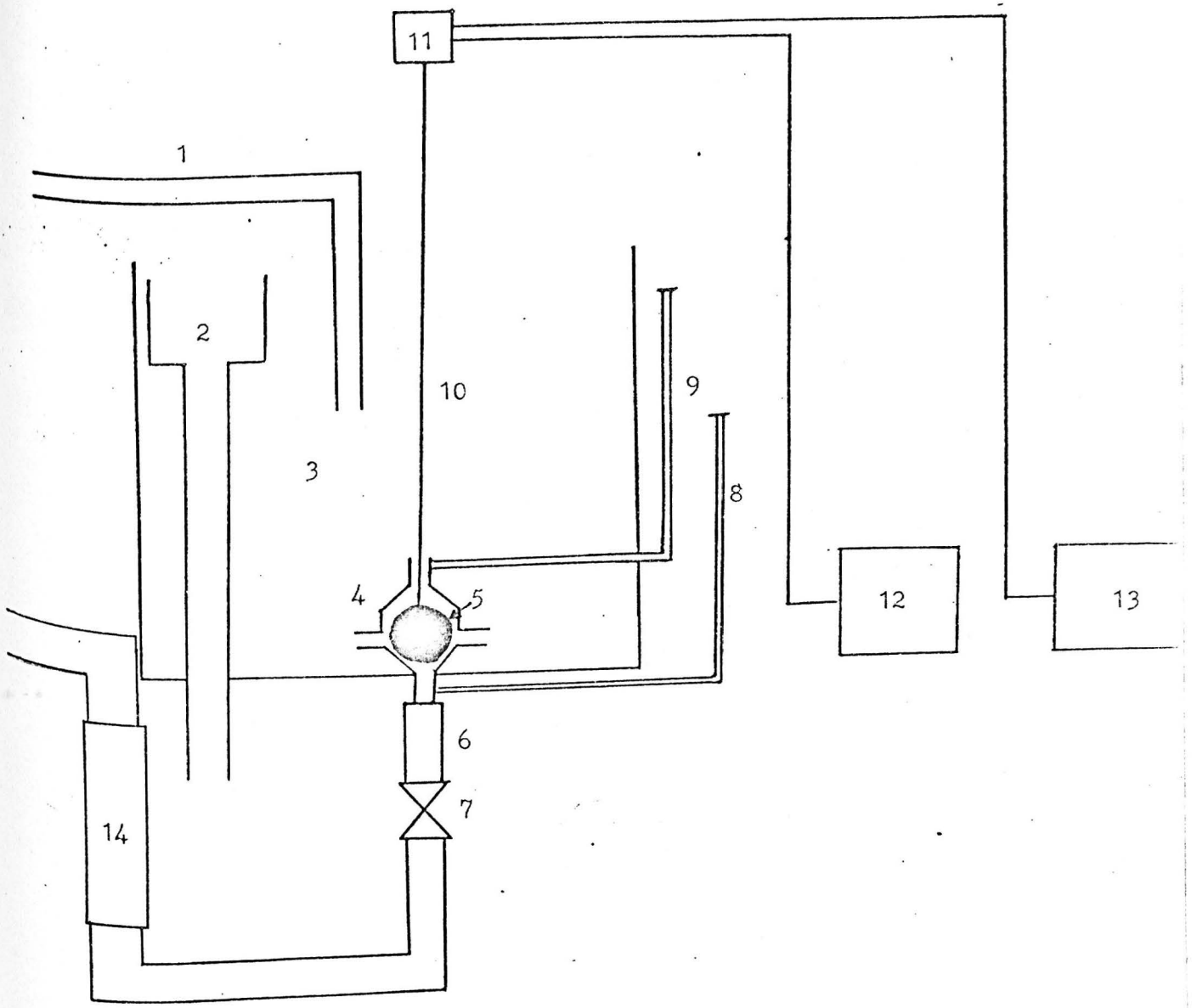

1. Pipe from the Pump.
2. Overflow Pipe.
3. Perspex Tank.
4. Model.
5. Ball.
6. Outlet Pipe.
7. Gate Valve.
8. Vertical Manometer.
9. Multitube Manometer.
10. String.
11. Force Transducer.
12. Power Supply.
13. Galvanometer.
14. Rotameter.

FIG. 9.2 LAYOUT OF THE TEST APPARATUS

Five enlarged models (A, B, C, D, and E) of different geometries of the injector valve were designed. Fig. (9.3) shows a photograph of the models, while the main dimensions of each model are given in table (9.1). The main dimensions of the model which is described in Chapter 7 are also given in this table. The model was made geometrically similar to the injector valve and the scale factor was 20.6. The boundaries of the models were made from perspex and in two parts. The upper part contained the top inlet and the lower part contained the outlet and the side inlets, or were without any side inlets (open all round). The two parts were connected by screws. The model was screwed to the bottom of the tank. The tank was made from perspex and was of dimensions 65 cm x 61 cm x 58 cm. The height of the tank was designed to give a suitable pressure head. The water was supplied to the tank by a pump. The level of the water in the tank was kept constant during the test by fixing an overflow pipe in the tank. The static pressure at the top inlet of the model was measured by a multitube manometer. The static pressure at the outlet of the model was measured by a vertical manometer. The total flow rate from the model was measured by a rotameter (Rotameter Manufacturing Co.) and controlled by a gate valve.

The ball was connected to the force transducer (Pye Ether, type UF1) by a strong wire. The other end of the ball was connected to a small piece of a brass bar passing through a guide to keep the centre of the ball always on the vertical centre line of the model. The force transducer was fixed rigidly on a plate which could be positioned anywhere along the length of a screw bar. This was achieved by means of two nuts. The electric power was supplied to

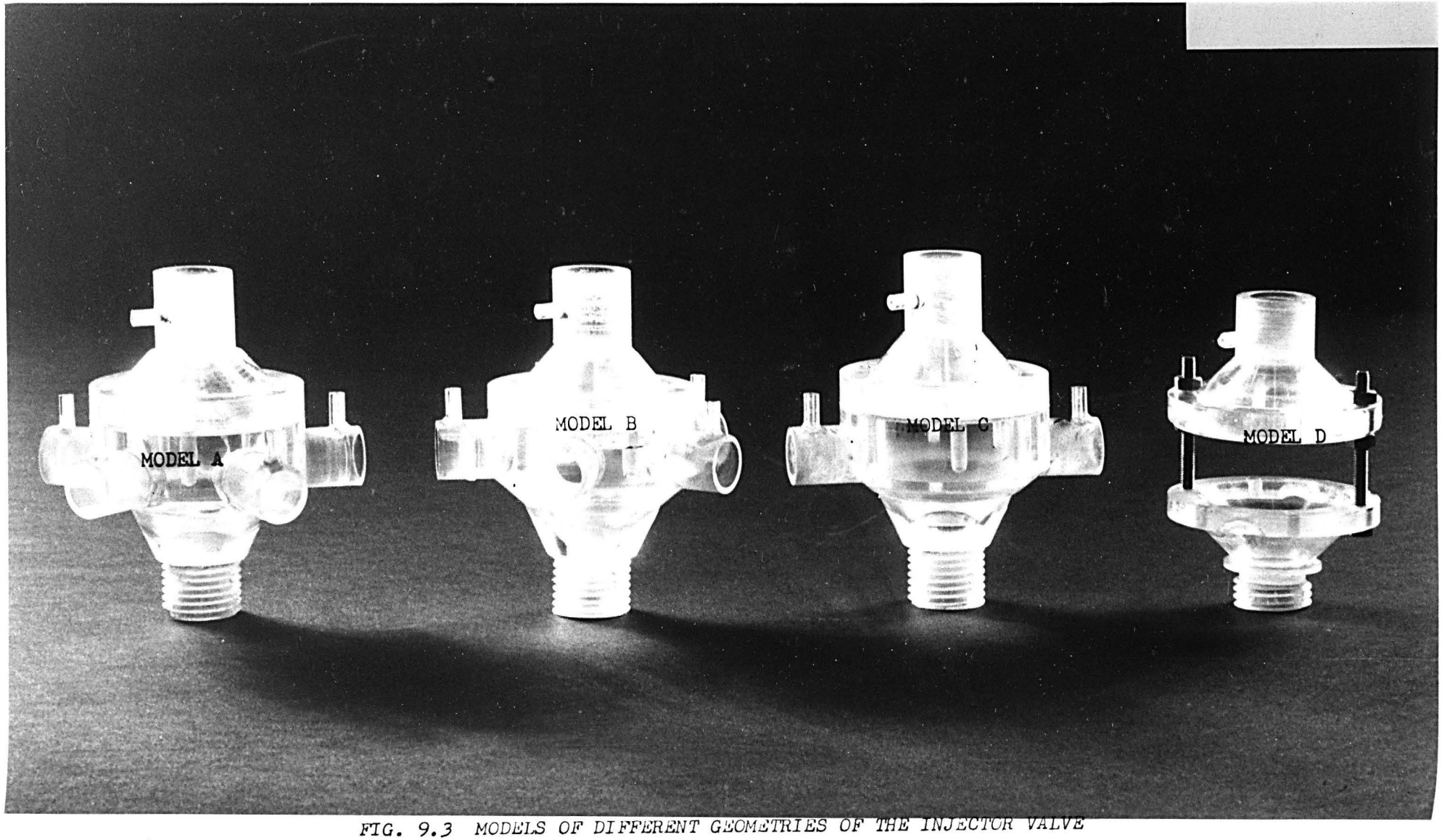

FIG. 9.3 MODELS OF DIFFERENT GEOMETRIES OF THE INJECTOR VALVE

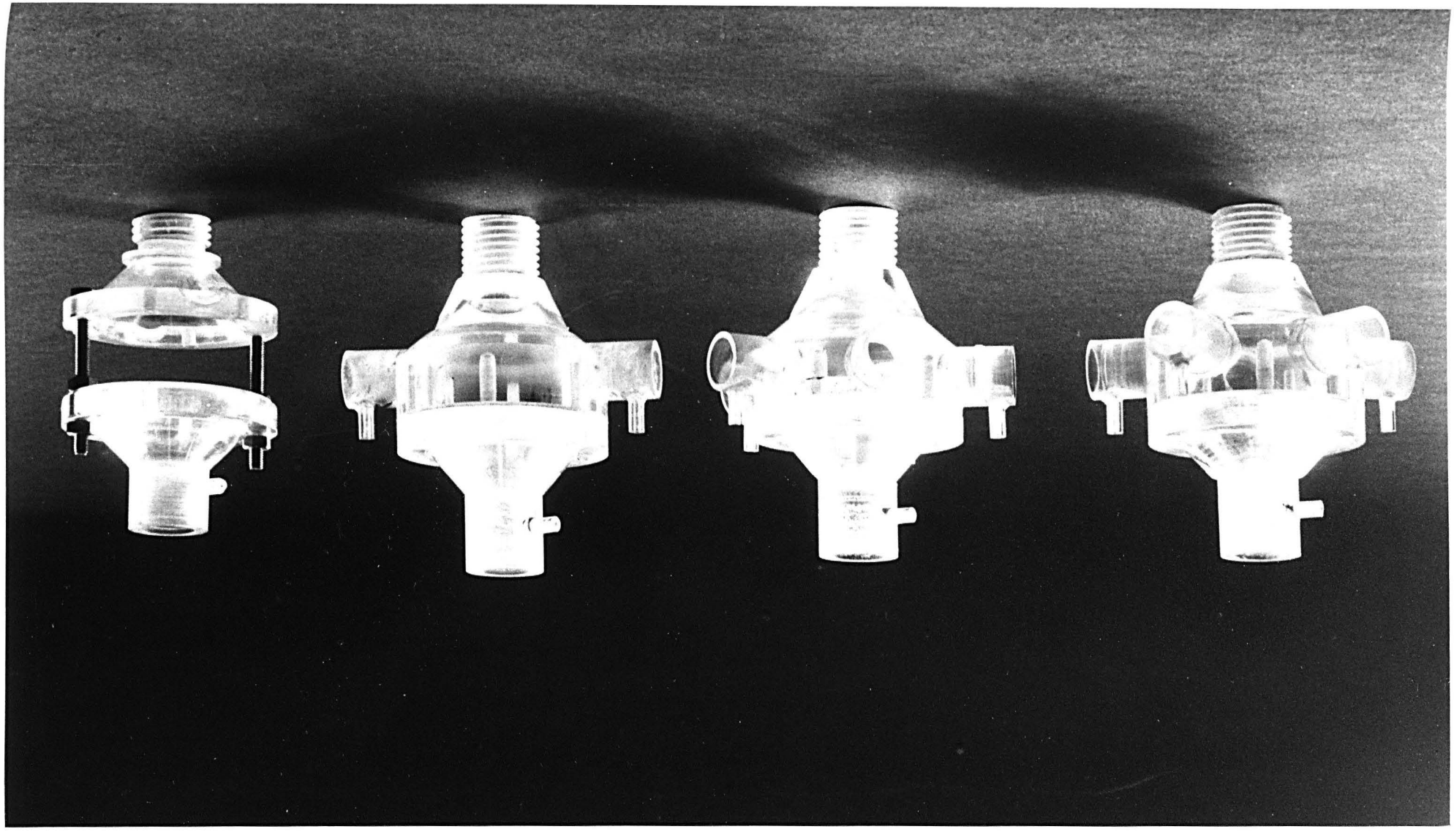

Model	n	a (cm)	b (cm)	c (cm)	d (cm)	e (cm)	f (cm)	A_1 (cm^2)	A_2 (cm^2)	A_3 (cm^2)	A_4 (cm^2)	A_5 (cm^2)
A	5	1.7	1.1	1.5	1.7	4.4	3	2.24	1.27	9.43	1.27	2.24
B	5	1.7	0.93	1.5	0.85	4.4	3	2.24	1.1	9.43	1.1	0.56
C	2	1.7	0.93	1.5	1.7	4.4	3	2.24	1.1	2.83	1.1	2.24
D	*	1.7	0.8	1.6	1.7	5	3	2.24	0.9	25.1	0.9	2.24
E	*	1.7	1.4	2.3	1.7	5	3	2.24	1.5	36.1	1.5	2.24
Chapter 7 model	2	1.7	0.97	1.5	1.7	5	3	2.24	1.16	2.83	1.16	2.24

n No. of Side Inlets
a Top Inlet Diameter
b Ball Travel
c Side Inlet Diameter
d Outlet Diameter
e Cavity Diameter
f Perimeter Diameter

A_1 Area of the Top Inlet
A_2 Area Above the Ball
A_3 Area of the Side Inlets
A_4 Area Under the Ball
A_5 Area of the Outlet
* Open all Round

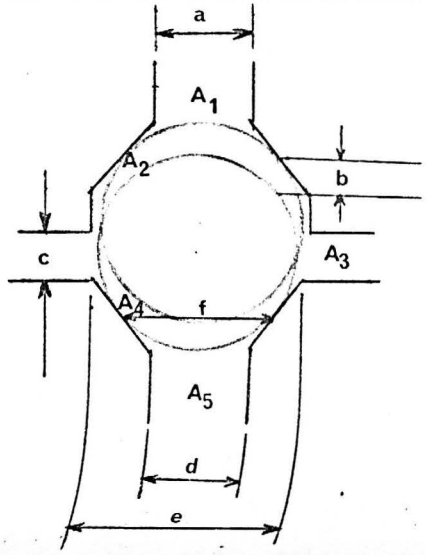

TABLE 9.1 MAIN DIMENSIONS OF THE MODELS

the force transducer by a power supply (Farnell, type E 30/2). The output of the force transducer was read on a galvanometer (W. G. Pye & Co. Ltd.).

9.3 TEST PROGRAM

In each test the flow forces on the ball, the total flow rate, the static pressure at the top inlet and the static pressure at the outlet were measured. These measurements were done for different positions of the ball in the model, and for a corresponding supply pressure of the injector valve. The test Reynolds numbers were those corresponding to 20 psi, 40 psi and 60 psi supply pressure to the injector valve.

9.4 TEST PROCEDURE

Before starting the test, the rotameter was calibrated by a weighing method. Also top inlet flow was calibrated* by a weighing method. The force transducer was also calibrated by putting weights on the ball which was connected by a wire to the force transducer, and reading the corresponding voltage on the galvanometer.

To start the test the ball was fixed at the upper wall of the model. The position of the force transducer was read by means of a rule fixed on a bar. The position of the transducer was considered as the zero position of the ball. The ball was then moved down 1 mm from the upper wall of the model. At this position the indicator of the galvanometer was fixed at zero on the scale. This position of the indicator represented zero fluid forces on the ball. The water was then delivered to the tank by switching on the pump.

* against the multitude manometer

After getting the constant level of the water in the tank, the static pressure at the outlet of the model was then fixed during the test by using the valve. The value of the static pressure at this point was calculated by equating Euler number between the top inlet and the outlet of this injector valve and that of the model.

$$\frac{P_{vt} - p^*_{vo}}{\frac{1}{2}\rho_v V^2_{vo}} = \frac{P_{mt} - p^*_{mo}}{\frac{1}{2}\rho_m V^2_{mo}}$$

where P_{vt} represents supply pressure at the top inlet of the valve, p^*_{vo} piezometric pressure at the outlet of the valve, ρ_v density of the liquid in the valve, V_{vo} flow velocity at the outlet of the valve, P_{mt} supply pressure at the top inlet of the model, p^*_{mo} piezometric pressure at the outlet of the model, ρ_m density of the liquid in the model and V_{mo} flow velocity at the outlet of the model.

The static pressure at the top inlet was measured by the multitube manometer. This measurement was done to calculate the flow rate at the top inlet from the calibration of the static pressure versus the flow rate at the top inlet.

The following readings were then taken:

1. The galvanometer reading.
2. The rotameter reading.
3. The multitube manometer reading.

The ball was then lowered in 1 mm steps and the procedure was repeated at 0.5 mm from the seat.

The same procedure was repeated for each test.

9.5 MEASURING ANALYSIS OF THE EXPERIMENTAL DATA

The measuring analysis of the experimental data was the same as that of Chapter 7 (see section (7.5)).

Eqn. (7.6) was used to calculate the flow rate (Q_{vt}) at the top inlet of the valve.

$$Q_{vt} = Q_{mt} \frac{d_{vt}}{d_{mt}} \frac{\nu_v}{\nu_m} \tag{9.1}$$

where Q_{mt} represents the flow rate at the top inlet of the model, d_{vt} diameter of the top inlet of the valve, d_{mt} diameter of the top inlet of the model, ν_v kinematic viscosity of the liquid in the valve and ν_m kinematic viscosity of the liquid in the model.

By the same procedure the total flow rate (Q_{vT}) from the valve was calculated. The side inlets flow rate (Q_s) was calculated by subtracting the top inlet flow rate from the total flow rate.

Eqn. (7.14) was used to calculate the flow force on the ball of the valve:

$$F_{vf} = F_{mf} \frac{\rho_v}{\rho_m} \left(\frac{D_v}{D_m}\right)^2 \left(\frac{V_{vt}}{V_{mt}}\right)^2 \tag{9.3}$$

where F_{vf} represents the flow force on the ball of the valve, F_{mf} flow force on the ball of the model, D_v diameter of the ball of the valve, D_m diameter of the ball in the model, V_{vt} flow velocity at the top inlet of the valve and V_{mt} flow velocity at the top inlet of the model.

Eqn. (7.15) was used to calculate the flow force on the ball of the model:

$$F_{mf} = F_e + F_{mb} \qquad (9.4)$$

where F_e represents the measured flow force on the ball of the model and F_{mb} the buoyancy force on the ball of the model.

9.6 TEST RESULTS AND DISCUSSIONS

9.6.1 Model A

Fig. (9.4) shows the relationship between the flow force (F_{vf}) on the ball of the injector valve and the position of the ball from the seat (y), for supply pressure 20 psi, 40 psi, and 60 psi. It can be seen from these figs. that the shape of the graphs is the same as the $F_{vf} - y$ graphs which are discussed in Chapter 7 (see fig. (7.15)).

Figs. (9.5- 9.7) show plots of the total flow rate from the injector valve (Q_{vT}), the side inlets flow rates (Q_{vs}) and the top inlets flow rate (Q_{vt}) versus y, for 20 psi, 40 psi, and 60 psi respectively. These figs. show that the shape of the $Q_{vs} - y$ and $Q_{vt} - y$ plots is respectively the same as the $Q_{vs} - y$ and $Q_{vt} - y$ plots which are discussed in Chapter 7 (see section (7.6)). These figs. also show that when Q_{vt} decreased due to the decrease in the area above the ball, Q_{vT} remained constant. This is because the total resistance which was composed of the resistance (R_1) (see fig. (7.13)) due to the area above the ball plus the resistance (R_2) due to the area of the top inlet in parallel with the resistance (R_3) due to the area of the side inlets was very small compared to the resistance (R_5) due to the area of the outlet (the resistance (R_4) due to the area under the

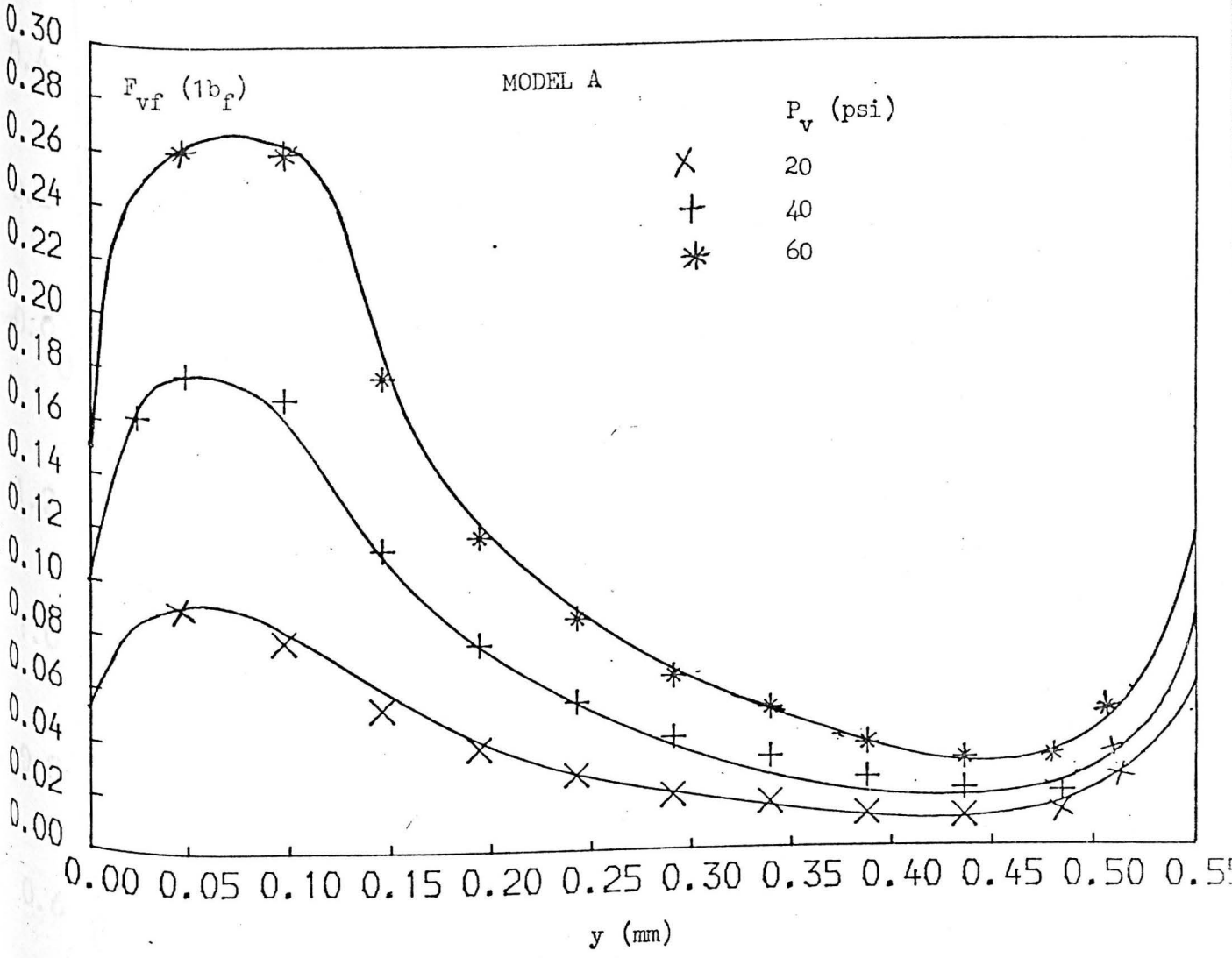

FIG. 9.4 FLOW FORCE - POSITION OF THE BALL FROM THE SEAT RELATIONSHIP

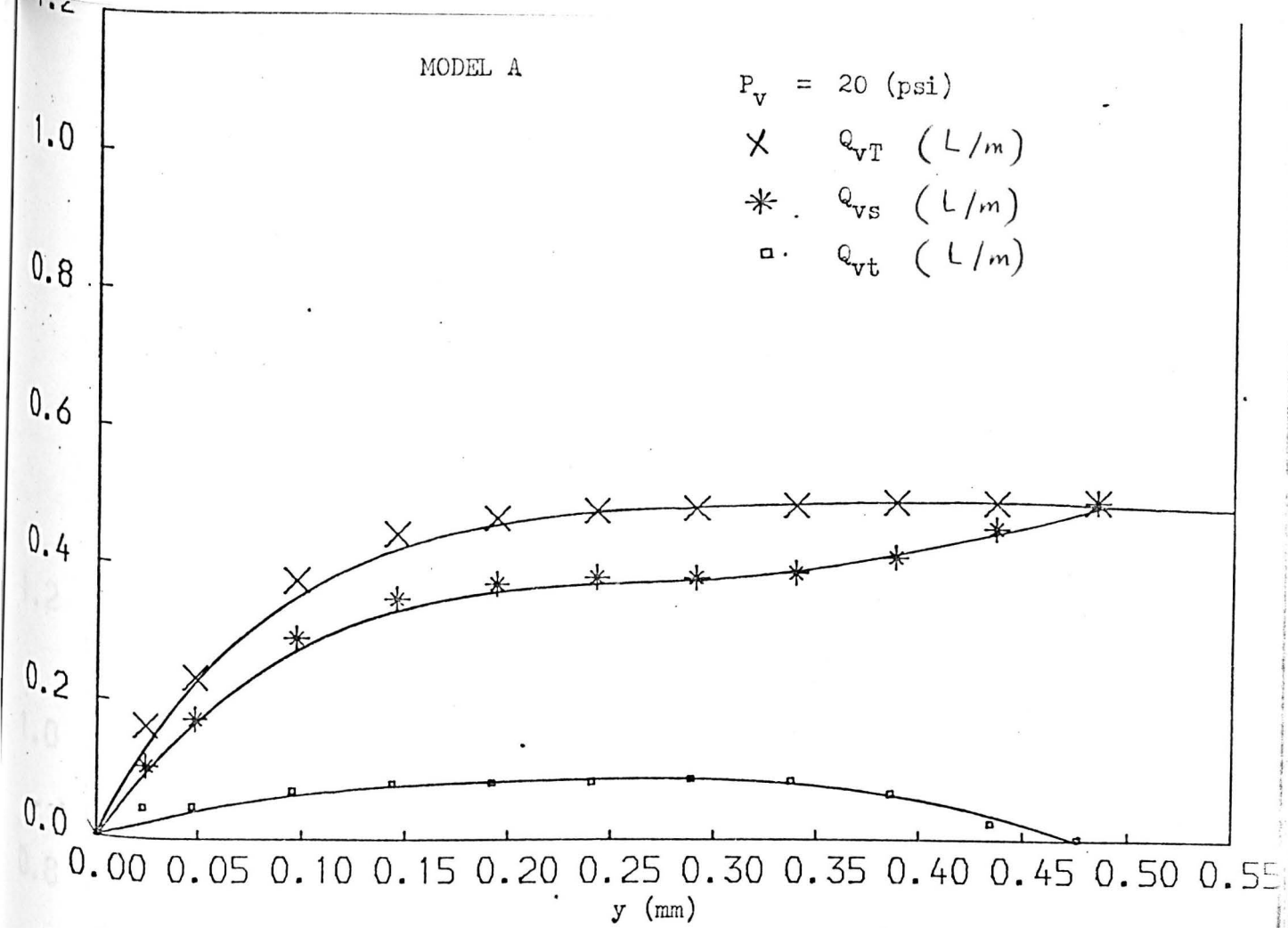

FIG. 9.5 FLOW RATES - POSITION OF THE BALL FROM THE SEAT RELATIONSHIP

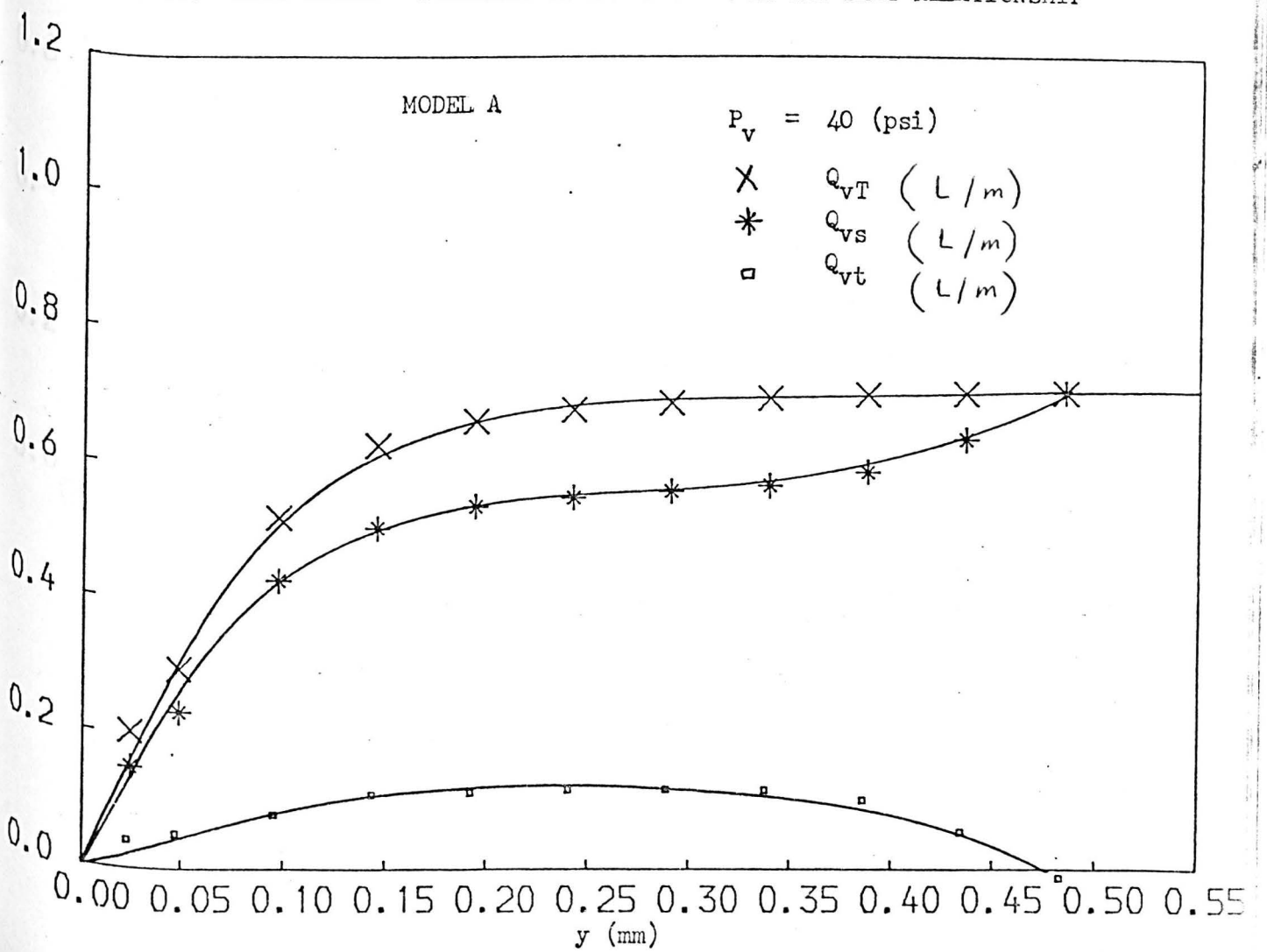

FIG. 9.6 FLOW RATES - POSITION OF THE BALL FROM THE SEAT RELATIONSHIP

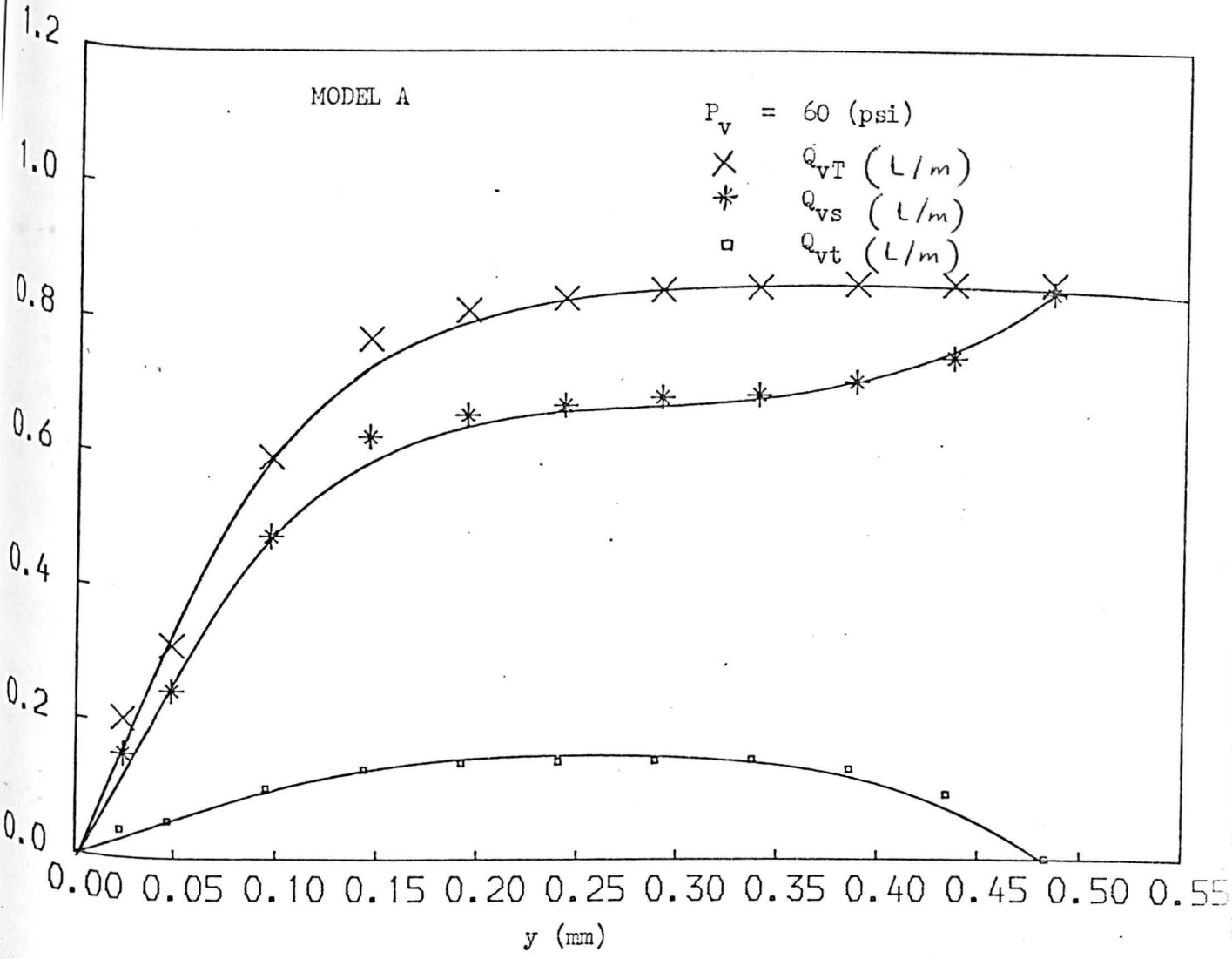

FIG. 9.7 FLOW RATES - POSITION OF THE BALL FROM THE SEAT RELATIONSHIP

ball was approximately negligible in this region). Hence the increase in the total resistance due to the increase of R_2 could not affect the total flow rate. These figs. show that when P_v was increased, Q_{vT}, Q_{vs} and Q_{vt} increased as nearly the square root of pressure.

9.6.2 Model B

Fig. (9.8) shows the relationship between the flow force (F_{vf}) on the ball of the injector valve and the position (y) of the ball from the seat, for supply pressure 20 psi, 40 psi and 60 psi. It can be seen from these figs. that the shape of the graphs is the same as the $F_v - y$ graph of model A (see section (9.6.1)). These figs. show that the maximum value of F_{vf} was smaller than the maximum value of F_{vf} of the model A. This is because in model B the resistance (R_5) due to the area of the outlet of the injector valve was very large compared to the resistance (R_4) due to the area under the ball. Hence the value of y in which R_4 would become negligible was smaller than that of model A.

Also it can be seen from this fig. that F_{vf} reduced to a minimum at lower value of y, and its value here was smaller than F_{vf} of model A. This is because R_5 was very large compared to the other resistances in the injector valve.

Figs. (9.9- 9.11) show plots of the total flow rate (Q_{vT}) from the injector valve and the top (Q_{vt}) and side (Q_{vs}) inlet flows versus y, for 20 psi, 40 psi and 60 psi. The shape of the plots is the same as those of model A (see section (9.6.1)) but the flow rates were smaller because R_5 was very large compared to the other resistances in this injector valve.

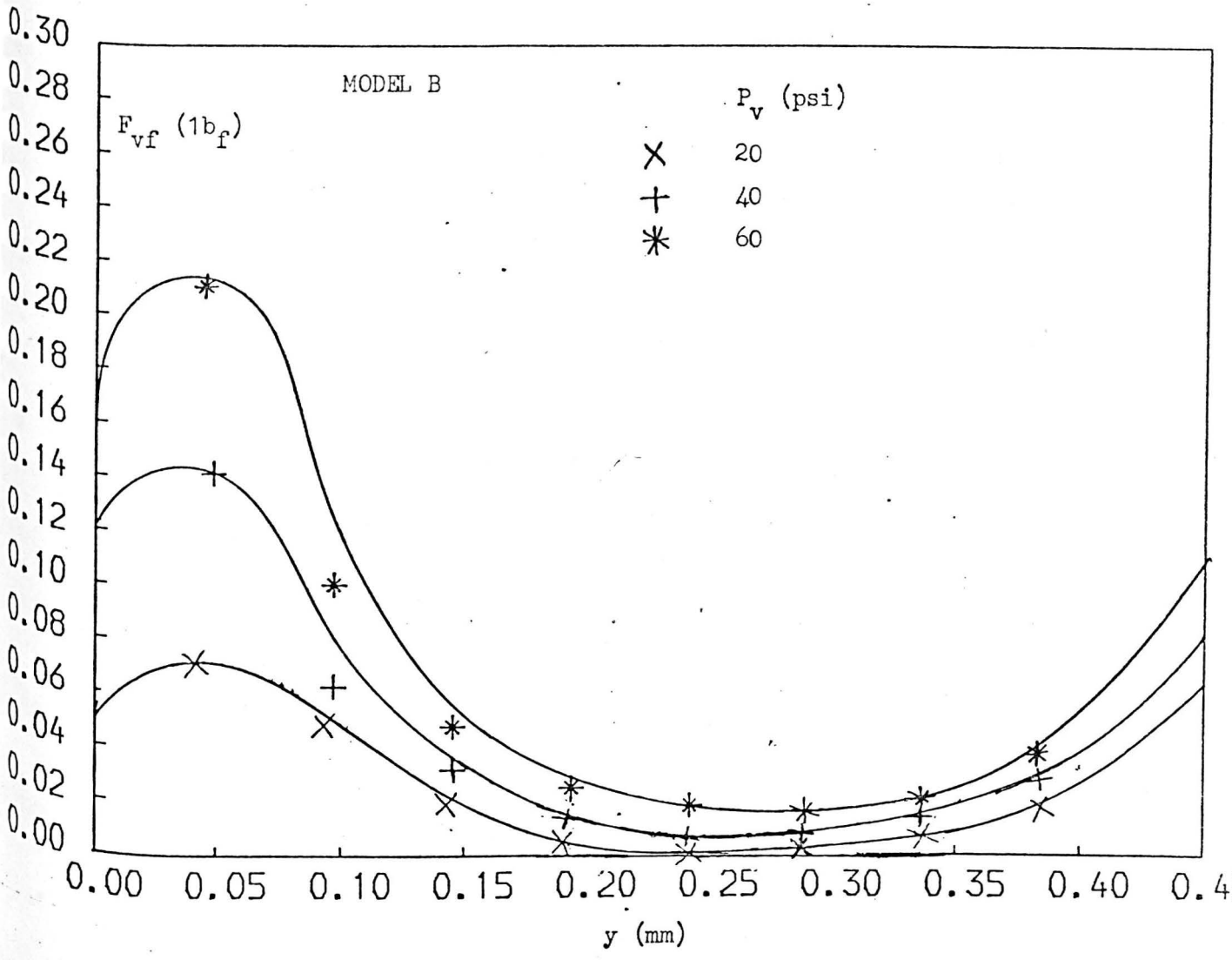

FIG. 9.8 FLOW FORCE - POSITION OF THE BALL FROM THE SEAT RELATIONSHIP

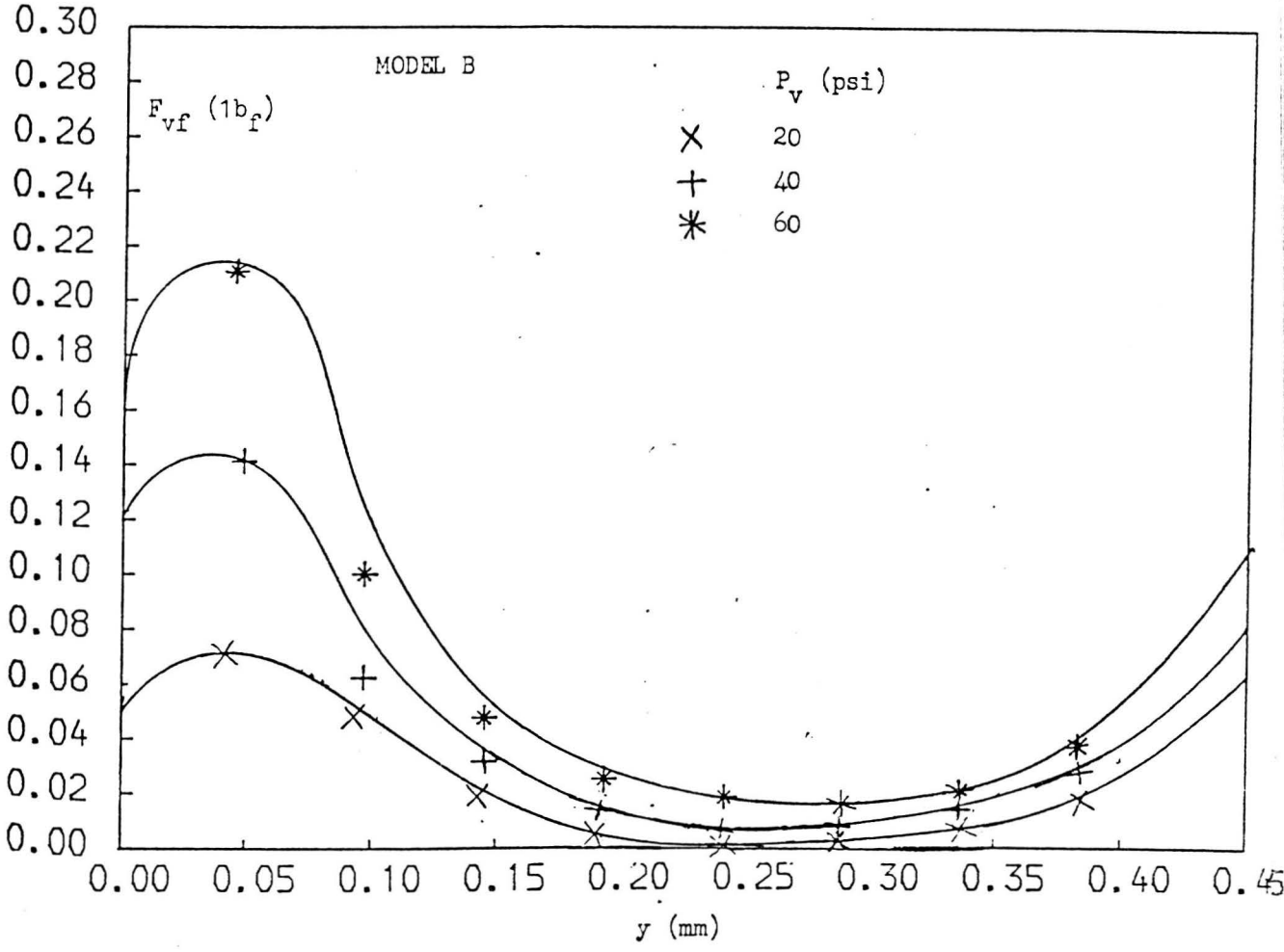

FIG. 9.8 FLOW FORCE - POSITION OF THE BALL FROM THE SEAT RELATIONSHIP

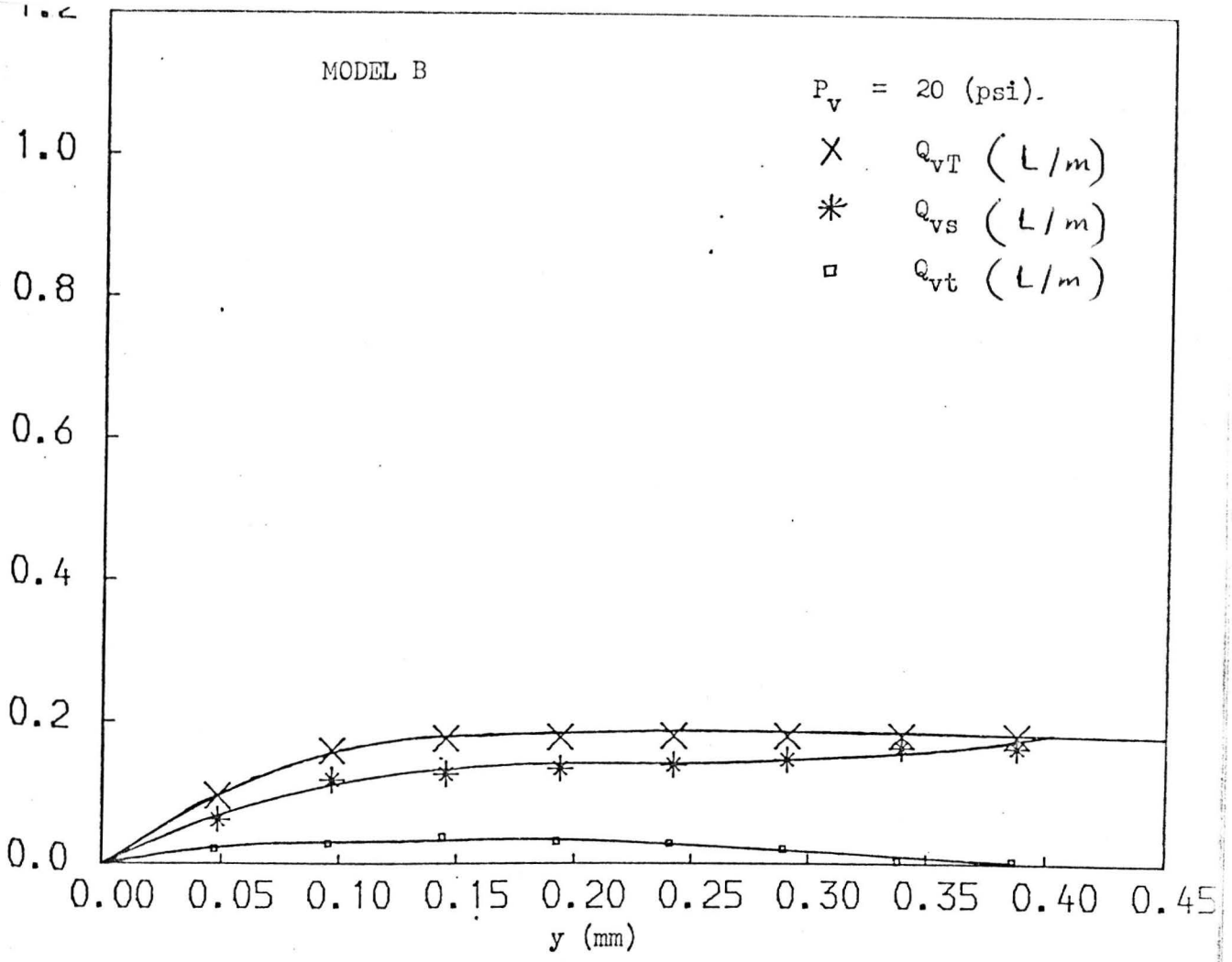

FIG. 9.9 FLOW RATES - POSITION OF THE BALL FROM THE SEAT RELATIONSHIP

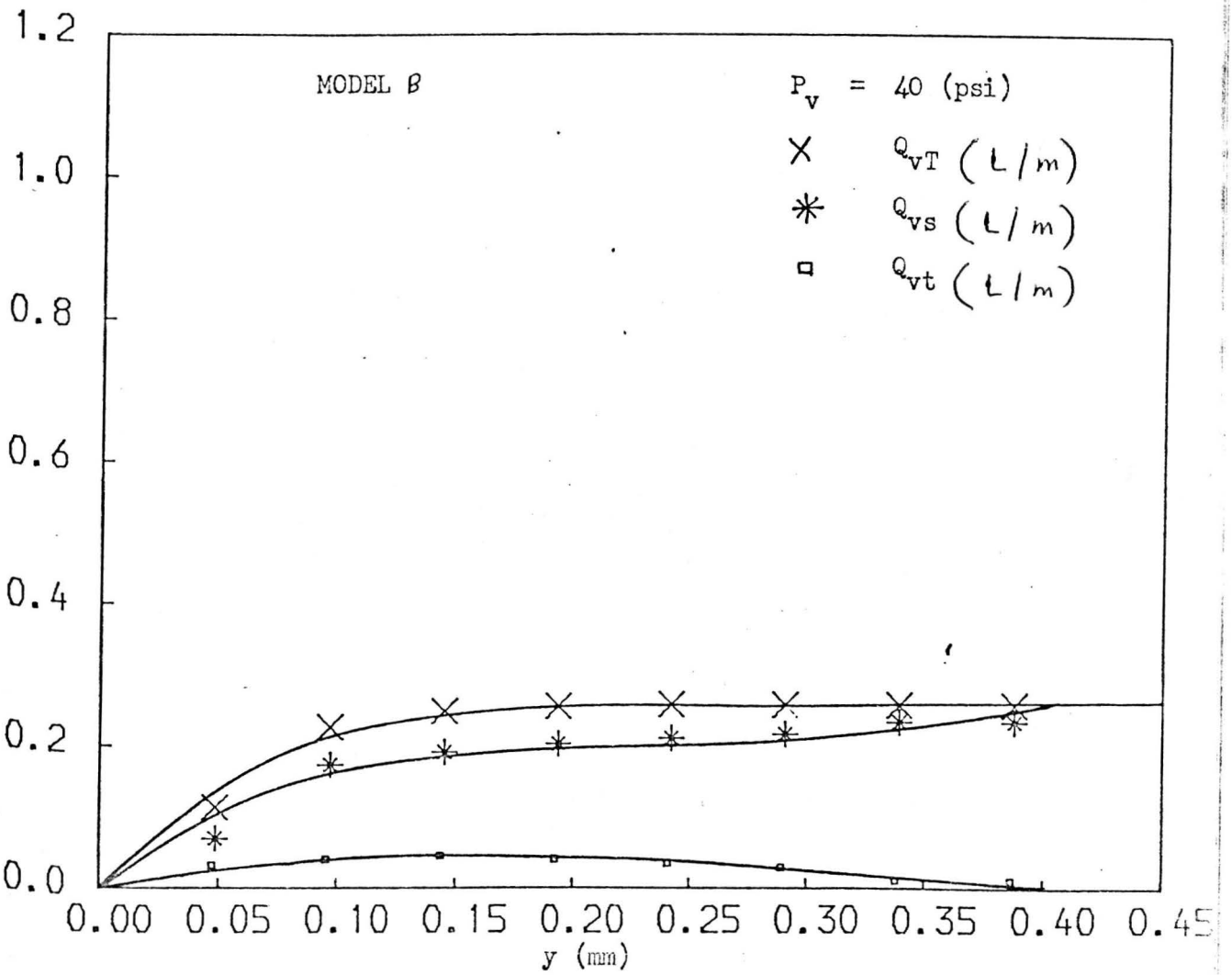

FIG. 9.10 FLOW RATES - POSITION OF THE BALL FROM THE SEAT RELATIONSHIP

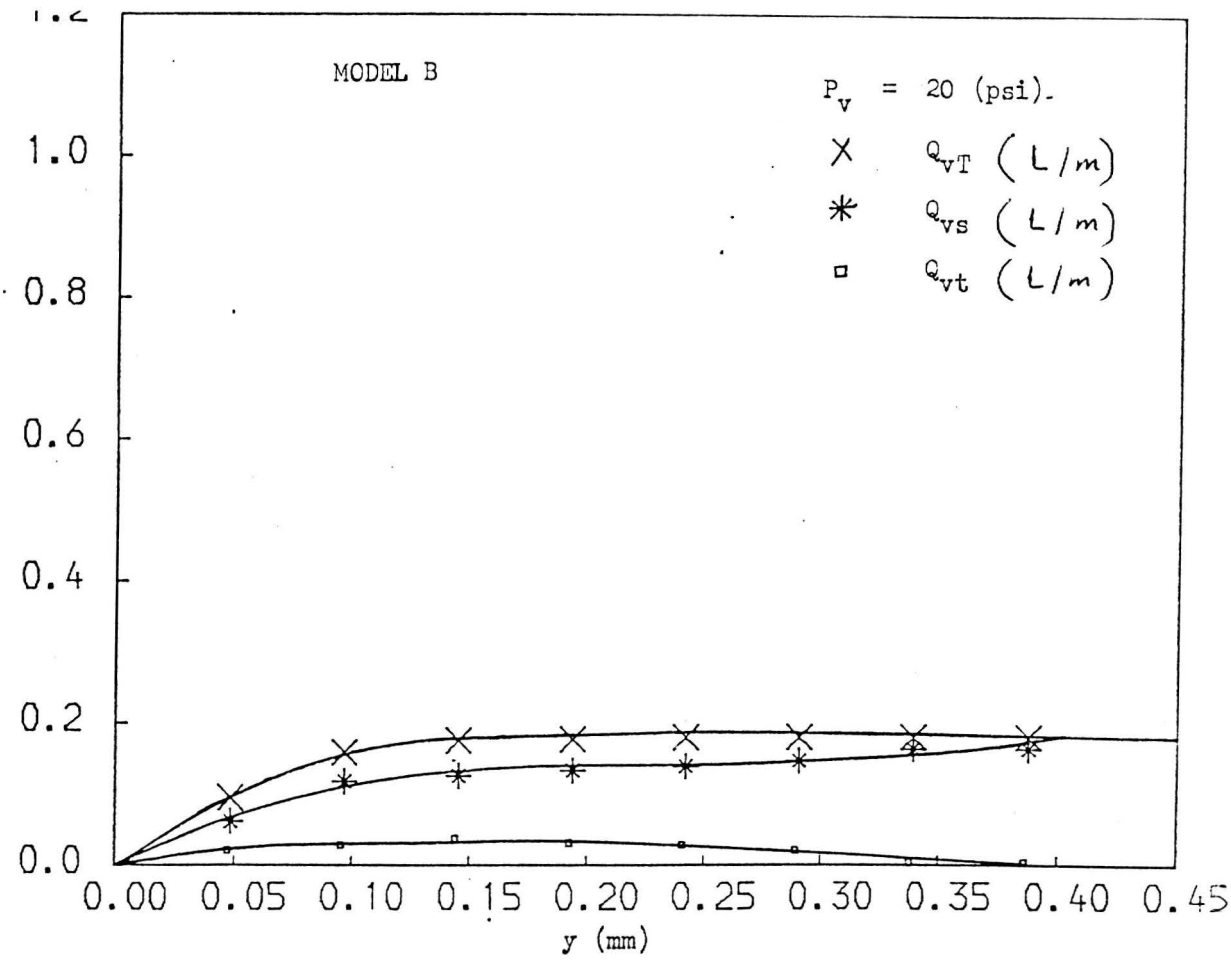

FIG. 9.9 FLOW RATES - POSITION OF THE BALL FROM THE SEAT RELATIONSHIP

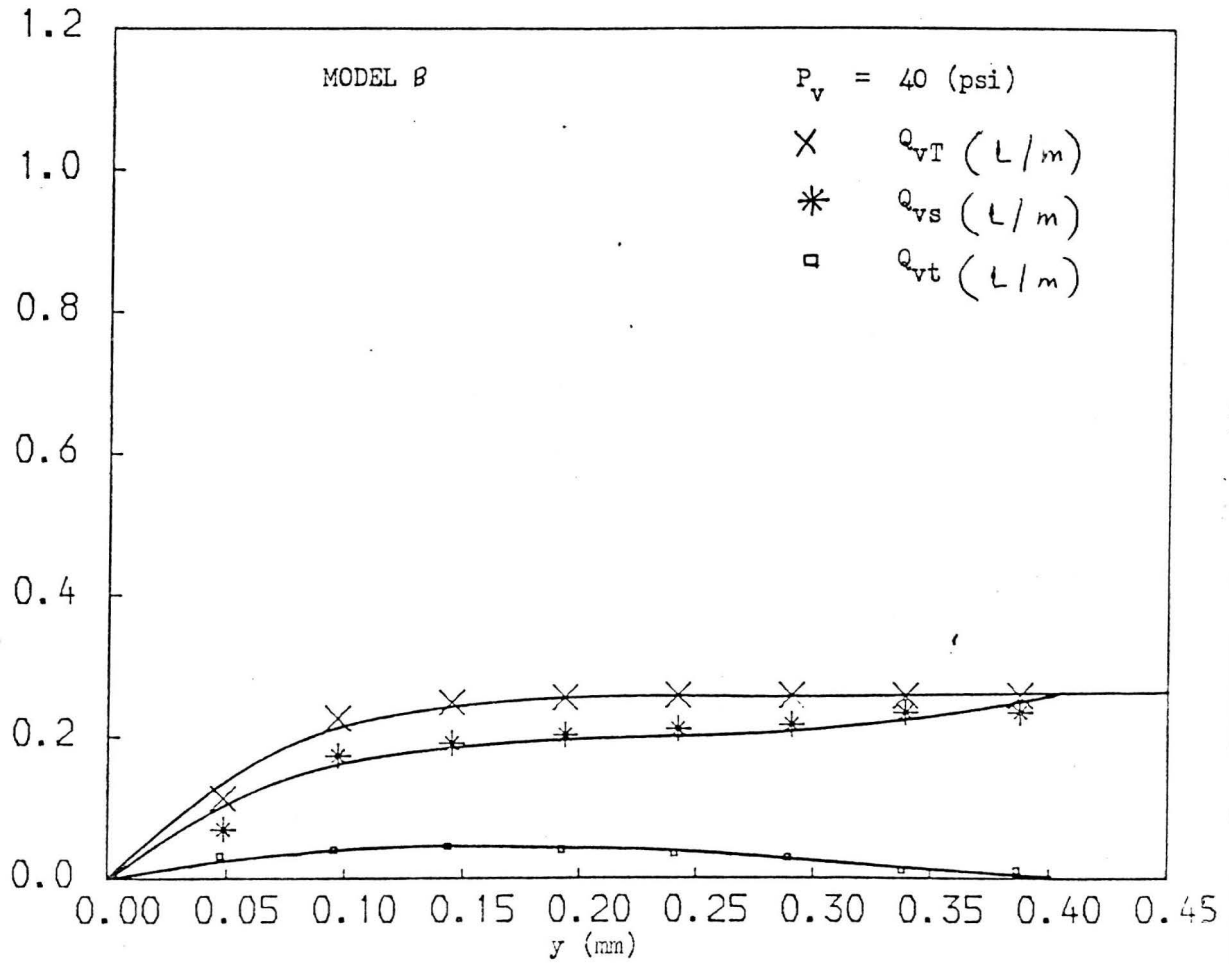

FIG. 9.10 FLOW RATES - POSITION OF THE BALL FROM THE SEAT RELATIONSHIP

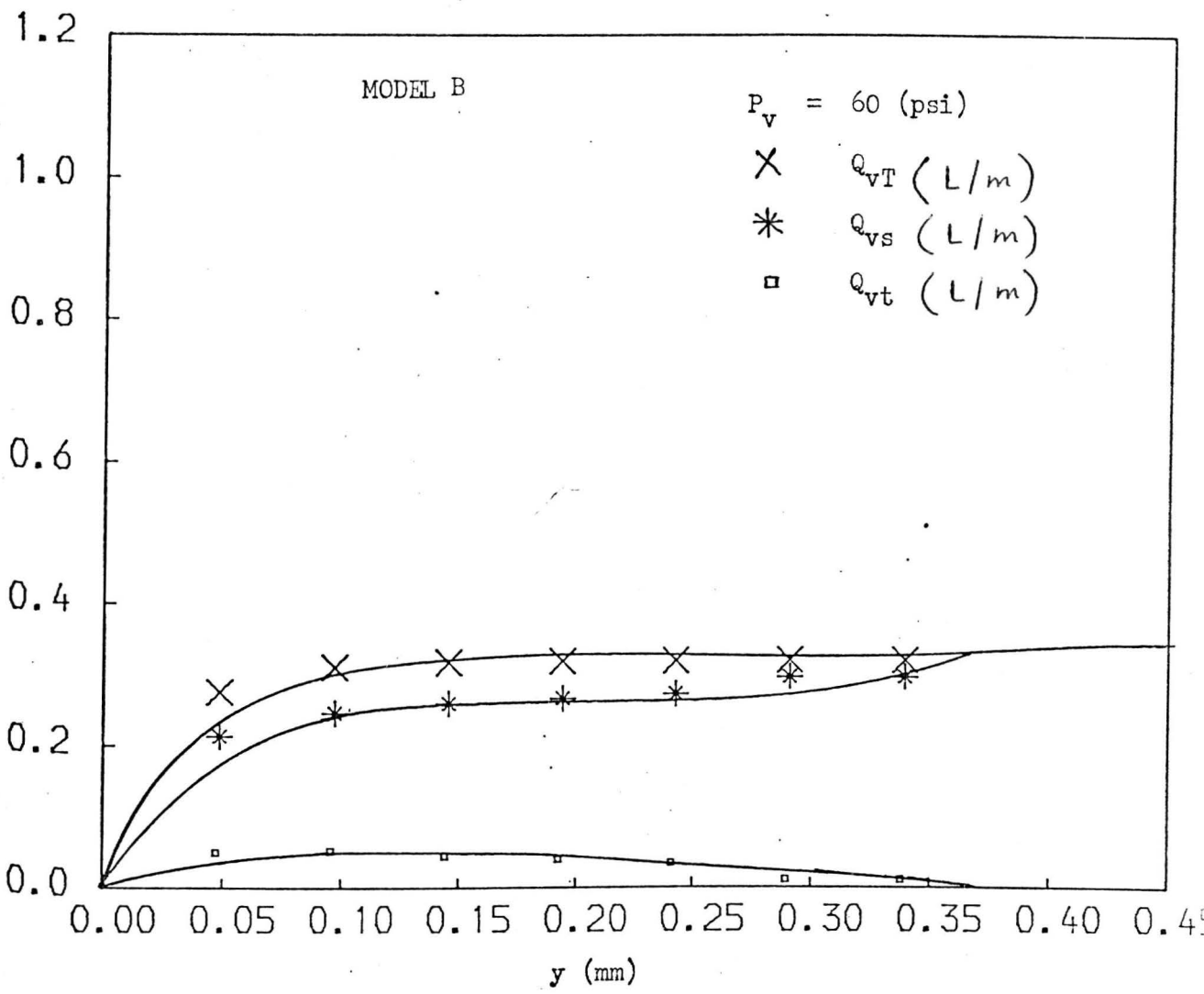

FIG. 9.11 FLOW RATES - POSITION OF THE BALL FROM THE SEAT RELATIONSHIP

These figs. show that the ratio of Q_{vs} to Q_{vt} at $y = 0.225$ mm (approximate middle position) was almost the same as for model A at the same value of y. This is because at this position in both the models the resistances (R_4) due to the area under the ball and the resistance (R_2) due to the area above the ball were almost negligible. Hence Q_{vs} and Q_{vt} were respectively proportional to the side and the top inlets areas which were the same in both the models.

Also, it can be seen from this fig. that Q_{vT} built up to its maximum value at smaller value of y compared to Q_{vT} of model A. This occurs because in model B, R_5 was very large and soon became larger than R_4 at small lift. Hence it could be considered the main controller of the flow rates.

9.6.3 Model C

Fig. (9.12) shows the relationship between the flow force (F_{vf}) on the ball and the position (y) of the ball from the seat, for supply pressure 20 psi, 40 psi and 60 psi. The general shape is the same as those of models A and B. It can be seen that the flow force (F_{vf}) on the ball did not stay constant when its value reached a minimum (as in models A and B). This is because in model C the resistance (R_3) due to the area of the side inlets was significant compared to the resistance (R_2) due to the area above the ball, while it was very small compared to R_2 in models in A and B. Hence the increase in R_2 caused an increase in the static pressure on the upper half of the ball. Figs. (9.13- 9.15) show plots of the flow rates versus y for

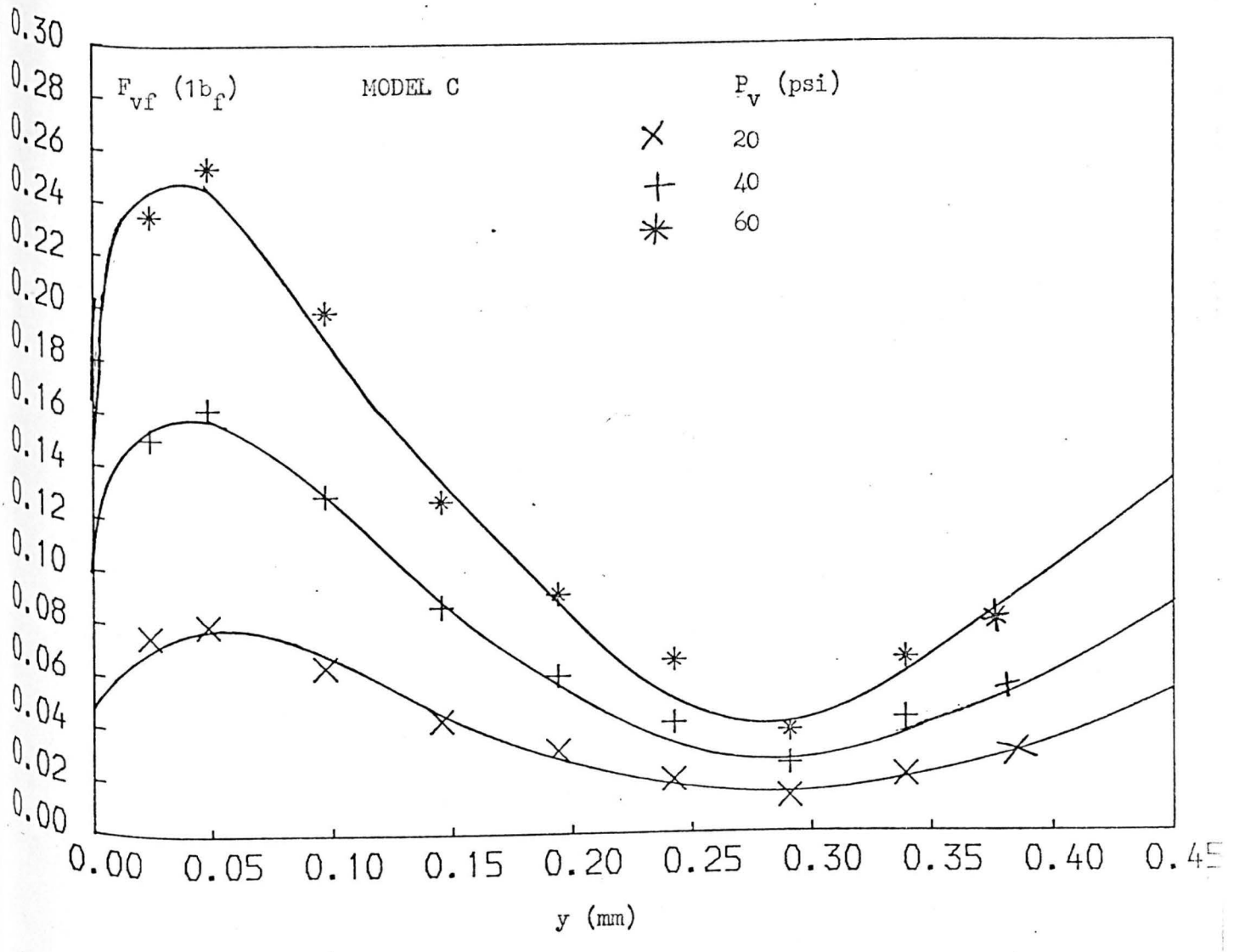

FIG. 9.12 FLOW FORCE - POSITION OF THE BALL FROM THE SEAT RELATIONSHIP

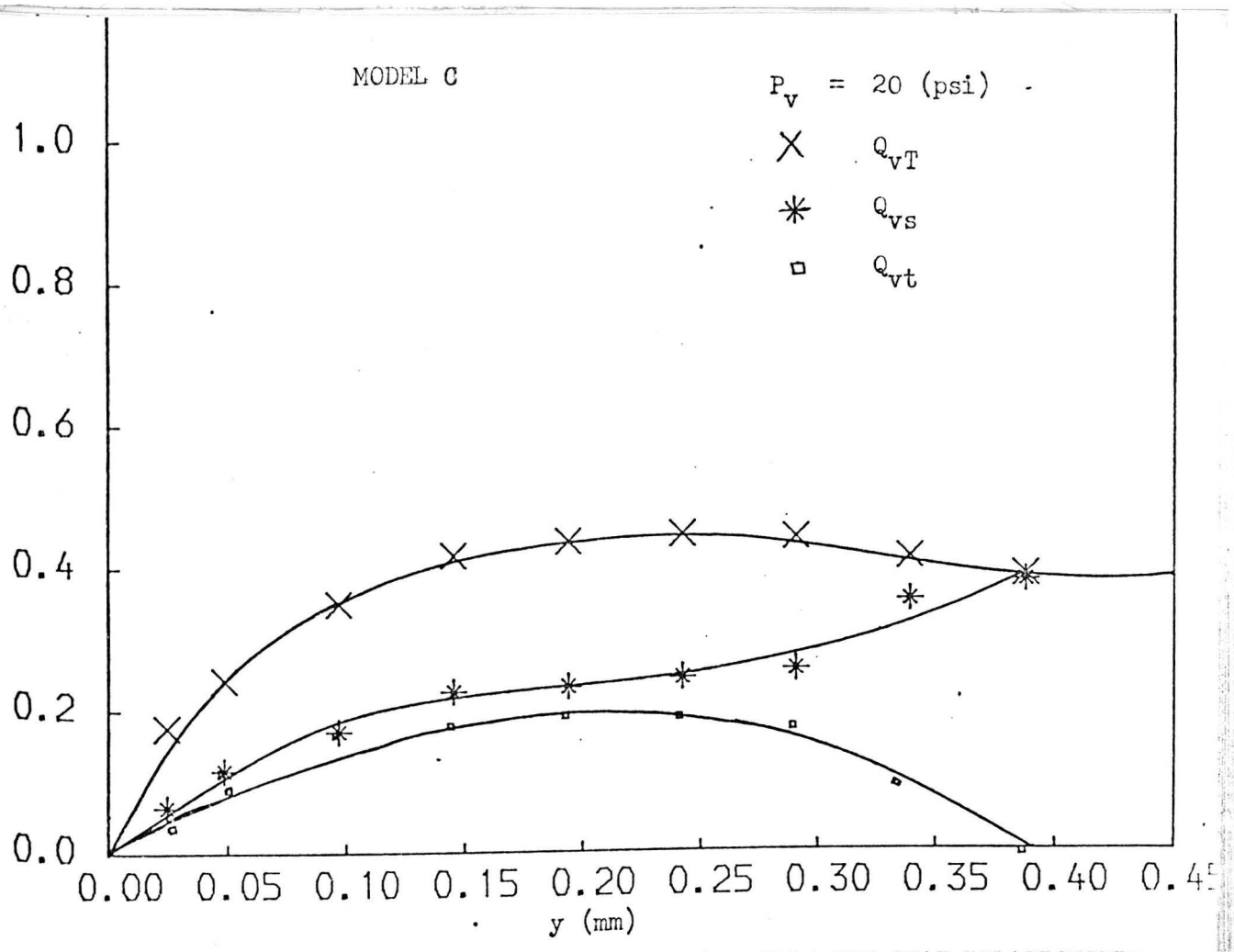

FIG. 9.13 FLOW RATES - POSITION OF THE BALL FROM THE SEAT RELATIONSHIP

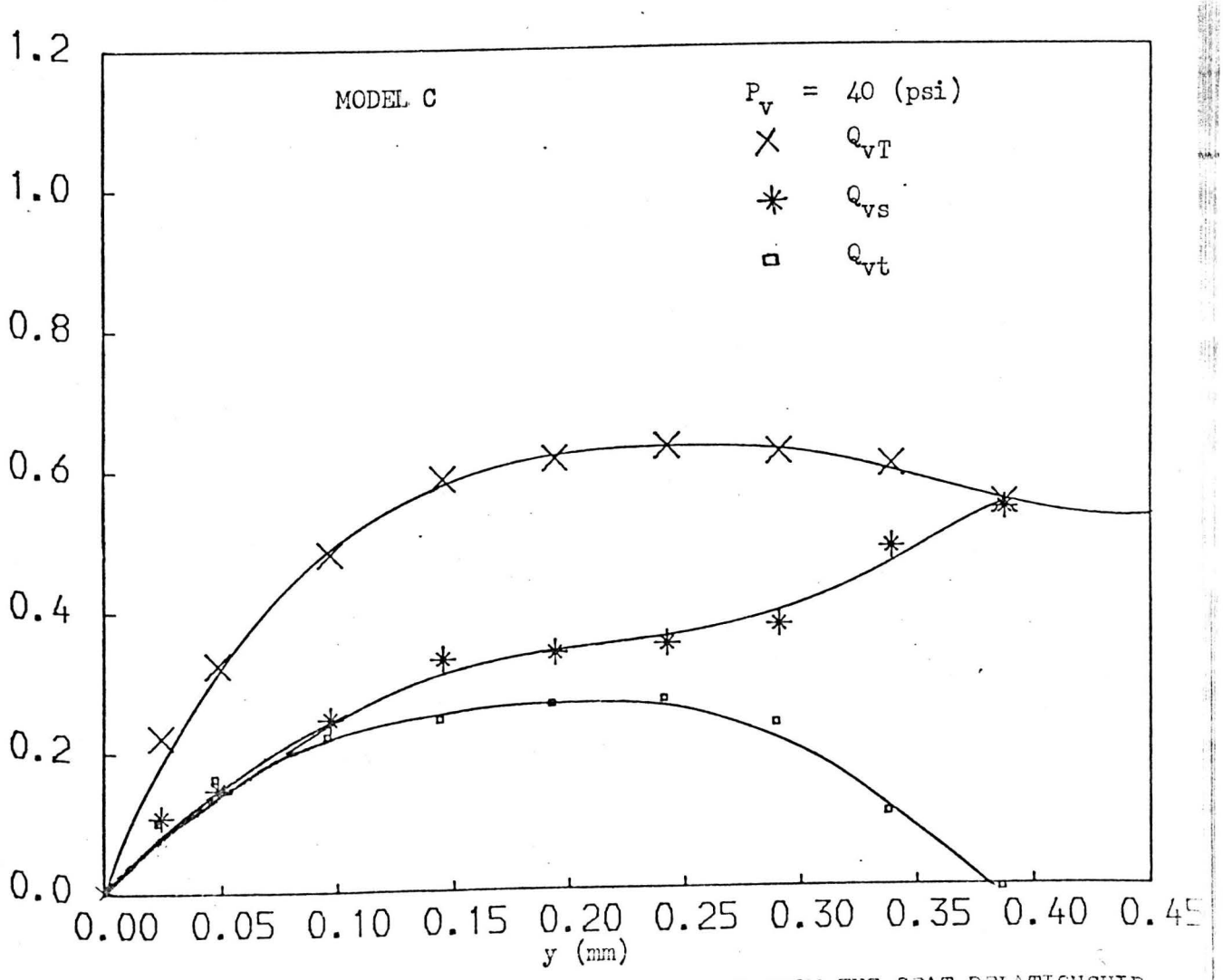

FIG. 9.14 FLOW RATES - POSITION OF THE BALL FROM THE SEAT RELATIONSHIP

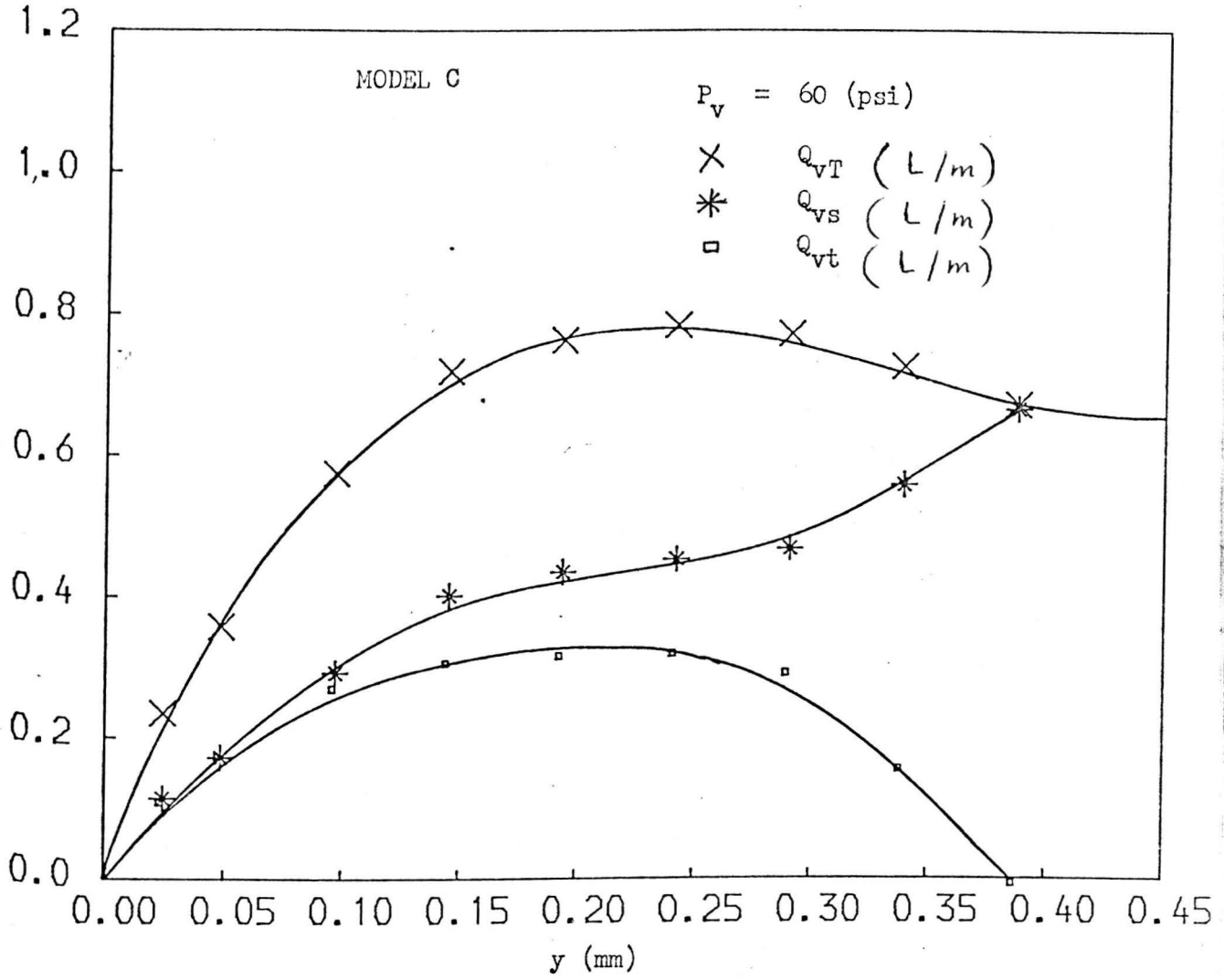

FIG. 9.15 FLOW RATES - POSITION OF THE BALL FROM THE SEAT RELATIONSHIP

20 psi, 40 psi and 60 psi. The shapes of the $Q_{vs} - y$ and the $Q_{vt} - y$ plots are respectively the same as those of models A and B. These figs. show that Q_{vT} decreased when the ball was lifted from $y = 0.25$ mm to $y = 0.45$ mm. This is because the increase in R_2 when the ball was lifted caused an increase in the total resistance of the parallel circuit which was slightly significant compared to the resistance (R_5) due to the area of the outlet. It can be seen from these figs. that the maximum value of Q_{vT} was slightly smaller than the maximum value of Q_{vT} of model A. This is because the increase in R_3 slightly increased the resistance of the parallel circuit.

9.6.4 Model D

Fig. (9.16) shows the relationship between the flow force (F_{vf}) on the ball of the injector valve and the position (y) of the ball from the seat, for supply pressure 20 psi and 40 psi. It can be seen from these figs. that the value of y for maximum F_{vf} was greater than that of models A, B and C. This occurs because in model D the resistance (R_3) due to the area of the side inlets was very small compared to the resistances (R_2) due to the area above the ball and the resistance (R_1) due to the area of the top inlet compared with models A, B and C. Hence when the ball was lifted in this region, the flow force on the upper half of the ball was due to the supply pressure and the flow force on the lower half of the ball was due to the static pressure which was decreased when the ball was lifted from the seat.

Also these figs. show that F_{vf} did not increase again as

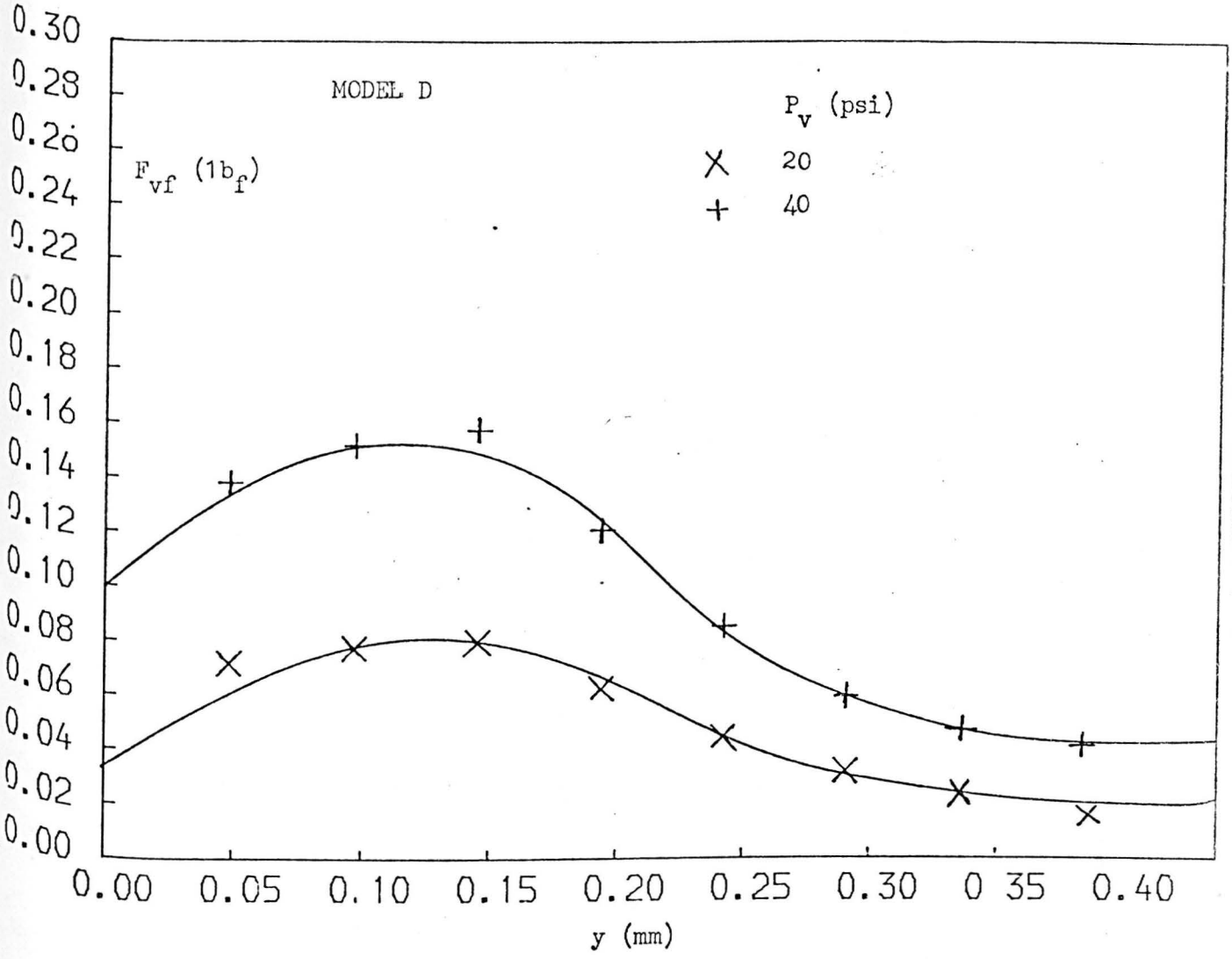

FIG. 9.16 FLOW FORCE - POSITION OF THE BALL FROM THE SEAT RELATIONSHIP

in models A, B and C. This is probably also because R_3 was very small compared to $R_1 + R_2$. Hence for any value of y, the flow force on the upper half of the ball was due to the supply pressure. For the same reason it can be seen from this fig. that the value of y for which F_{vf} fell to a minimum was greater than that of models A, B and C.

Figs. (9.17 - 9.18) show plots of the total flow rate (Q_{vT}) from the injector valve, the side inlets flow rates (Q_{vs}) and the top inlet flow rate (Q_{vt}) versus y, for 20 psi and 40 psi. These figs. show there was little or no flow rate from the top inlet of the injector valve because R_3 was so small compared to $R_1 + R_2$.

It can also be seen from this fig. that the maximum value of Q_{vT} was greater compared to models A and C because the total resistances of the parallel circuit was smaller due both to the low R_3 and also because the diameter of the cavity of the valve was larger. Thus the ball did not obstruct the side inlets.

9.6.5 Model E

Fig. (9.19) shows the relationship between the flow force (F_{vf}) on the ball of the injector valve and the gap (y) between the ball and the seat, for supply pressure 20 psi and 40 psi. These figs. show that the shape of the graphs is the same as the $F_{vf} - y$ graphs of model D (see section (9.6.4)). It can be seen from this fig. that the maximum value of F_{vf} was approximately the same as the maximum value of F_{vf} of model D because in both models the resistance (R_3) due to the area of the side inlets was almost negligible, i.e., the flow rate was not affected by the further

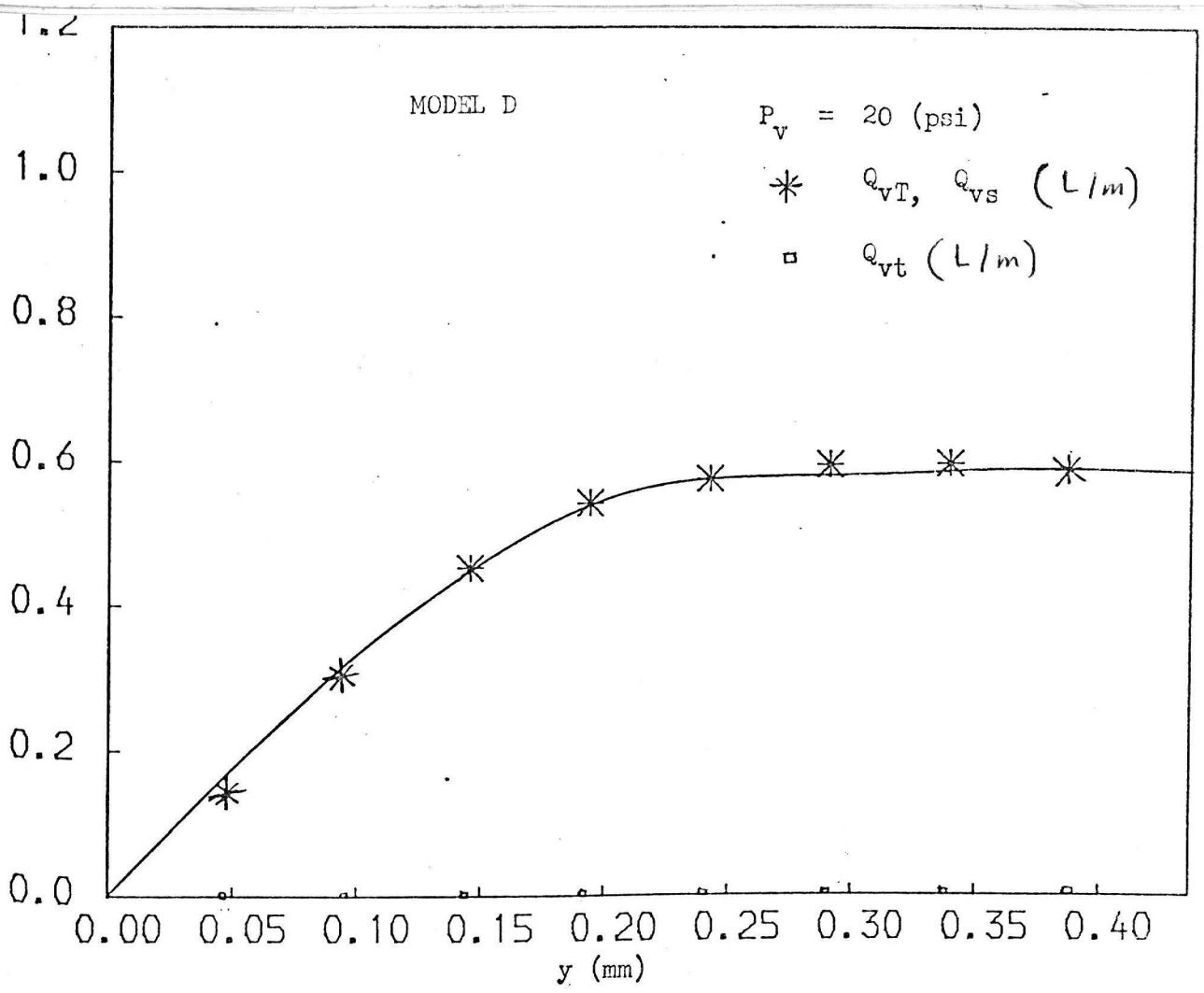

FIG. 9.17 FLOW RATES - POSITION OF THE BALL FROM THE SEAT RELATIONSHIP

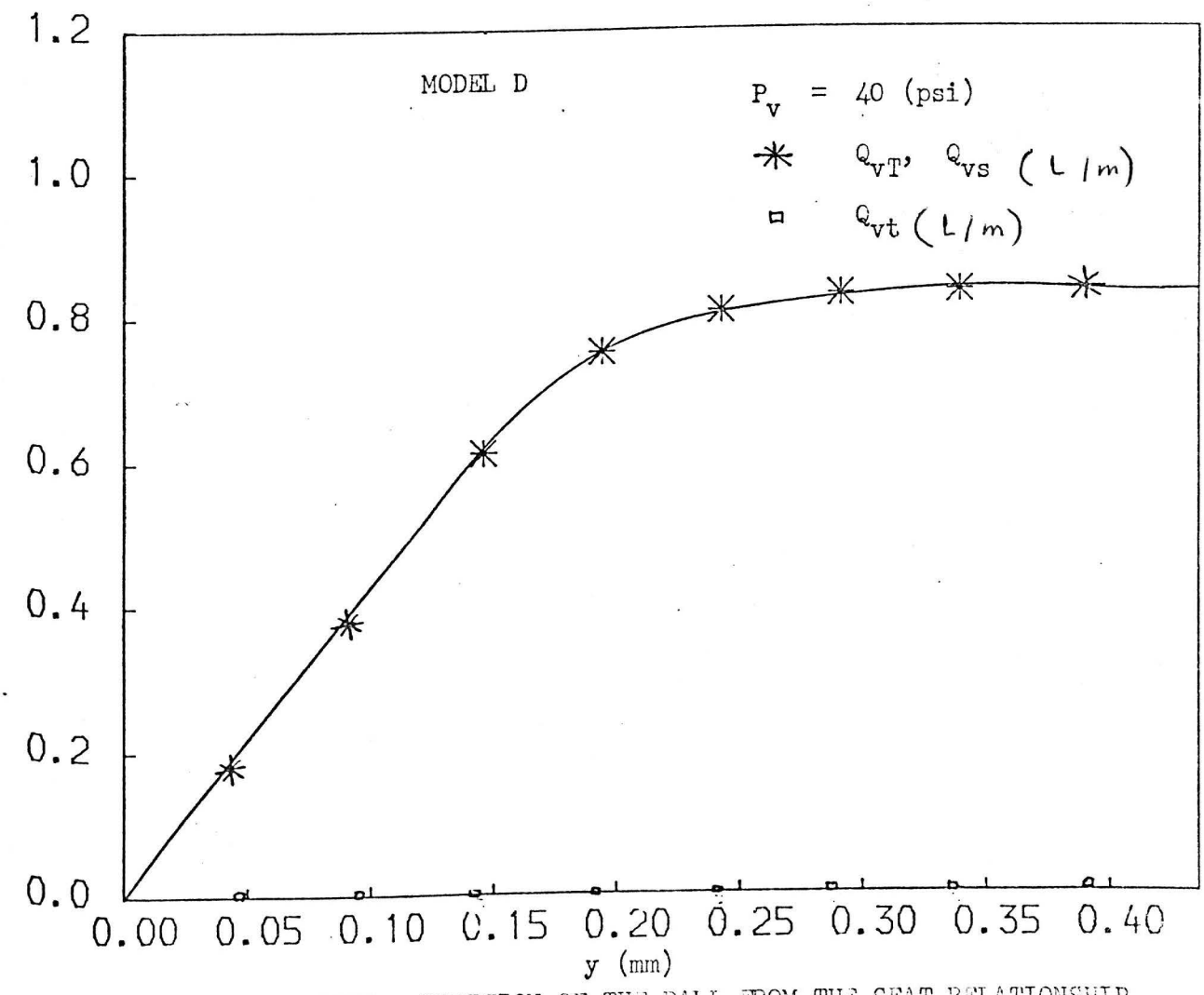

FIG. 9.18 FLOW RATES - POSITION OF THE BALL FROM THE SEAT RELATIONSHIP

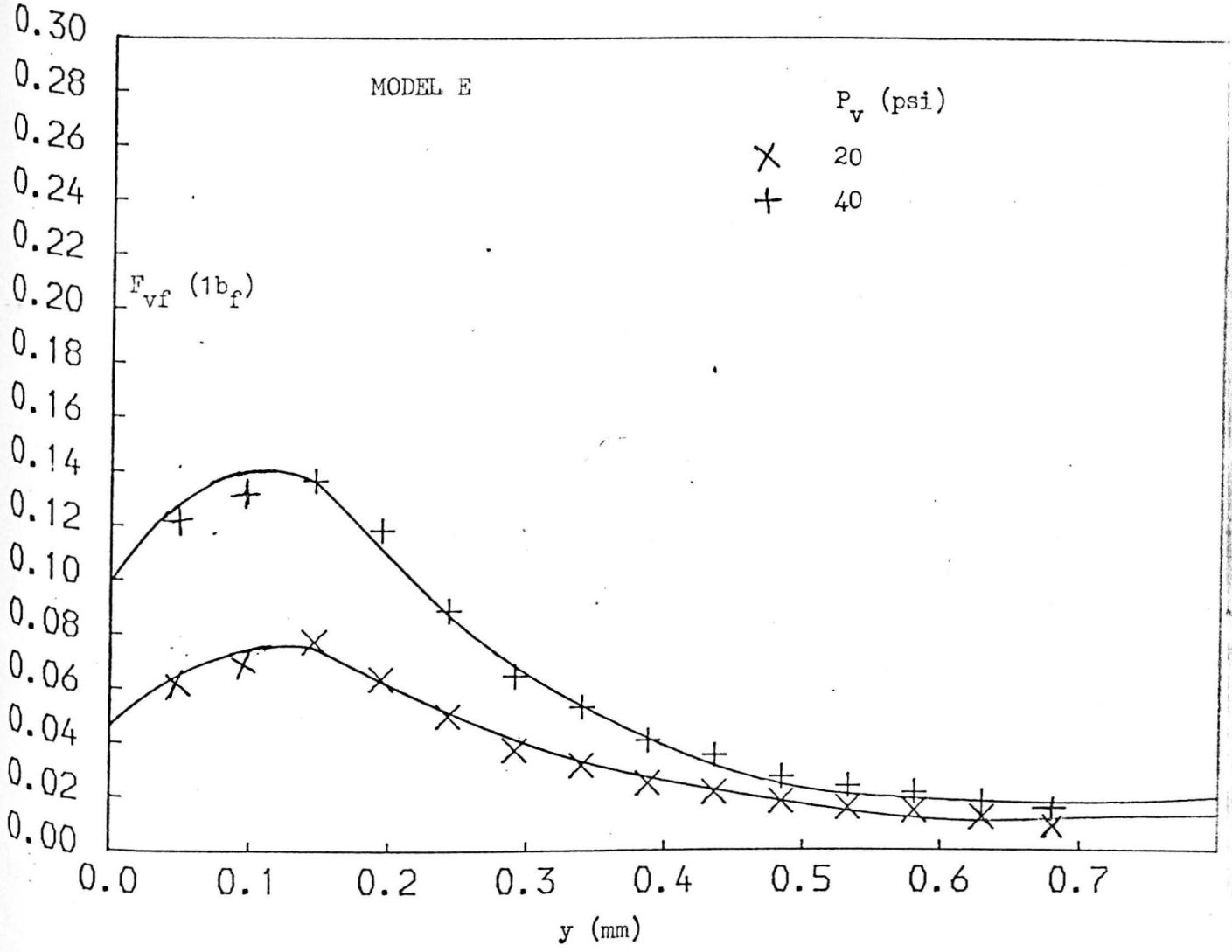

FIG. 9.19 FLOW FORCE - POSITION OF THE BALL FROM THE SEAT RELATIONSHIP

decrease of R_3.

Figs. (9.20 - 9.21) show plots of the total flow rate (Q_{vT}) from the injector valve, the side inlets flow rates (Q_{vs}) and the top inlet flow rates (Q_{vt}) versus y, for 20 psi and 40 psi. These figs. show that the shape of these graphs is the same as the $Q_{vT} - y$, $Q_{vs} - y$ and $Q_{vt} - y$ graphs of model D (see section (9.6.4)). It can be seen from these figs. that the maximum value of Q_{vT} was approximately the same as the maximum value of Q_{vT} of model D. This is again because R_3 was almost negligible, i.e., the flow rate was not affected by the decrease of R_3.

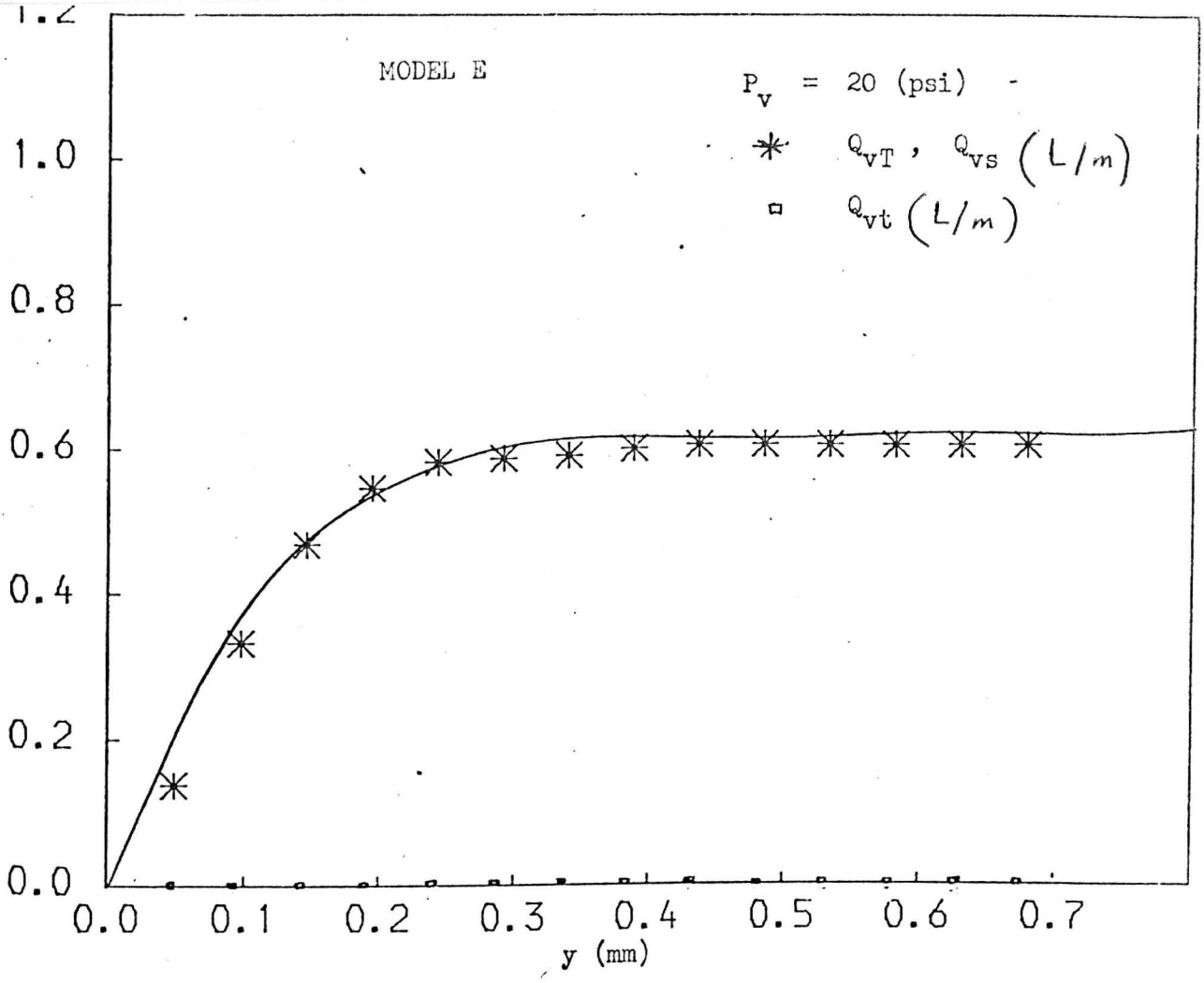

FIG. 9.20 FLOW RATES - POSITION OF THE BALL FROM THE SEAT RELATIONSHIP

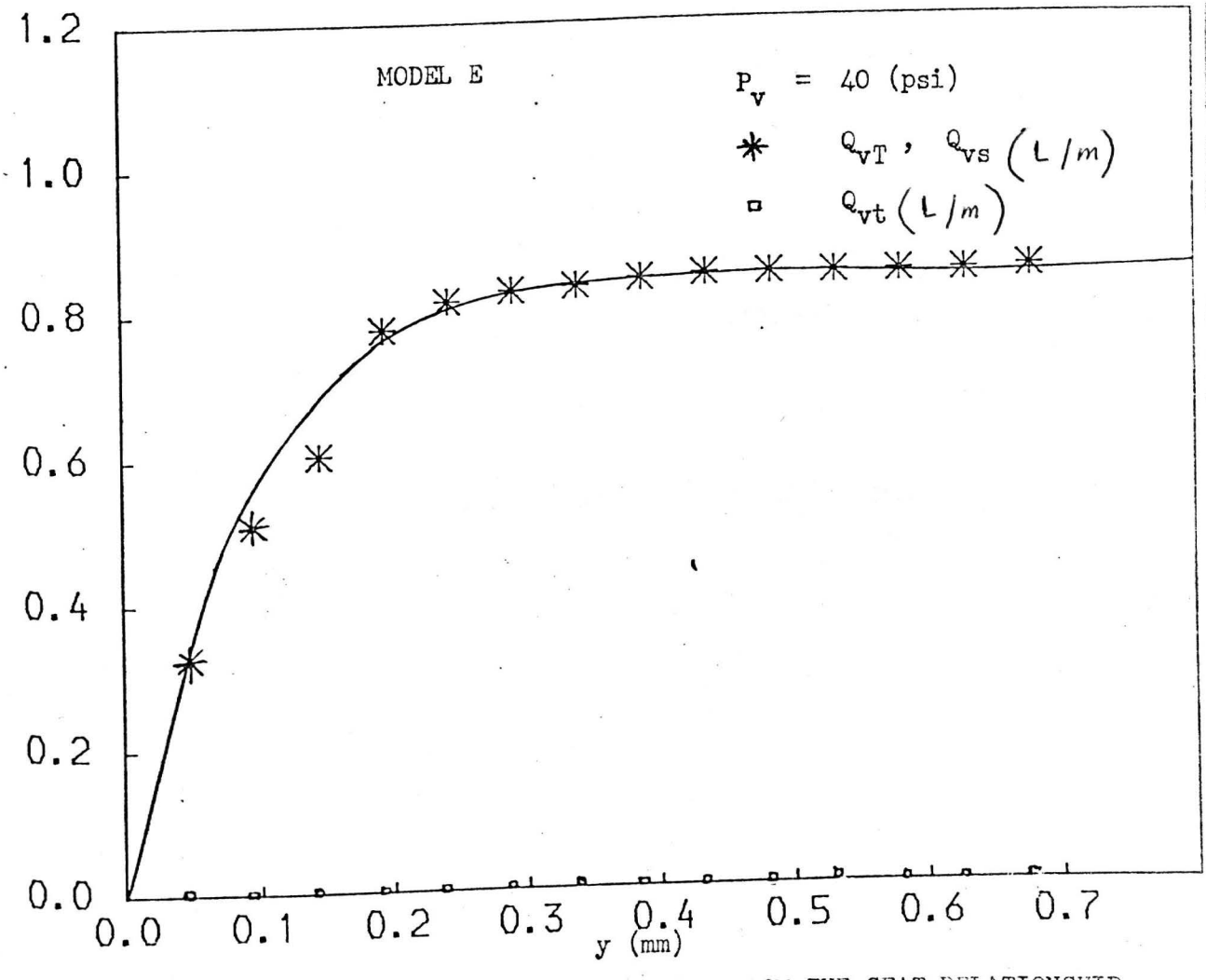

FIG. 9.21 FLOW RATES - POSITION OF THE BALL FROM THE SEAT RELATIONSHIP

9.7 PREDICTION OF THE FLOW FORCE ON THE BALL AND THE TOTAL FLOW RATE AT SMALL OPENING

9.7.1 Introduction

This section is devoted to predicting the flow force on the ball of the injector valve and the total flow rate from the injector valve. These predictions were done where the position of the ball was 1 mm from the seat.

The purpose of this investigation was to get a better understanding of the results of the models of the injector valve (which were described in Chapters 7 and 9).

The theory of the investigation and the results and the discussions are given below.

9.7.2 Theory

9.7.2.1 Prediction of the Total Flow Rate from the Injector Valve

The total flow rate was calculated where the position of the ball was 1mm from the seat. It was assumed that the liquid was ideal (so that no energy was dissipated by friction) and of constant density. The flow was assumed steady. It was assumed that the conditions over the cross sectional area (A_1) between the ball and the seat (see fig. (9.20) were uniform, and the streamlines were straight and parallel. To calculate the flow rate, Bernoulli's equation was applied between sections 1 and 6 (see fig. (9.20)). At section 6, it was assumed that the flow velocity was zero and the pressure was the supply pressure. At section 1 it was assumed that the pressure was atmospheric, and the separation of the flow

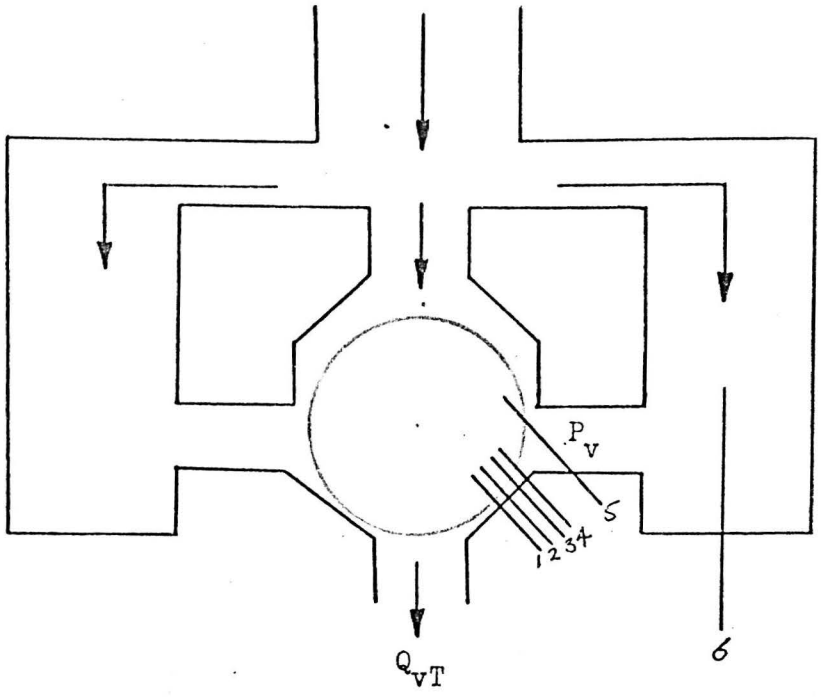

FIG. 9.20 LAYOUT OF THE INJECTOR VALVE

from the ball occurred at this section.

From Bernoulli's equation, the total flow rate:

$$Q_{vT} = A_1 \sqrt{\frac{2}{\rho_v} (p_6^* - p_1^*)} \qquad (9.5)$$

where A_1 was calculated from the design drawing of the injector valve, ρ_v represents the density of the liquid of the valve, p_6^* piezometric pressure at section 6 and p_1^* piezometric pressure at section 1.

9.7.2.2 Prediction of the Flow Force on the Ball of the Injector Valve

The flow force on the ball was calculated where the position of the ball was 1 mm from the seat.

The flow force on the upper half of the ball was assumed to be due to the supply pressure.

The flow force on the lower half of the ball was calculated by calculating the static pressure over several cross sectional areas between the ball and the lower wall of the injector valve. It was assumed that the static pressure acted on each small surface area of the lower half of the ball. It was assumed that the conditions over the cross sectional areas were uniform and that the streamlines there were straight and parallel.

The static pressure was calculated over three sectional areas between the ball and the lower wall of the injector valve (A_2, A_3 and A_4) (see fig (9.20)). By applying Bernoulli's equation between sections 6 and 2, the static pressure at A_2:

$$p_2^* = p_6^* - \frac{\rho_v}{2} \left(\frac{Q_{vT}}{A_2} \right)^2 \qquad (9.6)$$

Also eqn. (9.6) was used to calculate the atatic pressure over A_3 and A_4.

It was assumed that the static pressure over A_1 was atmospheric pressure. The separation of the flow from the ball was assumed to occur at section 1. Also it was assumed that at the surface area of the ball between sections 4 and 5, the static pressure was the supply pressure.

The flow force on the lower half of the ball was calculated from the following equation:

$$F_1 = p_2^* A_{1-2} + p_3^* A_{2-3} + p_4^* A_{3-4} + P_v A_{4-5} . \qquad (9.7)$$

where A_{1-2}, A_{2-3}, A_{3-4} and A_{4-5} were the projected areas between sections 1 and 2, 2 and 3, 3 and 4 and 4 and 5 respectively.

The flow force on the upper half of the ball was calculated from the following equation:

$$F_u = P_v A_r . \qquad (9.8)$$

where A_r was the projected area of the upper half of the ball.

The net flow force on the ball was calculated from the following equation:

$$F_{vf} = F_u - F_1 . \qquad (9.9)$$

9.7.3 Results and Discussions

Table (9.2) shows the calculated values of the flow force (F_{vf}) on the ball of the injector valve for each of six models, and the flow rate (Q_{vT}) from each valve, for supply pressure 40 psi. Model F is described in Chapter 7 and models A- E are described in Chapter 9. The table also shows the corresponding experimental values. It can be seen from this table that the calculated values of Q_{vT}, except for model B, were less than the corresponding experimental values. This is probably because the separation of the flow did not occur until after section 1 (the minimum area). Hence the static pressure at this section was less than atmospheric pressure and the flow velocity was greater than the flow velocity obtained by the assumption of atmospheric pressure. The lower static pressure would also cause a higher flow force on the ball. This is probably the reason why the calculated values of the flow force on the ball were less than the corresponding experimental values. The reason why the calculated value of Q_{vT} of model B was greater than the corresponding experimental value was probably because the outlet area of this model was smaller than the minimum cross sectional area (A_1). This would make the pressure over A_1 greater than atmospheric pressure.

Model	Q_{vT} Experimental (l/m)	Q_{vT} Theoretical (l/m)	F_{vf} Experimental (l/m)	F_{vf} Theoretical (l/m)
A	0.29	0.28	0.179	0.145
B	0.117	0.2	0.142	0.126
C	0.28	0.272	0.163	0.132
D	0.33	0.29	0.138	0.109
E	0.34	0.3	0.142	0.12
F	0.32	0.28	0.14	0.109

TABLE 9.2 COMPARISON BETWEEN THE EXPERIMENTAL AND THEORETICAL RESULTS

Chapter Ten

MEASURING THE FLOW RATE FROM THE INJECTOR VALVE BY USING LASER ANEMOMETRY

10.1 INTRODUCTION

The flow rate delivered from the injector valve is considered as the fundamental variable in the design of the injector. Hence the study of factors which affect these flow rate characteristics is central to the injector design.

It is very difficult (if not impossible) to measure directly the motion of the ball of the injector valve. Studying the behaviour of the flow itself might give a better understanding to the motion of the ball. In any case, it is the flow, and not the ball motion, which is ultimately to be controlled.

In this investigation a laser technique was employed to measure the flow rate - time relationship. This technique was used to obtain accurate information on this pulsatile flow probably unobtainable by more conventional techniques.

The details of test apparatus, test program, test procedure and results and discussions are given below.

10.2 TEST APPARATUS

The test apparatus comprised a special injector equipments set-up and laser anemometry equipments.

Fig. (10.1) shows a photograph for the apparatus.

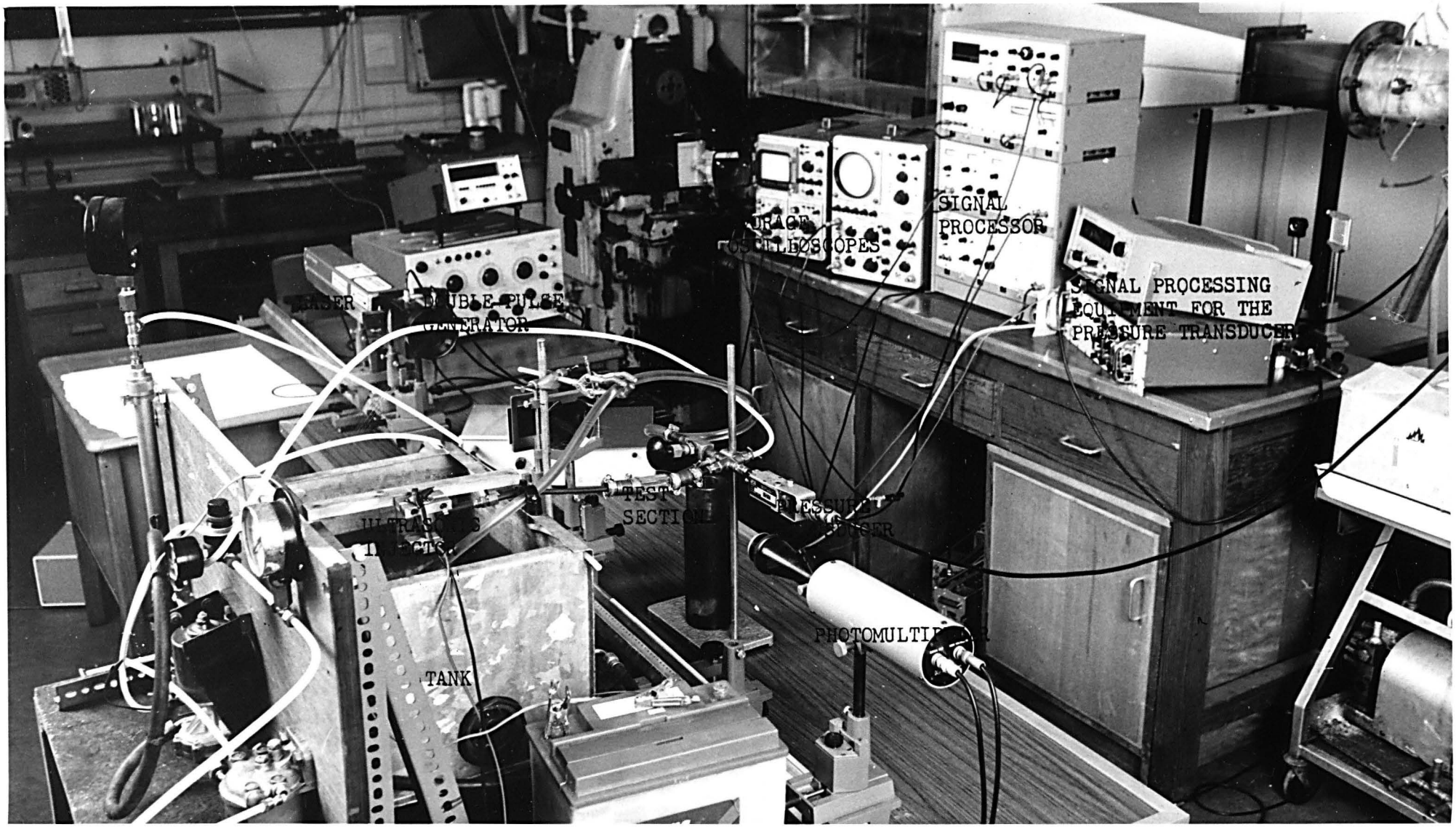

FIG. 10.1 APPARATUS FOR MEASURING FLOW RATE

10.2.1 Injector Equipments

Fig. (10.2) shows a layout of the injector equipments, while the layout of the injector valve is shown in fig. (10.3). The injector was fixed rigidly at the top of a tank. The tank was filled with kerosine. The kerosine was delivered from the tank to the injector by a pump (Lucas) of 120 psi maximum pressure. The supply pressure of the kerosine to the injector was controlled by a needle valve. The needle valve was set up on a tee junction. One outlet of the junction was connected to the tank, and the other was connected to the test section. By this arrangement the supply pressure to the injector was fixed. Also there was continuous flow (much greater than required by the injector) through the needle valve. Thus the change in pump flow when the injector was actuated was negligible. Also, the tee junction was placed close to the injector and test section, so that this length was the minimum possible. Thus only the fluid in this short line was accelerated when the injector was actuated., and the acceleration time was small.

A calibrated pressure transducer (SE, type 180/N/M/1/BB-200 PSI-D) was used for measuring the supply pressure. The signal from the pressure transducer was fed to the signal processing equipment (SE, type 429 P) which was connected to a digital voltmeter (Dalton, type 1051). To get an adequate amount of scattered light, the presence of particles in the flow was important. Hence the kerosine was not filtered, and Titanium Oxide particles were added.

The pulse width of any duty cycle was controlled by a double pulse generator (Magard Ltd., Type 5002 C). The test section (see fig. (10.4)) was made from a Perspex. The dimensions of the cross

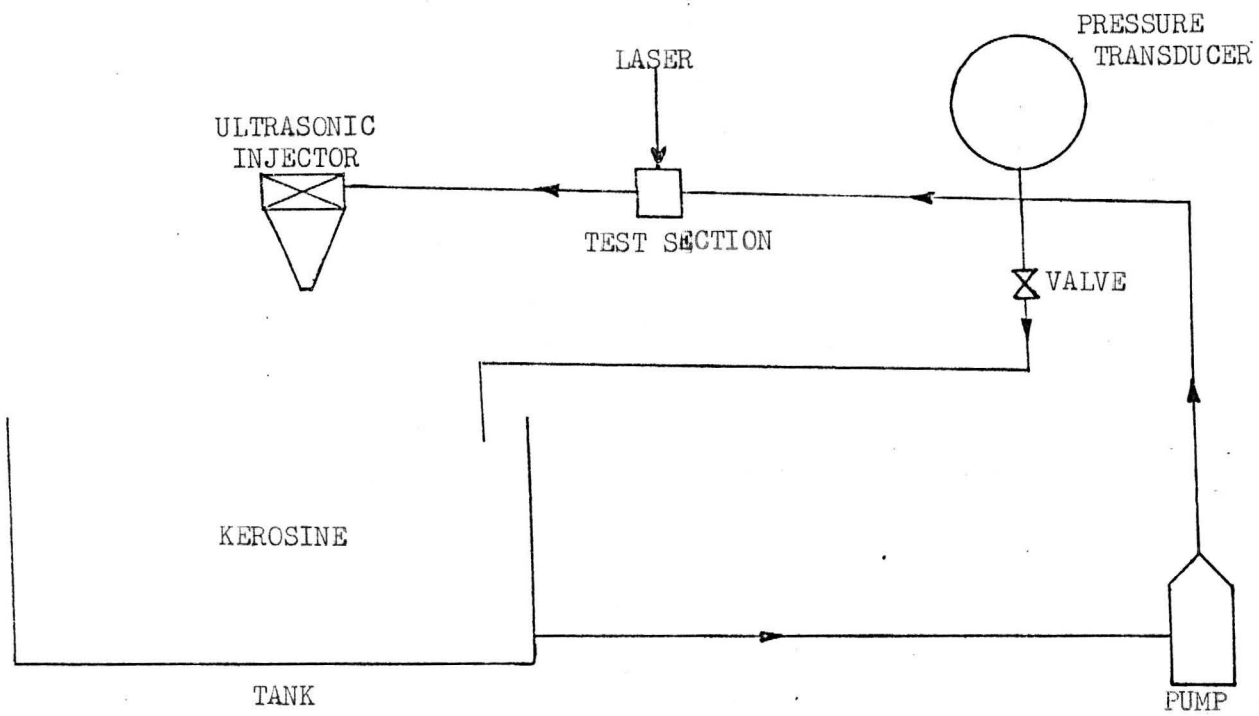

FIG. 10.2 LAYOUT OF THE INJECTOR EQUIPMENT

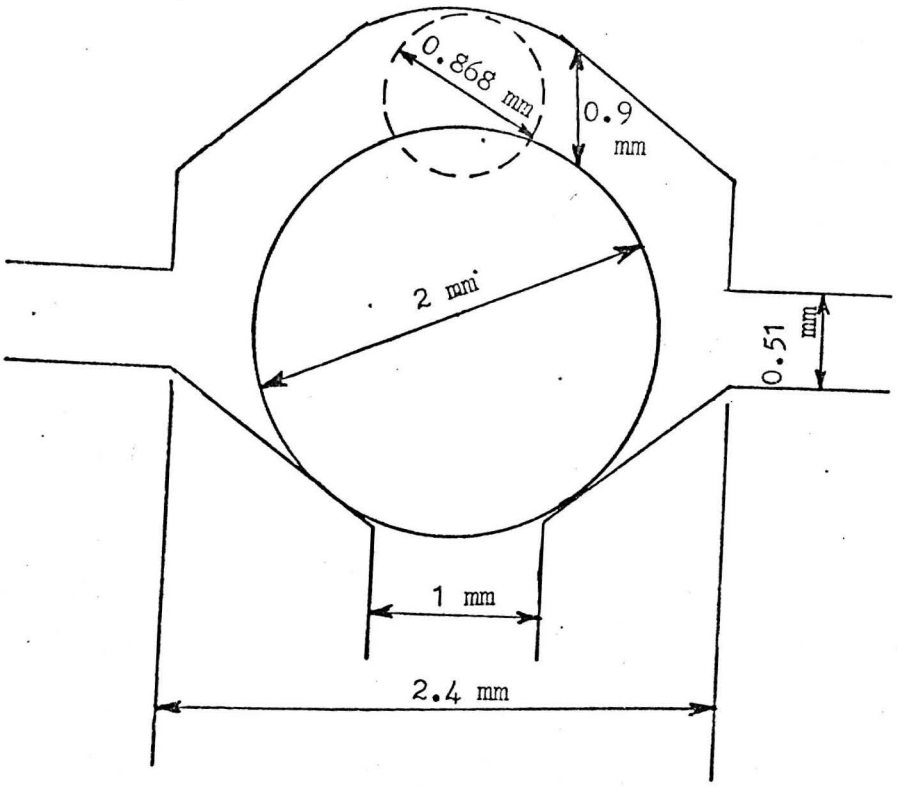

FIG. 10.3 LAYOUT OF THE INJECTOR VALVE

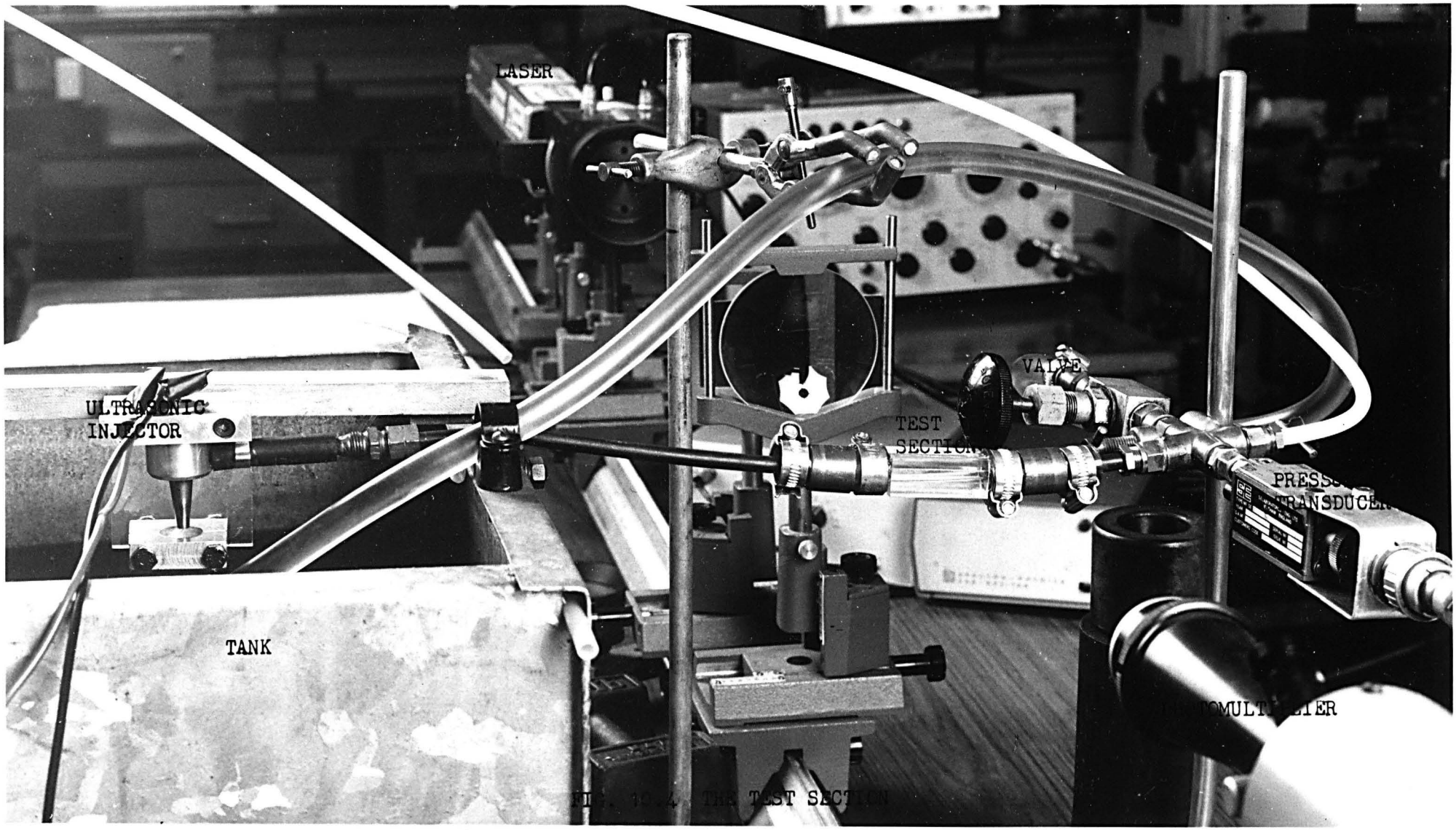

FIG. 19.4 THE TEST SECTION

section perpendicular to the direction of the flow were 0.6 x 0.9 mm. The test section was put near enough from the injector valve to allow the pressure waves to reach the test section in a negligible time. The pump was connected to the test section by a plastic tube. The test section was connected to the injector by a brass pipe of which the rigidity was adequate to avoid significant change in its cross section due to the increase in the supply pressure when the injector valve was closed instantaneously.

10.2.2 Laser Equipment

Fig. (10.5) shows a layout of the laser equipments. The laser equipment which was used for measuring the tip motion was also used here (see section (5.2.2)). The optical unit was operated in differential Doppler mode on forward scattered light. In this mode two beams of equal intensity were intersected at the flow in the test section. The beams were frequency shifted by ±3.75 MHz by the Bragg Cells. By this means zero velocity corresponds to a doppler frequency of 7.5 MHz and thus negative as well as positive velocities can be measured. The scattered light was picked up from the same direction of the two incident beams. The beam intersection angle was set up to 9.53 degrees.

10.3 TEST PROGRAM

In each test the maximum instantaneous Doppler frequency was measured for each pulse width of a specific pulse width range and for a specific supply pressure. The tests were conducted for a pulse width range 1 - 6 ms and supply pressure range 10 - 100 psi. The

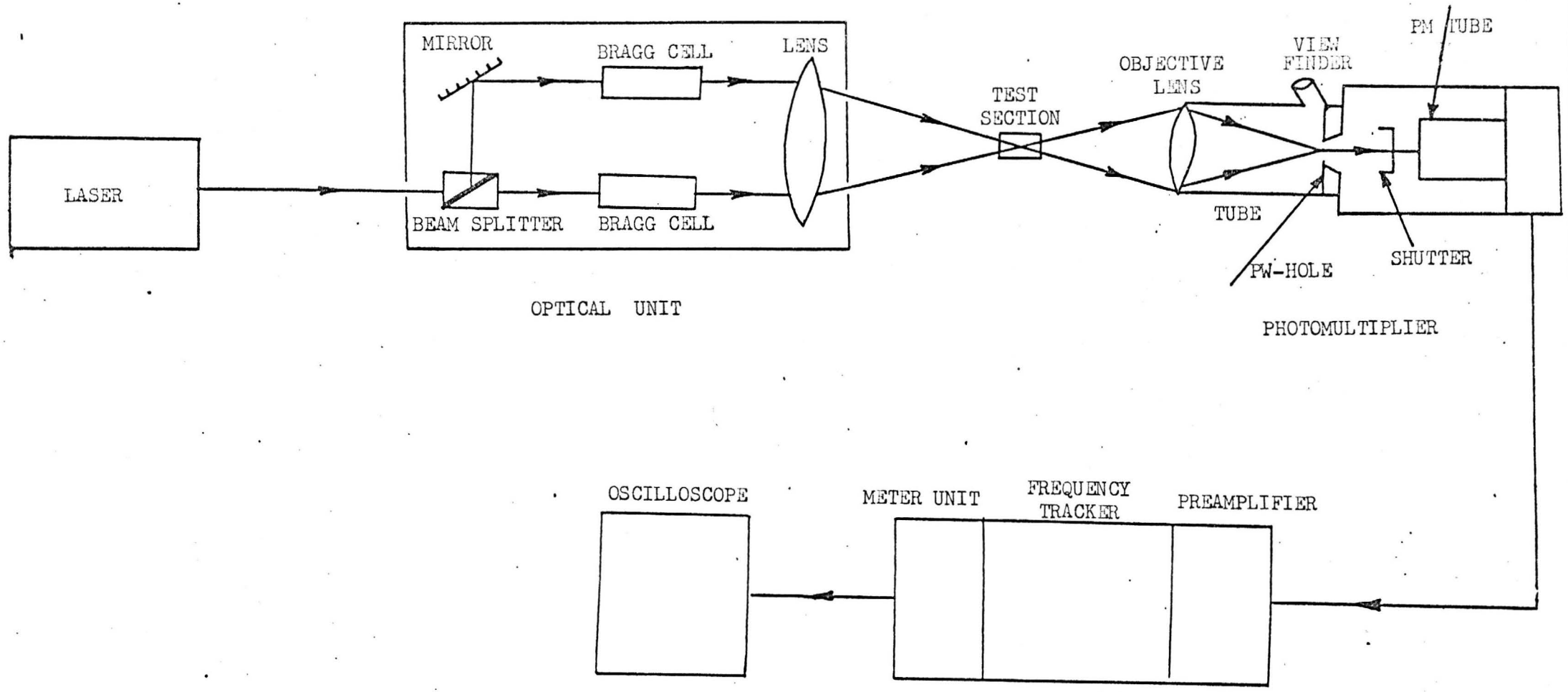

FIG. 10.5 LAYOUT OF THE LASER EQUIPMENTS

time interval between injection pulses was 6 ms (166.6 Hz). Thus the mark-space ratio varied from $\frac{1}{5}$ to ∞.

10.4 TEST PROCEDURE

The injection frequency was set to 166.6 Hz, and the pulse width and supply pressure were adjusted.

The procedure used for obtained the laser signal of the tip motion was also used here (see section (5.4)). When the laser signal (which represented the instantaneous velocity of the flow) was obtained on the oscilloscope, the injection frequency was reduced. This would obtain the signal of the zero value of the flow on the oscilloscope. The injection frequency was then reset to 166.6 Hz. The instantaneous Doppler frequency representing velocity was displayed on the storage oscilloscope and photographed. The maximum value was recorded. The pulse width was then increased to the other value, and the supply pressure was readjusted to the original value when the flow rate increased due to the increase of the pulse width. The procedure was repeated until the data for the required pulse width range was covered. The supply pressure was then changed to the other value, and the test was repeated until the data for the required supply pressure range was obtained.

10.5 MEASUREMENT ANALYSIS OF THE LASER OUTPUT

The instantaneous flow velocity at the test section was calculated from the following standard formula of doppler anemometry

$$V_{vL} = \frac{f_D \lambda}{2 \sin \theta/2} \qquad (10.1)$$

where f_D is the doppler shift frequency, λ the wavelength of the laser light and θ the angle of intersection of the beams. The instantaneous total flow rate from the injector valve was then calculated from

$$Q_{vL} = V_{vL} A_{cs} \qquad (10.2)$$

where A_{cs} is the area of the measuring cross-section.

10.6 TEST RESULTS AND DISCUSSIONS

Fig. (10.6) shows the relationship between the maximum flow rate with the pulse width, for supply pressure range 10 - 100 psi and injection frequency = 166.6 Hz. This fig. shows that when the pulse width was increased from 1 ms to 3 ms, the maximum flow rate increased due to the increase in the amplitude of the tip motion. The maximum flow rate remained constant as the pulse width was increased further. The reason for this is because the velocity of the tip was high enough at this range, and hence the ball spent more of its time at the larger gaps where it did not influence flow rate.

This fig. also shows that the maximum flow rate increased with the supply pressure. Fig. (10.7) shows a plot of the flow rate versus the pulse width, for supply pressure range 10 - 100 psi and injection frequency = 166.6 Hz. These measurements have been carried out by a weighing method. The aim of these measurements was to find the relationship between the average flow rate with the pulse width, and also to compare this relationship with the maximum flow rate - pulse width relationship which is shown in Fig. (10.6).

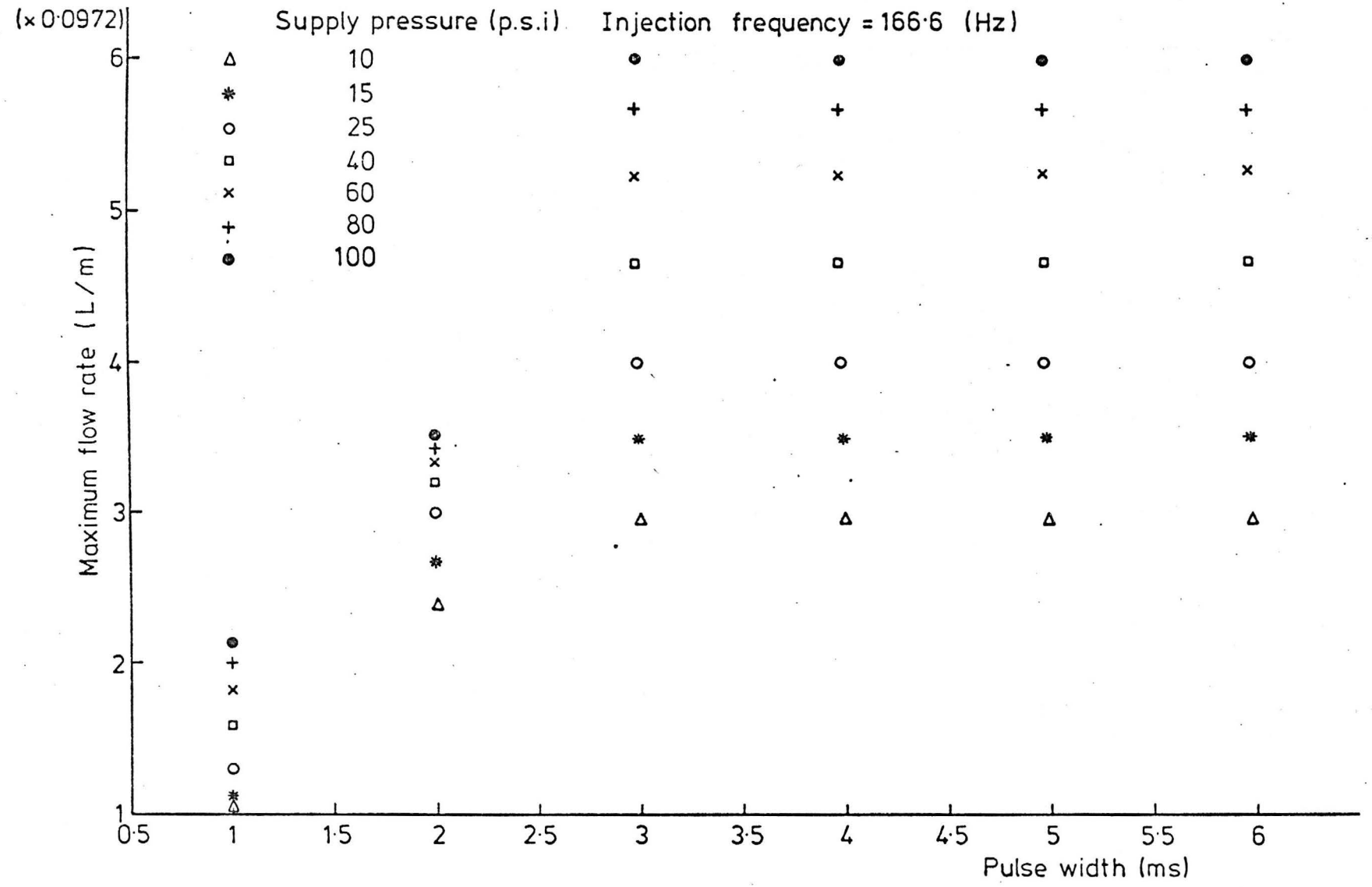

FIG.10-6 MAXIMUM FLOW RATE — PULSE WIDTH RELATIONSHIP FOR VARIOUS SUPPLY PRESSURES

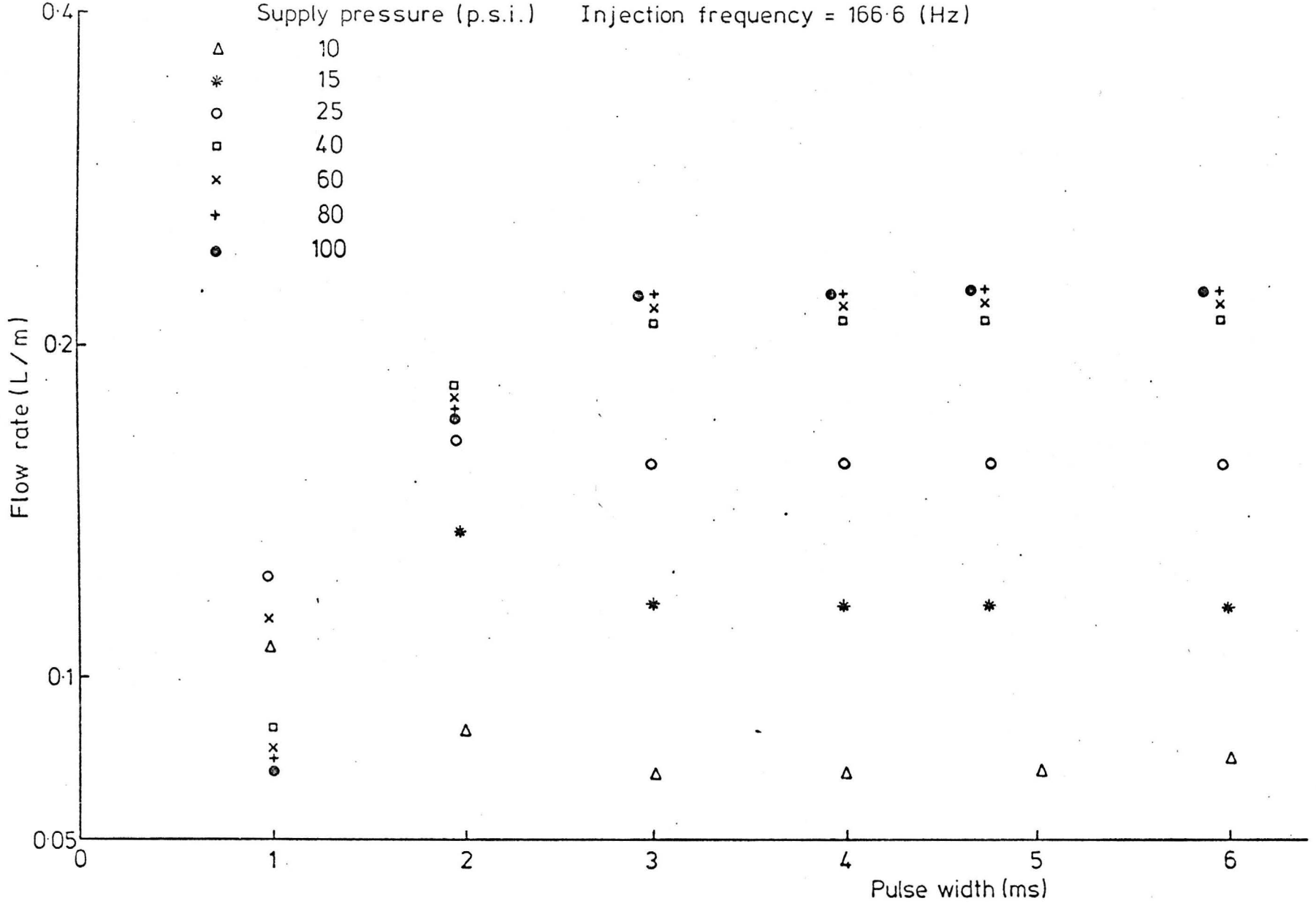

FIG.10-7 FLOW RATE – PULSE WIDTH RELATIONSHIP FOR VARIOUS SUPPLY PRESSURES

At 3 ms pulse width, it can be seen that the flow rate increased with increasing the supply pressure in the range 10 - 40 psi, and then remained approximately constant in the range 40 - 100 psi. This is probably because in the supply pressure range 10 - 40 psi the supply pressure was small and hence the effect of the increase in the supply pressure on the gaps was less than that on the flow rate itself. When the supply pressure was increased in the range 40 - 100 psi, the supply pressure was large, and the effect of the increase in the supply pressure on the gaps was approximately identical with that on the flow rate itself. The flow rate did not decrease when the supply pressure increased in the range 40 - 100 psi, as in 1 ms and 2 ms pulse widths. This is because the ball was moving in larger gaps.

Also this fig. shows that when the pulse width was increased from 3 ms to 6 ms, the flow rate remained the same. The reason for this is also because the ball spent more of its time at the larger gaps where it did not influence flow rate.

Fig. (10.8) shows a photograph of the laser signal for 4 ms pulse width, 166.6 Hz injection frequency and 40 psi supply pressure. The signal of the pulses is also shown on the photograph. This fig. shows that the flow rate built up to the steady state value in approximately 2.5 ms. This fig. also shows that after the injector was switched off, there was still flow because the ball continued bouncing, due to the decay in the motion of the tip. It can also be seen from this fig. that the injector was switched on when the flow was still decaying. Hence the tip might try to stop the motion

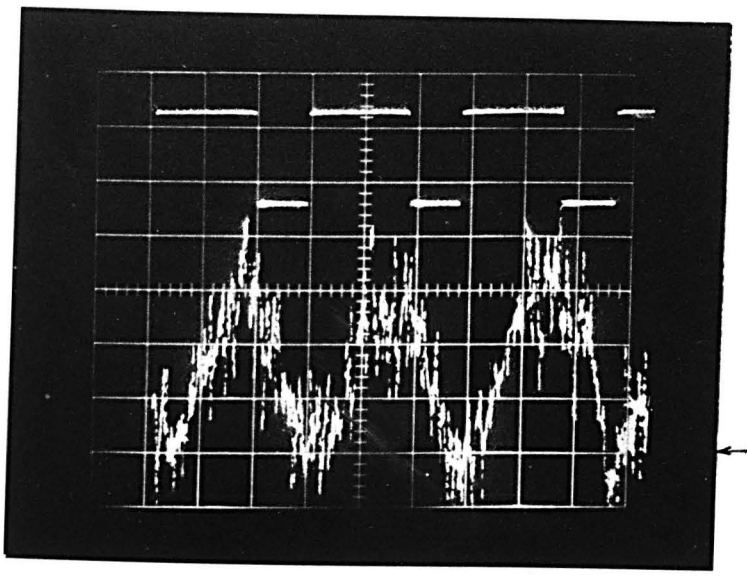

FIG. 10.8 - PHOTOGRAPH OF THE LASER SIGNAL AND OF THE PULSES SIGNAL
PW = 4 ms, INJECTION FREQUENCY = 166.6 Hz, P_v = 40 psi.

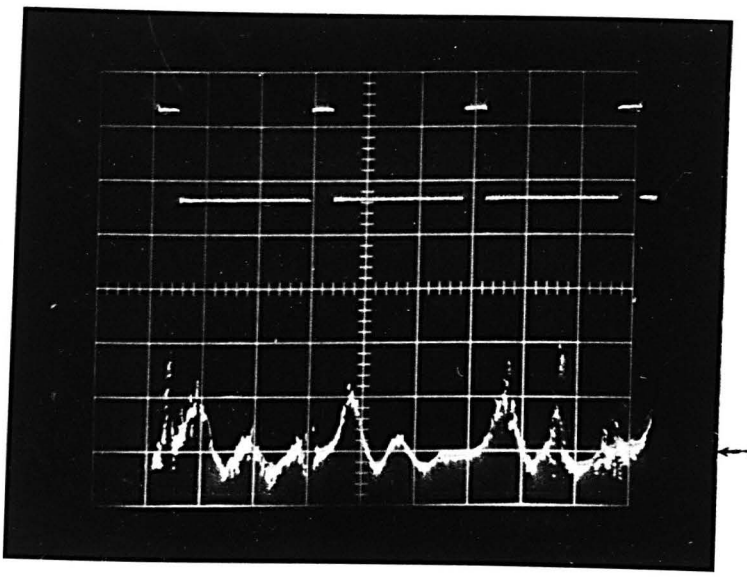

FIG. 10.9 - PHOTOGRAPH OF THE LASER SIGNAL AND OF THE PULSES SIGNAL
PW = 1 ms, INJECTION FREQUENCY = 166.6 Hz, P_v = 40 psi.

of the ball. Also this fig. shows that there was slight reverse flow, probably due to the reflections of waves after closing the valve.

The effect of the pulse width on the flow rate is indicated in fig. (10.9). This shows a photograph of the laser signal for 1 ms pulse width, 166.6 Hz injection frequency and 40 psi supply pressure. The signal of the pulses is also shown on the photographs. This fig. shows that the flow discharged from the injector valve after the injection pulse, i.e., phase shifted by about 1 ms. The fluctuation in the signal about the zero line was probably due to the wave reflections after switching off the valve. The effect of the supply pressure on the flow rate is indicated in fig. (10.10). This fig. shows a photograph of the laser signal for 3 ms pulse width, 166.6 Hz injection frequency and 10 psi supply pressure. This fig. shows that when the injector was switched on flow build up was delayed. This is probably because when the injector was switched on there was reverse flow.

Fig. (10.11) shows a photograph of the laser signal for 100 psi supply pressure, 20 Hz injection frequency and 10 ms pulse width. The pressure transducer signal is also shown on the photograph. This fig. shows that after switching off the injector there was slight flow in the direction of the supply tank. The flow then increased and then decayed to the zero value. The negative flow rate (flow in the direction of the supply tank) and the increase in the flow rate again, were probably due to the wave reflections after closing the valve. It can be seen from this fig. that the signal of the pressure transducer represented well the

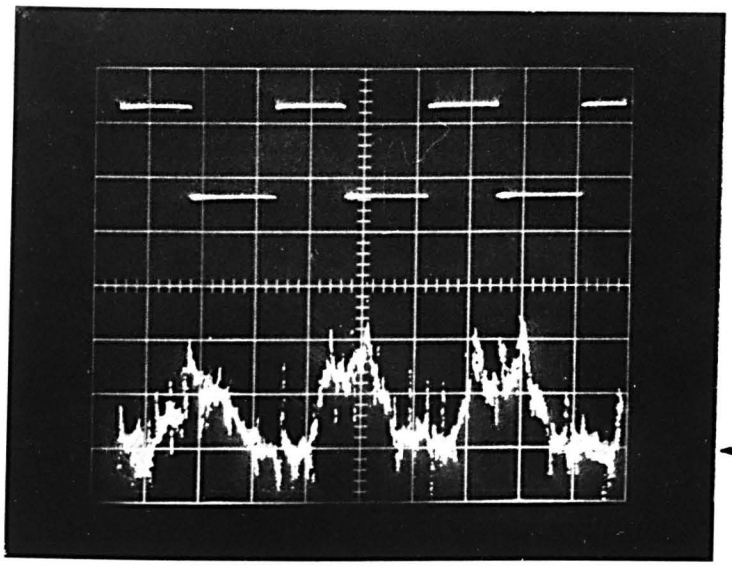

FIG. 10.10 - PHOTOGRAPH OF THE LASER SIGNAL AND OF THE PULSES SIGNAL
PW = 3 ms, INJECTION FREQUENCY = 166.6 Hz, P_v = 10 psi.

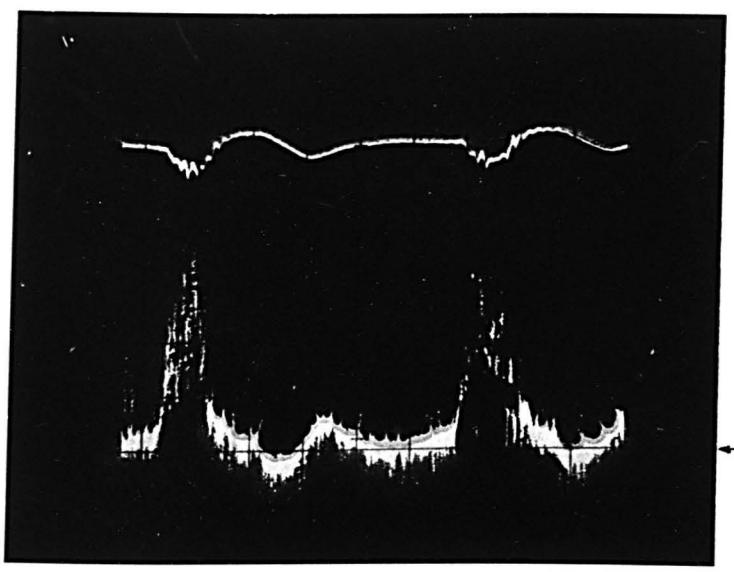

FIG. 10.11 - PHOTOGRAPH OF THE LASER SIGNAL AND OF THE PULSES SIGNAL
PW = 10 ms, INJECTION FREQUENCY = 20 Hz, P_v = 100 psi.

change of the flow rate with the time at the test section.

Fig. (10.12) shows a photograph of the laser signal for 100 psi supply pressure, 166.6 injection frequency and 4 ms pulse width. This photograph was taken during the build up of the flow. This fig. shows that the frequency of flow rate was of order 10 KHz. Hence the frequency of the ball was of order 10 KHz.

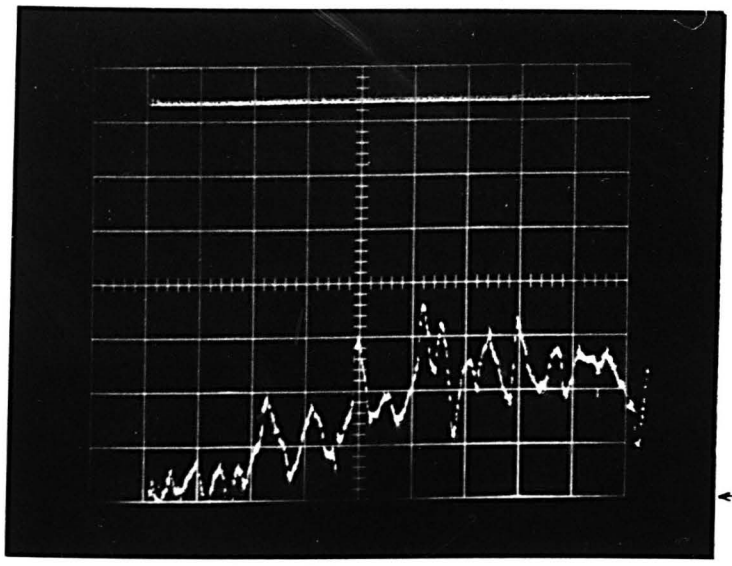

FIG. 10.12 - PHOTOGRAPH OF THE LASER SIGNAL AND OF THE PULSES SIGNAL

PW = 4 ms, INJECTION FREQUENCY = 166.6 Hz, P_v = 100 psi.

Chapter Eleven

GENERAL DISCUSSION

This chapter contains a short discussion and comments on the results reported in the different sections of this thesis.

The ball motion without liquid resistance and with the assumption of sinusoidal motion of the tip was investigated and the results are given in chapter 3. The period of the ball cycle plots (figs. (3.4 - 3.7)) indicated that the ball was moving with a random frequency. This means that the flow per cycle fluctuated.

These results also showed that sometimes the ball spent more than 1 ms in one cycle (although the injector was moving at a frequency of 60 KHz). Sometimes the ball spent 1.6×10^{-2} ms to complete one cycle. This indicates that the fluctuations in the flow per cycle were very large. Flow is also affected if random part-cycles occur as these may produce any flow quantity depending on their amplitude and time. The fluctuations in the flow per cycle during the flow pulse might have no effect upon the employment of the injector, but it is undesirable from the design point of view. The injector can be designed by controlling the motion of the ball, i.e., making the ball move in a steady state frequency, and in full amplitude, i.e., the flow per cycle is in a steady state. This will provide a linear flow-time relationship. This design is needed only when the flow rate is changing with the gap between the ball and the seat. When the flow rate becomes in a steady state as soon as the ball leaves the seat, the flow-time relationship will be linear.

Slow ball cycle is undesirable for fast response of the

injector. Also it is desirable to make the total number of the ball cycles in a pulse very large, so that the flow during a single ball cycle is negligible.

The best injector valve can be defined as the valve which possesses the following 'Ideal Requirements':

1. The ball leaves the seat as soon as the injector is switched on.
2. The time of impact between the ball and the seat is very small.
3. The ball closes the valve as soon as the injector is switched off.
4. The flow rate becomes in a steady state as soon as the ball leaves the seat.
5. The geometry of the valve provides a suitable flow rate.

It can be deduced from this definition that the ball motion could not affect the total flow rate if the second and fourth Ideal Requirements could be fulfilled.

It has been shown from the effect of the parameter D (ratio of the maximum amplitude of the injector tip to the maximum gap between the ball and the seat) on the ball motion (figs. (3.4 - 3.7)) that the period of the ball decreased when D increased and the parameter Z (ratio of the gravitational acceleration to the maximum acceleration of the injector tip) was kept constant. These results indicated that the frequency of the ball could be increased by reducing the maximum gap between the ball and the seat. To meet the third Ideal Requirement, the frequency of the ball should be high enough, i.e., the ball should return to its seat within a very short time. But a very high frequency may not be desirable if it makes the ball continue in the motion after the injector is switched off or causes

wear on the walls of the valve.

The results have also shown that the change in the maximum amplitude of the tip and also the frequency of the tip while keeping the maximum gap between the ball and the seat would change the period of the ball randomly. It was found also that when the ball was moving at the same frequency as the injector tip, the possibility of a steady state motion was higher.

The effect of changing the initial condition of the tip was found to change the motion of the ball, but the effect of the other parameters on the ball motion remained the same. It was concluded from the results of computing the time of impact that this was very small. This result meets the second Ideal Requirement (very small time of impact).

The ball motion was studied experimentally in a large model of the injector valve without any liquid resistance and the results are given in Chapter 4. The results of the measurements have shown the multiple impacts phenomenon. If this phenomenon occurs with the ball motion of the injector valve, this will increase the time of impact. The multiple impacts phenomenon has also been found from the results of Chapter 3.

It was also found from the measurements that the frequency of the ball was approximately identical with the excitation frequency in steady state. This probably means that the approach in the design of the injector valve with steady state motion was to make the ball move in the same frequency of the injector tip. But side effects, such as the wear on the walls of the valve and the possibility of the continuity of the motion of the ball after

switching off the injector, should be taken into consideration.

The results of measurements of the ball motion were in very good agreement with the corresponding results of the computer program of Chapter 3. This indicates that the results of the theoretical analysis of the ball motion without any fluid resistance were accurate. The injector tip motion was measured using laser anemometry, and the results are shown in Chapter 5. The effect of the pulse width and the supply pressure on the tip motion is shown in fig. (5.4). It was found that the pulse width had a significant effect on the tip motion. The tip motion built up in 5 ms to the steady state. This phenomenon must have a significant effect on the performance of the injector valve. It was found that the effect of the supply pressure on the tip motion was to reduce its amplitude. It was also found from the photographs of the signal of the tip motion that the tip motion took 1.5 ms to decay after switching off the injector. If the injector drive was switched on again in less than 1.5 ms, the phase of the electrical signal relative to the injector motion would be important. Therefore, variations in the ball motion due to this phase difference could be expected. This motion would affect the flow per pulse.

The flow force on the ball, the total flow rate and the inlet flow rates for each position of the ball were increased in a scale model of a general design of the injector valve. The results of the measurements were scaled to the injector valve and are given in Chapter 7. The plots of the total flow rate, the side inlets flow rates and the top inlet flow rate are shown in figs. (7.10 - 7.12). The total flow rate plots have shown that the total flow rate

became steady when the gap was approximately 30% of the maximum gap. It can thus be deduced that the ball position influenced the total flow rate only when the gap was approximately less than 30% of the maximum gap between the ball and the seat. The change in the total flow rate with the gap between the ball and the seat was caused by change in the resistance due to the area under the ball. This indicates that the fourth Ideal Requirement of the best injector valve could be met by controlling this resistance. The effect of this resistance on the flow rate can be reduced by increasing the resistance due to the area of the outlet, i.e., by reducing the area of the outlet (compare fig. (9.6) with fig. (9.10)). The resistance due to the area under the ball can be reduced by increasing the wall angle (the angle between the lower wall and horizontal line).

The plots of the flow force on the ball of the injector valve are presented in fig. (7.15). These plots have shown that the flow force on the ball increased when the ball was lifted from the seat until the gap was 17% of the maximum gap. (This increase in the flow force occurs because, due to the wall angle, the surface of minimum flow area is below the horizontal diameter of the ball. Pressures below this diameter therefore fall below supply pressure for small ball lifts.) The increase in the flow force is contradictory to the first Ideal Requirement (fast ball lift). Hence increasing the seat angle could provide a reduction in the flow force as soon as the ball leaves the seat. But increasing the seat angle increases the projected area (cross-section through the contact perimeter) of the ball, and hence the pressure force on the

seated ball increases.

These plots have also shown that the flow force then decreased until the gap was approximately $\frac{2}{3}$ of the maximum gap where the flow force on the ball is desirable. This will permit the ball to move faster, especially in the gap where the total flow rate is not in steady state. Also the increase in the flow force when the ball nears the top inlet is preferable. This could force the ball to come back to the seat in a suitable short time. This meets with the third Ideal Requirement (the ball closes the valve as soon as the injector is switched off). The forces due to the gravity and buoyancy were found very small and hence the flow force plots represented the net force on the ball.

The ball motion was studied theoretically with the fluid resistance and the results are presented in Chapter 8. The ball motion results (figs. (8.12 - 8.14)) have shown that the ball motion built up in 1.5- 2 ms. The flow resistance was found to have a significant influence on the ball motion. This was concluded clearly by comparing these results with the results of the theoretical analysis of the ball motion which were presented in Chapters 3 and 6. The decay in the ball motion (which is shown in fig. (8.17)) indicated that the ball could not come back as soon as the injector was switched off. This behaviour contradicts the third Ideal Requirement.

It can be concluded from the plots of the time of the ball cycle (fig. (8.16)) that the frequency of the ball was also random and the flow force had significant effect on the spectrum of the frequency. The total flow rate plots (figs. (8.18 - 8.20)) have

also shown build up in the total flow rate in 1.5- 2 ms. It was found that the total flow rate built up to 80% of the steady state value of the total flow rate in 0.5 ms. This indicated that the effect of the build up in the flow rate on the performance of the injector was very significant only when the pulse width was less than 0.5 ms.

The decay in the flow rate is shown in fig. (8.21). This fig. has shown that the decay in the flow rate was approximately in 3 ms. It can be deduced from this result that when the time in which the injector was switched off was less than 3 ms, the injector would be switched on whilst there was flow from the injector. This phenomenon is undesirable.

The flow plots (fig. (8.22)) indicated that the flow had linear characteristics after 1.5- 2 ms from switching on the injector. The linear characteristics of the total flow after 0.8 ms was also found by Martin and Sumal (3). The method of their investigation was not mentioned in their paper. Hence the reason of the difference in the results could not be known. These plots have also indicated that the effect of the increase in the supply pressure had no significant effect on the flow when the supply pressure was higher than 40 psi. This is probably the reason why the maximum amplitude of the tip was not affected by the increase of the supply pressure above 40 psi, (fig. (5.4)). It was found by (3) that the total flow rate from the injector valve was constant with changing the supply pressure. Also the method of the investigation of (3) was not mentioned in the paper.

It was found from the measurements of the flow rate per pulse

width (fig. (10.7)), that the flow rate was in a steady state after 2 - 3 ms from switching on the injector, i.e., the flow had linear characteristics after 2 - 3 ms. It was also found from these measurements that the flow rate was not affected by the increase of the supply pressure above 40 psi. Although these measurements have been done with injector valve of geometry different from that of Chapter 7 (the theoretical analysis was based on the data of Chapter 7), these theoretical and experimental results were in agreement. This is probably because the change in the geometry changed the flow rates but did not significantly change the flow force on the ball. Also the effect of the tip motion on the ball remained the same. Hence the ball motion was not significantly affected by the change in the geometry of the valve, i.e., the build up in the flow rate and the effect of the supply pressure remained the same.

It was found from these plots that the mean flow rate during the pulse was approximately 60% of the peak value. It can be concluded from this that if the peak flow rate could be estimated then the flow rate at any time during the pulse could be estimated.

The effect of the geometry of the injector valve on the flow force on the ball and on the flow rates were studied by making five scale models of different geometries of the injector valve. The flow rates plots of model A (figs. (9.5 - 9.7)) indicated that the increase of the number of the side inlets from 2 to 5 would cause an increase of 10% of the total flow rate. This was found by comparing model A with model C. It can be deduced from this that the increase in the area of the side inlets had no significant

influence on the maximum value of the total flow rate. Also the flow rates plots of model A indicated that the effect of the increase of the area of the side inlets would prevent the decrease in total flow rate when the ball was near the top inlet. This phenomenon meets with the fourth Ideal Requirement (the flow rate becomes in a steady state as soon as the ball leaves the seat). The plots of the flow rates of model B (figs. (9.9 - 9.11)) indicated that the decrease in the area of the outlet caused a significant decrease in the flow rate from the valve. It can be concluded that the outlet area could be considered as a controller of the total flow rate. Also the plots have shown that the gap in which the total flow rate built up to the steady state was smaller than that of model A. This indicated that the reduction in the outlet area caused the total flow rate to reach a steady state almost as soon as the ball left the seat. This satisfies the fourth Ideal Requirement. Hence to remove the effect of the ball motion on the flow rate from the injector valve, the outlet area should be reduced to a suitable value. This would however cause the total flow rate for a given pressure to reduce and also might be undesirable due to the difficulty of accurately manufacturing this hole.

The effect of the cavity diameter of the injector valve on the total flow rate was found by comparing the plots of the flow rates of model C (figs. (9.13 - 9.15)) with that of Chapter 7 (figs. (7.10 - 7.12)). It was found that the decrease in the cavity diameter caused the total flow rate to decrease because the gap between the ball and the side inlets would be smaller. Also the flow area between the ball and the side walls of the valve would

be smaller. The increased resistance due to this area would be complicated and might cause a reduction in the flow rates. The effect of this resistance could be made negligible by increasing the area of the side inlets.

The effect of the area of the side inlets on the flow rate of the top inlet was found from the plots of the flow rates of model D and E (figs. (9.17,18,20,21)). These results indicated that the increase in the area of the side inlets restricted the flow rate from the top inlet.

The plots of the flow force of model A (fig. (9.4)) indicated that the increase in the side inlets area would cause the flow force to stay constant for 0.1 mm at a minimum and to increase not sharply as in the case of models C and that of Chapter 7. The sharp increase of the flow force might force the ball to come back to the seat before reaching the top inlet. Hence the time in which the flow rate was in a steady state was reduced. This is contradictory to the fourth Ideal Requirement (the flow rate becomes in a steady state as soon as the ball leaves the seat).

Another effect of the side inlets area on the flow force was found from the plots of the flow force of models D and E. These results indicated that the increase in the side inlets area could cause the flow force to stay constant at a minimum until the ball was lifted to the top inlet. This phenomenon is contradictory to the third Ideal Requirement. (The ball comes back to the seat as soon as the injector is switched off.)

The decrease of the outlet area of the valve was found to cause a decrease in the values of the flow force. This was found

from the plots of the flow force of model B (figs. (9.8)). It was also found from these plots that F_{vT} decayed to a minimum at smaller value of the gap between the ball and the seat. This might prevent the ball coming back to the seat before reaching the top inlet. The flow force and the total flow rate were calculated where the ball was at 1 mm from the seat and the results are given in chapter 9 (table (9.2)). The results were in agreement with the experimental results.

The total flow rate- time relationship was studied experimentally by using laser techniques and the results are given in Chapter 10. The results indicated that there was approximately 2- 3 ms build-up in the total flow rate and the flow continued for approximately 2 ms after switching off the injector.

The photograph of the pressure transducer signal (fig. (10.11)) has indicated that measuring the pressure using electronic pressure transducer might be considered as an alternative way of measuring the total flow rate- time characteristics.

Chapter Twelve

CONCLUSIONS AND SUGGESTIONS FOR FURTHER WORK

12.1 CONCLUSIONS

The main conclusions of this investigation are the following:

1. The ball was moving with a random frequency when the effect of the liquid resistance was assumed negligible.
2. The increase in the maximum gap between the ball and the seat caused, in general, a decrease in the frequency of the ball.
3. The change in the maximum amplitude of the tip and also the frequency of the tip changed the frequency of the ball randomly.
4. When the ball was moving with the frequency of the injector tip, the possibility of the steady state motion was found higher.
5. The effect of the initial condition of the tip motion on the ball motion was found to change the ball motion, but the effect of the parameters such as the maximum amplitude of the tip, the frequency of the tip and the maximum gap between the ball and the seat remained the same.
6. Measurements of the ball motion in a large model of the injector valve without any liquid resistance were in agreement with the theoretical results of the ball motion without any liquid resistance. Multiple impact phenomena have been observed.
7. The time of impact was deduced to be very small compared to the time of the ball cycle.
8. The tip motion was found to build up in 5 ms to the steady state.
9. The increase of the supply pressure caused reduction of the amplitude of the tip motion.
10. A decay of 1.5 ms in the tip motion was observed after switching off the injector.

11. The resistance due to the area under the ball was found, in general, to prevent the flow rate to be in a steady state as soon as the ball left the seat.

12. The resistances due to the area above the ball and the area of the top inlet was found to cause a reduction in the total flow rate when the ball was near the top inlet. The existance of this reduction was found to depend on the ratio of the resistance due to the area of the side inlets to the resistances due to the area above the ball and the area of the top inlet.

13. The increase from two to five side inlets had no significant influence on the total flow rate. But the increase in the area of the side inlets caused a decrease in the flow rate of the top inlet. The value of the flow rate of the top inlet was found to be zero when the valve was opened completely around the side.

14. The area of the outlet of the injector valve was found to be an important controller of the total flow rate and the build-up of the total flow rate to the steady state. The decrease in the area of the outlet caused the total flow rate to decrease and the gap in which the total flow rate built up to the steady state to decrease also.

15. The diameter of the cavity of the valve was found to affect the total flow rate. The decrease in the cavity diameter caused the total flow rate to decrease.

16. The seat angle had influence on the flow force on the ball. It was concluded that the increase in the seat angle could provide a reduction in the flow force as soon as the ball leaves the seat.

17. In general the flow force increased when the ball was lifted

from the seat of the valve and then decreased until the ball was near the top inlet where the flow force increased again.

18. The area of the side inlets affected the flow force on the ball. The increase in the area of the side inlets caused the flow force to stay constant at a minimum, and prevented the flow force increasing sharply after it reached a minimum value. Also the increase in the side inlets area could prevent the flow force on the ball increasing again when the ball was lifted near the top inlet.

19. The outlet of the valve had influenced the flow force on the ball. The decrease in the area of the valve caused a decrease in the values of the flow force.

20. The ball motion was building up in 1.5 - 2 ms dependent on the supply pressure. It can be concluded that this is the reason for the fluctuation in the total flow rate per pulse at short pulse widths (1). The liquid resistance was found to have a significant influence on the ball motion. The ball motion has decayed for approximately 3 ms after switching off the injector. The ball was moving in a random frequency even with the existence of the liquid resistance.

21. The flow rate was found to build up to the steady state in 2 - 3 ms. The flow rate decayed for approximately 2 ms. It was estimated that the average flow rate was approximately 60% of the maximum value during the pulse.

22. The total flow was found to have linear characteristics after 1.5 - 2 ms from switching on the injector.

23. The supply pressure was found theoretically and experimentally

to have no significant influence on the total flow when the supply pressure was higher than 40 psi.

24. Computations of the flow force on the ball and the flow rate were in agreement with the experimental results. It can be concluded that Bernoulli's equation could be used in estimating the pressure and the flow rate at some positions in the valve.

25. It can be concluded from this investigation that parameters such as the gap between the ball and the seat, the frequency of the ball, the inertia of the horn of the injector, the area under the ball, the area above the ball, the area of the top inlet, the area of the side inlets, the area of the outlet, the diameter of the cavity, the supply pressure and the liquid resistance on the ball should be taken into consideration in the design of the ultrasonic fuel injector.

12.2 SUGGESTIONS FOR FURTHER STUDIES

Amongst the most important suggestions for consideration for further studies are the following:

1. In the measurements of the flow force on the ball, the total flow rate, the side inlets flow rate and the top inlet flow rate; by using a scale model of the injector valve, it was assumed that the flow passing the ball was in steady state. In fact the flow might be affected by the vibration of the tip. Hence studying the effect of the vibration of the flow on the ball motion is considered necessary.

2. Studying the wave action in the pipe between the valve which controls the supply pressure and the injector valve is considered

useful. By this study the total flow rate could be computed, and the effect of the wave action due to the instantaneous closure of the valve on the total flow rate would be known. The method of characteristics might be useful for this purpose.

3. Computing the pressure distribution on the ball might be useful to get better understanding of the flow force on the ball. The ideal fluid approach could be useful.

4. Making the ultrasonic fuel injector of valves of the different geometries which were described in Chapter 9, and measuring the total flow rate by using laser technique. This would enable us to find the effect of changing the geometry on the ball motion.

5. Studying the motion of the ball by making a model of the ultrasonic injector with the valve made of perspex. A very high speed camera could be used for this study.

6. Studying alternative design of the injector valve such as a valve with the ball fixed to a spring which is fixed to the wall of the valve. This study has been done theoretically and a computer program has been established (see Appendix 1). A modification to the theory is needed.

7. Measuring the flow force and the flow rates in a scale model of the valve of the ultrasonic fuel injector of type Ex 4 (flow rate- time and flow- pulse width relationships of this injector were measured and the results are presented in Chapter 10). The results of these measurements could be used as an input data to the computer program of the fluid flow (which is described in Chapter 8). Comparison between these theoretical results with the experimental results (which are presented in Chapter 10) could be made.

APPENDIX 1

THEORETICAL ANALYSIS ON ALTERNATIVE DESIGN OF THE INJECTOR VALVE

Since one of the best characteristics of the injector valve is that the ball comes back to the seat as soon as the injector is switched off, this could be achieved by fixing the ball to a spring (see fig. (A1.1)). It is assumed that the forces which could affect the ball are the forces due to the collision with the walls of the cavity, the spring force and the inertia force.

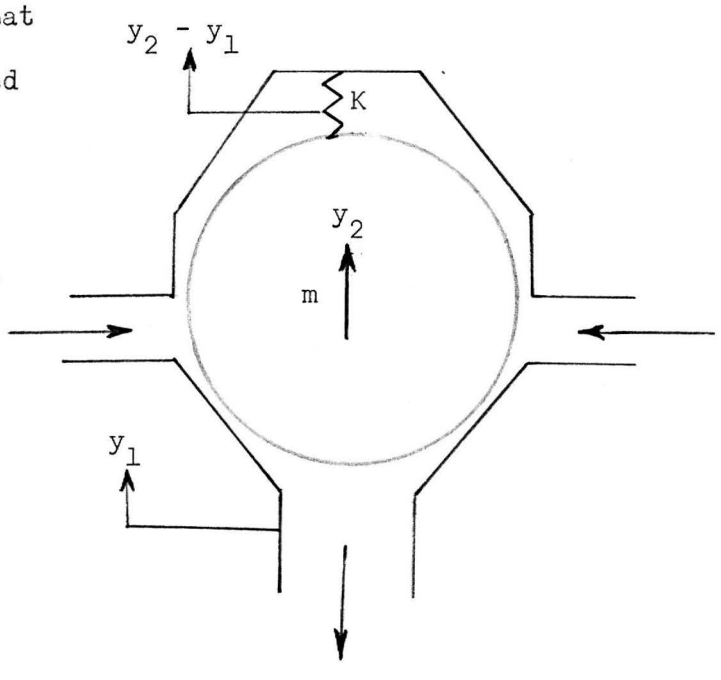

FIG.A1.1.

Hence the equation of motion will be:

$$m\ddot{y}_2 + K(y_2 - y_1) = 0 \qquad \text{(A1.1)}$$

where m represents mass of the ball, y_2 position of the ball from a fixed datum, K spring constant and y_1 position of the tip from a fixed datum.

Adding $-m\ddot{y}_1$ to the two sides:

$$m(\ddot{y}_2 - \ddot{y}_1) + k(y_2 - y_1) = -m\ddot{y}_1 \qquad \text{(A1.2)}$$

letting $y_2 - y_1 = y$ and dividing by m:

$$\ddot{y} + n^2 y = -\ddot{y}_1 \qquad \text{(A1.3)}$$

where n represents natural frequency of the ball-spring system.

The tip is assumed moving sinusoidally:

$$y_1 = y_x \sin(w_o t) \tag{A1.4}$$

where y_x maximum amplitude of the tip and w_o frequency of the tip.

$$\ddot{y}_1 = y_x w_o^2 \sin(w_o t) \tag{A1.5}$$

Eqn. (A1.3) becomes:

$$\ddot{y} + n^2 y = y_x w_o^2 \sin(w_o t) \tag{A1.6}$$

Taking Laplace transform:

$$S^2 Y - S y_i - \dot{y}_i + n^2 Y = y_x w_o^3 / S^2 + w_o^2 \tag{A1.7}$$

where y_i represents initial gap between the ball and the seat and $\dot{y}_i$ initial relative velocity between the ball and the tip, i.e.,

$$(S^2 + n^2) Y = S y_i + \dot{y}_i + y_x w_o^3 / S^2 + w_o^2 \tag{A1.8}$$

Assuming $y_i = o$ and $\dot{y}_i = o$:

$$Y = y_x w_o^3 / (S^2 + w_o^2)(S^2 + n^2) \tag{A1.9}$$

Transforming eqn. (A1.9) to t domain:

$$y = \frac{y_x w_o^3}{n^2 - w_o^2} \left[\frac{1}{w_o} \sin(w_o t) - \frac{1}{n} \sin(n t) \right] \tag{A1.10}$$

Hence the position of the ball from a fixed datum is:

$$y_2 = \frac{y_x w_o^3}{n^2 - w_o^2} \left[\frac{1}{w_o} \sin(w_o t) - \frac{1}{n} \sin(n t) \right] + y_x \sin(w_o t) \qquad \text{(A1.11)}$$

This equation is only valid before the first impact.

From (13), equation of motion due to sudden impulse is:

$$y_2 = \frac{\text{impulse}}{m\ n} \sin(nt) \qquad \text{(A1.12)}$$

Where

$$\text{impulse} = m(v_{o1} - v_{ib}) \qquad \text{(A1.13)}$$

where v_{o1} represents velocity of the ball after the collision and v_{ib} velocity of the ball before the collision.

Eqn. (3.6) is used to find v_{o1}:

$$v_{o1} = 2 v_f - v_{ib} \qquad \text{(A1.14)}$$

The velocity of the ball was found by taking the derivative of y_2 with respect to t:

$$v_b = \frac{y_x w_o^3}{n^2 - w_o^2} \left[\cos(w_o t) + \cos(nt) + y_x w_o \cos(w_o t) \right] \qquad \text{(A1.15)}$$

$v_{iv} = v_b$ at the instance of the impact.

Substituting eqn. (A1.13) in eqn. (A1.12), we have:

$$y_2 = \frac{v_{o1} - v_{ib}}{n} \sin(nt) \qquad \text{(A1.16)}$$

When one impulse of short duration follows another, it will initiate harmonic vibration produced by the first impulse. This independence stems from the fact that the equation of vibration for such a system is linear, and that the principle of superposition will apply (13).

Rewriting eqn. (A1.16) for the time t, the position of the ball due to the impulse in a sequence will be:

$$y_2 = \frac{v_{o1} - v_{ib}}{n} \sin(n(t - t_i)) \qquad \text{(A1.17)}$$

where t_i is the time at which the impulse was applied.

Hence the equation of the position of the ball at any instance will be:

$$y_2 = \frac{y_x w_o^3}{n^2 - w_o^2} \left[\frac{1}{w_o} \sin(w_o t) - \frac{1}{n} \sin(nt) + y_x \sin(w_o t) \right]$$

$$+ \frac{v_{o1} - v_{ib}}{n} \sin(n(t - t_i)) \qquad \text{(A1.18)}$$

Equation of the gap between the ball and the seat is:

$$y = y_2 - y_1 \quad ,$$

i.e.,

$$y = \frac{y_x w_o^3}{n^2 - w_o^2} \left[\frac{1}{w_o} \sin(w_o t) - \frac{1}{n} \sin(n t) \right] + \frac{v_{o1} - v_{ib}}{n}$$

$$\sin(n(t - t_i)) \qquad \text{(A1.19)}$$

Applying the dimensional analysis, eqn. (A1.19) will be:

$$\frac{y}{y_w} = \frac{\frac{y_x}{y_w}\left[\sin(w_o t) - \left(\frac{w_o}{n}\right)\sin\left(w_o t\left(\frac{n}{w_o}\right)\right)\right]}{\left(\frac{n}{w_o}\right)^2 - 1} + \left(\frac{v_{o1} - v_{ib}}{y_x \cdot w_o}\right)$$

$$\left(\frac{y_x}{y_w}\right) \cdot \left(\frac{w_o}{n}\right) \sin\left(\frac{(w_o t - w_o t_i)}{\left(\frac{w_o}{n}\right)}\right) \qquad \text{(A1.20)}$$

The computer program is shown in Appendix (A1.1).

APPENDIX A1.1

```
      LIBRARY(SUBGROUPNAGF)

      LIBRARY(SUBGROUPNAGG)
       LIBRARY(SUBGROUPGHOS)
      LIBRARY(SUBGROUPGHOS)

      PROGRAM(HUSSAIN)

      OUTPUT 3=LP0
      TRACE 2
      END
      MASTER MAIN
      EXTERNAL F3
       DIMENSION H(1000)

      COMMON D,A,H,I,V0,R
      DW=0.000
       WMAX=1000.
      D=0.1
      R=10.
      V0=0.000000001
      ETA=0.
      EPS=0.
      IFAIL=1
      W=0
      I=0
      N=1
      CALL PAPER(1)
      CALL MAP(0.,1000.,0.,5.)
      CALL CTRMAG(10)
      CALL AXESSI(0.00001,0.00001)
      CALL POINT(0.,0.)
      CALL PAPLEN(1000.)
      CALL BORDER
1     W=W+DW
      IF(W-WMAX)7,27,27
7     Y=(SIN(W)-D*SIN(R*W))/(R**2.-1)+V0*COS(R*W)
      IF(Y.EQ.0.)GO TO 3
       IF(I.EQ.0)GO TO 3
      DO 2 J=1,I
      Y=Y+D*A*SIN(W*R-R*H(J))
2     CONTINUE
3     IF(Y.EQ.0.)GO TO 6
      IF(N.GT.1)GO TO 9
      IF(Y.LT.0.)GO TO 4

9     A1=W-DW
       B1=W
       CALL COSACE(A1,B1,EPS,ETA,F3,X,IFAIL)
       IF(IFAIL.EQ.0)GO TO 35
      N=N+1

       IF(Y.LT.0.)CALL FERROR
4     GO TO 1
       A1=W-DW+0.000001
        B1=W
      IFAIL=1
```

```
5         CALL COSACF(A1,B1,EPS,ETA,F3,X,IFAIL)
        IF(IFAIL.EQ.1)X=B1
35      IFAIL=1
        W=X
        WRITE(3,15)X,A1,B1
15      FORMAT(/1X,'X=',E15.7,'A1=',E15.7,'B1=',E15.7/)

 6      W=W
          X5=W-X1
         X1=W
         CALL JOIN(W,X5)

        V1=(COS(W)-COS(R*W))/(R**2.-1.)-R*V0*SIN(R*W)+COS(W)
         IF(I.EQ.0)GO TO 10
         DO 11 J=1,I
        V1=V1+A*COS(R*W-R*H(J))
 11     CONTINUE

10      V2=2.*COS(W)


        A=V2-V1

        I=I+1
        H(I)=W
         N=1
        F0=0.
         GO TO 1
27       CALL GREND
          STOP
         END
         REAL FUNCTION F3(W)
         REAL W
        DIMENSION H(1000)

        COMMON D,A,H,I,V0,R


        Y=(SIN(W)-D*SIN(W*R))/(R**2.-1.)+V0*COS(R*W)
        IF(I.EQ.0)GO TO 22
        DO 21 J=1,I
21      Y=Y+D*A*SIN(W*R-R*H(J))
22      F3=Y
        RETURN
         END
         FINISH
****
```

```
      LIBRARY(SUBGROUPGHOS)
      LIBRARY(SUBGROUPGHOS)
      LIBRARY(SUBGROUPNAGF)
      LIBRARY(SUBGROUPNAGG)
       LIBRARY(SUBGROUPNAGH)

      PROGRAM(HUSS)
      INPUT 2=CR0
     OUTPUT 3=LP0
      TRACE 0
      END
     MASTER MAIN
      EXTERNAL F3,F4,F5,F6,F7,F8
      COMMON Z,D,S,Y3,A1,B1,W1,P ,WX1 ,A,B,WX2
      Z=0.0005
       S=4.0*ATAN(1.0)
      WMAX=6300.
      DW=0.4

       D=0.1
      J=0
      WG=0.
95    D=D+WG
      S1=0.
39    CALL PAPER(1)
      CALL MAP(0.,1000.,0.,30.)
        CALL GPINFO('INK PEN 7L-3 IN HOLDER 1,BLACK INK,PLEASE',42)
       CALL PSPACE(0.1,0.6,0.1,0.5)
       CALL CSPACE(0.,0.65,0.,0.55)
       CALL  CTRMAG(10)
     CALL AXESSI(0.00001,0.00001)
     CALL POINT(0.,0.)
      CALL PAPLEN(1000.0)
     CALL BORDER
202   TG=SIN(S)
      TGA=SIN(S+DW)
      WRITE(3,610)TG,TGA
610   FORMAT(/1X,'TG=',E15.7,'TGA=',E15.7/)
      I=0
     F0=0.
      W=0.

6
      W=W+DW

      WP=W
      Y1=-Z*D*W**2./2.
      Y2=D*SIN(S+  W)
      Y=Y1-Y2+P
     IF(Y.EQ.0)GO TO 5
     F1=Y
      B3=W
     IF(F1.GT.0.AND.F0.LT.0) GO TO 4
      IF(F1.LT.0.AND.F0.GT.0) GO TO 4
     F0=Y
     A3=W
4    GO TO 6
      ETA=0.
```

```
      EPS=0.
       IFAIL=0.
       CALL C05ACF(A3,B3,EPS,ETA,F3,X,IFAIL)

      WX1=X
       GO TO 100
5     Wx1=W
100    T=-Z*WX1
20     H=2.*COS(S+WX1)
       A=H-T
       AB=H/2.-T
14     B=SIN(S+  WX1)
       IF(AB.LT.0)AB=AB*(-1)
62     F0=0.
        WP=WX1
        Y=0.
        X5=WX1-S1

        WP=WP/(2*S)
        X5=X5/(2*S)

        IF(X5.LT.0.)CALL FERROR

       S1=WX1

        CALL JOIN(WP,X5)
      W=0.
       W=W+DW
      W2=W+WX1
       Y1=D*(-Z*W**2./2.+A*W+B)
      Y2=D*SIN(S+  W2)
       Y=Y1-Y2+P
       IF(Y.LT.0) GO TO 60
       W=0
10     W=W+DW
      W2=WX1+W
       Y1=D*(-Z*W**2./2.+A*W+B)
      Y2=D*SIN(S+  W2)
       Y=Y1-Y2+P
23     WP=WX1+W
       IF(W2-WMAX)51,37,37
51     IF(Y-1)9,27,27
9     WN2=A/7
        IF(WN2.LT.0.)WN2=-WN2
       WX2=WN2+WX1
       IF(W2-WX2)52,11,11
52     IF(Y.F0.0) GO TO 46
       F1=Y
       B6=W
      IF(F1.GT.0.AND.F0.LT.0) GO TO 45
      IF(F1.LT.0.AND.F0.GT.0) GO TO 45
       F0=Y
      A6=W
       GO TO 10
60     B6=W
       A6=W-DW+0.0000001
```

```
      Y1=D*(-Z*A6**2./2.+A*A6    +B)
     Y2=D*SIN(S+WX1+A6)
      Y=Y1-Y2
      WRITE(3,7) Y
7     FORMAT(/1X,'Y=',E15.7/)
45    CALL C05ACF(A6,B6,EPS,ETA,F6,X,IFAIL)
     WRITE(3,111) A6,B6,X
111   FORMAT(/1X,'A6=',E15.7,2X,'B6=',E15.7,3X,'X=',E15.7/)
      WN6=X
      GO TO 47
46    WN6=W
47    WX6=WN6+WX1
      Q6=-Z*WN6    +A
        H6=2.*COS( S+WX6)
      A6=H6-Q6
      AB=H6/2.-Q6
       IF(AB .LT.0)AB=AB*(-1)
     B6=SIN(S+WX6)
     A=A6
      B=B6
      WX1=WX6
      GO TO 62
11    W=0.
       F0=0.

      Y3=Y1
       W=W+DW
       W3=W+WX2
       IF(W3-WMAX)300,37,37
300    Y1=Y3-D*Z*W**2./2.
       Y2=D*SIN(S+W3)
       Y=Y1-Y2
       IF(Y.LT.0.)GO TO 301

       W=0.
12    W=W+DW
     W3=W+WX2
     IF(W3-WMAX)50,37,37
50    Y1=Y3-D*Z*W**2./2.
      Y2=D*SIN(S+W3)
      Y=Y1-Y2+P
3     IF(Y-1)3,27,27
      IF(Y.F0.0)GO TO 16
     F1=Y
     B4=W
      IF(F1.GT.0.AND.F0.LT.0) GO TO 13
      IF(F1.LT.0.AND.F0.GT.0) GO TO 13
      F0=Y
      A4=W
     WP=W+WX2
     GO TO 12
301     B4=W.
        A4=0.0000001

13    CALL C05ACF(A4,B4,EPS,ETA,F4,X,IFAIL)
       WRITE(3,206)X
```

```
206     FORMAT(/1X,'X2=',E15.7/)
        WN3=X
      GO TO 17
16      WN3=X
17      WX3=WX2+WN3
        IF(WX3-WMAX)88,37,37
88      WX1=WX3
        T=-Z*WN3
        GO TO 20

27       IF(Y.EQ.1.)GO TO 210
         B7=W
         A7=W-DW
           CALL C05ACF(A7,B7,EPS,ETA,F7,X,IFAIL)
         W=X
210      WN2=W

        Y=1.
        WP=WX1+WN2
        WX2=WN2+WX1
        Q=-Z*WN2+A
          H2=2.*COS(S+  WX2 )
108      A1=H2-Q
        AB=H2/2.-Q
105      B1=SIN(S+WX2)+(1./D)
        IF(AB.LT.0)AB=AB*(-1)
93      W=0.
          F0=0.
          W=W+DW
          W3=W+WX2
          IF(W3-WMAX)302,37,37
302       Y1=D*(-Z*W**2./2.+A1*W+B1)
          Y2=D*SIN(S+W3)
          Y=Y1-Y2
          IF(Y.LT.0.)GO TO 303

          W=0.
29      W=W+DW
        W3=W+WX2
        IF(W3-WMAX)53,37,37
53      Y1=D*(-Z*W**2./2.+A1*W+B1)
        Y2=D*SIN(S+W3)
        Y=Y1-Y2+P
        WP=W+WX2
        IF(Y-1) 80,81,81
81       IF(Y.EQ.1.)GO TO 211
         B8=W
         A8=W-DW+0.0000001
         CALL C05ACF(A8,B8,EPS,ETA,F8,X,IFAIL)
         W=X
211      WN2=W

        WX2=WX2+WN2
        Q=-Z*WN2+A1
          H2=2.*COS(S+WX2 )
        A1=H2-Q
        AB=H2/2.-Q
        B1=SIN(S+WX2)+(1./D)
```

```
      IF(AB.LT.0)AB=AB*(-1)
       Y=1.
      WP=WX2
      GO TO 93
80    IF(Y.EQ.0) GO TO 72
      F1=Y
     B5=W
      IF(F1.GT.0.AND.F0.LT.0) GO TO 73
      IF(F1.LT.0.AND.F0.GT.0) GO TO 73
      F0=Y
      A5=W

      GO TO 29
303    B5=W
       A5=0.0000001

73    CALL C05ACF(A5,B5,EPS,ETA,F5,X,IFAIL)
      WN3=X
      GO TO 74
72    WN3=W
74    WX3=WX2+WN3
      IF(WX3-WMAX)36,37,37
36    WX1=WX3
      T=-Z*WN3+A1
      GO TO 20
37    CALL FRAME

38    CALL GREND
      STOP
     END
      REAL FUNCTION F3(W)
       REAL W
      COMMON Z,D,S,Y3,A1,B1,W1,P ,WX1 ,A,B,WX2
      Y1=-D*Z*W**2./2.
      Y2=D*SIN(S+  W)
       F3=Y1-Y2+P
     RETURN
     END
      REAL FUNCTION F4(W)
      REAL W
      COMMON Z,D,S,Y3,A1,B1,W1,P ,WX1 ,A,B,WX2
     Y1=Y3-D*Z*W**2./2.
      Y2=D*SIN(S+W+WX2)
      F4=Y1-Y2+P
      RETURN
      END
      REAL FUNCTION F5(W)
      REAL W
      COMMON Z,D,S,Y3,A1,B1,W1,P ,WX1 ,A,B,WX2
      Y1=D*(-Z*W**2./2.+A1*W+B1)
      Y2=D*SIN(S+W+WX2)
     F5=Y1-Y2+P
      RETURN
     END
      REAL FUNCTION F6(W)
       REAL W
      COMMON Z,D,S,Y3,A1,B1,W1,P ,WX1 ,A,B,WX2
      Y1=D*(-Z*W**2./2.+A*W+B)
```

```
Y2=D*SIN(S+W+WX1)
 F6=Y1-Y2
 RETURN
  END
  REAL FUNCTION F7(W)
  REAL W
  COMMON Z,D,S,Y3,A1,B1,W1,P,WX1,A,B,WX2
Y1=D*(-Z*W**2./2.+A*W+B)
  Y2=D*SIN(S+W+WX1)
  F7=Y1-Y2-1.
  RETURN
  END
  REAL FUNCTION F8(W)
  REAL W
  COMMON Z,D,S,Y3,A1,B1,W1,P,WX1,A,B,WX2
  Y1=D*(-Z*W**2./2.+A1*W+B1)
  Y2=D*SIN(S+W+WX2)
  F8=Y1-Y2-1
  RETURN
  END


FINISH
```

APPENDIX 3

```
      LIBRARY(SUBGROUPGHOS)
      LIBRARY(SUBGROUPGHOS)
      LIBRARY(SUBGROUPNAGE)
      LIBRARY(SUBGROUPNAGG)
       LIBRARY(SUBGROUPNAGH)

      PROGRAM(HUSS)
      INPUT 2=CR0
     OUTPUT 3=LP0
      TRACE 0
      END
     MASTER MAIN
      EXTERNAL F3,F4,F5,F6,F7,F8
      COMMON Z,D,S,Y3,A1,B1,W1,P ,WX1 ,A,B,WX2
      Z=0.000005
       S=4.0*ATAN(1.0)
      WMAX=6300.
      DW=0.4

       VX=0.00000784
       W1=500000.
       D=0.01
      J=0
      WG=0.
95    D=D+WG
      S1=0.
39    CALL PAPER(1)
      CALL MAP(0.,0.01,0.,0.00001)
       CALL  CTRMAG(10)
        CALL GPINFO('INK PEN 7L-3 IN HOLDER 1,BLACK PEN,PLEASE',42)
        CALL PSPACE(0.1,0.6,0.1,0.5)
        CALL CSPACE(0.,0.65,0.,0.55)
     CALL POINT(0.,0.)
       CALL AXES
      CALL PAPLEN(1000.0)
     CALL BORDER
202   TG=SIN(S)
      TGA=SIN(S+DW)
      WRITE(3,610)TG,TGA
610   FORMAT(/1X,'TG=',E15.7,'TGA=',E15.7/)
      I=0
     F0=0.
      W=0.

6
      W=W+DW

      WP=W
      Y1=-Z*D*W**2./2.
      Y2=D*SIN(S+  W)
      Y=Y1-Y2+P
     IF(Y.EQ.0)GO TO 5
     F1=Y
      B3=W
     IF(F1.GT.0.AND.F0.LT.0) GO TO 4
      IF(F1.LT.0.AND.F0.GT.0) GO TO 4
     F0=Y
     A3=W
```

```
      GO TO 6
4      ETA=0.
      EPS=0.
       IFAIL=0.
       CALL C05ACF(A3,B3,EPS,ETA,F3,X,IFAIL)

      WX1=X
       GO TO 100
5     WX1=W
100   T=-Z*WX1
20    H=2.*COS(S+WX1)
      A=H-T
      AB=H/2.-T
14    B=SIN(S+  WX1)
      IF(AB.LT.0)AB=AB*(-1)
62    F0=0.
       WC=0.0000069*W1**0.8*YX**(-0.2)*AB**(-0.2)
       A=COS(S+WX1)+COS(S+WX1+WC)-T
       B=SIN(S+WX1+WC)
       WX1=WX1+WC
       TC=WC/W1

       WP=WX1
       Y=0.
       X5=WX1-S1

       WP=WP/(W1)
       X5=X5/(W1)

       IF(X5.LT.0.)CALL FERROR

      S1=WX1

         X5=TC/X5
       CALL JOIN(WP,TC)
      W=0.
       W=W+DW
      W2=W+WX1
       Y1=D*(-Z*W**2./2.+A*W+B)
      Y2=D*SIN(S+  W2)
       Y=Y1-Y2+P
       IF(Y.LT.0) GO TO 60
       W=0
10     W=W+DW
      W2=WX1+W
       Y1=D*(-Z*W**2./2.+A*W+B)
      Y2=D*SIN(S+  W2)
23     Y=Y1-Y2+P
       WP=WX1+W
51     IF(W2-WMAX)51,37,37
9      IF(Y-1)9,27,27
      WN2=A/Z
       IF(WN2.LT.0.)WN2=-WN2
      WX2=WN2+WX1
52     IF(W2-WX2)52,11,11
       IF(Y.F0.0) GO TO 46
       F1=Y
       B6=W
```

```
      IF(F1.GT.0.AND.F0.LT.0) GO TO 45
      IF(F1.LT.0.AND.F0.GT.0) GO TO 45
       F0=Y
      A6=W
       GO TO 10
60     B6=W
       A6=W-DW+0.0000001
       Y1=D*(-Z*A6**2./2.+A*A6    +B)
      Y2=D*SIN(S+WX1+A6)
       Y=Y1-Y2
       WRITE(3,7) Y
7      FORMAT(/1X,'Y=',E15.7/)
45     CALL C05ACE(A6,B6,EPS,ETA,F6,X,IFAIL)
      WRITE(3,111) A6,B6,X
111    FORMAT(/1X,'A6=',F15.7,2X,'B6=',E15.7,3X,'X=',F15.7/)
       WN6=X
       GO TO 47
46     WN6=W
47     WX6=WN6+WX1
       Q6=-Z*WN6    +A
         H6=2.*COS( S+WX6)
       A6=H6-Q6
       AB=B6/2.-Q6
        IF(AB .LT.0)AB=AB*(-1)
      B6=SIN(S+WX6)
      A=A6
       B=B6
       WX1=WX6
        T=Q6
       GO TO 62
11     W=0.
        F0=0.

       Y3=Y1
        W=W+DW
        W3=W+WX2
        IF(W3-WMAX)300,37,37
300    V1=Y3-D*Z*W**2./2.
        Y2=D*SIN(S+W3)
        Y=Y1-Y2
        IF(Y.LT.0.)GO TO 301

        W=0.
12     W=W+DW
      W3=W+WX2
      IF(W3-WMAX)50,37,37
50    V1=Y3-D*Z*W**2./2.
       Y2=D*SIN(S+W3)
       Y=Y1-Y2*P
3      IF(Y-1)3,27,27
       IF(Y.F0.0)GO TO 16
      F1=Y
      B4=W
       IF(F1.GT.0.AND.F0.LT.0) GO TO 13
       IF(F1.LT.0.AND.F0.GT.0) GO TO 13
       F0=Y
       A4=W
      WP=W+WX2
```

```
      GO TO 12
301     B4=W
        A4=0.0000001

13      CALL C05ACF(A4,B4,EPS,ETA,F4,X,IFAIL)
        WRITE(3,206)X
206     FORMAT(/1X,'X2=',E15.7/)
        WN3=X
      GO TO 17
16      WN3=X
17      WX3=WX2+WN3
        IF(WX3-WMAX)88,37,37
88      WX1=WX3
        T=-7*WN3
        GO TO 20

27       IF(Y.EQ.1.)GO TO 210
         B7=W
         A7=W-DW
           CALL C05ACF(A7,B7,EPS,ETA,F7,X,IFAIL)
         W=X
210      WN2=W

        Y=1.
        WP=WX1+WN2
        WX2=WN2+WX1
        Q=-2*WN2+A
          H2=2.*COS(S+  WX2 )
108     A1=H2-Q
        AB=H2/2.-Q
105      B1=SIN(S+WX2)+(1./D)
        IF(AB.LT.0)AB=AB*(-1)
93      W=0.
          WC=0.0000069*W1**0.8+YX**(-0.2)*AB**(-0.2)
         A1=COS(S+WX2)+COS(S+WX2+WC)-Q
         B1=SIN(S+WX2+WC)+(1./D)
         WX2=WX2+WC
         TC=WC/W1

         F0=0.
         W=W+DW
         W3=W+WX2
         IF(W3-WMAX)302,37,37
302      Y1=D*(-Z*W**2./2.+A1*W+B1)
         Y2=D*SIN(S+W3)
         Y=Y1-Y2
         IF(Y.LT.0.)GO TO 303

         W=0.
29      W=W+DW
        W3=W+WX2
        IF(W3-WMAX)53,37,37
53      Y1=D*(-7*W**2./2.+A1*W+B1)
        Y2=D*SIN(S+W3)
        Y=Y1-Y2+P
        WP=W+WX2
        IF(Y-1) 80,81,81
81       IF(Y.EQ.1.)GO TO 211
```

```
      B8=W
      A8=W-DW+0.0000001
      CALL C05ACF(A8,B8,EPS,ETA,F8,X,IFAIL)
      W=X
211   WN2=W

     WX2=WX2+WN2
     D=-Z*WN2+A1
       H2=2.*COS(S+WX2 )
     A1=H2-D
     AB=H2/2.-D
     B1=SIN(S+WX2)+(1./D)
     IF(AB.LT.0)AB=AB*(-1)
      Y=1.
     WP=WX2
     GO TO 93
80   IF(Y.EQ.0.) GO TO 72
     F1=Y
    B5=W
     IF(F1.GT.0.AND.F0.LT.0) GO TO 73
     IF(F1.LT.0.AND.F0.GT.0). GO TO 73
     F0=Y
     A5=W

     GO TO 29
303   B5=W
      A5=0.0000001

73   CALL C05ACF(A5,B5,EPS,ETA,F5,X,IFAIL)
     WN3=X
     GO TO 74
72   WN3=W
74   WX3=WX2+WN3
     IF(WX3-WMAX)36,37,37
36   WX1=WX3
     T=-Z*WN3+A1
     GO TO 20
37   CALL FRAME

38   CALL GREND
     STOP
    END
     REAL FUNCTION F3(W)
      REAL W
     COMMON Z,D,S,Y3,A1,B1,W1,P ,WX1 ,A,B,WX2
     Y1=-D*Z*W**2./2.
     Y2=D*SIN(S+  W)
      F3=Y1-Y2+P
    RETURN
    END
     REAL FUNCTION F4(W)
     REAL W
     COMMON Z,D,S,Y3,A1,B1,W1,P ,WX1 ,A,B,WX2
    Y1=Y3-D*Z*W**2./2.
     Y2=D*SIN(S+W+WX2)
     F4=Y1-Y2+P
     RETURN
     END
```

```
      REAL FUNCTION F5(W)
      REAL W
      COMMON Z,D,S,Y3,A1,B1,W1,P ,WX1 ,A,B,WX2
      Y1=D*(-Z*W**2./2.+A1*W+B1)
      Y2=D*SIN(S*W+WX2)
    F5=Y1-Y2+P
      RETURN
    END
      REAL FUNCTION F6(W)
       REAL W
      COMMON Z,D,S,Y3,A1,B1,W1,P ,WX1 ,A,B,WX2
      Y1=D*(-Z*W**2./2.+A*W+B)
    Y2=D*SIN(S+W+WX1)
      F6=Y1-Y2
      RETURN
       END
       REAL FUNCTION F7(W)
       REAL W
       COMMON Z,D,S,Y3,A1,B1,W1,P,WX1,A,B,WX2
    Y1=D*(-Z*W**2./2.+A*W+B)
       Y2=D*SIN(S+W+WX1)
       F7=Y1-Y2-1.
       RETURN
       END
       REAL FUNCTION F8(W)
       REAL W
       COMMON Z,D,S,Y3,A1,B1,W1,P,WX1,A,B,WX2
       Y1=D*(-Z*W**2./2.+A1*W+B1)
       Y2=D*SIN(S+W+WX2)
       F8=Y1-Y2-1
       RETURN
       END
```

APPENDIX 4

```
      LIBRARY(SUBGROUPGHOS)
      LIBRARY(SUBGROUPGHOS)
      LIBRARY(SUBGROUPNAGE)
      LIBRARY(SUBGROUPNAGG)
       LIBRARY(SUBGROUPNAGH)
      PROGRAM(HUSS)
      INPUT 2=CRO
     OUTPUT 3=LPO
      TRACE 1
      END
     MASTER MAIN
      EXTERNAL F3,F4,F5,F6,F7,F8,F9,F10,F11,F12
      COMMON Z,D,S,Y3,A1,B1,W1,P ,WX1 ,A,B,WX2,WM,GM,S1,W7,WX
      Z=0.0005
       S3=4.0*ATAN(1.0)
       S=S3
       IFAIL=0
      WMAX=6300.
      DW=0.4
       D=0.1

       WM=1.
         S1=S3/2.
      GM=0.0022

      J=0
      WG=0.
95    D=D+WG
39    CALL PAPER(1)
      CALL MAP(0.,1000.,0.,30.)
        CALL PSPACE(0.1,0.6,0.1,0.5)
       CALL CSPACE(0.,0.65,0.,0.55)
       CALL  CTRMAG(10)
       CALL AXES
       CALL GPINFO('INK PEN 7L-3 IN HOLDER 1,BLACK INK,PLEASE',42)
     CALL POINT(0.,0.)
      CALL PAPLEN(1000.0)
     CALL BORDER
202   TG=SIN(S)
      W7=DW
       TGA=D*WM*COS(W7/WM+S+S1)/EXP(W7*GM)+D*COS(W7+S-S1)

      WRITE(3,610)TG,TGA
610   FORMAT(/1X,'TG=',E15.7,'TGA=',E15.7/)
       W7=0.
501    WP=W7/(2.*S3)
       X5=0.
       CALL JOIN(WP,X5)
       W7=W7+0.017
       YD=D*WM*COS(W7/WM+S+S1)/EXP(W7*GM)+D*COS(W7+S-S1)
       YA=GM**2.*WM*COS(W7/WM+S+S1)/EXP(W7*GM)
     1 +2.*GM*SIN(W7/WM+S+S1)/EXP(W7*GM)
     1 -COS(W7/WM+S+S1)/(WM*EXP(W7*GM))-COS(W7+S-S1)
       WRITE(3,500)YD,YA
500    FORMAT(/1X,'YD=',E15.7,4X,'YA=',E15.7/)
       IF(YA.LT.0.AND.YD.GT.0.)GO TO 502
       IF(YA.GT.0.AND.YD.LT.0.)GO TO 505
```

```
          GO TO 501
502       IF(YA.LT.(-7))GO TO 503
          GO TO 501
503       IFAIL=0
          B9=W7
          A9=W7-0.017
          EPS=0.
          ETA=0.
          CALL C05ACF(A9,B9,EPS,ETA,F9,X,IFAIL)
          WRITE(3,504)A9,B9,X
504       FORMAT(/1X,'A9=',E15.7,3X,'B9=',E15.7,3X,'X=',E15.7/)
1000      WX1=X
          S11=X
          W7=X
           A=-GM*WM*COS(W7/WM+S+S1)/EXP(W7*GM)-SIN(W7/WM+S+S1)/
     1    EXP(W7*GM)-SIN(W7+S-S1)

          B=WM*COS(W7/WM+S+S1)/EXP(W7*GM)+COS(W7+S-S1)
          GO TO 62
505       IF(YA.GT.7)GO TO 506
          GO TO 501
506         IFAIL=0
          B10=W7
          A10=W7-0.017
          EPS=0.
          ETA=0.
             CALL C05ACF(A10,B10,EPS,ETA,F10,X,IFAIL)
           WRITE(3,507)A10,B10,X
507       FORMAT(/1X,'A10=',E15.7,3X,'B10=',E15.7,3X,'X=',E15.7/)
           GO TO 1000

          W7=X
          B=WM*COS(W7/WM+S+S1)/EXP(W7*GM)+COS(W+S-S1)
          WX=X
          W=0.
           GO TO 6

         I=0
        F0=0.
         W=0.

          WX1=0.
           A=1.
          B=0.
6         GO TO 62
         W=W+DW

         WP=W
         Y1=-Z*D*W**2./2.+B*D
          W7=W+WX

          Y2=D*WM*COS(W7/WM+S+S1)/EXP(W7*GM)+D*COS(W7+S-S1)

         Y=Y1-Y2+P
        IF(Y.EQ.0)GO TO 5
        F1=Y
         B3=W
        IF(F1.GT.0.AND.F0.LT.0) GO TO 4
```

```
      IF(F1.LT.0.AND.F0.GT.0) GO TO 4
      F0=Y
      A3=W
      GO TO 6
4     ETA=0.
      EPS=0.
      IFAIL=0.
      CALL C05ACF(A3,B3,EPS,ETA,F3,X,IFAIL)

      WX1=X+WX
      GO TO 100
5      W=WX+W
100   T=-Z*WX1
20      W7=WX1

       H=2.*(-GM*WM*COS(W7/WM+S+S1)/EXP(W7*GM)-SIN(W7/WM+S+S1)/
     1  EXP(W7*GM)-SIN(W7+S-S1))









      A=H-T
      AB=H/2.-T
14    B=WM*COS(W7/WM+S+S1)/EXP(W7*GM)+COS(W7+S-S1)

      IF(AB.LT.0)AB=AB*(-1)
62    F0=0.
       WP=WX1
       Y=0.
       X5=WX1-S11

       WP=WP/(2*S3)
       X5=X5/(2*S3)

       IF(X5.LT.0.)CALL FERROR

      S11=WX1



       CALL JOIN(WP,X5)
      W=0.
        WRITE(3,508)WP,X5
508    FORMAT(/1X,'UP=',E15.7,5X,'X5=',E15.7/)
       W=U+DW
      W2=U+WX1
       Y1=D*(-Z*W**2./2.+A*W+B)
        W7=W2
         Y2=D*WM*COS(W7/WM+S+S1)/EXP(W7*GM)+D*COS(W7+S-S1)

      Y=Y1-Y2+P
      IF(Y.LT.0) GO TO 60
```

```
      W=0
10    W=W+DW
      W2=WX1+W
      Y1=D*(-Z*W**2./2.+A*W+B)
       W7=W2


         Y2=D*WM*COS(W7/WM+S+S1)/EXP(W7*GM)+D*COS(W7+S-S1)

      Y=Y1-Y2+P
23    WP=WX1+W

      IF(W2-WMAX)51,37,37
51    IF(Y-1)9,27,27
9     WN2=A/7
       IF(WN2.LT.0.)WN2=-WN2
      WX2=WN2+WX1
      IF(W2-WX2)52,11,11
52    IF(Y.EQ.0) GO TO 46
      F1=Y
      B6=W
     IF(F1.GT.0.AND.F0.LT.0) GO TO 45
     IF(F1.LT.0.AND.F0.GT.0) GO TO 45
      F0=Y
     A6=W
      GO TO 10
60    B6=W
       A6=W-DW+0.000001
      Y1=D*(-Z*A6**2./2.+A*A6    +B)
        W7=WX1+A6
       Y2=D*WM*COS(W7/WM+S+S1)/EXP(W7*GM)+D*COS(W7+S-S1)

      Y=Y1-Y2
      WRITE(3,7) Y
7     FORMAT(/1X,'Y=',E15.7/)
       IFAIL=1
45    CALL CONACE(A6,B6,EPS,ETA,F6,X,IFAIL)
     WRITE(3,111) A6,B6,X
111   FORMAT(/1X,'A6=',E15.7,2X,'B6=',E15.7,3X,'X=',E15.7/)
       IF(IFAIL.EQ.1)GO TO 510
      WN6=X
      GO TO 47
46    WN6=W
510    W7=WX1
511    WP=W7/(2.*S3)
        X5=0.
       CALL JOIN(WP,X5)
        W7=W7+HK
        YD=D*WM*COS(W7/WM+S+S1)/EXP(W7*GM)+D*COS(W7+S-S1)
        YA=GM**2.*WM*COS(W7/WM+S+S1)/EXP(W7*GM)
     1  +2.*GM*SIN(W7/WM+S+S1)/EXP(W7*GM)
     1-COS(W7/WM+S+S1)/(WM*EXP(W7*GM))-COS(W7+S-S1)

       YV=-GM*WM*COS(W7/WM+S+S1)/EXP(W7*GM)-SIN(W7/WM+S+S1)/
     1   EXP(W7*GM)-SIN(W7+S-S1)
       IF(YD.GT.0.AND.YV.GT.0.)GO TO 512
       IF(YD.LT.0.AND.YV.LT.0.)GO TO 513
```

```
      GO TO 511
512   IF(YA.LT.(-7))GO TO 514
      HK=0.017
      GO TO 511
    IFAIL=0
      B11=W7
      A11=W7-0.017
      CALL COSACF(A11,B11,EPS,ETA,F11,X,IFAIL)
      WRITE(3,515)A11,B11,X
515   FORMAT(/1X,'A11=',E15.7,3X,'B11=',E15.7,3X,'X=',E15.7/)
514   WX1=W7
      S11=W7
      A=-GM*WM*COS(W7/WM+S+S1)/EXP(W7*GM)-SIN(W7/WM+S+S1)/
     1  EXP(W7*GM)-SIN(W7+S-S1)
      B=WM*COS(W7/WM+S+S1)/EXP(W7*GM)+COS(W7+S-S1)
      GO TO 62
513   IF(YA.GT.7)GO TO 516
      HK=0.017

       GO TO 511
      IFAIL=0
       B12=W7
        A12=W7-0.017
       ETA=0.
       CALL COSACF(A12,B12,EPS,ETA,F12,X,IFAIL)
        WRITE(3,517)A12,B12,X
517   FORMAT(/1X,'A12=',E15.7,3X,'B12=',E15.7,3X,'X=',E15.7/)
516    W=0.
       B=WM*COS(W7/WM+S+S1)/EXP(W7*GM)+COS(W7+S-S1)
        WX=W7
       IFAIL=0
      F0=0
        GO TO 6

       IFAIL=0
47    WX6=WN6+WX1
      Q6=-7*WN6    +A
       W7=WX6

       H6=2.*(-GM*WM*COS(W7/WM+S+S1)/EXP(W7*GM)-SIN(W7/WM+S+S1)/
     1 EXP(W7*GM)-SIN(W7+S-S1))


      A6=H6-Q6
      AB=H6/2.-Q6
       IF(AB .LT.0)AB=AB*(-1)
        W7=WX6
       B6=WM*COS(W7/WM+S+S1)/EXP(W7*GM)+COS(W7+S-S1)

     A=A6
      B=B6
      WX1=WX6
      GO TO 62
11    W=0.
       F0=0.

      Y3=Y1
       W=W+DW
```

```
      W3=W+WX2
      IF(W3-WMAX)300,37,37
300   Y1=Y3-D*Z*W**2./2.
       W7=W3
       Y2=D*WM*COS(W7/WM+S+S1)/EXP(W7*GM)+D*COS(W7+S-S1)

      Y=Y1-Y2
      IF(Y.LT.0.)GO TO 301

      W=0.
12     W=W+DW
      W3=W+WX2
      IF(W3-WMAX)50,37,37
50    Y1=Y3-D*Z*W**2./2.
       W7=W3
       Y2=D*WM*COS(W7/WM+S+S1)/EXP(W7*GM)+D*COS(W7+S-S1)


      Y=Y1-Y2+P
      IF(Y-1)3,27,27
3     IF(Y.EQ.0)GO TO 16
     F1=Y
     B4=W
      IF(F1.GT.0.AND.F0.LT.0) GO TO 13
      IF(F1.LT.0.AND.F0.GT.0) GO TO 13
      F0=Y
      A4=W
     WP=W+WX2
     GO TO 12
301    B4=W
       A4=0.0000001

13    CALL COSACF(A4,B4,EPS,ETA,F4,X,IFAIL)
       WRITE(3,206)X
206   FORMAT(/1X,'X2=',E15.7/)
      WN3=X
     GO TO 17
16    WN3=X
17    WX3=WX2+WN3
      IF(WX3-WMAX)88,37,37
88    WX1=WX3
      T=-Z*WN3
      GO TO 20

27     IF(Y.EQ.1.)GO TO 210
       B7=W
       A7=W-DW
         CALL COSACF(A7,B7,EPS,ETA,F7,X,IFAIL)
       W=X
210    WN2=W

      Y=1.
      WP=WX1+WN2
     WX2=WN2+WX1
      Q=-Z*WN2+A
       W7=WX2
       B2=2.*(-GM*WM*COS(W7/WM+S+S1)/EXP(W7*GM)-SIN(W7/WM+S+S1)/
    1EXP(W7*GM)-SIN(W7+S-S1))
```

```
108     A1=H2-Q
        AB=H2/2.-Q
150     B1=WM*COS(W7/WM+S+S1)/EXP(W7*GM)+COS(W7+S-S1)+(1./D)

        IF(AB.LT.0)AB=AB*(-1)
93      W=0.
        F0=0.
        W=W+DW
        W3=W+WX2
        IF(W3-WMAX)302,37,37
302     Y1=D*(-Z*W**2./2.+A1*W+B1)
        W7=W3

        Y2=D*WM*COS(W7/WM+S+S1)/EXP(W7*GM)+D*COS(W7+S-S1)

        Y=Y1-Y2
        IF(Y.LT.0.)GO TO 303

        W=0.
29      W=W+DW
        W3=W+WX2
        IF(W3-WMAX)53,37,37
53      Y1=D*(-Z*W**2./2.+A1*W+B1)
        W7=W3
        Y2=D*WM*COS(W7/WM+S+S1)/EXP(W7*GM)+D*COS(W7+S-S1)

        Y=Y1-Y2+P
        WP=W+WX2
        IF(Y-1) 80,81,81
81      IF(Y.EQ.1.)GO TO 211
        B8=W
        A8=W-DW+0.0000001
        CALL COSACF(A8,B8,EPS,ETA,F8,X,IFAIL)
        W=X
211     WN2=W

        WX2=WX2+WN2
        Q=-Z*WN2+A1
        W7=WX2
        H2=2.*(-GM*WM*COS(W7/WM+S+S1)/EXP(W7*GM)-SIN(W7/WM+S+S1)/
     1  EXP(W7*GM)-SIN(W7+S-S1))


        A1=H2-Q
        AB=H2/2.-Q
        B1=WM*COS(W7/WM+S+S1)/EXP(W7*GM)+COS(W7+S-S1)+(1./D)
        IF(AB.LT.0)AB=AB*(-1)
        Y=1.
        WP=WX2
        GO TO 93
80      IF(Y.EQ.0) GO TO 72
        F1=Y
        B5=W
        IF(F1.GT.0.AND.F0.LT.0) GO TO 73
        IF(F1.LT.0.AND.F0.GT.0) GO TO 73
```

```
      F0=Y
      A5=W

      GO TO 29
303    B5=W
       A5=0.0000001

73    CALL COSACF(A5,B5,EPS,ETA,F5,X,IFAIL)
      WN3=X
      GO TO 74
72    WN3=W
74    WX3=WX2+WN3
      IF(WX3-WMAX)36,37,37
36    WX1=WX3
      T=-Z*WN3+A1
      GO TO 20
37    CALL FRAME

38    CALL GREND
      STOP
      END
      REAL FUNCTION F3(W)
       REAL W
      COMMON Z,D,S,Y3,A1,B1,W1,P ,WX1 ,A,B,WX2,WM,GM,S1,W7,WX
      Y1=-D*Z*W**2./2.+B*D
       Y2=D*WM*COS((W+WX)/WM+S+S1)/EXP((W+WX)*GM)+D*COS((W+WX)+S-S1)

       F3=Y1-Y2+P
      RETURN
      END
       REAL FUNCTION F4(W)
       REAL W
       COMMON Z,D,S,Y3,A1,B1,W1,P ,WX1 ,A,B,WX2,WM,GM,S1,W7,WX
      Y1=Y3-D*Z*W**2./2.
       Y2=D*WM*COS((W+WX2)/WM+S+S1)/EXP((W+WX2)*GM)+D*COS((W+WX2)+S-S1)

       F4=Y1-Y2+P
       RETURN
       END
       REAL FUNCTION F5(W)
       REAL W
       COMMON Z,D,S,Y3,A1,B1,W1,P ,WX1 ,A,B,WX2,WM,GM,S1,W7,WX
       Y1=D*(-Z*W**2./2.+A1*W+B1)
       Y2=D*WM*COS((W+WX2)/WM+S+S1)/EXP((W+WX2)*GM)+D*COS((W+WX2)+S-S1)

      F5=Y1-Y2+P
       RETURN
      END
       REAL FUNCTION F6(W)
       REAL W
       COMMON Z,D,S,Y3,A1,B1,W1,P ,WX1 ,A,B,WX2,WM,GM,S1,W7,WX
       Y1=D*(-Z*W**2./2.+A*W+B)
       Y2=D*WM*COS((W+WX1)/WM+S+S1)/EXP((W+WX1)*GM)+D*COS((W+WX1)+S-S1)

       F6=Y1-Y2
       RETURN
       END
       REAL FUNCTION F7(W)
```

```
      REAL W
      COMMON Z,D,S,Y3,A1,B1,W1,P,WX1,A,B,WX2,WM,GM,S1,W7
     Y1=D*(-Z*W**2./2.+A*W+B)
      Y2=D*WM*COS((W+WX1)/WM+S+S1)/EXP((W+WX1)*GM)+D*COS((W+WX1)+S-S1)

      F7=Y1-Y2-1.
      RETURN
      END
      REAL FUNCTION F8(W)
      REAL W
      COMMON Z,D,S,Y3,A1,B1,W1,P,WX1,A,B,WX2,WM,GM,S1,W7
      Y1=D*(-Z*W**2./2.+A1*W+B1)

      Y2=D*WM*COS((W+WX2)/WM+S+S1)/EXP((W+WX2)*GM)+D*COS((W+WX2)+S-S1)

      F8=Y1-Y2-1
      RETURN
      END
      REAL FUNCTION F9(W)


       REAL W
       COMMON Z,D,S,Y3,A1,B1,W1,P,WX1,A,B,WX2,WM,GM,S1,W7
      F9=GM**2.*WM*COS(W/WM+S+S1)/EXP(W*GM)
1     +2.*GM*SIN(W/WM+S+S1)/EXP(W*GM)
1      -COS(W/WM+S+S1)/(WM*EXP(W*GM))
1     -COS(W+S-S1)
1      +Z
       RETURN
       END
       REAL FUNCTION F10(W)
       REAL W
       COMMON Z,D,S,Y3,A1,B1,W1,P,WX1,A,B,WX2,WM,GM,S1,W7
       F10=GM**2.*WM*COS(W/WM+S+S1)/EXP(W*GM)
1      +2.*GM*SIN(W/WM+S+S1)/EXP(W*GM)
1      -COS(W/WM+S+S1)/(WM*EXP(W*GM))
1       -COS(W+S-S1)-Z

        RETURN
         END
      REAL FUNCTION F11(W)

          REAL W
        COMMON Z,D,S,Y3,A1,B1,W1,P,WX1,A,B,WX2,WM,GM,S1,W7
        F11=GM**2.*WM*COS(W/WM+S+S1)/EXP(W*GM)
1      +2.*GM*SIN(W/WM+S+S1)/EXP(W*GM)

1-COS(W/WM+S+S1)/(WM*EXP(W*GM))
1     -COS(W+S-S1)+Z
      RETURN
      END
      REAL FUNCTION F12(W)
       REAL W
       COMMON Z,D,S,Y3,A1,B1,W1,P,WX1,A,B,WX2,WM,GM,S1,W7
        F12=GM**2.*WM*COS(W/WM+S+S1)/EXP(W*GM)
1     +2.*GM*SIN(W/WM+S+S1)/EXP(W*GM)
```

```
1   -COS(W/WM+S+S1)/(WM*EXP(W*GM))

1      -COS(W*S-S1)-Z
       RETURN
        END


 FINISH
```

APPENDIX 5

```
      LIBRARY (SUBGROUPNAGF)
      LIBRARY(SUBGROUPNAGG)
       LIBRARY(SUBGROUPNAGH)
      LIBRARY(SUBGROUPGHOS)
      LIBRARY(SUBGROUPGHOS)
      PROGRAM(RUSS)
      OUTPUT 3=LPO
      TRACE 2
      END
      MASTER MAIN
      DIMENSION WORK1(3,9),WORK2(2,9),A(9,9),S(9),X(10),Y(10)
     1   ,W(10),A1(10)

      M=9
      KPLUS1=9
      NROWS=9
      NPLUS1=9

      DO 1 I=1,M

      W(I)=1.
      X(1)=0.0
      X(2)=0.792
      X(3)=2.83
      Y(4)=4.416
      X(5)=5.47
      X(6)=6.53
      X(7)=7.58
      X(8)=8.64
      X(9)=0.47*20.637
      Y(1)=0.0994
      Y(2)=0.147
      Y(3)=0.114
      Y(4)=0.074
      Y(5)=0.04
      Y(6)=0.026
      Y(7)=0.0276
      Y(8)=0.0395
      Y(9)=0.051
      XMAX=X(9)/20.637
       XMIN=X(1)/20.637

      DO 9 I=1,M

        X(I)=X(I)/20.637
      IFAIL=0
      CALL E02ADF(M,KPLUS1,NROWS,X,Y,W,WORK1,WORK2,A,S,IFAIL)

      DO 2 IPLUS1=1,KPLUS1
       I=IPLUS1-1
       WRITE(3,4)I
       WRITE(3,5)(JPLUS1,A(IPLUS1,JPLUS1),JPLUS1=1,IPLUS1)
       WRITE(3,6)S(IPLUS1)
       CONTINUE
       FORMAT(//7H DEGREE, I4//8H I COEFF/)
       FORMAT(1X,I3,E20.5)
       FORMAT(//18H R.M.S  RESIDUAL =,E20.5)
```

```
DO 7 IPLUS1=1,KPLUS1
  DO 10 JPLUS1=1,IPLUS1
 A1(JPLUS1)=A(IPLUS1,JPLUS1)
NPLUS1=JPLUS1
 DO 8 I=1,M
 XCAP=(2.*X(I)-XMAX-XMIN)/(XMAX-XMIN)
 CALL E02AEF(NPLUS1,A1,XCAP,P,IFAIL)
 Y(I)=P
   WRITE(3,11)(Y(I),I=1,M)

    FORMAT(/1X,'Y=',E15.7/)

CALL PAPER(1)
CALL MAP(0.0,0.47,-0.015,0.146)
 CALL GPINFO('INK PEN 7L-3 IN HOLDER 1,BLACK PEN,PLEASE',42)
CALL PSPACE(0.1,0.6,0.1,0.5)
CALL CSPACE(0.,0.65,0.,0.55)
CALL AXES

 CALL CURVEO(X,Y,1,M)
 CALL FRAME
 CONTINUE



 CALL GREND

STOP
END
 FINISH
**
```

APPENDIX 6

```
      LIBRARY(SUBGROUPGHOS)
      LIBRARY(SUBGROUPGHOS)
        LIBRARY(SUBGROUPNAGF)
      LIBRARY(SUBGROUPNAGG)
      LIBRARY(SUBGROUPNAGH)
      PROGRAM(HUSS)
      OUTPUT 3=LPO
      TRACE 0
      END
      MASTER MAIN
      DIMENSION WORK1(3,9),WORK2(2,9),A(9,9),X(10),Y(10)
     1  ,Y1(5),G(5),YO(5),E(5),A1(5),B1(5),C1(5),D1(5),SS(10),
     1 W(10),AY(8000),BY(8000),TY(8000),WXY(8000),AYY(8000)
     1 ,GG(5),GGG(5)




      COMMON N,TM,YW,RM,A,XMAX,XMIN,D,WM,FREQ,S,S1,GM,XX,G1,BFI
         EXTERNAL F9,F10,DERIVE

      CALL PAPER(1)
      CALL MAP(0.,0.006,0.,40.)
      CALL GPINFO('INK PEN 7L-3 IN HOLDER 1,BLACK PEN,PLEASE',42)
      CALL PSPACE(0.1,0.625,0.1,0.5)
      CALL CSPACE(0.,0.625,0.,0.5)
       CALL BORDER
      CALL MAP(0.,0.006,-20.,20.)
       CALL POINT(0.,0.)
      M=9
      KPLUS1=9
      NROWS=9
      NPLUS1=9

      WMAX=2262.
      DO 1 I=1,M

      W(I)=1.
      X(1)=0.0
      X(2)=0.792
      X(3)=2.83
      X(4)=4.416
      X(5)=5.47
      X(6)=6.53
      X(7)=7.58
      X(8)=8.64
       X(9)=0.47*20.637
      Y(1)=0.0994
      Y(2)=0.147
      Y(3)=0.114
      Y(4)=0.074
      Y(5)=0.04
      Y(6)=0.026
      Y(7)=0.0276
```

```
      Y(8)=0.0395
      Y(9)=0.052
      XMAX=0.47
      XMIN=Y(1)/20.637

      DO 9 I=1,M

        X(I)=X(I)/20.637
      IFAIL=0


       CALL E02ADF(M,KPLUS1,NROWS,X,Y,W,WORK1,WORK2,A,SS,IFAIL)
      N=5
      TM=0.0000365
      PM=0.91
      YW=0.47

      FREQ=376991.11
       S3=4.0*ATAN(1.0)
      S=0.
      IFAIL=0
      DW=0.4
      D=0.00423/YW
      G1=0.0219708
      WM=1.
      S1=S3/2.
      GM=0.0022
      TG=SIN(S)
         BET=0.00002950 4
      W7=DW
      TGA=D*WM*COS(W7/WM+S+S1)/EXP(W7*GM)+D*COS(W7+S-S1)
      WRITE(3,10)TG,TGA

      FORMAT(/1X,'TG=',E15.7,4X,'TGA=',E15.7/)
      W7=0.0
      W7=W7+0.017
      YD=D*WM*COS(W7/WM+S+S1)/EXP(W7*GM)+D*COS(W7+S-S1)
      YA=GM**2.*WM*COS(W7/WM+S+S1)/EXP(W7*GM)
     1 +2.*GM*SIN(W7/WM+S+S1)/EXP(W7*GM)
     1 -COS(W7/WM+S+S1)/(WM*EXP(W7*GM))-COS(W7+S-S1)
      IF(YA.LT.0.AND.YD.GT.0.)GO TO 12
      IF(YA.GT.0.AND.YD.LT.0.)GO TO 28

      GO TO 11

      IF(YA.LT.-G1)GO TO 13
       GO TO 11

      B9=W7
      A9=W7-0.017
      EPS=0.0
      ETA=0.0
       IFAIL=0
       CALL C05ACF(A9,B9,EPS,ETA,F9,X6,IFAIL)
      WRITE(3,14)A9,B9,X6
      FORMAT(/1X,'A9=',E15.7,3X,'B9=',E15.7,3X,'X6=',E15.7/)
      WX0=X6
```

```
      S11=X6
      W7=X6

       XX=X6/FREQ
      WX1=X6
      YY=0.

       A2=-GM*WM*COS(W7/WM+S+S1)/EXP(W7*GM)-SIN(W7/WM+S+S1)/EXP(W7*GM)
     1   -SIN(W7+S-S1)
      IF(A2.LT.0.)GO TO 27

      VE=A2
          GO TO 15

       IF(YA.GT.G1)GO TO 29
      GO TO 11

      B10=W7
      A10=W7-0.017
      EPS=0.0
      ETA=0.0
      IFAIL=0
      CALL C05ADF(A10,B10,EPS,ETA,F10,X7,IFAIL)
      WRITE(3,30)A10,B10,X7
      FORMAT(/1X,'A10=',E15.7,3X,'B10=',E15.7,3X,'X7=',E15.7/)
      WX0=X7
      S11=X7
      W7=X7
      WX1=X7
      XX=X7/FREQ
      YY=0.0
      A2=-GM*WM*COS(W7/WM+S+S1)/EXP(W7*GM)-SIN(W7/WM+S+S1)/EXP(W7*GM)
     1  -SIN(W7+S-S1)
      VE=A2
      IF(A2.GT.0.)GO TO 27
      GO TO 15

         F0=0.
       Y1(1)=YD*YW
       Y1(2)=VE*D*YW*FREQ
      Y11=Y1(1)
      Y12=Y1(2)

       G(1)=0.000001
        G(2)=0.000001
       H=0.0000005
        DT=0.000001
        K=1
      T=0
           NN=2
        IFAIL=0
        T=0.
      X1=T

        WX1=WX1/FREQ
      VI=Y1(2)/1000.
      CALL JOIN(WX1,VL)
```

```
      T=T+DT
      CALL D02ABF(X1,Y1,G,K,NN,IFAIL,DT,H,DERIVE,YO,F,A1,B1,C1,D1)

      YB=Y1(1)/YW

        WX1=WX0+T*FREQ
      IF(WX1-WMAX)26,27,27

26    W7=WX1
      YD=D*WM*COS(W7/WM+S+S1)/EXP(W7*GM)+D*COS(W7+S-S1)

      YY=YB-YD
      I=I+1
      AY(I)=Y1(1)

      BY(I)=Y1(2)
      TY(I)=T
      WXY(I)=WX1
      AYY(I)=YY
      IF(DT.EQ.0.000000001)H=0.0000000005

      IF(YY-0.)18,45,19


19    IF(YY-1.)16,46,21

18    IF(I.EQ.1)GO TO 35
      GO TO 36
35    Y1(1)=Y11
      Y1(2)=Y12
      DT=0.000000001
      H=0.0000000005
      T=0
      X1=T
       GG(1)=0.000001
      GG(2)=0.000001
      T=T+DT

      CALL D02ABF(X1,Y1,GG,K,NN,IFAIL,DT,H,DERIVE,YO,F,A1,B1,C1,D1)
      YB=Y1(1)/YW
      WX1=WX0+T*FREQ
      IF(WX1-WMAX)37,27,27
37    W7=WX1

      YD=D*WM*COS(W7/WM+S+S1)/EXP(W7*GM)+D*COS(W7+S-S1)
      YY=YB-YD
      IF(YY-0.)38,38,40
40      BY(I)=Y1(2)
      TY(I)=T
      WXY(I)=WX1
      AYY(I)=YY
      H=0.0000000005
      GO TO 16
38      WXM=WX1
      BYM=Y1(2)
      GO TO 39
```

```
45      WXM=WX1
        BYM=Y1(2)
        GO TO 39
36      WXM=WXY(I)-((AYY(I)-0.)*(WXY(I)-WXY(I-1))/(AYY(I)-AYY(I-1)))

        TYM=(WXM-WX0)/FREQ
        BYM=BY(I)-((BY(I)-BY(I-1))*(TY(I)-TYM)/(TY(I)-TY(I-1)))
39      W7=WXM

        YD=D*WM*COS(W7/WM+S+S1)/EXP(W7*GM)+D*COS(W7+S-S1)
        A2=-GM*WM*COS(W7/WM+S+S1)/EXP(W7*GM)-SIN(W7/WM+S+S1)/EXP(W7*GM)
     1  -SIN(W7+S-S1)
        V0=BYM/(FREQ*D*YW)
        VE=2.*A2-V0
        WX1=WXM
        YY=0.

        WX0=WXM
        XX=WXM/FREQ
        GO TO 15

46      WXM=WX1
        BYM=Y1(2)
        GO TO 47
21      IF(I.EQ.1)GO TO 60
        GO TO 61
60      Y1(1)=Y11
        Y1(2)=Y12
        DT=0.000000001
        H=0.0000000005
        T=0.
        X1=T

        GGG(1)=0.000001
        GGG(2)=0.000001

        T=T+DT
        CALL D02ABF(X1,Y1,GGG,K,NN,IFAIL,DT,H,DERIVE,YO,E,A1,B1,C1,D1)
        YB=Y1(1)/YW
        WX1=WX0+T*FREQ
        IF(WX1-WMAX)62,27,27
62      W7=WX1
        YD=D*WM*COS(W7/WM+S+S1)/EXP(W7*GM)+D*COS(W7+S-S1)
        YY=YB-YD
        IF(YY-1.)64,63,63
64      BY(I)=Y1(2)
        TY(I)=T
        WXY(I)=WX1
        AYY(I)=YY
        H=0.0000000005
        GO TO 16
```

```
63      WXM=WX1
        BYM=Y1(2)
        GO TO 47

61    WXM=WXY(I)-((AYY(I)-1.)*(WXY(I)-WXY(I-1))/(AYY(I)-AYY(I-1)))
        TYM=(WXM-WX0)/FREQ
        BYM=BY(I)-((BY(I)-BY(I-1))*(TY(I)-TYM)/(TY(I)-TY(I-1)))
47    W7=WXM
        YD=D*WM*COS(W7/WM+S+S1)/EXP(W7*GM)+D*COS(W7+S-S1)
        A2=-GM*WM*COS(W7/WM+S+S1)/EXP(W7*GM)-SIN(W7/WM+S+S1)/EXP(W7*GM)
     1  -SIN(W7+S-S1)
        YD=YD+1.
        VO=BYM/(FREQ*D*YW)
        VE=2.*A2-VO
        WX1=WXM
        YY=1.
        WX0=WXM
        XX=WXM/FREQ
         GO TO 15

27       CALL GREND

         STOP


         END

          REAL FUNCTION F9(W)
        REAL W
        DIMENSION A(9,9)

      COMMON N,TM,YW,RM,A,XMAX,XMIN,D,WM,FREQ,S,S1,GM,XX,G1,BFI

         F9=GM**2.*WM*COS(W/WM+S+S1)/EXP(W*GM)
     1    +2.*GM*SIN(W/WM+S+S1)/EXP(W*GM)
     1     -COS(W/WM+S+S1)/(WM*EXP(W*GM))
     1      -COS(W+S-S1)+G1
          RETURN
           END
          REAL FUNCTION F10(W)
        REAL W
        DIMENSION A(9,9)
      COMMON N,TM,YW,RM,A,XMAX,XMIN,D,WM,FREQ,S,S1,GM,XX,G1,BFI
        F10=GM**2.*WM*COS(W/WM+S+S1)/EXP(W*GM)
     1  +2.*GM*SIN(W/WM+S+S1)/EXP(W*GM)
     1  -COS(W/WM+S+S1)/(WM*EXP(W*GM))
     1  -COS(W+S-S1)-G1

        RETURN
        END

          SUBROUTINE DERIVE(F1,Y1,X1)
        REAL F1,Y1,X1
        DIMENSION F1(2),Y1(2),A(9,9)
        COMMON N,TM,YW,RM,A,XMAX,XMIN,D,WM,FREQ,S,S1,GM,XX,G1,BFI
        F1(1)=Y1(2)
        F1(2)=-4.448222*1000.*(0.5*A(N,1)/TM
```

```
1   +A(N,2)*((2.*(Y1(1)-(YW*D*WM*COS(FREQ*(X1+XX)/WM+S+S1)
1   /EXP(FREQ*(X1+XX)*GM)+YW*D*COS(FREQ*(X1+XX)+S-S1)))-XMAX-XMIN)
1   /(YMAX-YMIN))/TM
1   +A(N,3)*(2.*(((2.*(Y1(1)-(YW*D*WM*COS(FREQ*(X1+XX)/WM+S+S1)
1   /EXP(FREQ*(X1+XX)*GM)+YW*D*COS(FREQ*(X1+XX)+S-S1)))-XMAX-XMIN)
1   /(XMAX-XMIN))**2)-1.)/TM
1   +A(N,4)*(4.*(((2.*(Y1(1)-(YW*D*WM*COS(FREQ*(X1+XX)/WM+S+S1)
1   /EXP(FREQ*(X1+XX)*GM)+YW*D*COS(FREQ*(X1+XX)+S-S1)))-XMAX-XMIN)
1   /(YMAX-YMIN))**3)
1   -(3.*((2.*(Y1(1)-(YW*D*WM*COS(FREQ*(X1+XX)/WM+S+S1)
1   /EXP(FREQ*(X1+XX)*GM)+YW*D*COS(FREQ*(X1+XX)+S-S1)))-XMAX-XMIN)
1   /(XMAX-XMIN)))/TM
1   +A(N,5)*(8.*(((2.*(Y1(1)-(YW*D*WM*COS(FREQ*(X1+XX)/WM+S+S1)
1   /EXP(FREQ*(X1+XX)*GM)+YW*D*COS(FREQ*(X1+XX)+S-S1)))-XMAX-XMIN)
1   /(YMAX-XMIN))**4)
1   -(8.*(((2.*(Y1(1)-(YW*D*WM*COS(FREQ*(X1+XX)/WM+S+S1)
1   /EXP(FREQ*(X1+XX)*GM)+YW*D*COS(FREQ*(X1+XX)+S-S1)))-XMAX-XMIN)
1   /(XMAX-XMIN))**2))+1.)/TM)-RM*9800.+BFI*1000./TM
    RETURN
    END

    FINISH
**
```

APPENDIX 7

```
      LIBRARY (SUBGROUPNAGE)
      LIBRARY(SUBGROUPNAGG)
          LIBRARY(SUBGROUPNAGH)
      LIBRARY(SUBGROUPGHOS)
      LIBRARY(SUBGROUPGHOS)
      PROGRAM(HUSS)
      OUTPUT 3=LP0
      INPUT 1=CR0
      INPUT 2=CR1
      INPUT 10=CR2
      INPUT 4=CR3
      INPUT 5=CR4
      INPUT 6=CR5
      INPUT 7=CR6
      INPUT 8=CR7
      INPUT 9=CR8

      TRACE 0
      END
      MASTER MAIN
      DIMENSION WORK1(3,10),WORK2(2,10),A(10,10),X(10),Y(10)
     1  ,Y1(5),G(5),Y0(5),E(5),A1(5),B1(5),C1(5),D1(5),SS(10),
     1 W(10),AY(2000),BY(2000),TY(2000),WXY(2000),AYY(2000)
     1 ,GG(5),GGG(5),PE(20),FR(20),WORKK1(3,6),WORKK2(2,6),AA1(6,6)
     1  ,AAA1(10),WORKK3(3,9),WORKK4(2,9),AA2(9,9),AAA2(10)
     1 ,WORKK5(3,10),WORKK6(2,10),AA3(10,10),AAA3(10)
     1 ,WORKK7(3,10),WORKK8(2,10),AA4(10,10),AAA4(10)
     1 ,WORKK9(3,9),WORKK10(2,9),AA5(9,9),AAA5(10)
     1 ,WORKK11(3,9),WORKK12(2,9),AA6(9,9),AAA6(10),WORKK13(3,10)
     1 ,WORKK14(2,10),AA7(10,10),AAA7(10)
     1 ,WORKK15(3,10),WORKK16(2,10),AA8(10,10),AAA8(10)
     1 ,WORKK17(3,6),WORKK18(2,6),AA9(6,6),AAA9(10)
     1 ,AA(10),PE1(10),XH(10),WWW(15),DDD(15)
      COMMON N,TM,YW,RM,FI,XMAX,XMIN,D,WM,FREQ,S,S1,GM,XX,G1,BFI
         EXTERNAL F9,F10

       X8X=0.
      KNN=0

      N=5
      CALL PAPER(1)
      CALL MAP(0.,0.008,0.,1.)

      CALL PSPACE(0.1,0.625,0.1,0.5)
      CALL CSPACE(0.,0.675,0.,0.55)
      CALL GPINFO('INK PEN 7L-3 IN HOLDER 1,BLACK PEN,PLEASE',42)
       CALL CTRMAG(10)
      CALL AXESSI(0.001,0.0005)
      CALL BORDER
      M=10
      MPLUS1=10
      NROWS=10
      NPLUS1=10

      WMAX=3016.
      DO 1 I=1,M
```

```
1       W(I)=1.
        X(1)=0.0
        X(2)=0.792
        X(3)=1.77
        X(4)=2.83
        X(5)=4.416
        X(6)=5.47
        X(7)=6.53
        X(8)=7.58
        X(9)=8.64
         X(10)=0.47*20.637
        Y(1)=0.0
        Y(2)=0.147
        Y(3)=0.264
        Y(4)=0.355
        Y(5)=0.37
        Y(6)=0.411
        Y(7)=0.405
        Y(8)=0.305
          Y(9)=0.223
        Y(10)=0.0
        XH(1)=0.0

        XH(2)=1.77
        XH(3)=2.83
        XH(4)=4.416
        XH(5)=5.47
        XH(6)=6.53
        XH(7)=7.58
        XH(8)=8.64
        XH(9)=0.47*20.637
        XMAX=0.47
        XMIN=X(1)/20.637

        DO 9 I=1,M

9         X(I)=X(I)/20.637
        IFAIL=0


         CALL E02ADF(M,KPLUS1,NROWS,X,Y,W,WORK1,WORK2,A,SS,IFAIL)
        DO 106 I=1,8
106     AA(I)=A(8,I)
        M=6
        KPLUS1=6
        NROWS=6
        DO 70 I=1,M
70      READ(1,71)RE(I),FR(I)
71      FORMAT(E20.10,E20.10)
        CALL E02ADF(M,KPLUS1,NROWS,RE,FR,W,WORKK1,WORKK2,AA1,SS,IFAIL)
        DO 72 I=1,N
72    AAA1(I)=AA1(N,I)

        M=9
        KPLUS1=9
        NROWS=9
        DO 74 I=1,M
```

```
74      READ(2,75)RE(I),FR(I)
75      FORMAT(E20.10,E20.10)
        CALL E02ADF(M,KPLUS1,NROWS,RE,FR,W,WORKK3,WORKK4,AA2,SS,IFAIL)
        DO 76 I=1,N
76    AAA2(I)=AA2(N,I)



        M=10
        KPLUS1=10
        NROWS=10
        DO 78 I=1,M
78      READ(10,79)RE(I),FR(I)
79      FORMAT(E20.10,E20.10)
        CALL E02ADF(M,KPLUS1,NROWS,RE,FR,W,WORKK5,WORKK6,AA3,SS,IFAIL)
        DO 80 I=1,N
80        AAA3(I)=AA3(N,I)
        M=10
        KPLUS1=10
        NROWS=10
        DO 82 I=1,M
82      READ(4,83)RE(I),FR(I)
83      FORMAT(E20.10,E20.10)
        CALL E02ADF(M,KPLUS1,NROWS,RE,FR,W,WORKK7,WORKK8,AA4,SS,IFAIL)
        DO 84 I=1,N
84      AAA4(I)=AA4(N,I)

        M=9
        KPLUS1=9
        NROWS=9
         DO 86 I=1,M
86      READ(5,87)RE(I),FR(I)
87      FORMAT(E20.10,E20.10)
        CALL E02ADF(M,KPLUS1,NROWS,RE,FR,W,WORKK9,WORKK10,AA5,SS,IFAIL)
        DO 88 I=1,N
88      AAA5(I)=AA5(N,I)
        M=9
        KPLUS1=9
        NROWS=9

        DO 90 I=1,M

90      READ(6,91)RE(I),FR(I)
91      FORMAT(E20.10,E20.10)
        CALL E02ADF(M,KPLUS1,NROWS,RE,FR,W,WORKK11,WORKK12,AA6,SS,IFAIL)
        DO 92 I=1,N
92      AAA6(I)=AA6(N,I)
        M=10
        KPLUS1=10
        NROWS=10

        DO 94 I=1,M
94      READ(7,95)RE(I),FR(I)
95      FORMAT(E20.10,E20.10)
        CALL E02ADF(M,KPLUS1,NROWS,RE,FR,W,WORKK13,WORKK14,AA7,SS,IFAIL)
        DO 96 I=1,N
96      AAA7(I)=AA7(N,I)
```

```
      M=10
      KPLUS1=10
      NROWS=10
      DO 98 I=1,M
98    READ(8,99)RE(I),FR(I)
99    FORMAT(E20.10,E20.10)
      CALL E02ADF(M,KPLUS1,NROWS,RE,FR,W,WORKK15,WORKK16,AA8,SS,IFAIL)
      DO  100 I=1,N
100   AAA8(I)=AA8(N,I)
      M=6
      KPLUS1=6
      NROWS=6
      DO 102 I=1,M
102    READ(9,103)RE(I),FR(I)
103   FORMAT(E20.10,E20.10)
      CALL E02ADF(M,KPLUS1,NROWS,RE,FR,W,WORKK17,WORKK18,AA9,SS,IFAIL)
      DO 104 I=1,N
104   AAA9(I)=AA9(N,I)
      TM=0.0000365
      RM=0.91
      FIF=0.4421532*1000.
      AR=0.5281
      DD=2.
      VV=0.5759988
      RMAX=70000.
      RMIN=0.
      HH=0.000000718
      YW=0.47

      FREQ=376991.11
       S3=4.0*ATAN(1.0)
      S=0.
      IFAIL=0
      DW=0.4
       GGM=0.007
      D=0.00423/YW
      G1=0.0219708
      WM=1.
      S1=S3/2.
      GM=0.0021
      TG=SIN(S)
         BET=0.00002950 4
      W7=DW
      TGA=D*WM*COS(W7/WM+S+S1)/EXP(W7*GM)+D*COS(W7+S-S1)
      W7=0.0
11    W7=W7+0.017
      YD=D*WM*COS(W7/WM+S+S1)/EXP(W7*GM)+D*COS(W7+S-S1)
      YA=GM**2.*WM*COS(W7/WM+S+S1)/EXP(W7*GM)
     1.  +2.*GM*SIN(W7/WM+S+S1)/EXP(W7*GM)
     1  -COS(W7/WM+S+S1)/(WM*EXP(W7*GM))-COS(W7+S-S1)
      IF(YA.LT.0.AND.YD.GT.0.)GO TO 12
      IF(YA.GT.0.AND.YD.LT.0.)GO TO 28

      GO TO 11

12    IF(YA.LT.-G1)GO TO 13
       GO TO 11
```

```
13      B9=W7
        A9=W7-0.017
        EPS=0.0
        ETA=0.0
         IFAIL=0
         CALL COSACF(A9,B9,EPS,ETA,F9,X6,IFAIL)
        WRITE(3,14)A9,B9,X6
14      FORMAT(/1X,'A9=',E15.7,3X,'B9=',E15.7,3X,'X6=',E15.7/)
        WX0=X6
        W7=X6

        WX1=X6
        YY=0.

         A2=-GM*WM*COS(W7/WM+S+S1)/EXP(W7*GM)-SIN(W7/WM+S+S1)/EXP(W7*GM)
     1    -SIN(W7+S-S1)
        IF(A2.LT.0.)GO TO 27

        YD=D*WM*COS(W7/WM+S+S1)/EXP(W7*GM)+D*COS(W7+S-S1)
        VE=A2
            GO TO 15

28       IF(YA.GT.G1)GO TO 29
        GO TO 11

29      B10=W7
        A10=W7-0.017
        EPS=0.0
        ETA=0.0
        IFAIL=0
        CALL COSACF(A10,B10,EPS,ETA,F10,X7,IFAIL)
        WRITE(3,30)A10,B10,X7
30      FORMAT(/1X,'A10=',E15.7,3X,'B10=',E15.7,3X,'X7=',E15.7/)
        WX0=X7
        W7=X7
        WX1=X7
        YY=0.0
        A2=-GM*WM*COS(W7/WM+S+S1)/EXP(W7*GM)-SIN(W7/WM+S+S1)/EXP(W7*GM)
     1  -SIN(W7+S-S1)
        YD=D*WM*COS(W7/WM+S+S1)/EXP(W7*GM)+D*COS(W7+S-S1)
        VE=A2
        IF(A2.GT.0.)GO TO 27
        GO TO 15

15         F0=0.
         Y1(1)=YD*YW
         Y1(2)=VE*D*YW*FREQ
        Y11=Y1(1)
        Y12=Y1(2)

        FI=FIF
          DT=0.000001
        T=0
          IFAIL=0
          T=0.
```

```
16        WX1=(WX1+X8X)/FREQ
      CALL JOT4(WX1,YY)

        T=T+DT

       Y1(1)=0.5*T**2.*(-FI/TM-9800.*RM+1000.*BFI/TM)
     1 +Y1(2)*T+Y1(1)
       Y1(2)=T*(-FI/TM-9800.*RM+1000.*BFI/TM)+Y1(2)

       YB=Y1(1)/YU

        WX1=WX0+T*FREQ
       IF(WX1-WMAX)26,27,27

26     W7=WX1
       YD=D*WM*COS(W7/WM+S+S1)/EXP(W7*GM)+D*COS(W7+S-S1)

        IF(KNN.EQ.1)GO TO 153

        YDD=YD/D
        IF(YDD.GE.0.99.OR.YDD.LE.-0.99)GO TO 151
       GO TO 154
151    KNN=KNN+1
       YBX=WX0
       WX0=0
       T=DT
153    WX1=WX0+T*FREQ
       W7=WX1
       YD=D*COS(W7/WM)/EXP(W7*GGM)

154    YY=YB-YD
       I=I+1
       AY(I)=Y1(1)

       BY(I)=Y1(2)
       TY(I)=T
       WXY(I)=WX1
       AYY(I)=YY

       IF(YY-0.)18,45,19


19     IF(YY-1.)116,46,21

 18    IF(I.EQ.1)GO TO 35
       GO TO 36
35     Y1(1)=Y11
       Y1(2)=Y12
       DT=0.000000001
       T=0
       T=T+DT

       Y1(1)=0.5*T**2.*(-FI/TM-9800.*RM+1000.*BFI/TM)
     1 +Y1(2)*T+Y1(1)
       Y1(2)=T*(-FI/TM-9800.*RM+1000.*BFI/TM)+Y1(2)
       YB=Y1(1)/YU

       WX1=WX0+T*FREQ
       IF(WX1-WMAX)37,27,27
```

```
37      W7=WX1

        IF(KNN.EQ.1)GO TO 157
        YD=D*WM*COS(W7/WM+S+S1)/EXP(W7*GM)+D*COS(W7+S-S1)
         YDD=YD/D
        IF(YDD.GE.0.99.OR.YDD.LE.-0.99)GO TO 156
        GO TO 158
156      KNN=KNN+1
         X8X=WX0
         WX0=0
         T=DT
157      WX1=WX0+T*FREQ
         W7=WX1

         YD=D*COS(W7/WM)/EXP(W7*GGM)

158     YY=YB-YD
        IF(YY-0.)38,38,40
40        BY(I)=Y1(2)
        TY(I)=T
        WXY(I)=WX1
        AYY(I)=YY
        GO TO 116
38        WXM=WX1
        BYM=Y1(2)
        GO TO 39


45       WXM=WX1
        BYM=Y1(2)
         GO TO 39
36        WXM=WXY(I)-((AYY(I)-0.)*(WXY(I)-WXY(I-1))/(AYY(I)-AYY(I-1)))




        TYM=(WXM-WX0)/FREQ
        BYM=BY(I)-((BY(I)-BY(I-1))*(TY(I)-TYM)/(TY(I)-TY(I-1)))
39      W7=WXM

        YD=D*WM*COS(W7/WM+S+S1)/EXP(W7*GM)+D*COS(W7+S-S1)
          IF(KNN.EQ.1)YD=D*COS(W7/WM)/EXP(W7*GGM)

        A2=-GM*WM*COS(W7/WM+S+S1)/EXP(W7*GM)-SIN(W7/WM+S+S1)/EXP(W7*GM)
     1  -SIN(W7+S-S1)
        IF(KNN.EQ.1)A2=-GGM*COS(W7/WM)/EXP(W7*GGM)-1./WM*SIN
     1  (W7/WM)/EXP(W7*GGM)
          V0=BYM/(FREQ*D*YD)
        VE=2.*A2-V0
        WX1=WXM
        YY=0.

        WX0=WXM
        GO TO 15
```

```
46      WXM=WX1
        BYM=Y1(2)
        GO TO 47
21       IF(I.EQ.1)GO TO 60
        GO TO 61
60      Y1(1)=Y11
        Y1(2)=Y12
        DT=0.000000001
        T=0.


        T=T+DT
         Y1(1)=0.5*T**2.*(-FI/TM-9800.*RM+1000.*BFI/TM)
     1  +Y1(2)*T+Y1(1)
        Y1(2)=T*(-FI/TM-9800.*RM+1000.*BFI/TM)+Y1(2)
        YB=Y1(1)/YU
        WX1=WX0+T*FREQ
        IF(WX1-WMAX)62,27,27
62      W7=WX1
        IF(KNN.EQ.1)GO TO 161
        YD=D*WM*COS(W7/WM+S+S1)/EXP(W7*GM)+D*COS(W7+S-S1)
        YDD=YD/D
        IF(YDD.GE.0.99.OR.YDD.LT.-0.99)GO TO 160
         GO TO 162
160     KNN=KNN+1
        YSY=WX0
        WX0=0
        T=DT
161     WX1=WX0+T*FREQ
         W7=WX1
         YD=D*COS(W7/WM)/EXP(W7*GGM)

162     YY=YB-YD
        IF(YY-1.)64,63,63
64      BY(I)=Y1(2)
        TY(I)=T
        WXY(I)=WX1
        AYY(I)=YY
        GO TO 116
63      WXM=WX1
        BYM=Y1(2)
        GO TO 47

61     WXM=WXY(I)-((AYY(I)-1.)*(WXY(I)-WXY(I-1))/(AYY(I)-AYY(I-1)))
       TYM=(WXM-WX0)/FREQ
       BYM=BY(I)-((BY(I)-BY(I-1))*(TY(I)-TYM)/(TY(I)-TY(I-1)))
47     W7=WXM
       YD=D*WM*COS(W7/WM+S+S1)/EXP(W7*GM)+D*COS(W7+S-S1)
        IF(KNN.EQ.1)YD=D*COS(W7/WM)/EXP(W7*GGM)
       A2=-GM*WM*COS(W7/WM+S+S1)/EXP(W7*GM)-SIN(W7/WM+S+S1)/EXP(W7*GM)
     1 -SIN(W7+S-S1)
       IF(KNN.EQ.1)A2=-GGM*COS(W7/WM)/EXP(W7*GGM)-1./WM*SIN
     1 (W7/WM)/EXP(W7*GGM)
       YD=YD+1.
       V0=BYM/(FREQ*D*YU)
       VF=2.*A2-V0
       WX1=WXM
```

```
      YY=1.
      WW0=WXM
       GO TO 15

116   AX=YY*YW

      XCAP=(2.*AX-XMAX-XMIN)/(XMAX-XMIN)
      IFAIL=0
      CALL E02AEF(8,AA,XCAP,PR,IFAIL)


      PR=PR*16666.666
      VR=PR/AR
      VRI=-VR-Y1(2)
      IF(VRI.LT.0.)VRI=-VRI
      RR=VRI*DD/VV

       IF(RR.GT.20000)GO TO 27
      RCAP=(2.*RR-RMAX-RMIN)/(RMAX-RMIN)
      CALL E02AEF(N,AAA1,RCAP,PF,IFAIL)
      PFI(1)=PF
      CALL E02AEF(N,AAA2,RCAP,PF,IFAIL)
      PFI(2)=PF
      CALL E02AEF(N,AAA3,RCAP,PF,IFAIL)
      PFI(3)=PF
      CALL E02AEF(N,AAA4,RCAP,PF,IFAIL)

      PFI(4)=PF
      CALL E02AEF(N,AAA5,RCAP,PF,IFAIL)
      PFI(5)=PF
      CALL E02AEF(N,AAA6,RCAP,PF,IFAIL)
      PFI(6)=PF
       CALL E02AEF(N,AAA7,RCAP,PF,IFAIL)
       PFI(7)=PF
       CALL E02AEF(N,AAA8,RCAP,PF,IFAIL)
       PFI(8)=PF
       CALL E02AEF(N,AAA9,RCAP,PF,IFAIL)
       PFI(9)=PF

       N2=9-1

       IG=15

      XAA=AX*20.637
      CALL E01AEF(N2,XAA,XH,PFI,WWW,DDD,IG,VAL)

       FI=VAL*(VRI**2.)*(DD**2.)*HH
       GO TO 16


27    WRITE(3,119)RR
119   FORMAT(1X,'RR=',E15.7)
      CALL GREND

       STOP


       END
```

```
      REAL FUNCTION F9(W)
     REAL W

    COMMON N,TM,YW,RM,FI,XMAX,XMIN,D,WM,FREQ,S,S1,GM,XX,G1,BFI

      F9=GM**2.*WM*COS(W/WM+S+S1)/EXP(W*GM)
     1  +2.*GM*SIN(W/WM+S+S1)/EXP(W*GM)
     1   -COS(W/WM+S+S1)/(WM*EXP(W*GM))
     1    -COS(W+S-S1)+G1
      RETURN
       END
      REAL FUNCTION F10(W)
     REAL W
    COMMON N,TM,YW,RM,FI,XMAX,XMIN,D,WM,FREQ,S,S1,GM,XX,G1,BFI
     F10=GM**2.*WM*COS(W/WM+S+S1)/EXP(W*GM)
     1  +2.*GM*SIN(W/WM+S+S1)/EXP(W*GM)
     1  -COS(W/WM+S+S1)/(WM*EXP(W*GM))
     1  -COS(W+S-S1)-G1

     RETURN
     END


      FINISH
****
```

APPENDIX 8

```
      LIBRARY (SUBGROUPNAGF)
      LIBRARY(SUBGROUPNAGG)
          LIBRARY(SUBGROUPNAGH)
      LIBRARY(SUBGROUPGHOS)
      LIBRARY(SUBGROUPGHOS)
      PROGRAM(HUSS)
      OUTPUT 3=LP0
      INPUT 1=CR0
      INPUT 2=CR1
      INPUT 10=CR2
      INPUT 4=CR3
      INPUT 5=CR4
      INPUT 6=CR5
      INPUT 7=CR6
      INPUT 8=CR7
      INPUT 9=CR8

      TRACE 0
      END
      MASTER MAIN
      DIMENSION WORK1(3,10),WORK2(2,10),A(10,10),X(10),Y(10)
     1  ,Y1(5),G(5),Y0(5),E(5),A1(5),B1(5),C1(5),D1(5),SS(10),
     1 V(10),AY(2000),BY(2000),TY(2000),WXY(2000),AYY(2000)
     1 ,GG(5),GGG(5),RE(20),FR(20),WORKK1(3,6),WORKK2(2,6),AA1(6,6)
     1  ,AAA1(10),WORKK3(3,9),WORKK4(2,9),AA2(9,9),AAA2(10)
     1 ,WORKK5(3,10),WORKK6(2,10),AA3(10,10),AAA3(10)
     1 ,WORKK7(3,10),WORKK8(2,10),AA4(10,10),AAA4(10)
     1 ,WORKK9(3,9),WORKK10(2,9),AA5(9,9),AAA5(10)
     1 ,WORKK11(3,9),WORKK12(2,9),AA6(9,9),AAA6(10),WORKK13(3,10)
     1 ,WORKK14(2,10),AA7(10,10),AAA7(10)
     1 ,WORKK15(3,10),WORKK16(2,10),AA8(10,10),AAA8(10)
     1 ,WORKK17(3,6),WORKK18(2,6),AA9(6,6),AAA9(10)
     1 ,AA(10),PFI(10),XH(10),WWW(15),DDD(15),RRR(15),ZZZ(15)
     1 ,YF(15)
      COMMON N,TM,YW,RM,FI,XMAX,XMIN,D,WM,FREQ,S,S1,GM,XX,G1,BFI
         EXTERNAL F9,F10

       X8X=0.
      KNN=0

      N=5
      CALL PAPER(1)
      CALL MAP(0.,0.008,0.,1.)

      CALL GPIN=0('INK PEN 71-3 IN HOLDER 1,BLACK PEN,PLEASE',42)
      CALL PSPACE(0.1,0.625,0.1,0.5)
      CALL CSPACE(0.,0.675,0.,0.55)
      CALL CTRMAG(10)
      CALL AXESSI(0.001,0.0005)
      CALL BORDER
      M=10
      KPLUS1=10
      NPLUS=10
      NPLUS1=10

      WMAX=3016.
      DO 1 I=1,N
```

```
1       U(1)=1.
        X(1)=0.0
        X(2)=0.792
        X(3)=1.77
        X(4)=2.83
        X(5)=4.416
        X(6)=5.47
        X(7)=6.53
        X(8)=7.58
        X(9)=8.64
         X(10)=0.47*20.637
        Y(1)=0.0
        Y(2)=0.147
        Y(3)=0.264
        Y(4)=0.355
        Y(5)=0.37
        Y(6)=0.411
        Y(7)=0.405
        Y(8)=0.305
          Y(9)=0.223
        Y(10)=0.0
        YF(1)=0.
        YF(2)=0.3
        YF(3)=0.54
        YF(4)=0.71
        YF(5)=0.729
        YF(6)=0.758
        YF(7)=0.776
        YF(8)=0.776
        YF(9)=0.76
        YF(10)=0.74

        XH(1)=0.0

        XH(2)=1.77
        XH(3)=2.83
        XH(4)=4.416
        XH(5)=5.47
        XH(6)=6.53
        XH(7)=7.58
        XH(8)=8.64
        XH(9)=0.47*20.637
        XMAX=0.47
        XMIN=X(1)/20.637

        DO 9 I=1,M

9         X(I)=X(1)/20.637
        IFAIL=0


         CALL E02ADF(M,KPLUS1,NROWS,X,Y,W,WORK1,WORK2,A,SS,IFAIL)
        DO 106 I=1,8
106     AA(I)=A(8,I)
        M=6
        KPLUS1=6
        NROWS=6
```

```
      DO 70 I=1,M
70    READ(1,71)RE(I),FR(I)
71    FORMAT(E20.10,E20.10)
      CALL E02ADF(M,KPLUS1,NROWS,RE,FR,W,WORKK1,WORKK2,AA1,SS,IFAIL)
      DO 72 I=1,N
72   AAA1(I)=AA1(N,I)

      M=9
      KPLUS1=9
      NROWS=9
      DO 74 I=1,M
74    READ(2,75)RE(I),FR(I)
75    FORMAT(E20.10,E20.10)
      CALL E02ADF(M,KPLUS1,NROWS,RE,FR,W,WORKK3,WORKK4,AA2,SS,IFAIL)
      DO 76 I=1,N
76   AAA2(I)=AA2(N,I)



      M=10
      KPLUS1=10
      NROWS=10
      DO 78 I=1,M
78    READ(10,79)RE(I),FR(I)
79    FORMAT(E20.10,E20.10)
      CALL E02ADF(M,KPLUS1,NROWS,RE,FR,W,WORKK5,WORKK6,AA3,SS,IFAIL)
      DO 80 I=1,N
80      AAA3(I)=AA3(N,I)
      M=10
      KPLUS1=10
      NROWS=10
      DO 82 I=1,M
82    READ(4,83)RE(I),FR(I)
83    FORMAT(E20.10,E20.10)
      CALL E02ADF(M,KPLUS1,NROWS,RE,FR,W,WORKK7,WORKK8,AA4,SS,IFAIL)
      DO 84 I=1,N
84    AAA4(I)=AA4(N,I)

      M=9
      KPLUS1=9
      NROWS=9
       DO 86 I=1,M
86    READ(5,87)RE(I),FR(I)
87    FORMAT(E20.10,E20.10)
      CALL E02ADF(M,KPLUS1,NROWS,RE,FR,W,WORKK9,WORKK10,AA5,SS,IFAIL)
      DO 88 I=1,N
88    AAA5(I)=AA5(N,I)
      M=9
      KPLUS1=9
      NROWS=9

      DO 90 I=1,M

90    READ(6,91)RE(I),FR(I)
91    FORMAT(E20.10,E20.10)
      CALL E02ADF(M,KPLUS1,NROWS,RE,FR,W,WORKK11,WORKK12,AA6,SS,IFAIL)
      DO 92 I=1,N
```

```
92      AAA6(I)=AA6(N,I)
        M=10
        KPLUS1=10
        NROWS=10

        DO 94 I=1,M
94      READ(7,95)RE(I),FR(I)
95      FORMAT(E20.10,E20.10)
        CALL E02ADF(M,KPLUS1,NROWS,RE,FR,W,WORKK13,WORKK14,AA7,SS,IFAIL)
        DO 96 I=1,M
96      AAA7(I)=AA7(N,I)

        M=10
        KPLUS1=10
        NROWS=10
        DO 98 I=1,M
98      READ(8,99)RE(I),FR(I)
99      FORMAT(E20.10,E20.10)
        CALL E02ADF(M,KPLUS1,NROWS,RE,FR,W,WORKK15,WORKK16,AA8,SS,IFAIL)
        DO  100 I=1,N
100     AAA8(I)=AA8(N,I)
        M=6
        KPLUS1=6
        NROWS=6
        DO 102 I=1,M
102      READ(9,103)RE(I),FR(I)
103     FORMAT(E20.10,E20.10)
        CALL E02ADF(M,KPLUS1,NROWS,RE,FR,W,WORKK17,WORKK18,AA9,SS,IFAIL)
        DO 104 I=1,N
104     AAA9(I)=AA9(N,I)
        TM=0.0000365
        PM=0.91
        FIF=0.4421532*1000.
        AD=0.5281
        DD=2.
        VW=0.5759988
        RMAX=70000.
        RMIN=0.
        BB=0.000000718
        YW=0.47

        FREQ=376991.11
         S3=4.0*ATAN(1.0)
        S=0.
        IFAIL=0
        DW=0.4
         GGM=0.007
        D=0.00423/YW
        G1=0.0219708
        WM=1.
        S1=S3/2.
        GM=0.0021
        TG=SIN(S)
           BET=0.00002950 4
        W7=DW
        TGA=D*WM*COS(W7/WM+S+S1)/EXP(W7*GM)+D*COS(W7+S-S1)
        W7=0.0
11      W7=W7+0.017
```

```
      YD=D*WM*COS(W7/WM+S+S1)/EXP(W7*GM)+D*COS(W7+S-S1)
      YA=GM**2.*WM*COS(W7/WM+S+S1)/EXP(W7*GM)
     1  +2.*GM*SIN(W7/WM+S+S1)/EXP(W7*GM)
     1  -COS(W7/WM+S+S1)/(WM*EXP(W7*GM))-COS(W7+S-S1)
      IF(YA.LT.0.AND.YD.GT.0.)GO TO 12
      IF(YA.GT.0.AND.YD.LT.0.)GO TO 28

      GO TO 11

12    IF(YA.LT.-G1)GO TO 13
       GO TO 11

13    B9=W7
      A9=W7-0.017
      EPS=0.0
      ETA=0.0
       IFAIL=0
       CALL COSACE(A9,B9,EPS,ETA,F9,X6,IFAIL)
      WRITE(3,14)A9,B9,X6
14    FORMAT(/1X,'A9=',E15.7,3X,'B9=',E15.7,3X,'X6=',E15.7/)
      WX0=X6
      W7=X6

      WX1=X6
      YY=0.

       A2=-GM*WM*COS(W7/WM+S+S1)/EXP(W7*GM)-SIN(W7/WM+S+S1)/EXP(W7*GM)
     1   -SIN(W7+S-S1)
      IF(A2.LT.0.)GO TO 27

      YD=D*WM*COS(W7/WM+S+S1)/EXP(W7*GM)+D*COS(W7+S-S1)
      VE=A2
          GO TO 15

28     IF(YA.GT.G1)GO TO 29
      GO TO 11

29    B10=W7
      A10=W7-0.017
      EPS=0.0
      ETA=0.0
      IFAIL=0
      CALL COSACE(A10,B10,EPS,ETA,F10,X7,IFAIL)
      WRITE(3,30)A10,B10,X7
30    FORMAT(/1X,'A10=',E15.7,3X,'B10=',E15.7,3X,'X7=',E15.7/)
      WX0=X7
      W7=X7
      WX1=X7
      YY=0.0
      A2=-GM*WM*COS(W7/WM+S+S1)/EXP(W7*GM)-SIN(W7/WM+S+S1)/EXP(W7*GM)
     1  -SIN(W7+S-S1)
      YD=D*WM*COS(W7/WM+S+S1)/EXP(W7*GM)+D*COS(W7+S-S1)
      VE=A2
      IF(A2.GT.0.)GO TO 27
      GO TO 15
```

```
15          F0=0.
            Y1(1)=YD*YW
            Y1(2)=VF*D*YW-FREQ
            Y11=Y1(1)
            Y12=Y1(2)

            FI=FIF
              DT=0.000001
            I=0
              IFAIL=0
              T=0.

16            WX1=(WX1+X8X)/FREQ
            CALL JOIN(WX1,DT)

              T=T+DT

            Y1(1)=0.5*T**2.*(-FI/TM-9800.*RM+1000.*BFI/TM)
     1      +Y1(2)*T+Y1(1)
            Y1(2)=T*(-FI/TM-9800.*RM+1000.*BFI/TM)+Y1(2)

            YB=Y1(1)/YW

              WX1=WX0+T*FREQ
            IF(WX1-WMA))26,27,27

26          W7=WX1
            YD=D*WM*COS(W7/WM+S+S1)/EXP(W7*GM)+D*COS(W7+S-S1)

             IF(KNN.EQ.1)GO TO 153

            YDD=YD/D
             IF(YDD.GE.0.99.OR.YDD.LE.-0.99)GO TO 151
            GO TO 154
151         KNN=KNN+1
            X8X=WX0
            WX0=0
            T=DT
153         WX1=WX0+T*FREQ
            W7=WX1
            YD=D*COS(W7/WM)/EXP(W7*GGM)

154         YY=YB-YD
            I=I+1
            AY(I)=Y1(1)

            BY(I)=Y1(2)
            TY(I)=T
            WY(I)=WX1
            AYY(I)=YY

            IF(YY-0.)18,45,19


19          IF(YY-1.)116,46,21

  18        IF(I.EQ.1)GO TO 35
            GO TO 36
```

```
35      Y1(1)=Y11
        Y1(2)=Y12
        DT=0.000000001
        T=0
        T=T+DT

        Y1(1)=0.5*T**2.*(-FI/TM-9800.*RM+1000.*BFI/TM)
     1  +Y1(2)*T+Y1(1)
        Y1(2)=T*(-FI/TM-9800.*RM+1000.*BFI/TM)+Y1(2)
        YB=Y1(1)/YY

        WX1=WX0+T*FREQ
        IF(WX1-WMAX)37,27,27
37      W7=WX1

        IF(KNN.EQ.1)GO TO 157
        YD=D*WM*COS(W7/WM+S+S1)/EXP(W7*GM)+D*COS(W7+S-S1)
         YDD=YD/D
        IF(YDD.GE.0.99.OR.YDD.LE.-0.99)GO TO 156
        GO TO 158
156      KNN=KNN+1
         X8X=WX0
         WX0=0
         T=DT
157      WX1=WX0+T*FREQ
         W7=WX1

         YD=D*COS(W7/WM)/EXP(W7*GGM)

158     YY=YB-YD
        IF(YY-0.)38,38,40
40        BY(I)=Y1(2)
        TY(I)=T
        WXY(I)=WX1
        AYY(I)=YY
        GO TO 116
38        WXM=WX1
        BYM=Y1(2)
        GO TO 39


45       WXM=WX1
        BYM=Y1(2)
         GO TO 39
36        WXM=WXY(I)-((AYY(I)-0.)*(WXY(I)-WXY(I-1))/(AYY(I)-AYY(I-1)))




        TYM=(WXM-WX0)/FREQ
        BYM=BY(I)-((BY(I)-BY(I-1))*(TY(I)-TYM)/(TY(I)-TY(I-1)))
39      W7=WXM

        YD=D*WM*COS(W7/WM+S+S1)/EXP(W7*GM)+D*COS(W7+S-S1)
          IF(KNN.EQ.1)YD=D*COS(W7/WM)/EXP(W7*GGM)
```

```
      A2=-GM*WM*COS(W7/WM+S+S1)/EXP(W7*GM)-SIN(W7/WM+S+S1)/EXP(W7*GM)
     1  -SIN(W7+S-S1)
        IF(KNN.EQ.1)A2=-GGM*COS(W7/WM)/EXP(W7*GGM)-1./WM*SIN
     1  (W7/WM)/EXP(W7*GGM)
          V0=BYM/(FREQ*D*YW)
        VE=2.*A2-V0
        WX1=WXM
        YY=0.

        WX0=WXM
         QT=0.
        GO TO 15

46      WXM=WX1
        BYM=Y1(2)
        GO TO 47
21       IF(I.EQ.1)GO TO 60
        GO TO 61
60      Y1(1)=Y11
        Y1(2)=Y12
        DT=0.000000001
        T=0.


        T=T+DT
         V1(1)=0.5*T**2.*(-FI/TM-9800.*RM+1000.*BFI/TM)
     1  +Y1(2)*T+Y1(1)
        Y1(2)=T*(-FI/TM-9800.*RM+1000.*BFI/TM)+Y1(2)
        YR=Y1(1)/YW
        WX1=WX0+T*FREQ
        IF(WX1-WMAX)62,27,27
62      W7=WX1
        IF(KNN.EQ.1)GO TO 161
        YD=D*WM*COS(W7/WM+S+S1)/EXP(W7*GM)+D*COS(W7+S-S1)
        YDD=YD/D
        IF(YDD.GE.0.99.OR.YDD.LT.-0.99)GO TO 160
         GO TO 162
160     KNN=KNN+1
        X8X=WX0
        WX0=0
        T=DT
161     WX1=WX0+T*FREQ
         W7=WX1
         YD=D*COS(W7/WM)/EXP(W7*GGM)

162     YY=YR-YD
        IF(YY-1.)64,63,63
64      BY(I)=Y1(2)
        TY(I)=T
        WXY(I)=WX1
        AYY(I)=YY
        GO TO 116
63      WXM=WX1
        BYM=Y1(2)
        GO TO 47
```

```
61      WXM=WXY(I)-((AYY(I)-1.)*(WXY(I)-WXY(I-1))/(AYY(I)-AYY(I-1)))
          TYM=(WXM-WY0)/FREQ
          BYM=BY(I)-((BY(I)-BY(I-1))*(TY(I)-TYM)/(TY(I)-TY(I-1)))
47      W7=WYM
          YD=D*WM*COS(W7/WM+S+S1)/EXP(W7*GM)+D*COS(W7+S-S1)
           IF(KNN.EQ.1)YD=D*COS(W7/WM)/EXP(W7*GGM)
          A2=-GM*WM*COS(W7/WM+S+S1)/EXP(W7*GM)-SIN(W7/WM+S+S1)/EXP(W7*GM)
     1    -SIN(W7+S-S1)
          IF(KNN.EQ.1)A2=-GGM*COS(W7/WM)/EXP(W7*GGM)-1./WM*SIN
     1    (W7/WM)/EXP(W7*GGM)
          YD=YD+1.
          V0=BYM/(FREQ*D*YW)
          VF=2.*A2-V0
          WX1=WXM
          YY=1.
          WX0=WXM
            QT=YF(10)
           GO TO 15

116       AX=YY*YW

          XCAP=(2.*AX-XMAX-XMIN)/(XMAX-XMIN)
          IFAIL=0
          CALL E02AEF(8,AA,XCAP,PF,IFAIL)


           NJ=10-1
            INK=15
          CALL E01AEF(NJ,AX,X,YF,BBB,ZZZ,INK,QT)
          PR=PR*16666.666
          VR=PR/AR
          VRI=-VR-Y1(2)
          IF(VRI.LT.0.)VRI=-VRI
          RR=VRI*DD/VV

           IF(RR.GT.70000)GO TO 27
          RCAP=(2.*RR-RMAX-RMIN)/(RMAX-RMIN)
          CALL E02AEF(N,AAA1,RCAP,PF,IFAIL)
          PFI(1)=PF
          CALL E02AEF(N,AAA2,RCAP,PF,IFAIL)
          PFI(2)=PF
          CALL E02AEF(N,AAA3,RCAP,PF,IFAIL)
          PFI(3)=PF
          CALL E02AEF(N,AAA4,RCAP,PF,IFAIL)

          PFI(4)=PF
          CALL E02AEF(N,AAA5,RCAP,PF,IFAIL)
          PFI(5)=PF
          CALL E02AEF(N,AAA6,RCAP,PF,IFAIL)
          PFI(6)=PF
           CALL E02AEF(N,AAA7,RCAP,PF,IFAIL)
           PFI(7)=PF
           CALL E02AEF(N,AAA8,RCAP,PF,IFAIL)
           PFI(8)=PF
           CALL E02AEF(N,AAA9,RCAP,PF,IFAIL)
           PFI(9)=PF

          N2=9-1
```

```
      IG=15

      XAA=AX*20.637
      CALL E01ADF(N2,XAA,XH,PFI,WWW,DDD,IG,VAL)

      FI=VAL*(VPI**2.)*(DD**2.)*HH
      GO TO 16


27    WRITE(3,119)RR
119   FORMAT(1X,'RR=',E15.7)
      CALL GREND

      STOP


      END

       REAL FUNCTION F9(W)
      REAL W

     COMMON N,TM,YW,RM,FI,XMAX,XMIN,D,WM,FREQ,S,S1,GM,XX,G1,BFI

       F9=GM**2.*WM*COS(W/WM+S+S1)/EXP(W*GM)
     1  +2.*GM*SIN(W/WM+S+S1)/EXP(W*GM)
     1   -COS(W/WM+S+S1)/(WM*EXP(W*GM))
     1    -COS(W+S-S1)+G1
       RETURN
        END
       REAL FUNCTION F10(W)
      REAL W
     COMMON N,TM,YW,RM,FI,XMAX,XMIN,D,WM,FREQ,S,S1,GM,XX,G1,BFI
      F10=GM**2.*WM*COS(W/WM+S+S1)/EXP(W*GM)
     1  +2.*GM*SIN(W/WM+S+S1)/EXP(W*GM)
     1  -COS(W/WM+S+S1)/(WM*EXP(W*GM))
     1  -COS(W+S-S1)-G1

      RETURN
      END


      FINISH
****
```

REFERENCES

1. GRUBB, J. A., MILSOM, R. F., and ABRAM, R. A. — "Progress Report of Work on the Ultrasonic Fuel Injector." Allen Clark Research Centre, The Plessey Company Limited, Caswell, Towcester, Northants, January 1977.

2. MARTIN, B. J. — "An Advanced Fuel and Engine Control System." Plessey Group Publication, Publication No. 5517.

3. MARTIN, B. J., SUMAL, J. S. — "The Ultrasonic Fuel Injector - Its Development as an Alternative to the Solenoid Injector." Proc. of the 2nd Int. Conf. on Automotive Electronics, 29 Oct. - 2 Nov. 1979, pp. 130.

4. SMITH, A. W,, and COOPER, J. N. — "Elements of Physics." McGraw-Hill, Inc., 8th edition, 1972, pp. 53.

5. HUNTER, S. C. — "Energy Absorbed by Elastic Waves During Impact", J. Mech. Phys. Solids, Vol. 5, 1957, pp. 162.

6. LOVE, A. E. H. — "Mathematical Theory of Elasticity." C.U.P., 4th edition, pp. 1, 8.

7. GOODIER, J. N., JAHSMAN, W. E., RIPPERGER, E. A. — "An Experimental Surface-Wave Method for Recording Force-Time Curves in Elastic Impacts", Journal of Applied Mechanics, Vol. 26, Trans. ASME, Vol. 81, March 1959, pp. 3.

8. LIFSHITZ, J. M., and KOLSKY, H. — "Some Experiments on an Elastic Rebound", J. Mech. Phys. Solids, Vol. 12, 1964, pp. 35.

9. RAMAN, C. V. — "On Some Applications of Hertz's Theory of Impact", Phys. Rev., Vol. 15, 1920, pp. 277.

10. VELUSWAMI, M. A. — "Vibroimpacts of a ball between restraints" Ph.D. dissertation, University of Massachusetts, Amhers, Mass., 1973.

11. DISA Information and Documentation Department — "DISA Type 55L Laser Doppler Anemometry", Instruction Manual, 1972.

12. FRENCH, A. P. "Vibrations and Waves", The M.I.T. Introductory Physics Series, 1971.

13. BURTON, R. "Vibration and Impact", Addison-Wesley Publishing Company, Inc., Reading, Massachusetts, U.S.A., 1958.